UNIVERSITY OF BIRMINGHAM

Statistical Modelling of the Transition Toughness Properties of Low Alloy Pressure Vessel Steels Volume 1: Main Body

by

DANIEL J. COGSWELL

A thesis submitted to the
Department of Metallurgy and Materials, School of Engineering, The University of Birmingham

For the degree of
Engineering Doctorate in Engineered Materials for High Performance Applications in Aerospace and Related Technologies

Structural Materials Research Centre
School of Engineering
The University of Birmingham
Birmingham
UK
July 2010

Synopsis

The transition toughness of low alloy steels used in pressure vessels is of key importance to establishing the safe operation of a number of structures; of these, the integrity of a nuclear reactor vessel is of greatest concern. The through life toughness of such vessels is a combination of the start of life properties and irradiation damage response of the material. Modelling of the inherent scatter of toughness measurements has received much academic interest since the mid-twentieth century and is found to be dependent on a number of metallurgical factors and failure modes; therefore, the micro-mechanisms of the ductile and brittle failure are explored and an assessment of the current best thinking on the modelling of crack arrest toughness is also considered. It has been established in this work that a highly accurate representation of a large toughness database can be achieved by the inclusion of constraint loss effects and the interaction between initiation and arrest toughness distributions.

Acknowledgements

This work would not have been possible without the support and aide of a number of people. The author has been on a roller-coaster ride of learning and understanding to be able to produce this thesis. This would not have been possible without technical discussions with a rather large and learned group of people.

Many technical discussions have been undertaken along the way, and without them, this work would not have followed the path that it has. Initial discussions with Paul Bowen, John Knott and Milorad Novovic proved invaluable in the early stages of this work and continue to be of great importance to maintain physical realism to the modelling work.

The members of the DISFRAC collaboration have provided an opportunity to discuss ideas on the mechanisms of failure at a level of detail that few would have gone to before. The knowledge gained simply from interaction with this group cannot be underestimated. Mark EricksonKirk in particular deserves a special mention for supplying the initial database that started this entire avenue of research.

The Nuclear Materials and Chemistry Support Department of Rolls-Royce was a great environment to allow completion of this work; providing a highly technical, yet amusing, place to work shows the quality of people within the organisation, both past and present.

Without a steady hand at the tiller this investigation may have ended up in any number of rabbit holes along the way; thanks is given to Tim Williams for guiding this work while allowing the author time to explore and unravel some of the mysteries of an incredibly interesting field.

The mathematical nature of this investigation has generated more than its fair share of questions, some much harder than others. Special credit must be awarded to Michael Asprey

for answering an incalculable number of ‘how do I do this?’ questions with the minimum of indignation. Statistics can often be confusing and counter intuitive so having communications with Daniel Eno has been very valuable in the closing stages of this work.

Particular gratitude is given to David Swan for his unfailing support and ability to find time for discussion. This work would have not been possible without his enthusiastic input and considerable experience.

The Engineering and Physical Sciences Research Council and Rolls-Royce Plc have supported the author in this work; their financial contributions are gratefully received. Thanks must also be given to Paul Bowen for the provision of research facilities at the University of Birmingham.

Thesis Outline

This thesis broadly contains three sections, each intended to provide part of the reasoning for this work and the mechanics involved in completing the statistical assessment of modelling methods suitable to the transition toughness behaviour of low alloy ferritic steels. The power generation industry requires that operational envelopes are widened and plant life times are increased in order to see the largest possible fiscal return on the high capital expenditure required to build a nuclear power plant. Increasing plant lifetimes by the reduction of conservatism in assessment methods is very appealing; the operational limits of a pressurised water reactor are, at least partially, directly set by the estimated toughness of key primary components such as the reactor pressure vessel (RPV). Any reduction in conservatism requires that a fully robust model is used or a lack of understanding could lead to unwanted and possibly dangerous optimism.

Chapter A details the background issues within the nuclear industry that have lead to the need for improvements in toughness assessment methods. A number of factors affect the through life toughness of RPV low alloy steels (LAS) and these can be modelled to various degrees of success; however, the output from these models, commonly a toughness shift, are added together in a linear fashion and the total affect is assumed to be a relative shift of the toughness curve from the start of life position. Improvements are being sought in all areas that affect through life toughness models. One area that presents significant benefit for the reduction of conservatism is toughness estimation. This can lead to benefits in safety margins at all points of plant life and help in the justification of yet longer planned plant lifetimes, reducing or eliminating the need for expensive plant life extension activities in the future.

Chapter B provides the physical understanding that directs the development of toughness assessment. This chapter reviews and comments on the current best thinking of the physical processes of fracture toughness behaviour of LAS, both the modelling methods employed

and the micro-mechanisms are considered. The review also contains a number of deductions and highlights based on the comments of the literature, helping to inform the important factors used in the database assessment of Chapter C.

Chapter C details an assessment of toughness estimation methods via the interrogation of a large database of toughness measurements in a variety of low alloy steels in various conditions, including irradiated data. The most widely accepted method for toughness estimation is the Master Curve (MC) concept developed by K. Wallin. This provides a mathematically robust and simply applied model; the physical and mathematical basis of this model however, is highly complex due to the underlying micro-mechanisms of fracture reviewed and developed in Chapter B.

The MC method allows the determination of toughness from a small volume of materials compared to elastic K_{Ic} measurements, or elastic plastic measurements across a wide temperature range. This stems from the setting of key variables in the mathematical model to known and consistent constants. This reduces the number of fitted parameters from three to one, thereby greatly increasing the accuracy of the estimate of the remaining variable. It is then feasible to generate meaningful estimates of toughness behaviour across a wide temperature range from a limited number of tests. The MC has been used to aid toughness determinations and improve margins of problematic real world structures.

Many studies show that the MC applies for a wide range of ferritic steels. Combined with the statistical nature of the fitting procedure it becomes appealing to adopt the MC for probabilistic assessments for the incredibility of failure for high integrity components. Exploring a large toughness database helps to provide support to use of the MC in assessments of this type.

The assumptions of the MC require assessment and validation against a large database to verify the use of the MC in probabilistic failure assessments (PFA) or risk informed

deterministic analysis. Industrial pressure to improve the lower bound toughness in such assessments is incompatible with one of the underlying assumptions of the MC method, a temperature independent lower bound to toughness in the transition region. This presents a problem for risk informed deterministic or full probabilistic assessments, as it is feasible that very low levels of toughness can be estimated at near upper shelf temperatures. This is contradictory to observation and informed scientific expectation of toughness behaviour. A physically based methodology is required to adjust the lower bound to produce a monotonically increasing lower bound of toughness within the transition region. Chapter C details a method to alter the lower tail of the MC distribution to correctly account for specimen geometry effects and the micro-mechanisms of fracture. This method has been established from statistical assessment of a large toughness database and the physical insights obtained from Chapter B.

This Engineering Doctorate has been conducted entirely within Rolls-Royce Nuclear Materials and Chemistry In-service Support and has had a significant impact on the development of work of this type. This work is largely classified, however, declassified summaries of directly relevant investigations and a strategy document have been included in the appendices. This work has directly affected the future toughness assessment strategy and direction of toughness research within Rolls-Royce Plc.

Nomenclature

K = stress intensity factor

G_f = geometric factor of defect

σ_{app} = applied stress across cross section

a = defect depth

σ_Y = the yield stress of the material

σ_0 = the internal resistance to dislocation motion, also known as the friction stress

k_y = the materials dependent strengthening coefficient

d = the grain diameter

σ_{ZA} = Zerilli-Armstrong stress

σ_G = internal resistance to dislocation motion (material constant)

k = grain boundary strengthening coefficient (material constant)

B_0 = material constant

β_0 = material constant

β_1 = material constant

$\dot{\varepsilon}$ = strain rate

T = temperature

V_p = the volume of the plastic zone

σ_1 = the maximum principal stress in an element

ΔV = the volume of element experiencing the principal stress, σ_1

V_0 = a small arbitrary reference volume

m = the inhomogeneity modulus of the Weibull model

σ_w = the Weibull stress

σ_u = the cleavage failure stress of the matrix

b = the ligament width, i.e $b = W - a$

M = a factor establishing a limit of constraint or constraint loss

J_{avg} = the externally applied load expressed as a J-integral

α_{RO} = a material dependent factor

n = the strain hardening exponent

σ_0 = the yield stress of the material

α = Weibull Scale parameter

β = Weibull Shape parameter

γ = Weibull Offset parameter

y_i = the actual number of events in bin i

$f(x_i)$ = the predicted number of events in bin i

B_{gross} = actual specimen thickness

B_{true} = crack front length corresponding to reduced stressed volume

K_{min} = temperature independent lower bounding toughness of the Master Curve, 20 $MPam^{0.5}$

$K_{Jc(med)}$ = median, 50 %, toughness of the Master Curve distribution

K_{Jc} = material toughness determined from J-integral at failure

$K_{Jc}B_i$ = material toughness determined for a crack front length of B_i

$K_{Jc}B_0$ = material toughness corrected to reference crack front length, B_0

$K_{J0}B_0$ = constraint corrected material toughness corrected to reference crack front length, B_0

Chapter A

Nuclear Power Generation

A Nuclear Power Generation

Contents

A Nuclear Power Generation....1

A.1 World Power Usage....4

A.2 Atmospheric CO2 Measurements....6

A.3 Nuclear Fission....7

A.4 Low Alloy Pressure Vessel Steels....12

A.4.1 Production of High Integrity Low Alloy Steel Forgings....12

A.4.2 Forming....13

A.4.3 Heat Treatment....16

A.4.4 Heavy Section Vessel Fabrication....19

A.4.5 Low Alloy Steel Microstructures....21

A.5 Effects of Neutron Embrittlement on the Mechanical Properties of Low Alloy Steels....23

A.6 UK Reactor Types....29

A.7 Age of Reactors....33

A.8 Defect Tolerant Design....35

A.9 Deterministic and Probabilistic Assessment Methods....43

A.10 Figures....46

A.11 References....82

Figures

Figure A-1 - Energy Consumption by Sector....46

Figure A-2 - World Energy Prices, 1980-2030....47

Figure A-3 - World Utility Power Generation....48

Figure A-4 - Energy Consumption by Source....49

Figure A-5 - Electricity Generation by Fuel, 1980-2030.....50

Figure A-6 - Location of atmospheric CO2 monitoring stations.....51

Figure A-7 - Direct Atmospheric CO2 Measurement.....52

Figure A-8 - Binding Energy of Atomic Nuclei.....53

Figure A-9 - Typical Reaction Products from the Fission of a U235 Nucleus.....54

Figure A-10 - Fission Chain Reaction of U235.....55

Figure A-11 - General Structure of an As-Cast ingot.....56

Figure A-12 - Iron-Carbon Phase Diagram.....57

Figure A-13 - Initial forging route for high integrity forgings.....58

Figure A-14 - Barrel forging procedure schematic.....59

Figure A-15 - Domed and shell forging process schematic.....60

Figure A-16 - Primary heat treatment profile.....61

Figure A-17 - Quality heat treatment profile.....62

Figure A-18 - Submerged Arc Welding Schematic.....63

Figure A-19 - Multi-pass Weld Structure.....64

Figure A-20 - Typical TTT Curve for ASTM A508-3 Material and Resultant Microstructure for Fast and Slow Cooling Rates.....65

Figure A-21 - Variety of Carbides in Tempered ASTM A508-3 Material.....66

Figure A-22 - Fast Neutron Interaction with Solid Materials.....67

Figure A-23 - Effect of Neutron Irradiation on the Hardness of Low Alloy Steel.....68

Figure A-24 - Effect of Neutron Irradiation on the Yield and Fracture Stress of low Alloy Steel.....69

Figure A-25 - Effect of Neutron Irradiation on the Charpy Impact Transition of Low Alloy Steel.....70

Figure A-26 - Effect of Neutron Irradiation on the Toughness Transition of Low Alloy Steel.....71

Figure A-27 - Magnox Reactor Schematic.....72

Figure A-28 - Advanced Gas Cooled Reactor (AGR) Schematic.....73

Figure A-29 - Pressurised Water Reactor (PWR) Schematic.....74

Figure A-30 - Age in Operation of World Utility Nuclear Power Reactors.....75

Figure A-31 - Expected Operational Life of USA Utility Nuclear Power Reactors.....76

Figure A-32 - UK Nuclear Power Generating Capacity of Current Plants, 2005-2040

.....77

Figure A-33 - Weld Defects.....78

Figure A-34 - Deterministic Assessment of Data.....79

Figure A-35 - Probability Plot of Variable x.....80

Figure A-36 - Combination of Probability Distributions.....81

A.1 World Power Usage

With the further industrialisation of the world outside Europe and North America, the world energy demands continue to increase significantly. An analysis of the usage of fuels in the USA shows that the majority of energy is used in transportation and industrial applications, with transportation usage predicted to increase further in the future (see Figure A-1). Residential and commercial usage has also shown a steady increase in recent years and will only continue to rise. Utility generation will provide the energy for all but transportation usage and reducing the cost (see Figure A-2 and Figure A-3) and increasing the security of supply is one of the key challenges facing governments in the future. The USA currently relies on nuclear power for 19% of electricity generation [1] (a similar figure also applies to the UK); however the steady state situation existing between decommissioning and commissioning nuclear plants will lead to a near constant supply from nuclear (see Figure A-4 and Figure A-5). The situation is mirrored in the UK and the age of current plants will be discussed later; however, it should be noted that the time required to build nuclear plants is considerably longer than fossil fuelled plants, approximately ten years compared to four years.

In order to meet the shortfall in energy demand, other fuels sources will need to be employed. It is most likely that emphasis will be placed on coal to provide the majority of utility energy in the near future. The supply of coal greatly outreaches that of gas or oil by some considerable margin; current predictions put reserves at 290, 15.7 and 18.4 ZJ (1 ZJ = 1×10^{21}J) respectively [2]. This is reflected in the predicated dependence on coal to provide the vast majority of utility power generation in the next 20 years.

The current demand is being met by what could be considered conventional supplies of fossil fuels, hydro electricity and nuclear fission. However all of these have a trade-off in other areas. Fossil fuels although cheap are in limited supply and produce green house gases during burning. Hydro electricity can supply large amounts of power but large areas of land have to be sacrificed in order to sustain a viable energy source. Nuclear fission is currently seen as the stopgap energy supply until nuclear fusion becomes economically viable. Nuclear fission also produces by products, a viable method of disposal for nuclear waste is yet to be discovered; however fission power plants occupy no more space than a fossil fuelled power plant yet produce only a small fraction of the carbon dioxide. If the challenges of reducing CO_2 emissions, to stop or reverse the effects of climate change, are to be met then nuclear fission appears to be the only well established technology capable of supplying the energy needs of the world.

Energy prices are set to increase in the future due to the lack of security within the energy supply market and increased demand by consumers. In recent years the price of wholesale oil and gas has fluctuated considerably leading to series of several consumer price increases and reductions. Nuclear provides more secure and reliable supply as the fuel is produced by either reprocessing or procured from politically stable and friendly nations such as Canada and Australia.

A.2 Atmospheric CO_2 Measurements

Atmospheric CO_2 measurements have been conducted by scientific and government observatories for many decades. This has lead to a good understanding of the recent changes in atmospheric CO_2 on a seasonal and annual basis. The global measurement is a weighted average of direct atmospheric CO_2 from over 50 laboratories situated all over the world [3] (see Figure A-6). The longest running continuous measurements have been made at the Mauna Loa Observatory in Hawaii, where measurements began in March 1958 and continue to this day [4]. The observations have been plotted in Figure A-7.

The Mauna Loa Observatory is situated at an altitude of 3400 m and as such the measurements from this site will differ from the global average; however, the trends in both datasets correlates well and it is undeniable that atmospheric CO_2 is increasing at an ever increasing rate. The Mauna Loa measurements show an increase of 20 % over approximately five decades and the global measurements show an increase of 13 % in 28 years. The measurements, in both cases, show a monotonically increasing trend and the data can be modelled well by a quadratic function. Fitting a quadratic to the global marine surface data and extrapolating into the future demonstrates that the current situation of CO_2 production from human activities cannot be sustained into the future without possibly irrevocable changes to global climate.

A.3 Nuclear Fission

Nuclear fission is a naturally occurring process in which a heavy nucleus, those with large atomic numbers, is disintegrated into two lighter nuclei [5]. This process is possible due to the differences in binding energies between the two states of matter. A heavy nucleus is imbalanced between the forces holding it together and those trying to push it apart, this creates a driving force for nuclear fission (and fusion for light nuclei). The forces are found to balance each other in isotopes with an atomic number of 50-65 with the best balanced achieved at nickel-62 [6], hence the natural abundance of iron and nickel found in the universe (see Figure A-8). It is preferential for matter to be in this state, and given the correct input of energy, can undergo fission to reach this condition.

When a fission reaction takes place the mass of the system changes; the two smaller nuclei will have a lower mass than the original large nucleus. The amount of energy is released can be calculated according to Albert Einstein's famous equation [7].

Equation A-1 $E = mc^2$

For example the fission of uranium 235 requires the kinetic energy and extra mass afforded by a neutron in order for the reaction to take place:

Equation A-2 $^{235}_{92}\mathrm{U} + {}^{1}_{0}\mathrm{n} \rightarrow {}^{236}_{92}\mathrm{U} \rightarrow {}^{141}_{56}\mathrm{Ba} + {}^{92}_{36}\mathrm{Kr} + 3\,{}^{1}_{0}\mathrm{n} + \text{Energy}$

The energy released by the above reaction is 186.4 MeV, calculated from the change in mass. This reaction is one of any number that may take place in the fission of uranium; however, the template is the same for all. A neutron adds mass, the

unstable nucleus then decays into two reaction products of varying mass, neutrons are released and energy is created (see Figure A-9). The amount of energy released varies due to varying mass of the reaction products but is about 200MeV for the fission of a uranium atom, the majority of which (~80 %) goes into providing kinetic energy to the reaction products. The reaction products themselves are commonly radioactive and their further decay releases yet more energy (~10 %). The remaining 10 % of the energy emerges as kinetic energy of the neutrons, moving at high speed interact with surrounding matter; however, due to the high velocities of these neutrons they may not cause fission in uranium-235 but can cause fission of uranium-238 leading to plutonium production which again is fissionable (this is the operating principle of the fast breeder reactor which generates more fissionable material than is consumed during operation).

As fission of uranium-235 can be caused more readily by a slow moving neutron a moderator material must be used in the reactor. Fast neutrons emitted by the fission process interact with these materials causing them to slow, losing kinetic energy and become thermal neutrons; these are easily absorbed by uranium-235 leading to further reactions. Different materials have differing levels of moderation on the fast neutrons, carbon (as graphite in Magnox and advanced gas reactors [AGR]) has a larger effect than light water (as used in a pressurised water reactor [PWR]) so more neutrons are slowed to take part in the next phase of reactions. This allows the use of natural or slightly enriched fuel in Magnox and AGR plants; however, particularly enriched fuel must be used in a light water reactor to sustain a reaction. This process of release and capture of neutrons can be used in a controlled chain reaction if a balance can be found between the number of neutrons emitted and absorbed (see Figure A-10).

The radioactive nature of uranium was discovered by Henri Becquerel in 1896 when he exposed photographic plates to a uranium salt and found that the plates became fogged [8]. This was the first proof of radioactivity and Henri Becquerel shared the 1903 Nobel Prize in physics with Marie and Pierre Currie for this discovery [9]. Since the discovery of uranium in 1789 by Martin Klaproth [10] it had been considered a safe substance and in fact had been in use for thousands of years in the form of the natural oxide as a colourant in glass. A physical understanding of radioactivity observed by Becquerel would not be published until 43 years after his discovery.

Lise Meitner and Otto Frisch correctly interpreted the discovery of barium in uranium subject to neutron bombardment as the splitting of the uranium atom in 1938 [11-12]. The field then moved very rapidly as scientists fled Europe following the rise of the Nazis to power, the majority settling in the United States. The knowledge of nuclear fission was taken to America by a number of scientists, most notably Niels Bohr, and a number of conferences and meetings would take place, further spreading the discovery of nuclear fission. During this time the first nuclear fission experiment was conducted at Columbia University by a team led by Enrico Fermi [13] , who had also been heavily involved with the earlier work on neutron bombardment of uranium, to establish the energy released during fission.

It had been predicted by Leo Szilard (also working at Columbia University), as early as 1933 (filing a patent for a simple reactor design in 1934 [14]), that a nuclear chain reaction could be possible; however, he predicted that it would be with light neutron rich elements not with a heavy nucleus as found in uranium. Upon hearing the discovery of secondary neutron emissions Szilard immediately saw the potential for a sustained chain reaction with uranium. Fermi and Szilard conducted experiments which would prove a chain reaction was possible [15] and eventually lead Szilard to the conclusion that production of a nuclear bomb would be inevitable.

It was found to be very difficult to initiate a chain reaction in natural uranium due to the low proportion of uranium-235. A German team had attempted to create a reactor using natural uranium as a fuel and graphite as a moderator. The production method for the German graphite blocks used included the use of boron carbide rods. Boron is a potent absorber of neutrons and Szilard concluded that the boron impurity in the graphite was preventing the chain reaction.

Aware of the problems with boron impurity in graphite Szilard commissioned graphite made without boron used during manufacture. By using natural uranium and high purity graphite Szilard and Fermi where able to produce the first sustained nuclear chain reaction with the Chicago Pile 1 [16]. Pile 1 was built under the direction of Fermi on a racquets court under a disused stadium at Chicago University; the first controlled reaction took place in 1942. Literally a pile of graphite blocks separating uranium oxide pellets; a central core of uranium metal was used to provide a good neutron source. The reaction was controlled by the use of cadmium (a neutron absorptive material) coated rods that could be removed from the pile to allow the neutron density to increase to allow the chain reaction.

Concerned at the implications of a Nazi Germany developing weapons based on nuclear fission Szilard drafted a letter to the current president, Franklin Roosevelt, which was signed by Albert Einstein [17]. This letter explained the possibility of nuclear weapons and that Nazi Germany may have the capability to develop these new weapons, to counter this he suggested that the United States embark on their own program of weapons development. This was the catalyst that began the Manhattan Project.

From the Manhattan Project many developments were made both in the field of reactor design and nuclear engineering. In order to create a uranium-based nuclear weapon of practical size the uranium used in the bomb must be highly enriched. Ways of enriching natural uranium therefore had to be developed, which in turn has lead to the creation of slightly enriched fuels. These allow a much greater power density to be obtained for a given amount of uranium and also allow the use different moderator materials, such as light water (H_2O). Different reactor designs require different levels of enrichment to function and these developments allowed for the use of nuclear power for energy generation.

A.4 Low Alloy Pressure Vessel Steels

A.4.1 Production of High Integrity Low Alloy Steel Forgings

Low alloy steels exhibit a ductile-to-brittle transition which would suggest that they are unsuitable for high-integrity applications; however, the high level of toughness achieved in the ductile failure region for the relatively low cost of the material provides a substantial driver for there use. If the ductile-to-brittle transition temperature can be effectively managed in the material by accurate controls during processing by a robust understanding of the microstructure, then the use of low alloys steel is highly acceptable.

The vast majority of pressure vessel steel forgings are manufactured from ASME Section II SA508 Grade 3 Class 1 material [18]. This a low carbon (~0.2 wt%) steel primarily strengthened by additions of manganese, nickel, molybdenum and chromium. The specification calls for a minimum yield strength of 345 MPa and tensile strength range of 550 to 725 MPa.

The quality of melt control and secondary steel making processes has improved greatly in the past two decades, allowing achievement of tight aim compositions and the removal of impurities such as phosphorus and sulphur. It can therefore be assumed that the heat-to-heat variability of composition has little effect on the resultant mechanical properties of these materials. In general, the mechanical properties of these materials is determined by two factors; the forming process used to provide the correct geometry for the component and the heat treatment applied to the forging following the forming process.

To fabricate a vessel, the forgings must be joined. Very early pressure vessels and high integrity structures featured riveted plates, modern vessels are all fabricated using welding. The wall thickness of heavy section vessels has traditionally limited options to high deposition rate processes but the drive to match the properties and integrity of parent materials has forced other options to be considered.

A.4.2 Forming

All nuclear quality forgings will be made using electric arc remelted scrap steel; the quality of this scrap is paramount to achieving the compositional requirements. Residual chemical analysis for embrittlement causing elements, such as phosphorus , copper, bismuth etc., will be used to determine if the scrap is suitable for ingot production. The remelted steel is then vacuum stream degassed during ingot pouring to remove residual hydrogen, oxygen and nitrogen. This provides a very high quality ingot with limited inclusions which is then passed hot to the heavy forge to allow processing without re-heating.

The intention of the forging process is produce the required geometry of the component while also offering sufficient work to break up inclusion clusters but more importantly to provide dynamic recrystallisation of the ingot. Upon solidification, the ingot will have a characteristic macro structure as shown in Figure A-11. The coarse microstructure and compositional variability due to macro-segregation within the ingot is highly undesirable undesirable. The goal of the forgemaster is a monolithic forging with (if possible) a homogeneous grain size distribution.

Attempts are made to help break up the structure of the ingot by the use of multi-fluted ingot moulds. These offer more surface area than a simple cylindrical mould and also a multitude of directions for the solidification front to grow and interact, help

to limit the growth of very large columnar grains which form in the chill length of the mould.

The macro-segregation of the ingot is easily dealt with by what appears to be an extreme measure. Following initial processing of the ingot, a significant proportion (<20%) of the ingot is parted from top and bottom to remove as much of the V and A segregate regions as possible. The parted material is not wasted, and will be added to the next furnace charge for production of the next forging.

The forging process for heavy section components used for high integrity applications is broadly similar in the initial stages no-matter what final geometry is required. All forging operations take place above the Ae3 temperature (a phase diagram for the Fe-C system is shown in Figure A-12), a range of 880 to 1250 °C is commonly used to ensure that the forging remains fully austenitic during forming. The forging will be re-heated as required through out the forging process. Figure A-13 details the early stages of the forging process: cogging, removal of discards, and upsetting.

Cogging forms the ingot into either a plain sided cylinder or one with a hexagonal or octagonal cross sections. Here the forging is worked perpendicular to the axial length to break up the columnar structure in the chill length by dynamic recrystallisation of the forging. This also helps to consolidate the central region of the forging which may contain pores caused by solidification shrinkage.

The discards will then be removed either by oxygen cutting or mechanical parting. This operation removes the macro-segregated regions, known as the V and A segregates, from the forging. In some instances the lower A segregate will not be

removed to provide integral thermal buffers for the forging (the use for buffers will be discussed below as these are required for heat treatment).

The forging is then subjected to a major upsetting operation along the axial length. The working achieved during this operation allows for large amounts of dynamic recrystallisation and effectively breaks up any remnants of the as-cast structure of the ingot. The forging, at this stage, is a thick disc and the remaining operations are dependent on the required geometry of the component. A number of possible routes can be chosen but fall broadly into two categories; barrel forgings and shaped shell forgings.

The forging operations required to produce a barrel forging a shown in Figure A-13. To produce a barrel forging, first the upset disc has to be either pierced or trepanned to create a central hole through the length of the forging. Trepanning is preferable as this removes the central, potentially segregated, region of the forging, yet further improves the macro-homogeniety of the forging. The forging is then repeatedly worked in the radial direction.

The next operation is to beck the forging such that the internal bore is large enough to use a substantial mandrel bar. The forging is worked with a thin tool parallel to the supporting bar; this forces material to the sides of the tool, increasing the bore and reducing the wall thickness. The forging is then rotated slightly on the smaller mandrel bar and the operation repeated, potentially hundreds of times on a large forging, to increase the bore such that a large mandrel bar can be used for the following operations.

With the bore increased, the forging must then be drawn to length. Here the tool is used perpendicular to the mandrel bar; as before the material is forced to the side of

the tool, increasing the length of the forging while reducing the wall thickness (the bore remains constant in this operation). After each operation the forging is moved relative to the press and at the end of each axial run the forging is rotated about the mandrel bar; again potentially hundreds of operations are required to achieve the required length of the component.

Finally, a becking operation is used to achieve the required wall thickness and bore of the component. The working required in each operation is planned to be balanced, i.e. the forging receives approximately equal longitudinal and circumferential working . In this way, anisotropic mechanical properties are largely avoided in the finished component.

Shell forgings and shaped forgings are made in a much simpler process. If the press utilised has suitable capacity then the shape of the forging can be achieved by one single axis-symmetric forging operation (see Figure A-15). The forging can be upset using shaped tools to produce thick section dome forgings or if thin section forgings are required then these can be achieved using either shaped tools as with thicker sections or by upsetting to the final thickness and then lightly working the forging over shaped tools.

A.4.3 Heat Treatment

All forgings require heat treatment, this performed in two stages,primary and quality. Primary heat treatment is performed directly after forging (see Figure A-16) and is purely to provide sufficient transparency for ultra-sonic inspection. Quality heat treatment (see Figure A-16) is performed in a near net shape geometry and is the main driver for the mechanical properties achieved by the forging.

The stages of primary heat treatment are transformation from forging, degas, homogenisation, optional austenitisation and tempering:

Following the final forging operation the forging is air cooled and is then held for sufficient time below 500 °C to allow for complete transformation of the forging from austenite to ferrite. At this time the forging temperature is not allowed to drop below 250 °C to prevent hydrogen cracking of the forging. Hydrogen cracking poses a significant risk to a forging and can result in a through thickness failure from which the only recovery is re-melting. The forging can be held at this temperature for any length of time dependent on the availability of equipment required for the following operations.

Upon heating to the homogenisation heat treatment, the forging will be held at ~600-650 °C to allow for complete hydrogen diffusion to free surfaces, where it simply evaporates to the atmosphere. The time is dependent on the recorded hydrogen level from the ladle analysis and the thickness of the forging; this can be several hundred hours when a very thick (>500 mm) section thickness is considered. While the forging is hot it is much easier to cut using oxy-parting; at this stage the ends of the forging are squared to allow easier handling in machining operations. Depending on the wall thickness and size of the forging, oxy-parting can take several hours and this time is factored into degas calculations.

Homogenisation is conducted at 900-950 °C to allow for complete dissolution of second phase particles for a time appropriate to ensure that the mid-wall of the thickest section is affected. The forging will either be air-cooled or water quenched to allow complete transformation from austenite to ferrite. Recent trends have been for water quenching to improve the number and quality of grain refining heat treatments. An optional second austenitisation (860-890 °C) and water quench may also be

performed to improve through thickness properties and therefore attenuation for ultrasonics.

Finally the forging is tempered in the region of 600-650 °C to soften the material to aid machining. The surface of the forging is skimmed to remove surface scale and provide a smooth surface for ultrasonic inspection. The forging is commonly rectilinear at this stage, therefore all areas of the forging can be assessed by ultrasonics for embedded defects. Following a successful ultrasonic inspection the forging is machined to quality heat treatment dimensions.

The quality heat treatment profile is near net shape to reduce the wall thickness and weight of the forging to absolute minimum while being able to maintain dimensional stability through heat treatment. By reducing the overall weight of the forging the quench efficiency is increased, i.e. by reducing the thermal mass the forging, it can be cooled quicker for a given quenching set-up. By minimising the wall thickness and therefore the amount of cover on the forging, the quench rate effect exhibited by low alloy steels can be taken advantage of. The mechanical properties achieved are dependent on the hardenabilty of the alloy chemistry chosen, the quench rate effect is symptomatic of this hardenabilty and the mechanical properties can be expected to be better near surface and lessen at greater depths.

To allow for assessment of the mechanical properties of the forging test rings will be used. These will be located either end of a barrel forging and at the single free end of a domed forging. In order to make the material in these ring representative of the bulk material, thermal buffers are required to limit the quench rate effect from end surfaces. These buffers can be integral (part of the forging) or welded-on using partial penetration welds (made from low alloy steel but not necessarily of the same specification as the forging being treated).

The forging may see repeated austenitisation and water quench cycles. These will be deliberately stepped down in temperature between cycles, the intention to produce no worse grain growth than the previous treatment. In reality the temperature control for large masses at these temperatures is not completely accurate so the temperature range is decreased, i.e. the first soak will be conducted at 870-890 °C and the second at 860-880 °C. The cooling rates achieved during the water quenches determine the resultant microstructures and hence are a major control on the mechanical properties achieved.

The final operation is a tempering heat treatment. This softens the material, trading strength for ductility, and the temperature and time are controlled strictly by material specifications [18]. The forging is then finish machined and prepared for welding to other forgings which form the vessel. A major vessel can be made up of many forgings and the quality of the welds used is often the limiting feature in the mechanical performance of the vessel.

A.4.4 Heavy Section Vessel Fabrication

Selection of the welding process used to join the plates is a balance between quality and time. Flux based processes allow large deposition rates but increase the likelihood of inclusion defects. Tungsten inert gas (TIG) welds offer greatly improved properties but have slow deposition rates. In general submerged arc welding (SAW) is used for vessel manufacture as acceptable properties can be achieved on a consistent basis (see Figure A-18). These welds are multi-pass and receive only minimal heat treatment as it is not practical to perform a full quality heat treatment on a finished vessel.

Without further heat treatment, the material therefore will have a characteristic cross section (see Figure A-19). Here the microstructure of each zone is controlled by the cooling rates achieved during deposition; these zones can be clearly defined as the parent, fine and coarse grained heat affected zone (HAZ), and the as deposited material.

The parent material is the unaffected material of the forgings to be joined. These will by definition, will have identical mechanical properties to the forgings. As deposited material is material which has been unaffected by subsequent weld passes; this will have columnar coarse grained structure and represents the weakest microstructure in the vessel.

The fine grained HAZ is formed by parent material which has been heated by the welding process and then due to rapid heat transfer to forging has been cooled very quickly. The fast cooling rates achieved afford a fine structure which has superior properties to the weld but due to induced residual stress, may be poorer than the parent material. The coarse grained HAZ forms in the weld deposited material, but due to the higher temperature of the recently solidified weld deposit, the cooling rates here are insufficient to produce a fine structure; however, the microstructure is refined over the as deposited structure.

Residual stresses in a weld can be high, and are often predicted to be larger than the primary pressure loads on the vessel. To reduce these stresses, the whole vessel receives post weld heat treatments. These are performed at temperatures slightly lower than the tempering temperature of the forgings with the intention of making no changes to the mechanical properties of the forgings while affording sufficient stress relaxation to reduce residual stresses in the welds.

A.4.5 Low Alloy Steel Microstructures

As can be seen from above, the primary control of the microstructure of the low alloy steel used for vessel construction is the cooling rate from the austenite phase field. In general faster cooling rates yield better mechanical properties (improved toughness and strength) by inducing a finer structure prior to tempering. Figure A-20 shows the Time Temperature Transformation (TTT) diagram and effect of cooling rate on the microstructure of ASTM A508-3 material. The structures that form are discussed below.

The slow cooling rate passes through the Pearlite nose of the TTT diagram causing a diffusional transformation in the material. This process is slow and allows for organisation of the material at the sub-structure level [19-20]. This leads to a cellular structure of moderately sized ferrite grains (~10-50 μm). These grains exhibit significant sub-structure suggesting that a simple model relating microstructure to mechanical properties is unlikely. The fast cooling curve passes to the left of the Pearlite nose. The structure produced in this case is of accicular ferrite with a correspondingly smaller grain size (~1-10 μm). This structure is not formed by diffusion but by shear [19, 21], creating a bainitic material with improved mechanical properties. The finer grain size will improve all mechanical properties, i.e. both strength and toughness will increase rather than achieving one at the expense of the other [22]. Faster cooling rates could lead to a martensitic material; however, the cooling rates required are so high (>50 °C/sec) that this is unachievable for heavy section forgings used for vessel production.

Currently the best mechanical properties achieved by inducing the accicular structure shown in Figure A-20; however this is only one element of the microstructure which needs to be considered. Ferritic steels are strengthened by a number of

mechanisms, grain boundary strengthening due to grain size being only one of these factors. Solid solution strengthening is is also important and controlled largely by chemistry but heat treatment can affect this by precipitation of strengthening elements. Carbon has low solubility in ferrite and so forms carbides, predominantly with iron but also with carbide forming alloy additions, such as molybdenum and chromium [23]. These carbides precipitate during the tempering of the material and can form in a number of morphologies. The size and shape of the carbides is dependent on the thermal history of the material and can range from needles, through plates to spherical. A high resolution electron microscope image of un-etched ASTM A508-3 material is shown Figure A-21; this highlights the variety of carbide sizes and morphology that can be achieved in a nominally homogeneous commercial steel.

A.5 Effects of Neutron Embrittlement on the Mechanical Properties of Low Alloy Steels

Fast neutrons escape from the fission chain reaction. Passing through the moderator without being slowed, these neutrons may interact with the support or containment structure of the reactor. For reactor designs that use a steel pressure vessel the results of this interaction is well documented [24-26], yet not completely understood. The mechanical properties, particularly the materials resistance to brittle fracture, can be greatly reduced by exposure to even a modest amount of neutron bombardment [25, 27]. There are a number of ways in which a fast neutron colliding with the steel crystal structure may result in changes to the properties of the material.

When a fast neutron collides with the crystal lattice of the steel pressure vessel the kinetic energy of the neutron will result in local disordering as a burst of thermal energy. Atoms will also be dislodged from their ordered positions in the crystal lattice, these will in turn collide with the lattice atoms again, and so on until all available kinetic energy is converted to thermal energy, creating a cascade (see Figure A-22). This resulting crystal will contain point defects, such as vacancies or a local irregular crystal structure. The irregularities in the structure will produce stress-fields on the crystal lattice affecting the movement of dislocations through the structure; this effect can be described as ‘matrix hardening’. This has the effect of inhibiting slip within the grains increasing the yield stress of the material and preventing the blunting of micro-cracks within the material. Both of these are perceived to be detrimental to toughness in low alloy steels.

The second mechanism for embrittlement follows directly from the irregular crystal structure caused by displacement cascades. The defects created by the neutron

bombardment will produce stresses in the deformed matrix. The stresses and increased vacancy concentration present allow normally immobile atoms to diffuse at temperatures much lower than can be attributed to solely thermal diffusion. The material will reorder itself to a configuration with the lowest stored energy; this commonly involves the development of clusters and precipitates of impurities and alloying additions.

One impurity that becomes mobile with the aid of irradiation is copper. The concentration of copper can be readily related to the amount of embrittlement evident in irradiated steels. However, utility reactor vessels are normally constructed from a number of rolled plates joined by submerged arc welding (see Figure A-18). In order to protect the welding consumables from corrosion in storage, the filler wires were coated with copper; this was considered good practice to prevent the use of corroded wires that may introduce welding defects into the structure. This increased the concentration of copper in the exact areas where embrittlement must be avoided; the welds will have the least refined microstructure and therefore the poorest start of life toughness, combining this with the highest level embrittlement presents many challenges to those looking to operate a utility reactor. The problem of copper precipitation came to light in the 1960's, although it took considerably longer for it to be recognised as a threat to plant integrity; now, the concentration of copper in materials used to construct reactor pressure vessels is carefully monitored by accurate control of the scrap steel used for production and welding consumables.

The precipitates act as barriers to dislocation motion within the matrix and therefore increase the strength and hardness, while reducing the toughness of the material. Fortunately the low concentration of copper in these alloys limits the formation of these precipitates; however, there is a sufficient level to have a considerable effect on the mechanical properties of the steel subject to bombardment. Although the

effect is constrained by the limited availability of copper to form the precipitates this also prevents the over ageing of the precipitates, i.e. they will always remain coherent to the matrix and provide an ever-increasing strengthening effect until all copper has migrated to the precipitates. Precipitates also form with high levels of nickel and manganese, key alloying additions to low alloy steels, a balance is therefore struck between start of life and end of life properties.

Another impurity element to cause disadvantageous changes to properties is phosphorus. Normally locked within solid-solution in the steel matrix, the increased vacancy and interstitial concentration due to irradiation permits diffusion of phosphorus. Phosphorus, unlike copper, does not form precipitates; however, phosphorus does migrate to grain boundaries causing severe embrittlement [28-29]. The presence of weakened grain boundaries presents another problem, inter-granular failure. Here the grains literally separate at the boundaries creating narrow and possibly atomically sharp defects within the material. The occurrence of these sharp defects will increase the chances of brittle failure as a sharp defect will increase the stress intensification for a given applied stress.

The effect of phosphorus on steels has been understood for many years [30] and the above process of grain boundary embrittlement is common in steels with a high level of phosphorus and the effect can be exaggerated by a temper embrittlement heat treatment [31]. By holding the steel at a temperature suitable for diffusion of phosphorus, 350-400 °C, the grain boundaries can be decorated with phosphorus atoms; this is now performed mostly as a research method for checking susceptibility to embrittlement. The level of phosphorus is now closely monitored in almost all fields of steel production and alloy development; some high hardness and high strength steels have been created which use the very potent effect of solid solution hardening from phosphorus.

The essential elimination of copper in modern alloys has yielded great benefits in through life toughness prediction; in recent years a new effect of neutron embrittlement in modern high toughness, ultra clean steels has been observed. The presence of increased alloying additions has led to the likelihood of late blooming phases [32-34]. Alloy rich precipitates may begin to form at very high doses in a process similar to copper precipitation. The formation of these precipitates is not limited in the same way as copper formation, due to the higher abundance of the alloying elements (nickel, manganese and silicon are of greatest concern) they contain giving rise to a highly accelerated form of irradiation embrittlement. These precipitates, once nucleated, grow very rapidly.

The three mechanisms of damage outlined above, matrix hardening, precipitation hardening and grain boundary embrittlement, cause different effects on the material (see Figure A-23). The hardening mechanisms increase the yield stress of the material, whereas the grain boundary embrittlement lowers the fracture stress of the material. This is commonly expressed on plot of the yield and fracture stress against temperature (see Figure A-24). This provides a measure of the change in ductile to brittle transition temperature (DBTT), in this case the change is absolute, i.e. below the DBTT no plastic deformation will take place giving a rather simplistic view of fracture. This, however, does provide a very basic framework for assessing the effects of neutron embrittlement and a simple way of applying a metric to this effect, the change in DBTT.

Difficulties in measuring the fracture stress of a material and the inability to relate the combination of yield and fracture stresses to the toughness of low alloy steel precludes this from being a useful assessment. From a toughness perspective, there are a number of ways to measure the DBTT. The oldest of these methods is impact

testing. Adopted primarily by the ship building industry after a number of very high profile failures impact testing provides a comparable measure of toughness, although not a measure that can be used to establish the severity of defects. Researchers have employed several different methods of impact testing, all essentially involve striking a standard test piece with a known kinetic energy supplied by a hammer or drop weight.

The Charpy [35] and Izod test both use a swinging hammer to strike a constrained test piece; the energy input is controlled by the height the hammer is raised and by measuring the height the hammer reaches on the follow through after the strike the amount of energy absorbed by the test piece during failure can be established. An impact test in this manner shows a transition from a brittle lower shelf to a tough upper shelf. Irradiation affects this transition in three ways; the entire curve is shifted to higher temperatures, the upper shelf is lowered, and the gradient of the transition is lessened (see Figure A-25).

There are a number of ways to assess the DBTT of an impact transition, the simplest being the temperature corresponding to half way between the upper and lower shelves; however the changes to the transition outlined above make this inappropriate. To provide a simple comparison between conditions, given the above changes in the shape of the transition, an energy level can be selected and the shift in temperature assessed at the reference energy level. The temperature shift provides a surprisingly good correlation to other mechanical property changes and is widely used as an assessment method for irradiation damage. Irradiation surveillance programmes commonly use impact test pieces due to their small size and desire for a measure of toughness comparable to those taken at the start of operation.

The shift in hardness has also been found to be good and transferable measure of irradiation damage; however, difficulties in repeatability common with hardness testing can result in small changes due to irradiation being lost in scatter. A hardness test can be conducted on a small fraction of the material required for almost any other mechanical testing providing a large number of test results for a given volume, increasing accuracy at the expense of precision. As hardness provides a good approximation to the tensile properties of a material the measured change in hardness unsurprisingly corresponds well to the change in tensile and other mechanical properties. The mechanical change in a material due to irradiation is hardening; this is the cause of all other mechanical property change. The effect is a reduction in the toughness and impact resistance of the material.

Recent developments in the understanding of the stresses experienced in standard test piece geometries have begun a renaissance in the assessment of through life toughness. By using smaller, even impact sized, specimens valid toughness data can be generated from valuable and limited irradiated material (see Figure A-26). The use of direct measurement to establish toughness eliminates some of the uncertainty and conservatism when estimating the resultant effects of irradiation embrittlement. Use of the Master Curve concept, to be described later, has created a framework to estimate the toughness of a component from a low number of small test pieces [36-37]. It is believed that the low level of irradiation that is experienced by a reactor vessel affects the toughness transition in only one way. The relative temperature dependence of the transition remains constant and the curve is simply shifted on the temperature axis.

A.6 UK Reactor Types

A utility power plant is made up of the same basic components no matter which fuel is used. A heat source is used to raise steam that is used to turn a turbine, which in turn, is used to power a turbo generator [38]. Steam is used due to the very high mass flow rates for a gas that can be achieved and thus the high energy density allowing smaller turbines to be used. This in turn reduces the rotating mass of the turbines that is highly desirable when engineering the structure. The rotational motion from the turbine is used to turn a coil within a magnetic field, or vice versa, to produce an alternating electric current, which is then supplied to a national grid. A nuclear power plant works in the same manner described above however there is a large diversity in the details of how the heat is generated. All reactors require a coolant and a moderator, the coolant is required to remove heat from the fuel elements and the moderator is required to slow the fast neutrons liberated by the nuclear reaction to a point were they can once again interact with the fuel. The variety of power reactors stems from the many different combinations of coolant and moderator used in these designs.

The majority of reactors used for power generation are light water reactors using light water (H_2O) as both coolant and moderator [39]. These produce steam either directly by boiling water within the reactor vessel (boiling water reactor, BWR) or by using pressurised light water as a coolant and indirectly raising steam via a heat exchanger (pressurised water reactor, PWR) [27]. Currently only one PWR, Sizewell B, is used in the UK to provide utility power; all other nuclear utility generation is produced by gas cooled reactors, of which two designs exist, one being a development of the other.

There are currently three reactor designs used for utility power generation within the United Kingdom, the reason for which use due to the availability of technology. Following World War II a limited number of facilities existed which could be used for the production of nuclear materials; a heavy water (D_2O) production plant existed in Canada so the Canadian design utilised heavy water as a coolant and moderator, the USA ended the war with a uranium enrichment plant and as such was able to produce enriched fuel required for light water reactor designs. The UK, however, only had access to un-enriched uranium from Australia and so a design was created which could best use this resource.

The Magnox reactor design (see Figure A-27) was developed in the early 1950s to provide a source of plutonium for nuclear weapons development, however emphasis soon switched to power generation as the energy demands of the UK increased. The first power reactor to supply energy to a national grid was a Magnox design, Calder Hall in 1956 [40]. The design was continually developed and improved over the next 15 years and as such no plants are exactly the same. The design takes its name from the alloy used to clad the uranium fuel, magnesium oxide, hence Magnox. By using carbon dioxide at high pressures as the coolant and graphite as the moderator the costs of production materials was relatively low, however the use of natural uranium fuel meant that the plant had to refuelled much more frequently than other designs [41]. The plant design was not without its problems, oxidation of low alloy steel components within the supporting structure of the core being the most widely reported and damaging[27].

The improvement in access to enriched fuels resulted in an evolution of the Magnox design, the advanced gas reactor or AGR (see Figure A-28). The heat exchangers were now brought inside the primary vessel and, like some of the later Magnox reactors, a large reinforced concrete pressure vessel was used allowing higher gas

pressures to increase efficiency and power output. The thermal efficiency of an AGR is very good, in the region of 40 % which is higher than a modern PWR (~35 %), due to the high temperatures achieved. The high temperatures of ~640 °C are passed onto the secondary coolant giving steam conditions similar to those found in a fossil fuelled power plant. The AGR was designed for online refuelling, originally to be undertaken at full power; however, problems with vibration in the fuel elements during reloading eventually lead to abandonment of full power refuelling. The AGR can still be refuelled at partial load, mitigating some of the lost power generating capacity.

The PWR design is very different from the gas cooled type reactors. Light water is used as both coolant and moderator for the reactor offering higher core power densities; however, due to the higher attenuation of fast neutrons achieved with water, slightly enriched fuel must be used in this design. The light water must be kept in a liquid state by the use of a pressuriser or the water may boil in the core therefore eliminating cooling due to the formation of a steam blanket around the fuel. If the fuel is not constantly cooled during power operations then a meltdown could result. As with both gas cooled reactors steam is generated indirectly by the use of a heat exchanger that boils secondary water to produce steam for the turbines. Some large PWRs will have several of these steam generator loops.

Unlike the gas cooled reactors, the PWR cannot be refuelled online and must be completely shut down and the top closure head removed to replace spent fuel. This must be carried out in a sealed space; hence PWRs have a secondary containment shield of concrete around the primary systems giving rise to the characteristic large dome or cylinder of the main reactor building seen at PWR sites. Currently the UK only has one PWR supplying utility power, Sizewell B. First operation began in 1995 following a very lengthy planning and consultation stage that delayed the project by

several years. PWR designs with simplified pipework layouts and reduced numbers of valves will most likely be built in the UK in the coming years. These contain a range of passive safety features, which greatly simplify the design and decrease greatly the risk of an incident due to human or operational errors. For instance, emergency make-up coolant is stored in a large tank above the reactor, the coolant is therefore gravity-fed. This design eliminates a pump critical for emergency operation which, would require redundancy in order to meet regulation requirements.

A.7 Age of Reactors

The population of nuclear reactors used for utility power generation is ageing rapidly. The International Atomic Energy Agency (IAEA) maintains an accurate database of information on utility power reactors [39] and a simple analysis of the age of these reactors shows that only 25 % have been in operation for less than 20 years (see Figure A-30). A balanced situation of new build and decommissioning of old plant is yet to be reached due to the relative infancy of the technology. The majority of reactors were originally commissioned with an expected 40 year operational life and hence the current crop of reactors can be considered to be the second generation of power reactors. New build is currently under way, or being considered, in several countries which will help to address the balance of new and old plants in operation.

The operational life of a power plant can be extended by a change in analysis methods moving from highly conservative estimates to demonstrably more accurate techniques. If this increase in operational life cannot be demonstrated then the plant will have to be shut-down and decommissioned. The USA has been conducting a review of the reactors used to supply utility power and where possible increasing the expected life from 40 to 60 years (see Figure A-31) [42]. This will allow a smooth transition between reliance on older plants and accommodate the delay in the construction of new plants.

The situation in the UK is very different from the USA and currently the operation life of almost all UK reactors cannot be extended at the present time. UK reactors were constructed using a very different design type to those in the USA. All except Sizewell B are gas-cooled reactors; these require the use of graphite to act as a moderator on the nuclear reactions. The graphite in the UK reactors has been highly adversely affected by neutron bombardment and cannot be replaced limiting the

expected life of these reactors to 40 years. Within 10 years the generating capacity will be reduced to just 35 % of the current level (see Figure A-32) leading to further reliance on fossil fuels to fill the gap until new plants can be constructed [43].

A.8 Defect Tolerant Design

Material defects can be found in all materials. The size, severity and density of these defects can be controlled by the processing method employed in manufacture; commonly, methods that provide the best quality materials and components are the greatest in expense. Ideally the best possible materials or components would be used for critical parts but in reality a balance must be found between the cost of manufacture and the requirements of the component in service, the fit for purpose concept. Although a material that exhibited no ductile to brittle transition, such as an austenitic stainless steel, would solve a large number of problems associated with irradiation damage, the cost of using such a material for manufacture of reactor pressure vessels is prohibitive and has only been performed when absolutely necessary.

It is more economical to produce a reactor pressure vessel made from an inexpensive yet tough material that exhibits a toughness transition, such as low alloy ferritic steels, and justify the use of the material through engineering analysis. By selecting this method, the defects within the material, or those introduced during manufacture, need to be understood and possibly eliminated. The defects contained in a low alloy steel reactor vessel can come from a number of sources but broadly fall into three categories: material, welding and forging.

Material defects form during the processing of the raw material to produce the final engineering material and cannot be removed by subsequent handling. Produced by chemical reactions between alloying elements or unwanted impurities during the molten stages of manufacture, hard non-metallics and soft inter-metallics can be formed [19-20]. Hard particles can act as initiation sites for brittle fracture and the

presence of clusters of soft particles will reduce the tensile properties of the material. The mechanisms of these effects will be discussed later.

There are a large number of different defect types that can be created during the steel making process. Some defects can be designed out by accurate control and intelligent processing, however, some are inherent and cannot be removed. These are melt defects created during the liquid stages of process by chemical reactions between impurities and alloy additions creating thermally stable phases which will be carried over into the ingot. These inclusions can take many forms, by far the most common in low alloy steel production are oxide and sulphide inclusions, large carbo-nitrides can also be of concern due to their angular structures. These inclusions will have different densities to liquid steel and this fact can be used to provide a way of removing them from the melt. By holding the steel as a liquid for a set length of time the inclusions can literally be floated out of the melt and retained in the slag layer.

In order to make large forgings a large ingot is required. The ingot must also be made over sized to permit the removal of the V and A segregates [44] (see Figure A-11), located at the upper and lower regions of the ingot, respectively. Segregation of alloy elements and impurities causes areas of solute rich material that may differ markedly from the homogeneous centre and columnar regions. The segregation is formed by a difference in melting temperature between the lean and rich phases that can be formed from the material. Commonly a material is a mixture of several phases, one solute rich the others lean, one of which will solidify at a lower temperature forcing the remaining liquid to become rich in the element that is not required to form the lower temperature phase. This creates a solute gradient in the solidification region in which the mechanical properties are difficult to estimate.

Due to the complex shapes required in certain areas of the reactor vessel and the required properties that can only come from forging of the material, it is difficult and impractical to construct the vessel in one piece. The vessel is made from a number of smaller components joined by welding. There are a number of welding techniques, again balancing cost and time against quality, but the types of defects that may be created are similar; although the size and the frequency will depend on the technique employed. Lack of fusion defects (see Figure A-33), caused by insufficient heat input to melt the substrate and form a good bond to the deposited material, and stop-start defects, caused by an interruption in the melting of filler material, are common to all types of welding.

The depth of weld required suggests a process requiring high deposition rate of material; therefore, the submerged arc welding process is commonly used (see Figure A-18). The submerged arc process deposits a large amount of material in each pass compared with most other welding processes resulting in a larger as-deposited bead and less refinement in the reheated region (see Figure A-19). As welding is a molten process, inclusions may also form in the weld bead as they would in the original melting of the material. As the actual time the material is molten is very short diffusion is limited so it is more likely that these inclusion will be formed from impurities in the filler material or reactions with the surrounding atmosphere. The submerged arc process forms a protective gaseous layer over the weld by vaporising the flux used to protect the weld surface.

The final source of defects in a reactor pressure vessel is the forging process. Incorrect design of the forging steps necessary to produce the properties and shape required could create serious defects that will prevent the use of the forging [44]. Of most concern are hot tears and folds. Hot tears form where the local stress exceeds the ultimate tensile strength of the material, which is severely reduced by the

increased temperatures. Folds are simply the creation of creases in the material during upsetting operations; the two surfaces brought together will not form a strong bond due to the presence of an oxidised layer on the surfaces. This may create a very large embedded defect that fortunately can be detected by ultrasonic inspection, which is conducted frequently during production of reactor vessel forgings. Folds and tears can be prevented by a good understanding of the flow properties of these materials at high temperatures and careful design of the tooling and forces applied during forging.

From the above we can see that the presence of some form of defect is almost inevitable in a reactor vessel. The materials ability to sustain a load given the presence of defects is known as the material fracture toughness. For many years toughness was estimated or asserted by the use of indirect measurement, such as impact testing. By taking direct measurement of material toughness, the severity of these defects can be established. The development of a critical stress intensity factor as a measure of toughness that was applicable to geometries other than that used for standard test pieces created a whole new field of engineering assessment, fracture mechanics [45]. For the first time it was possible to decide on the suitability of a structure by means of an assessment of the material, the defects that could be sized and the stresses with in the structure.

Failure of a material due to the presence of a defect occurs when the critical value of stress intensity factor is reached. For low alloy steels on the lower shelf and in the transition region this critical value will correspond to a catastrophic brittle failure of the component. The condition under which this value is measured becomes important, as the transferability of a laboratory measurement to a real world situation is highly complex. The three dimensional stress fields acting on a defect in an actual component can produce complex opening stresses on the defect. To produce a

viable measure of the material toughness the opening stress must be maximised; this is achieved by a simple tensile opening of the defect. However, the geometry of the defect must be strictly controlled to ensure that the applied force is a simple opening of the defect.

By following some simple assessment rules it is possible to form a first approximation to the real world situation using basic linear elastic fracture mechanics methods. A simplifying assumption that the deformations in the test piece or component remain linear elastic allows the use of a simple equation combining the defect geometry and applied load to produce a quantitative measure of stress intensity factor[46].

Equation A-3 $K = G_f \sigma_{app} \sqrt{\pi a}$

where K = stress intensity factor

G_f = geometric factor of defect

σ_{app} = applied stress across cross section

a = defect depth

As stated above, the limit to the stress intensity factor that can be accommodated is a material property, i.e. one independent of the geometry of the material, such as yield stress or thermal expansion. For a linear elastic approximation in tensile opening this limit takes on a very specific meaning; *the toughness of a material is the stress intensity factor that will cause catastrophic failure of a material subject to a monotonically increasing mode I (tensile) opening stress*. For high toughness materials, such as low alloy steels, it becomes difficult to replicate linear elastic conditions due relative size of the process zone and the specimen, leading to the loss of constraint both across the crack front and due to the presence of the back

face of the specimen. The effect of loss of constraint can be minimised by using large specimens, and early research on toughness resorted to the use of very large specimens to produce viable toughness data.

By using the equation above (Equation A-3) the severity of a defect can be established, i.e. it becomes feasible to use a component containing defects as long as the stress intensity factor can be accurately established and it is within the safety limits set by the regulator or designer. In reality a defect caused during processing or manufacture is unlikely to be of concern due to the high levels of toughness that can be obtained with low alloy steel; these defects, however, represent initiation sites for fatigue cracks. These will form the most damaging geometries of deep and sharp defects and their growth may require periodic monitoring in the most damaging situations.

In order to assess the suitability of a material and component design three factors must be known: the applied stress, the defect geometry and the material toughness. This allows the designer to assess when a crack will reach a critical size, i.e. a critical stress intensity factor for given loading situation. Commonly the elastic stresses, even for complex geometries, can be calculated accurately from finite element analysis of the component and applied loads [47]. The defect geometry can be measured and fatigue growth can be modelled via the Paris law [48], or alternatively periodically measured. The material toughness is constant for the majority of analyses of this type but the effects of neutron embrittlement require that this becomes a variable through life. This makes the assessment somewhat more complicated requiring the presence of increased safety factors and margins.

An elastic analysis contains one assumption that leads to a large overestimation of the stresses involved in the assessment. The stress increases exponentially as it

approaches the defect, giving rise conceptually to an infinite stress at the defect root. This, of course, is impossible and would result in the instant failure of all components once they have been loaded. Material plasticity comes to the aid of the component by limiting the maximum stress ahead of the notch root to a multiple of the yield stress of the material [49-50], commonly understood to be 3-5 times the yield stress, σ_y. The material will flow to dissipate the stress at the notch root causing crack blunting; this is especially evident in low alloy steels in the transition region where a small amount of blunting and stretch zone is observed on fracture surfaces between the pre-fatigued crack and cleavage failure at higher temperatures.

Plasticity alters the stress distribution ahead of the crack tip from an asymptote to a smoothed curve whose severity is controlled by the diameter of the crack tip. This moves the point of peak stress into the material and away from the defect (discussed in a later section).

One assumption that must be made to create the solutions for LEFM is that the defect is embedded in a semi-infinite plate. This must be done for simplicity, as even a simple elastic analysis of actual specimen geometries will result in non-linear deformation; by assuming that the plate is infinite and no deformations occur within it then solutions can be established analytically. This assumption holds true if the relative size of the component to the defect is very large. Once the size of defect is comparable to the component, such as in a test piece, the effect of the finite geometry becomes more important.

In small components or for shallow defects the loss of constraint at the defect tip becomes very pronounced. Most noticeable as shear lips on the flat sides of specimens, the formation of these plastic regions absorbs a large amount of energy

and creates a distorted measure of the toughness of the material. To mitigate the presence of shear lips on test specimens, specimen size effects must be taken into account. In the early stages of LEFM this was achieved by using large test specimens so that the effect of shear lips was reduced to the point where pseudo-elastic measurement of material toughness could be made; for high toughness materials, such as low alloy steels, the required specimen size can reach gigantic proportions.

A.9 Deterministic and Probabilistic Assessment Methods

Unsurprisingly, the outcome of a structural assessment can be modified by selection of the input parameters: the defect size and shape, component loads, and material toughness. In the case of a nuclear power plant, the difference between being overly conservative and overly optimistic can result in either the shut-down of a very expensive asset or the endangerment of the public. The correct choice of inputs for the assessment is difficult and requires engineering judgement to maintain the correct balance of conservatism and optimism. Two methods exist for performing a structural assessment, a deterministic method and a probabilistic method.

A deterministic assessment is essentially based on the perceived worst case of defect, loading and material toughness. This can be very hard to determine absolutely and commonly an element of engineering judgement is required; as data are difficult to generate for these cases an estimate must be made of the input parameters. In establishing the worst case the resultant analysis tends to be highly conservative; however, the parameters selected are based on a perception of the defect, stress and material involved. This perception can be incorrect and can to lead errors of both being too conservative or too optimistic, both outcomes are not desirable but being too optimistic can result in potentially safety critical failures.

A deterministic approach is adopted when a lower bounding curve is applied to empirical data, an example is provided in Figure A-34 using a dummy dataset. To prevent the assessment from being non-conservative safety factors are applied to the inputs to maintain a conservative approach. This further moves the assessment away from reality, with the additional factor applied also based on engineering judgement. This commonly results in the adopted method being so conservative that the assessment can have little resemblance to the true reality of the situation.

A more realistic view of safety may be afforded by a probabilistic method (see Figure A-35). This relies on data generated from the structure or testing of material factors in representative situations. For example the assessment of belt line weld defects requires knowledge of the defects that can be found in the weld, the stresses that may be experienced, the initial material toughness, and the expected through life shift. For each of these a probability distribution may be generated, again for example material toughness has an inherent scatter making it very difficult to establish the worst case. By random sampling from each of the controlling distributions a single estimate of the safety of the component can be generated (see Figure A-36). If this process is repeated several million times then a probability distribution of the outcomes can be established, from this it is possible to determine the probability of failure of the component.

Different probabilities of failure are required for different areas of a structure dependent on the expected consequences due to failure. Different international regulatory bodies use slightly different target probabilities of failure per year but commonly they are of the order of 1 in 10^6 [51]. Performing a number of simulations to a few orders of magnitude higher than the required probability of failure gives enough definition to the probability distribution to give an accurate description at these very low probabilities of failure. As this method is based on actual data it provides a better representation of the component than a deterministic assessment; however, even with 10^8 simulations the worst case may not be sampled so the deterministic case cannot be established from a probabilistic assessment.

As a component nears the end of life the judgement of the safety factors becomes more important; closing a plant before it is necessary could cost millions of pounds in lost revenue but operating beyond safe limits endangers public safety. At this stage

in the components life a combination of deterministic and probabilistic methods can be employed to provide a ‘risk informed’ assessment. Here the suitability of the structure is still assessed on the deterministic case, however, the probabilistic case is used to reinforce the assumptions of the deterministic case to confirm the precision of the estimate with respect to safety factors.

A.10 Figures

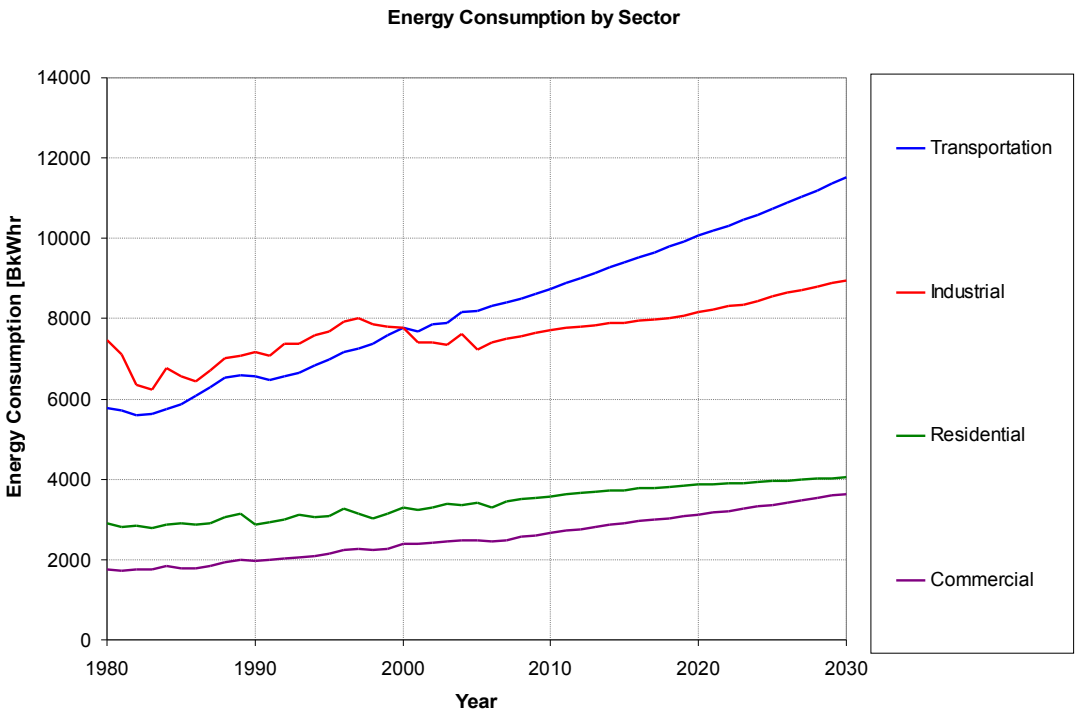

(Information from [1])

Figure A-1 - Energy Consumption by Sector

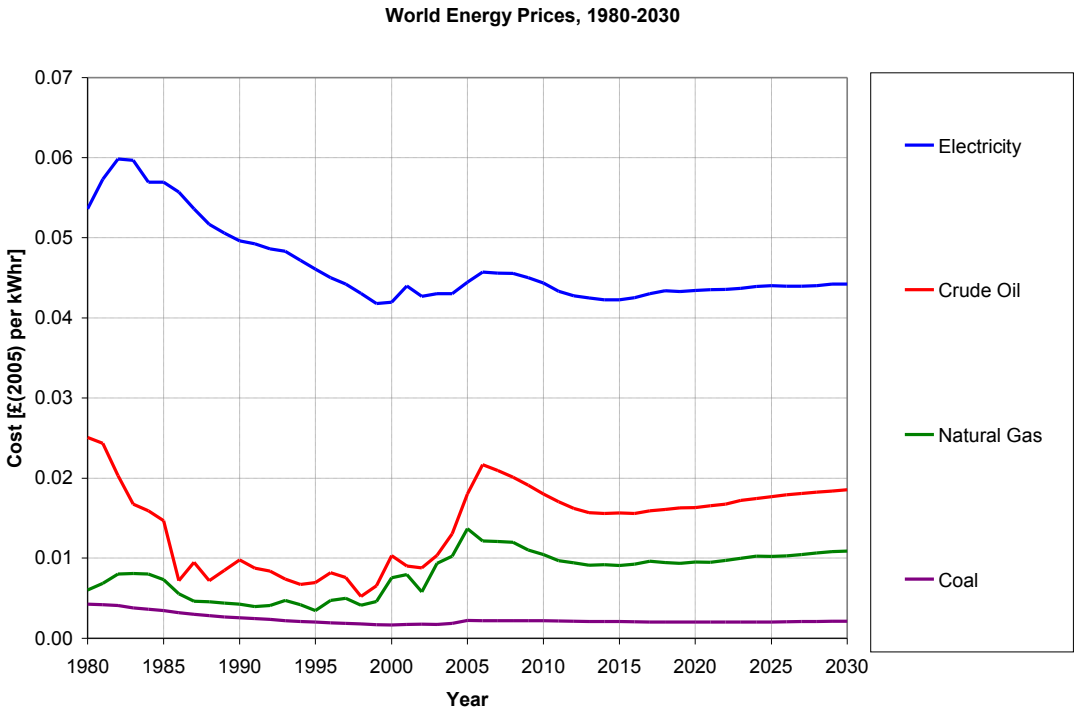

(Information from [1])

Figure A-2 - World Energy Prices, 1980-2030

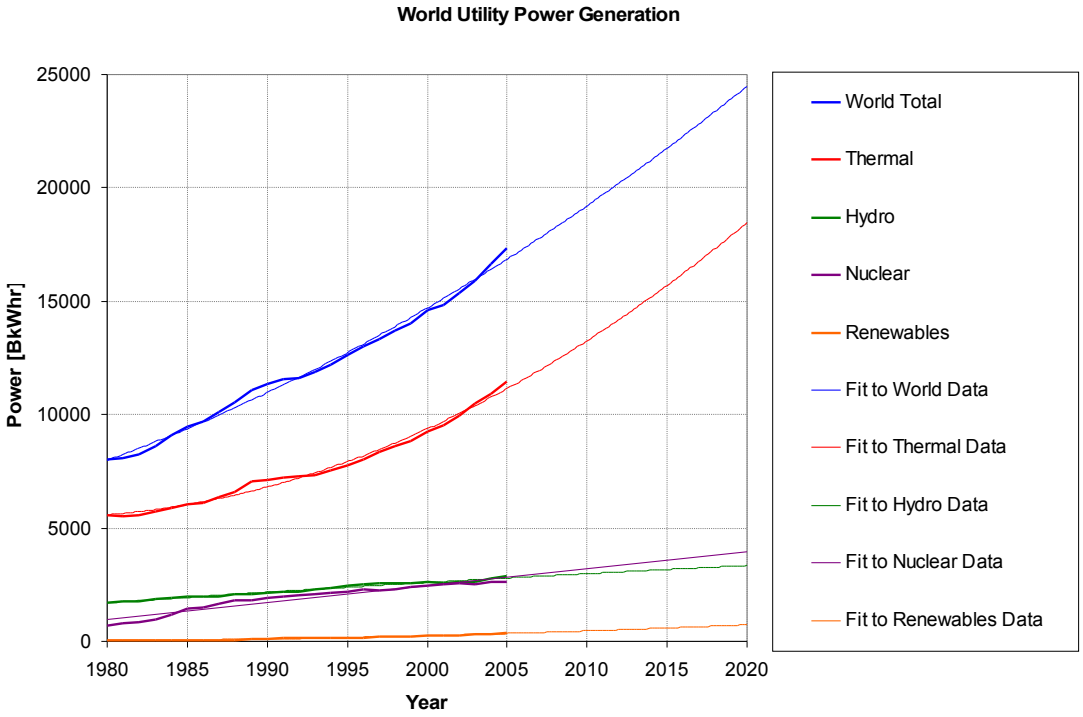

(Information from [2])

Figure A-3 - World Utility Power Generation

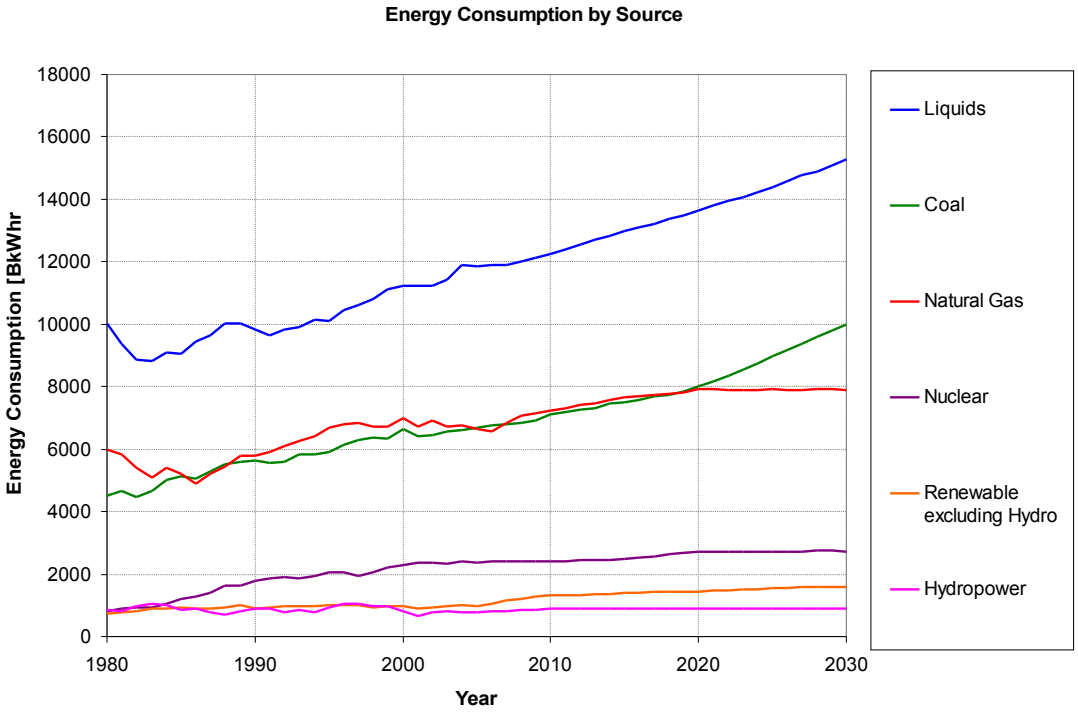

(Information from [1])

Figure A-4 - Energy Consumption by Source

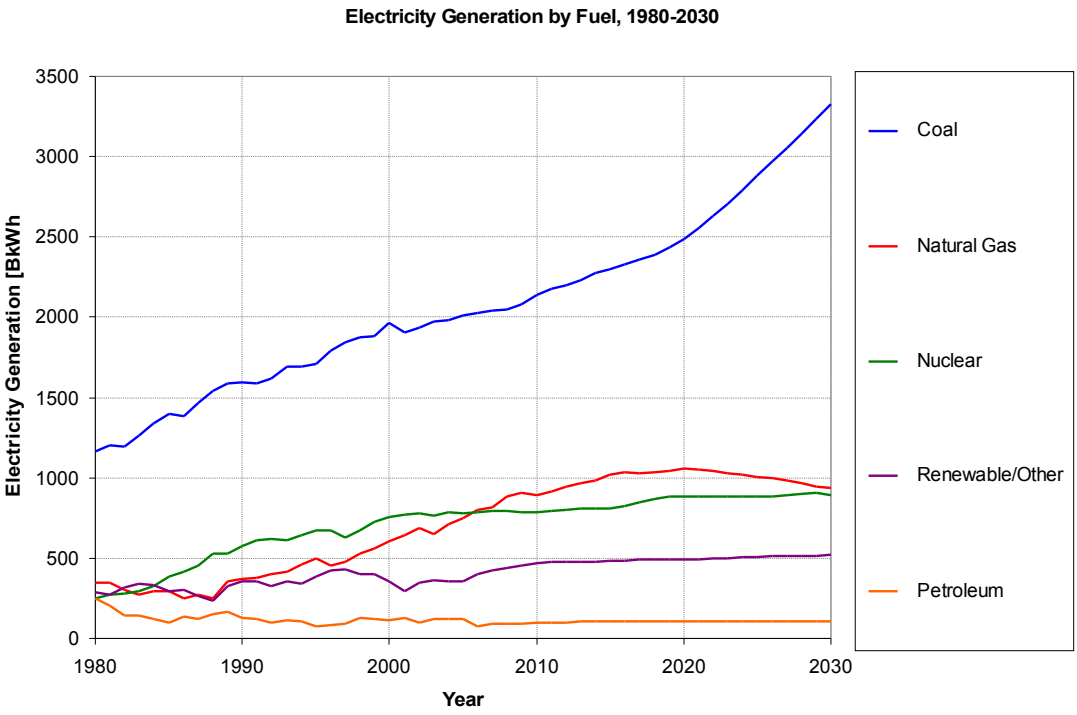

(information from [1])

Figure A-5 - Electricity Generation by Fuel, 1980-2030

(south pole station not shown, taken from [52])

Figure A-6 - Location of atmospheric CO_2 monitoring stations

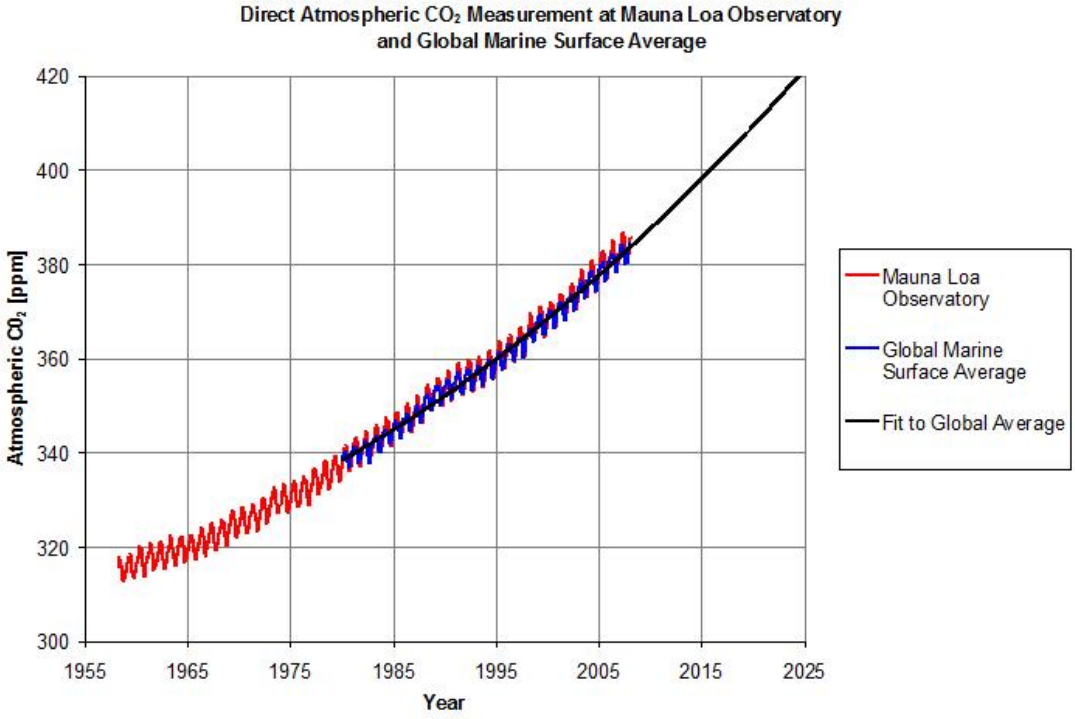

Figure A-7 - Direct Atmospheric CO_2 Measurement

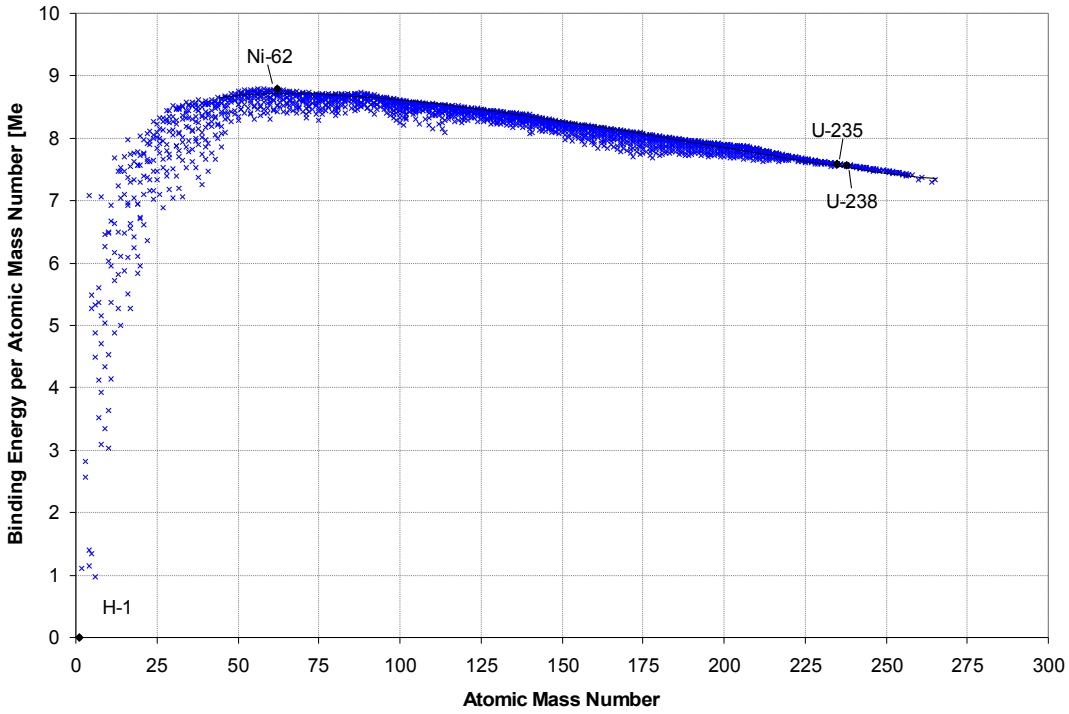

Figure A-8 - Binding Energy of Atomic Nuclei

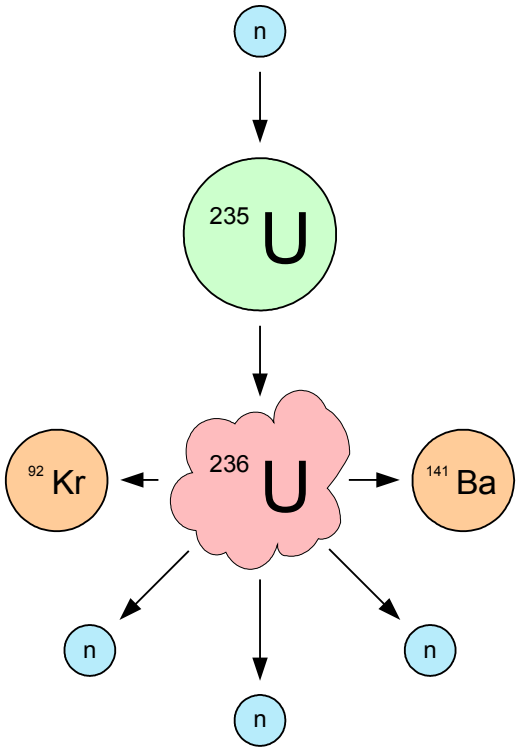

Figure A-9 - Typical Reaction Products from the Fission of a U_{235} Nucleus

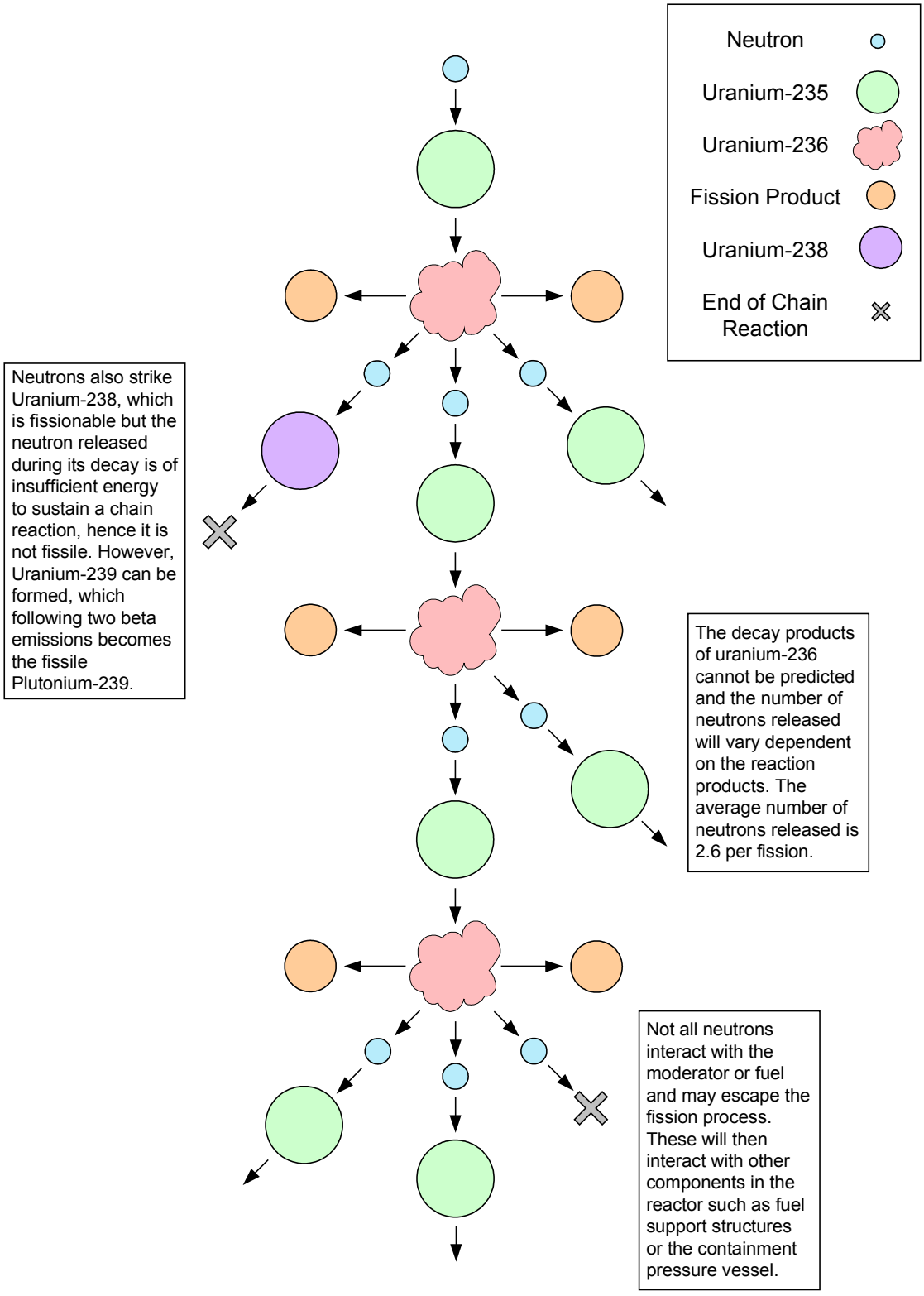

Figure A-10 - Fission Chain Reaction of U_{235}

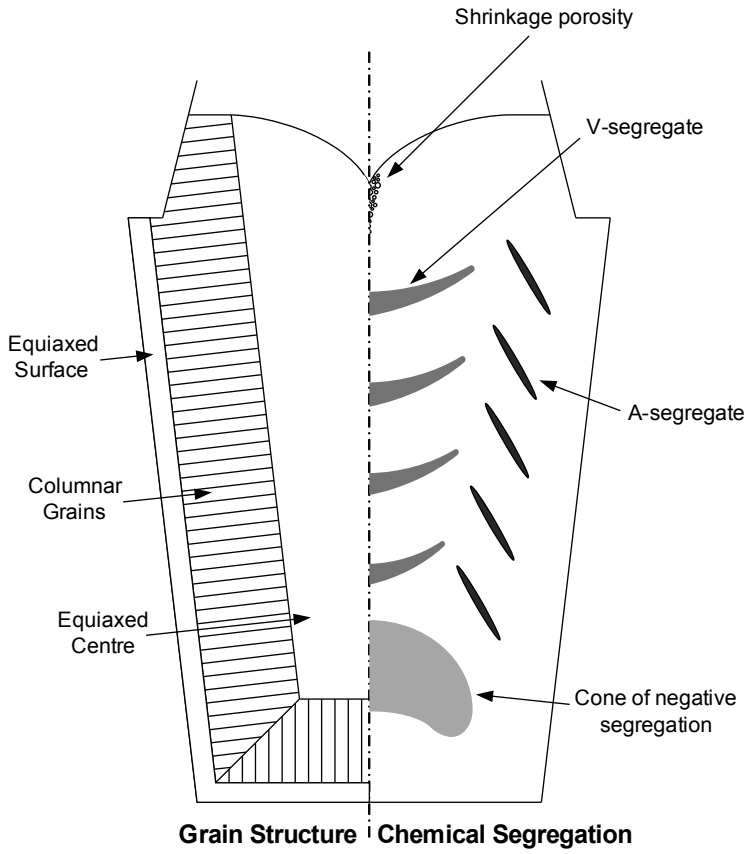

Figure A-11 - General Structure of an As-Cast ingot

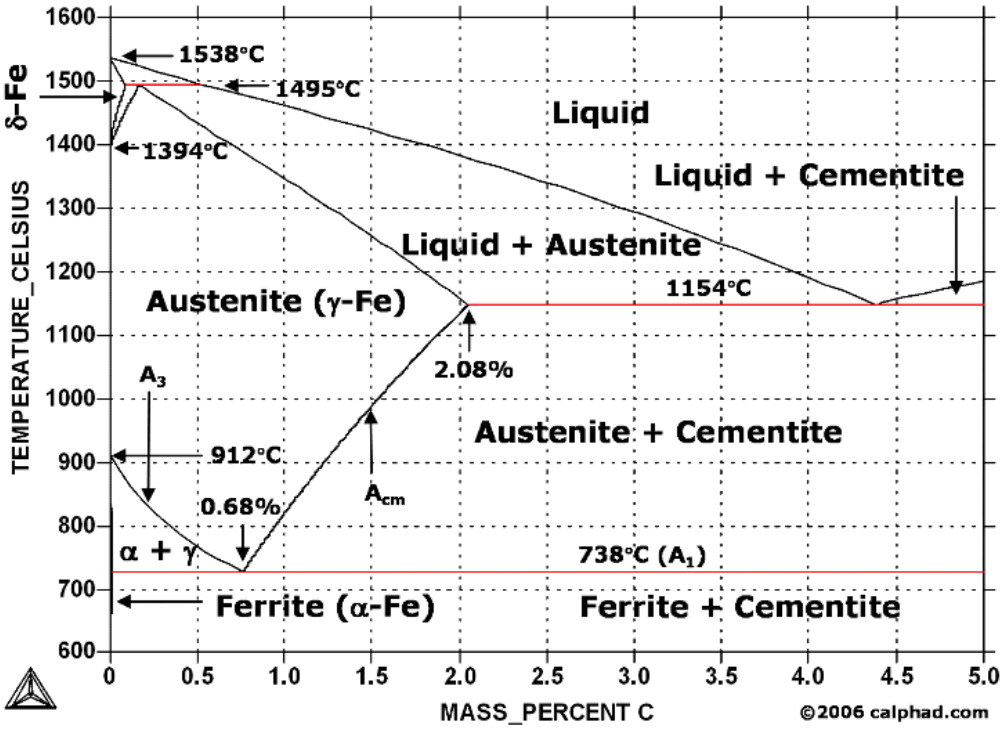

Figure A-12 - Iron-Carbon Phase Diagram

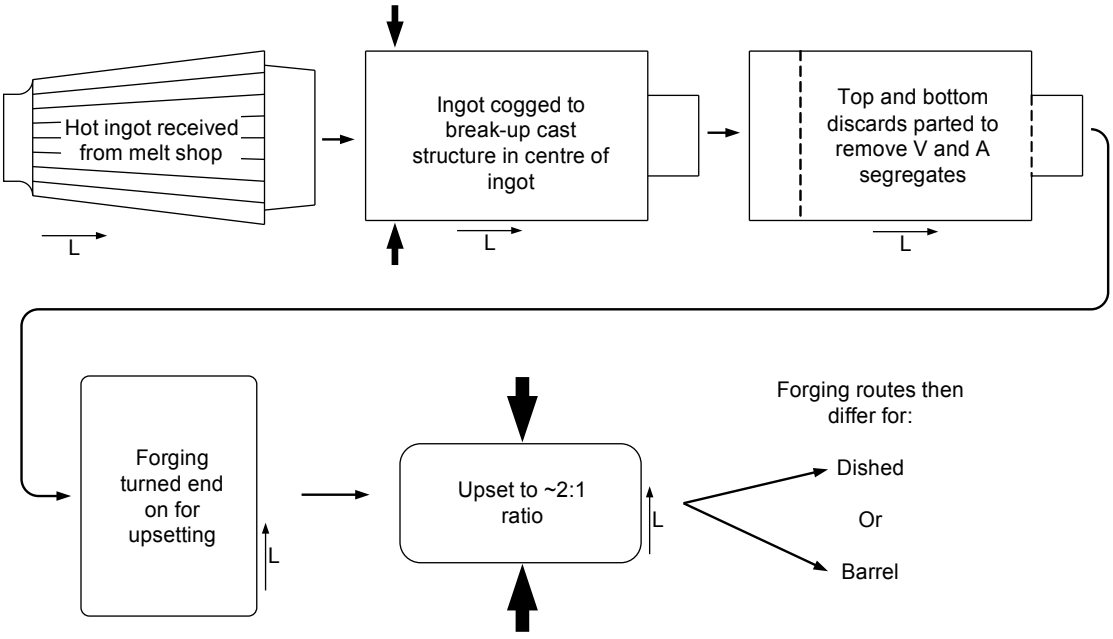

Figure A-13 - Initial forging route for high integrity forgings

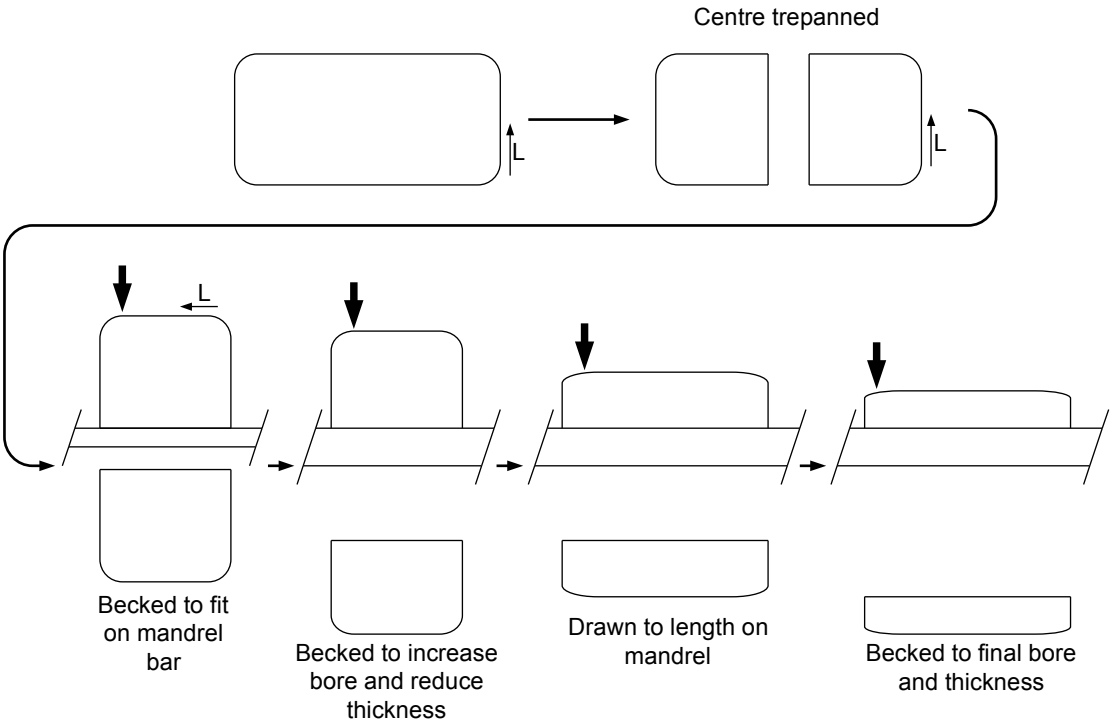

Figure A-14 - Barrel forging procedure schematic

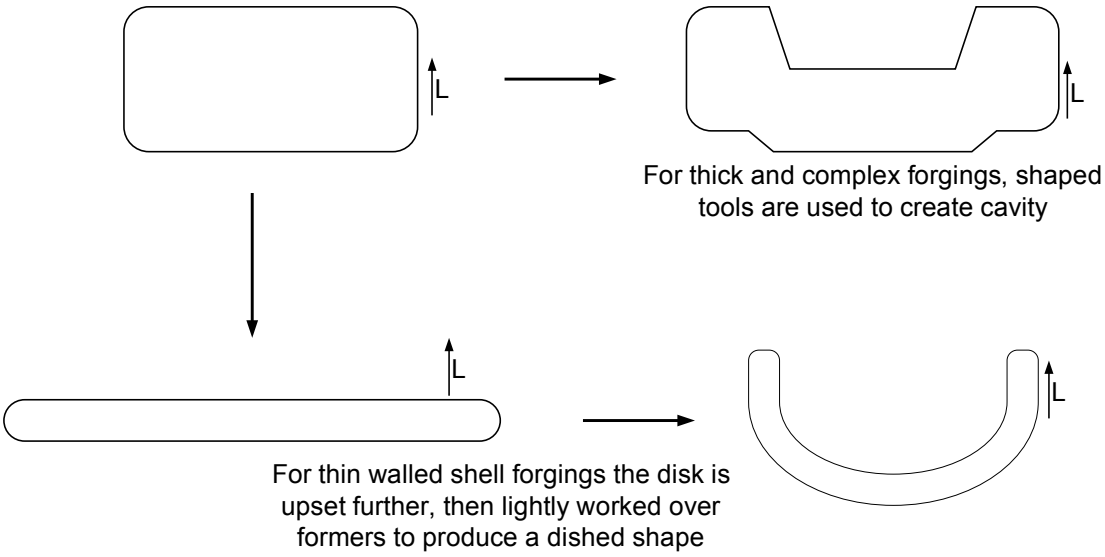

Figure A-15 - Domed and shell forging process schematic

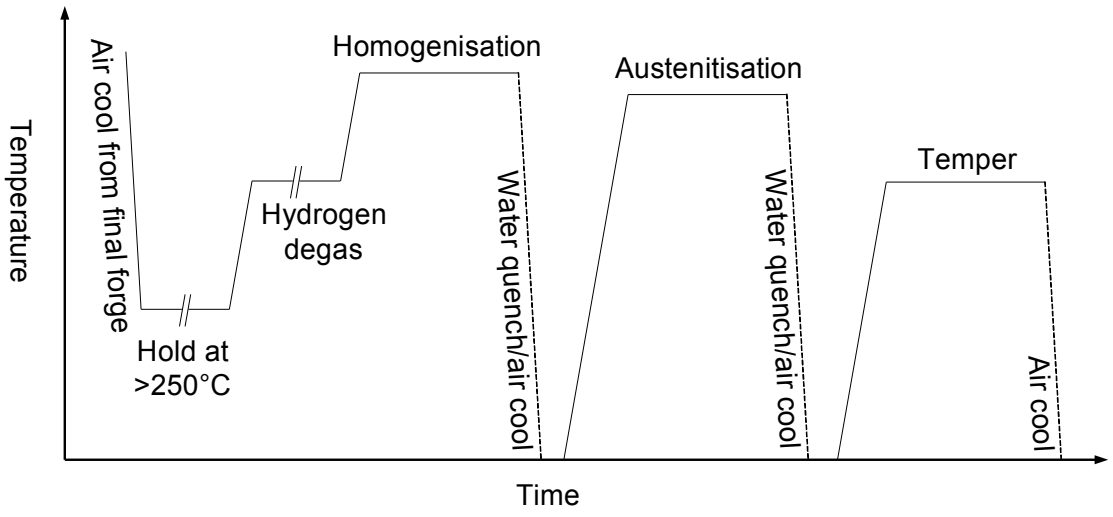

Figure A-16 - Primary heat treatment profile

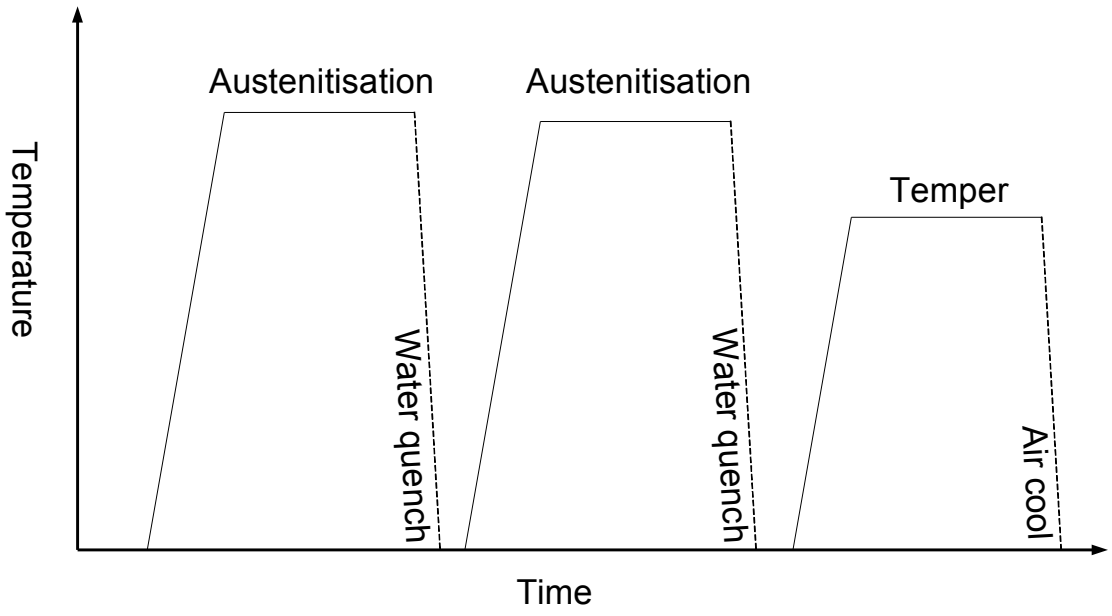

Figure A-17 - Quality heat treatment profile

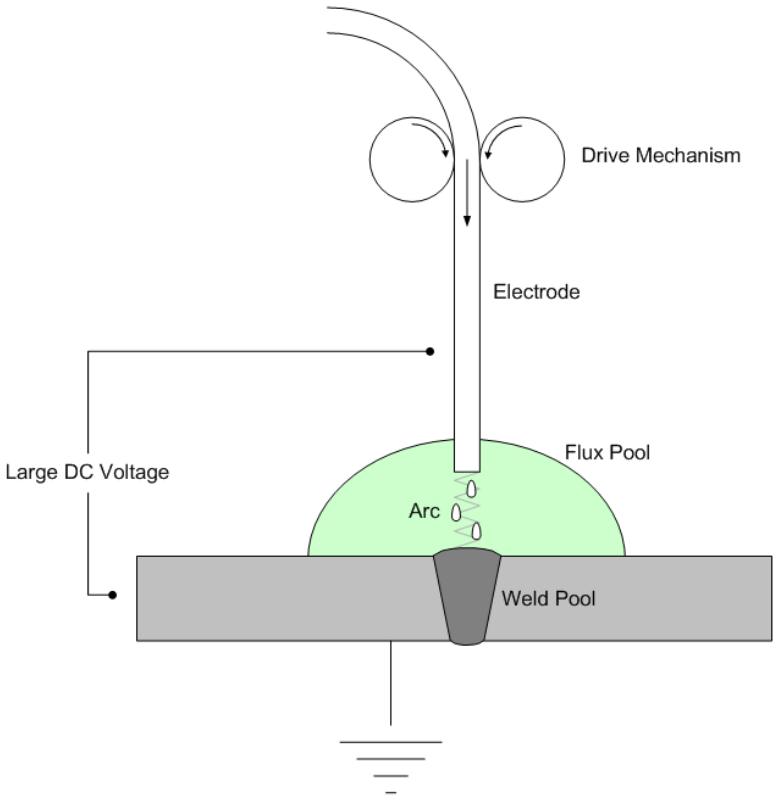

Figure A-18 - Submerged Arc Welding Schematic

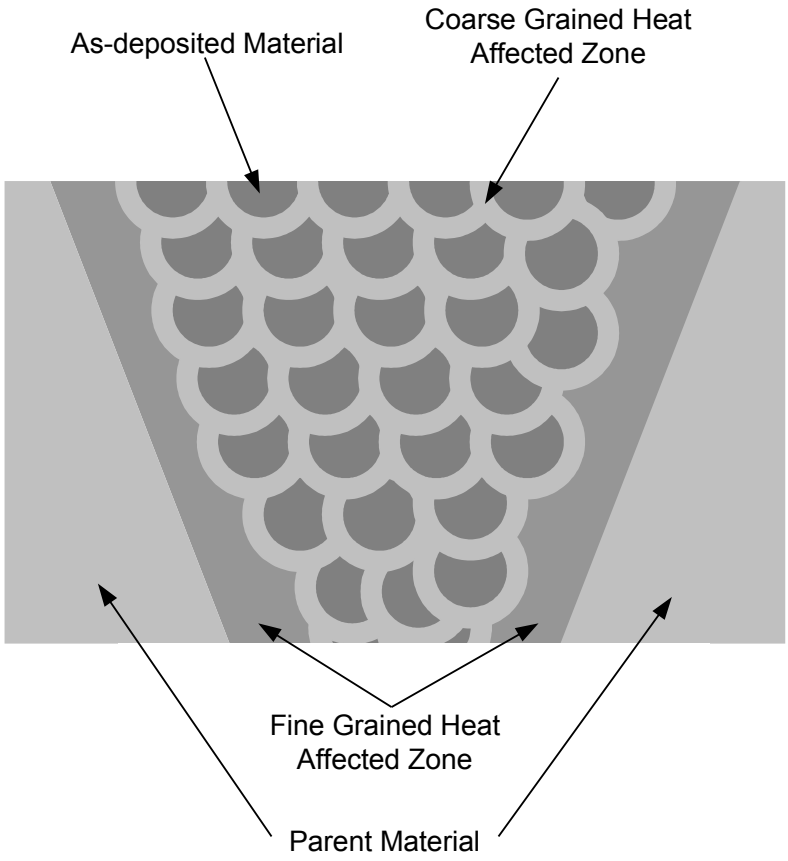

Figure A-19 - Multi-pass Weld Structure

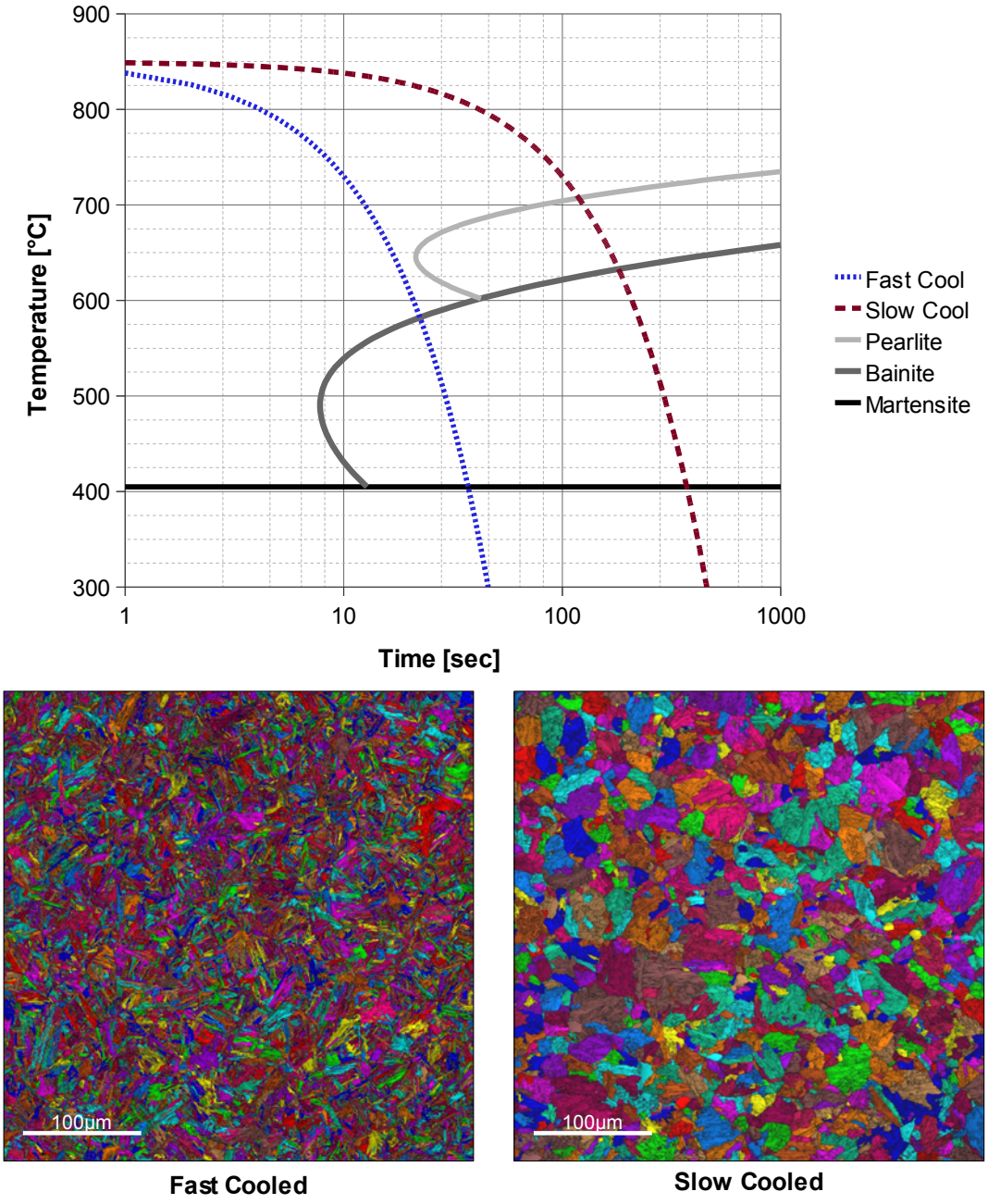

Figure A-20 - Typical TTT Curve for ASTM A508-3 Material and Resultant Microstructure for Fast and Slow Cooling Rates

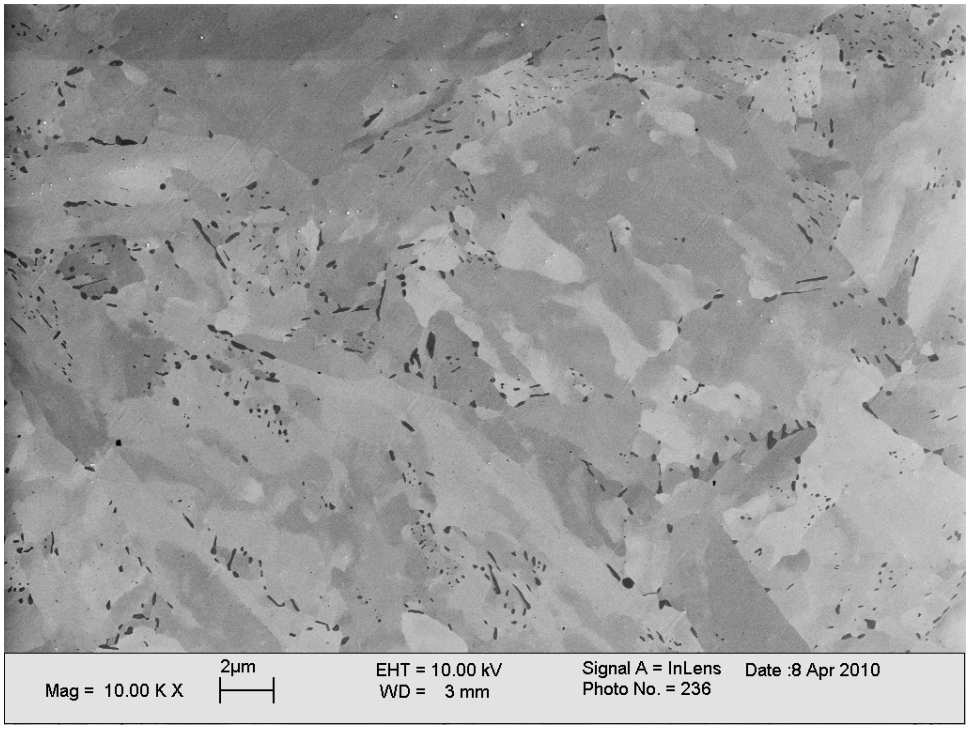

Figure A-21 - Variety of Carbides in Tempered ASTM A508-3 Material

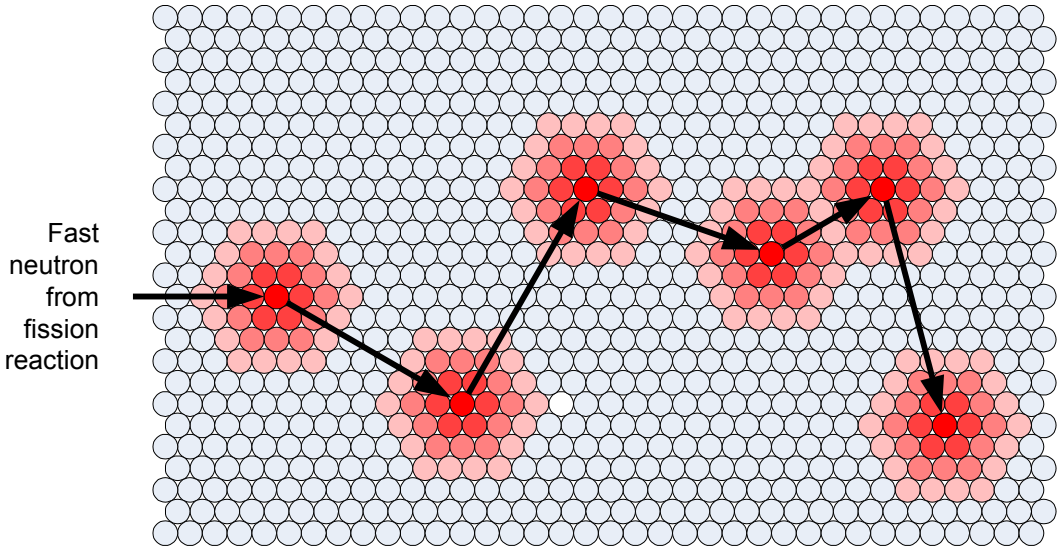

The fast neutron from the fission reaction collides with an atom of the crystal structure, knocking the atom from position and releasing some of the kinetic energy as heat. The primary knock-on atom then collides with the structure knocking another atom from position, and so on, causing a cascade until all the available kinetic energy is captured.

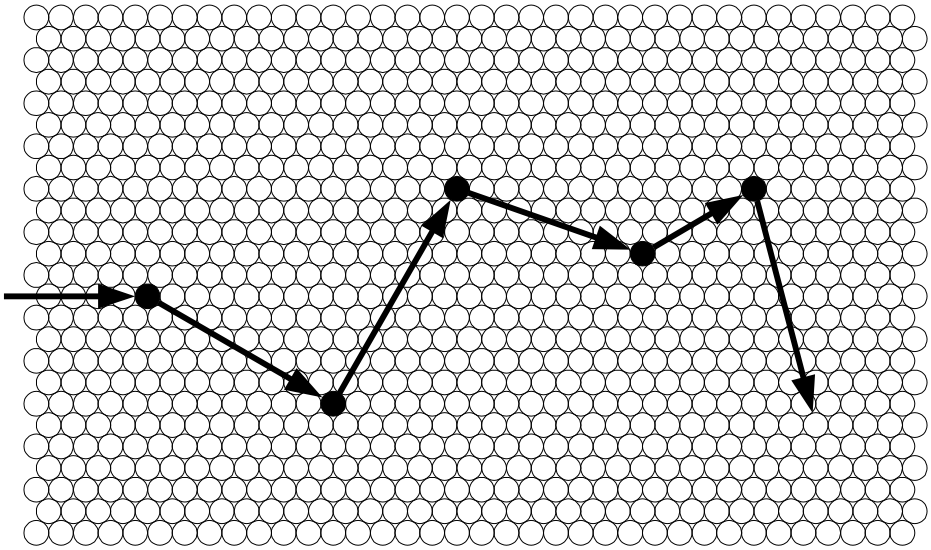

The resulting structure will contain a number of point defects where the atoms involved in the cascade have been knocked from position. This creates a number of small stress fields in the structure.

Figure A-22 - Fast Neutron Interaction with Solid Materials

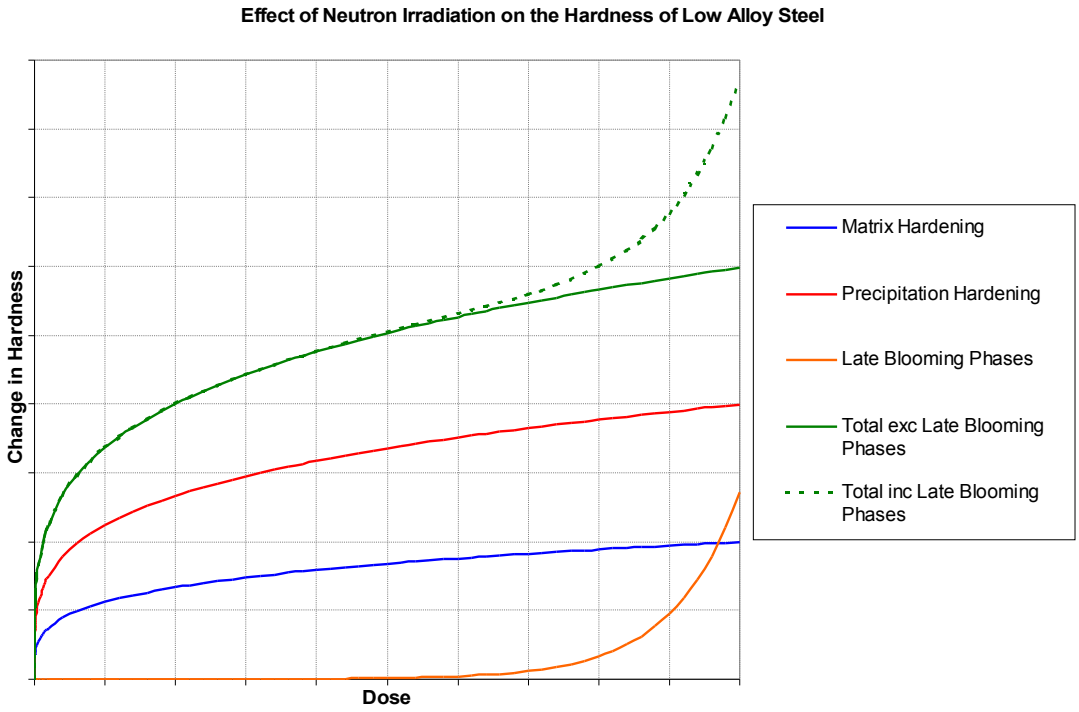

Figure A-23 - Effect of Neutron Irradiation on the Hardness of Low Alloy Steel

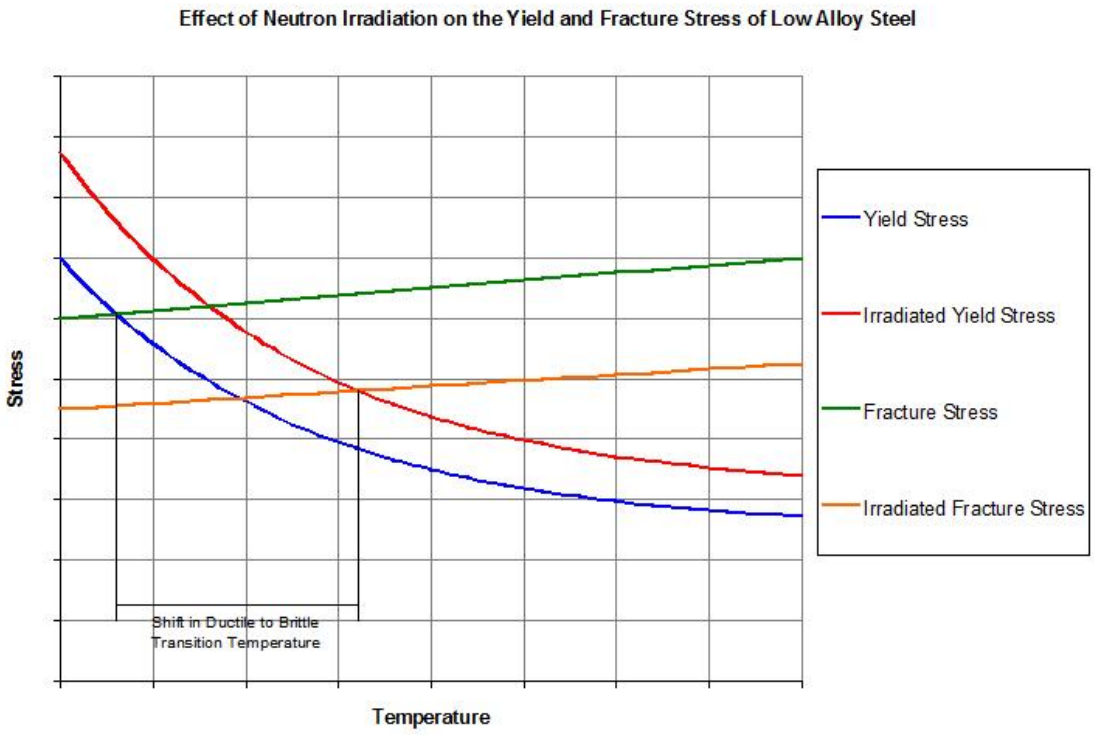

Figure A-24 - Effect of Neutron Irradiation on the Yield and Fracture Stress of low Alloy Steel

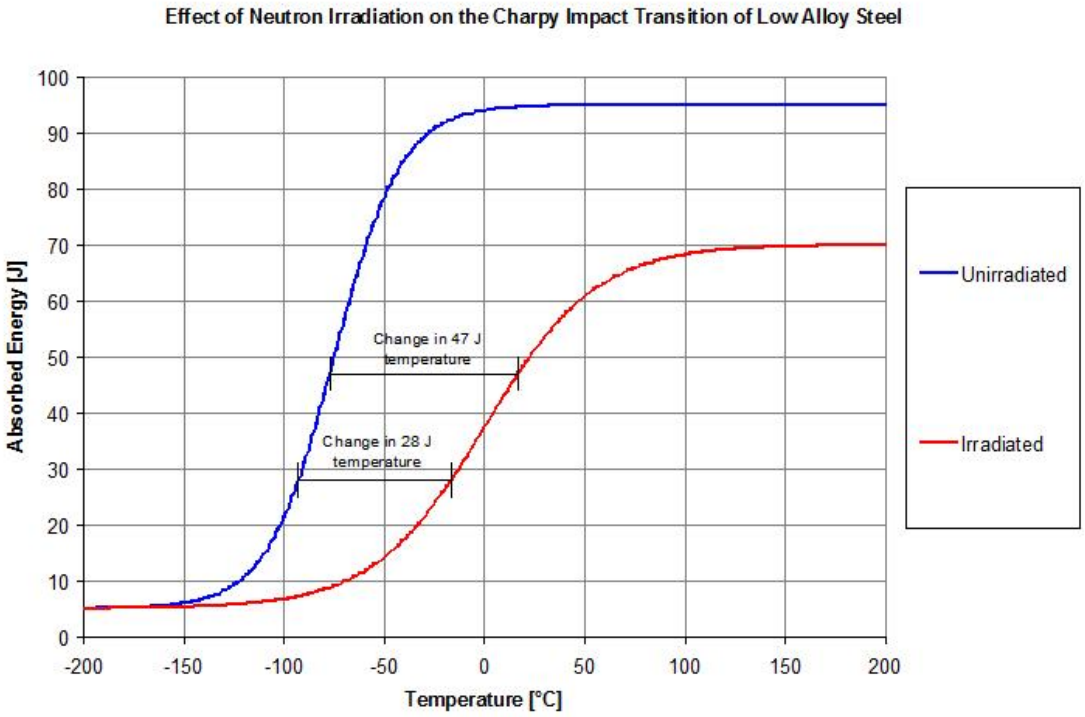

Figure A-25 - Effect of Neutron Irradiation on the Charpy Impact Transition of Low Alloy Steel

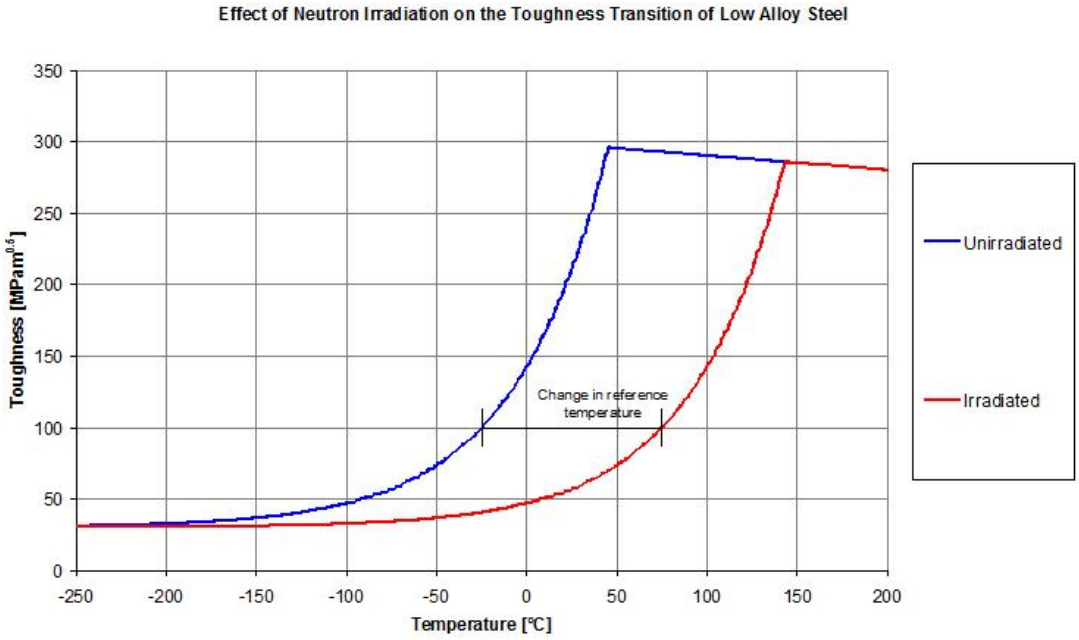

Figure A-26 - Effect of Neutron Irradiation on the Toughness Transition of Low Alloy Steel

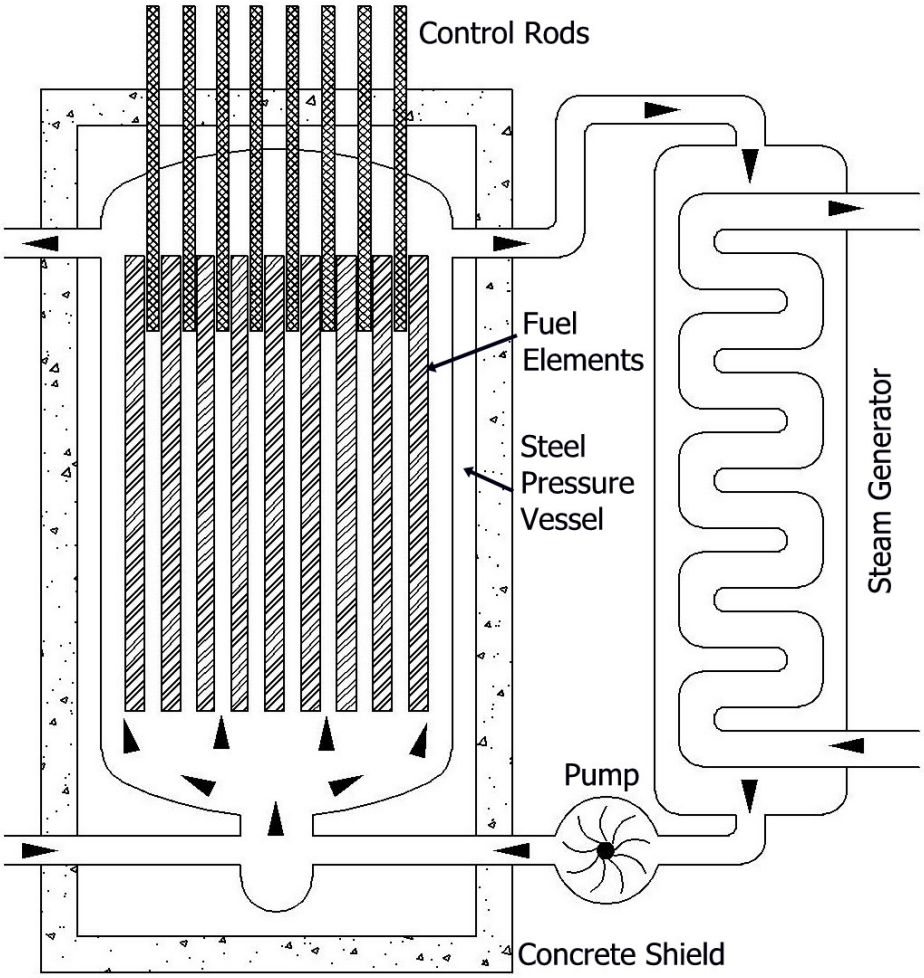

Figure A-27 - Magnox Reactor Schematic

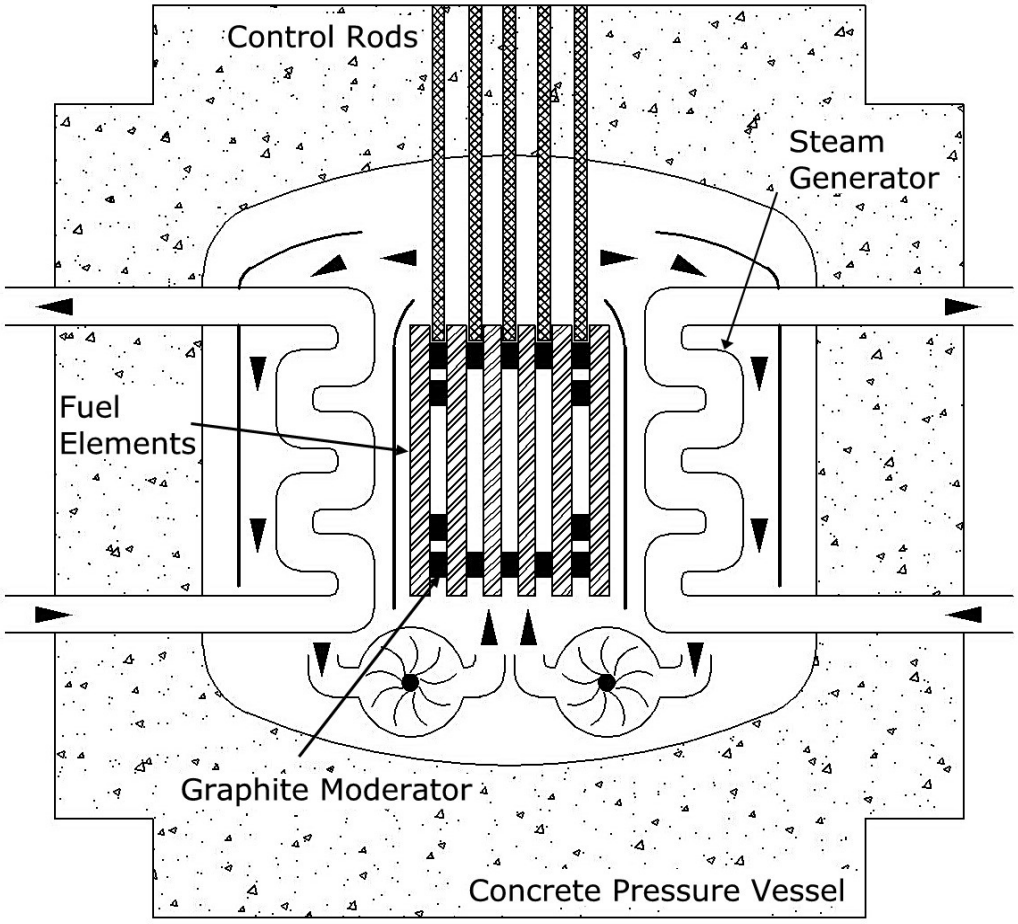

Figure A-28 - Advanced Gas Cooled Reactor (AGR) Schematic

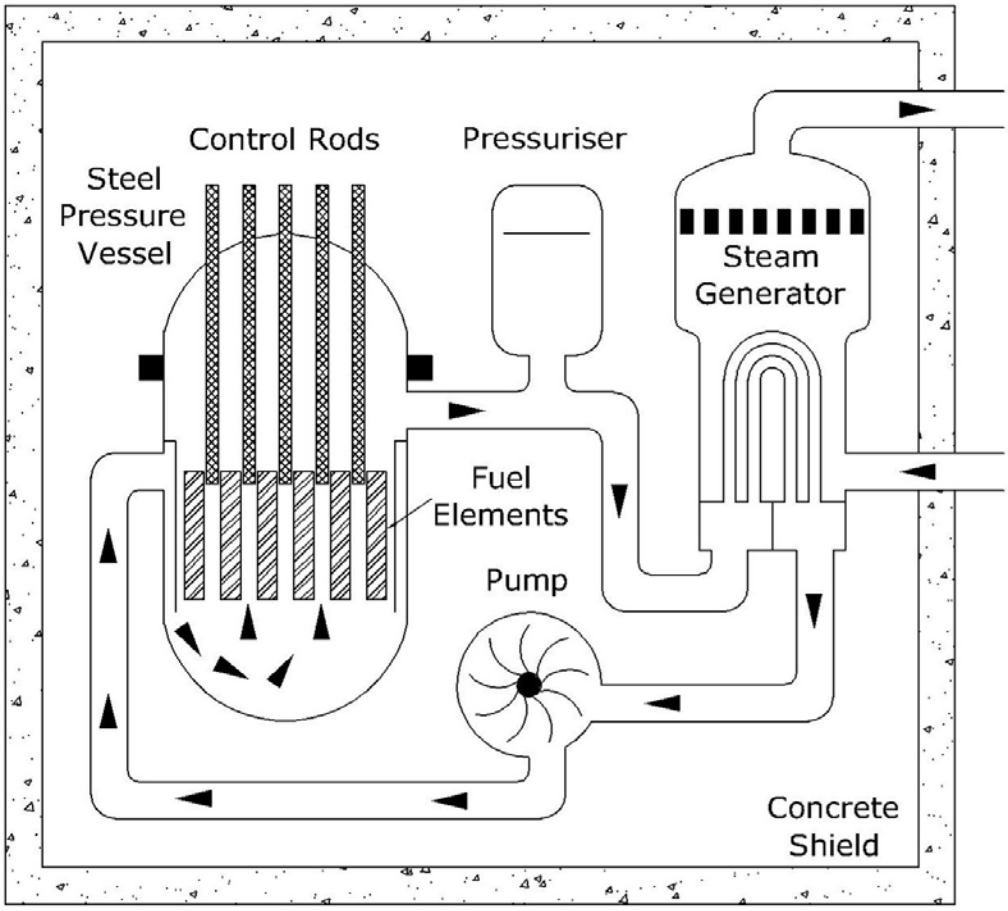

Figure A-29 - Pressurised Water Reactor (PWR) Schematic

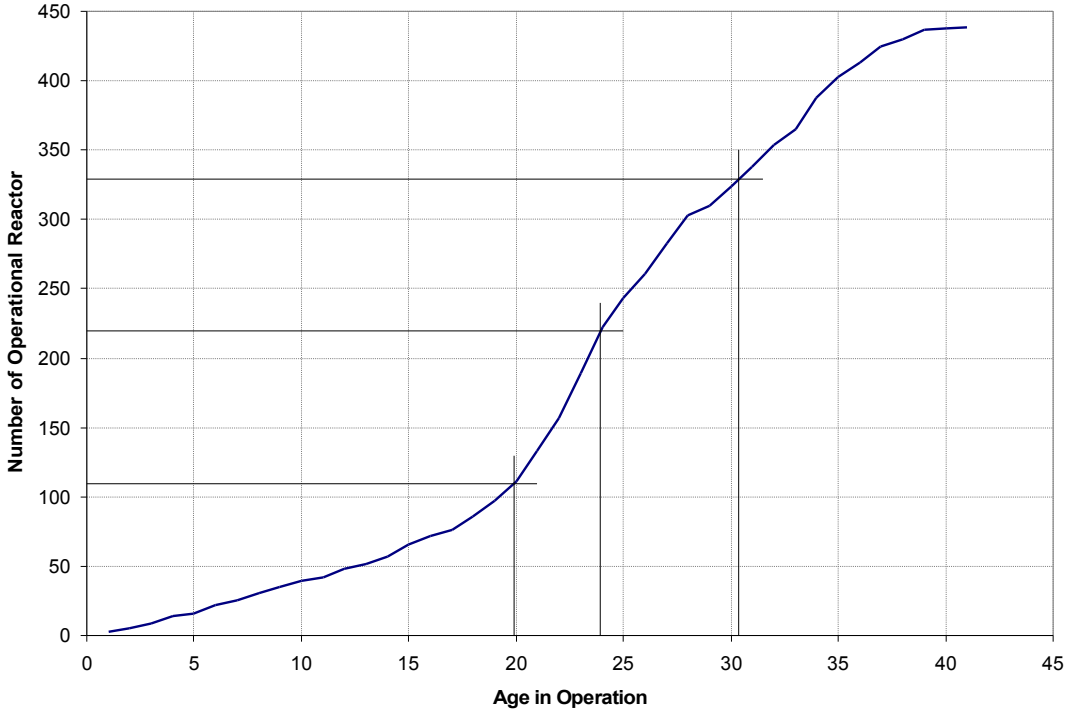

Figure A-30 - Age in Operation of World Utility Nuclear Power Reactors

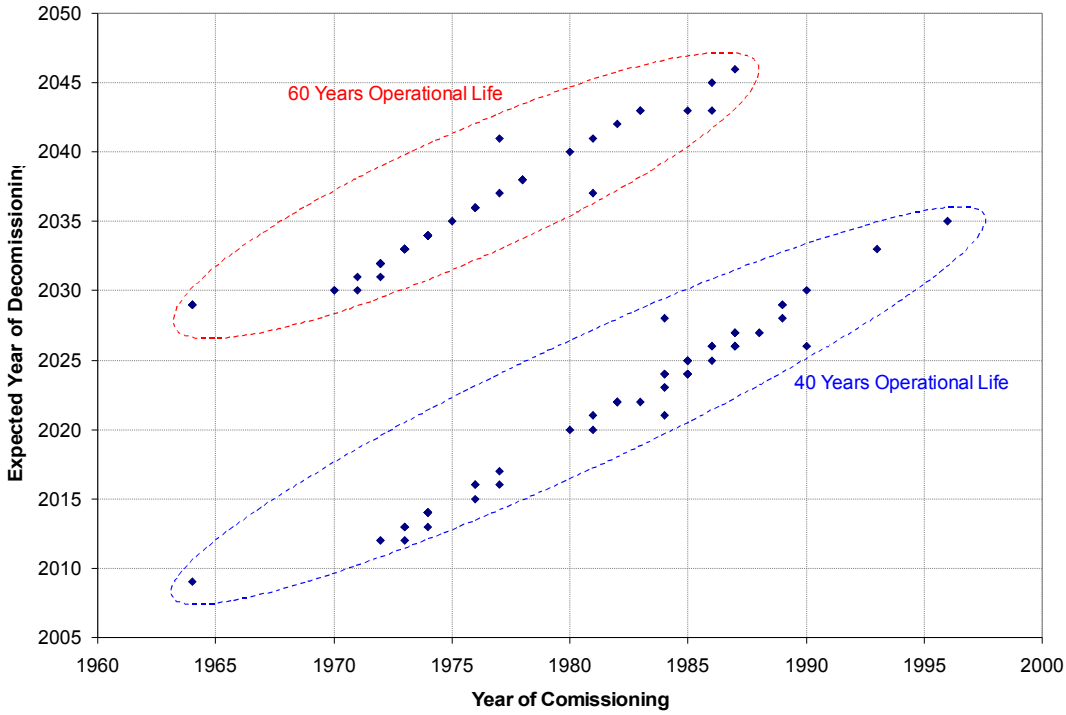

Figure A-31 - Expected Operational Life of USA Utility Nuclear Power Reactors

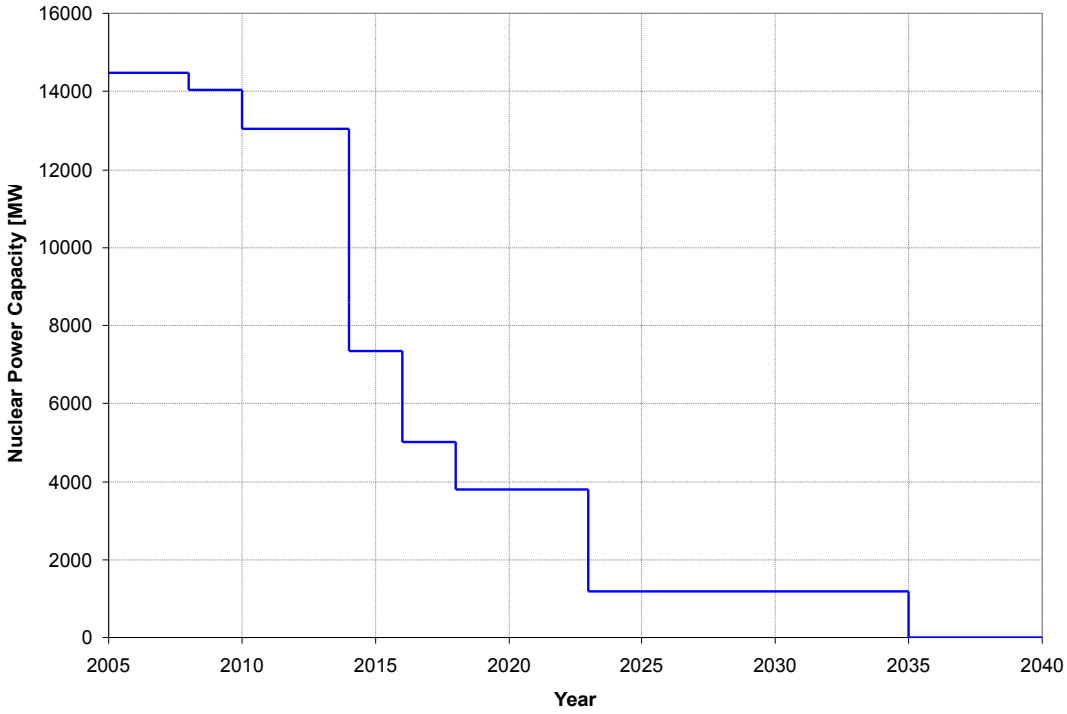

Figure A-32 - UK Nuclear Power Generating Capacity of Current Plants, 2005-2040

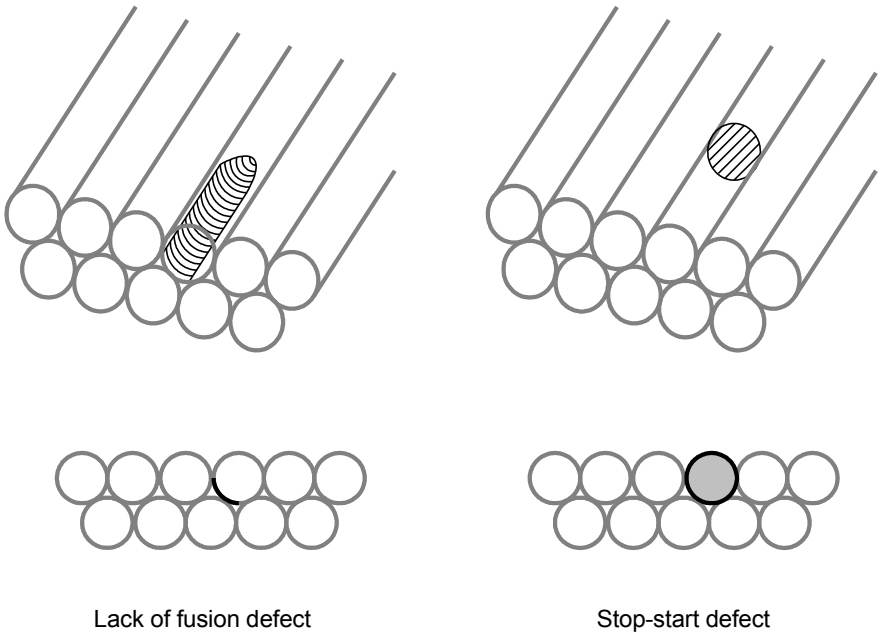

Figure A-33 - Weld Defects

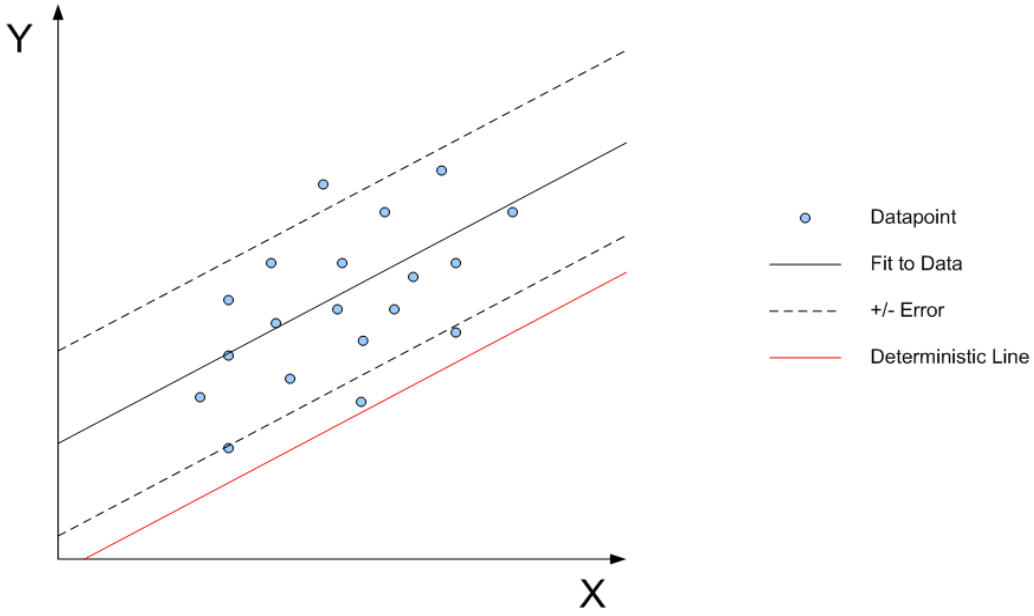

Figure A-34 - Deterministic Assessment of Data

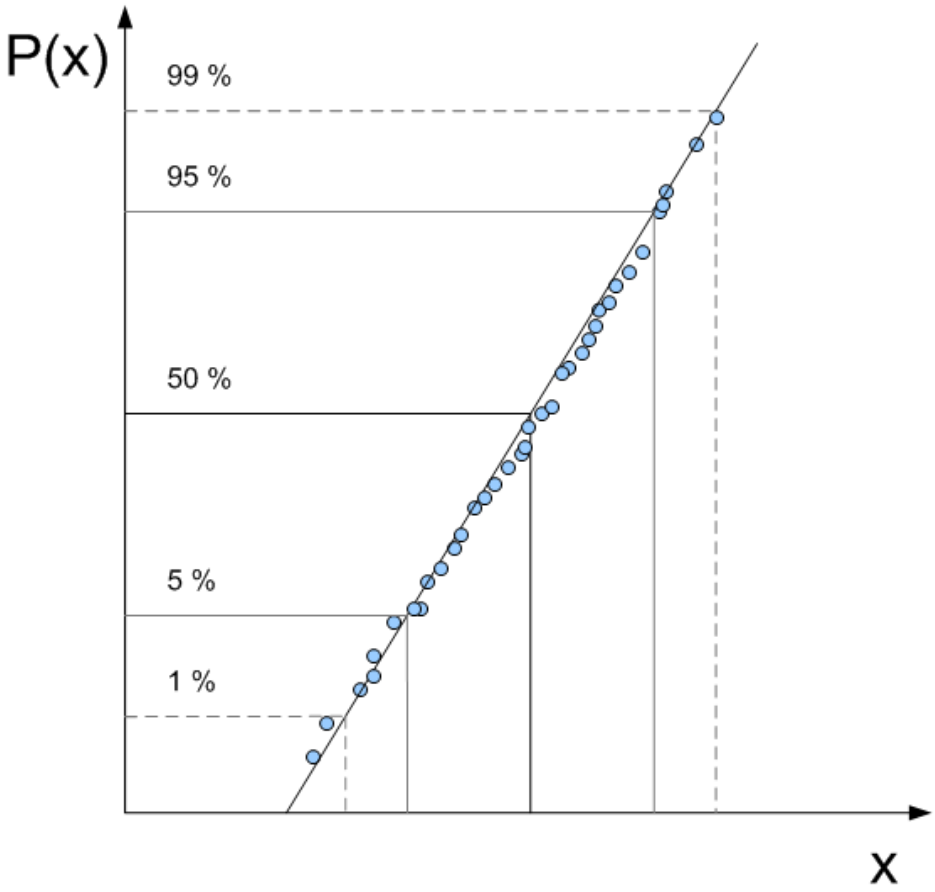

Figure A-35 - Probability Plot of Variable x

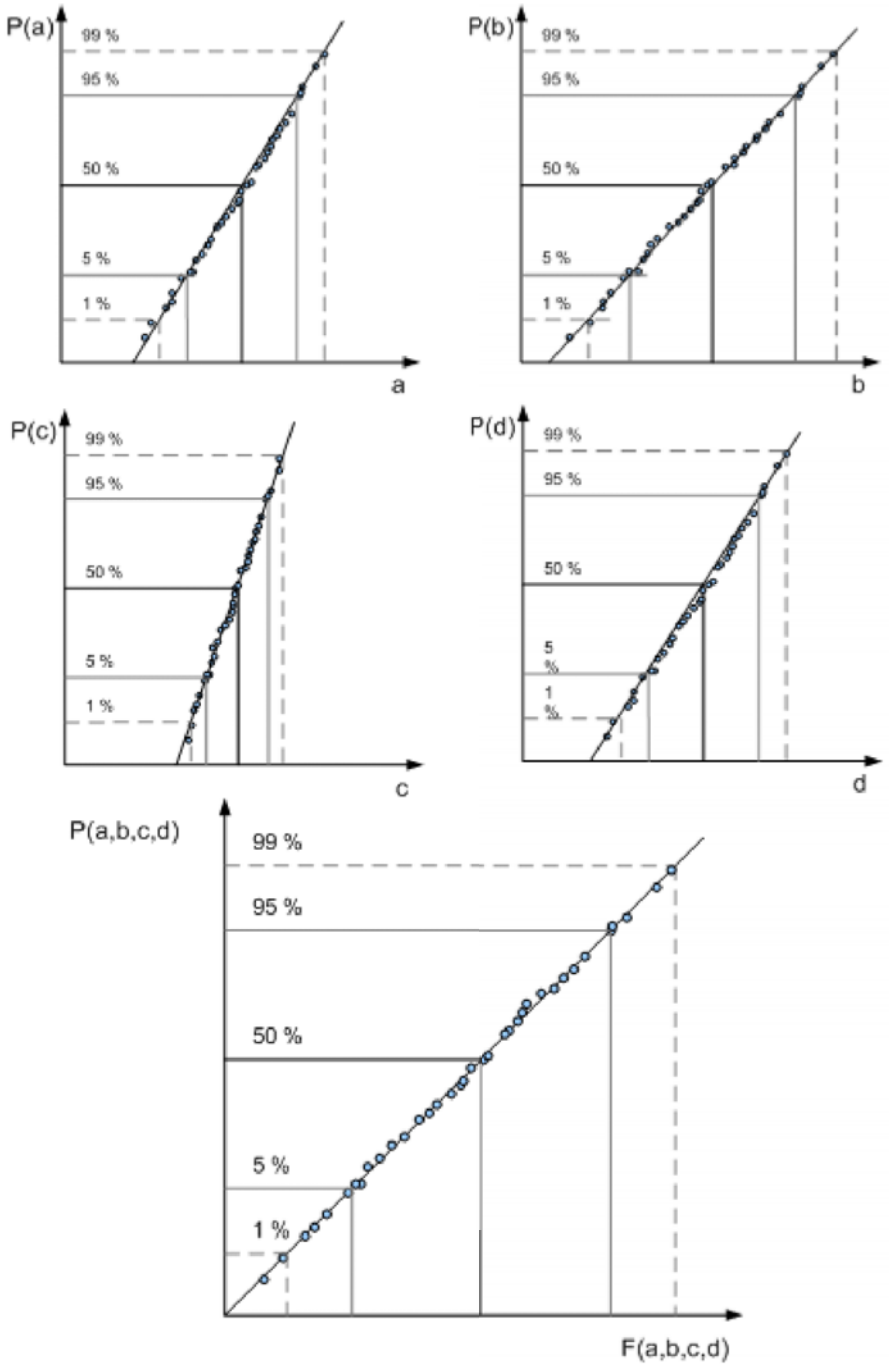

Figure A-36 - Combination of Probability Distributions

A.11 References

1. *Annual Energy Outlook 2007 with Projections to 2030 DOE/EIA-0383(2007)*. 2007.
2. *International Energy Annual 2005*. 2005, Energy Information Administration.
3. Conway, T.J., P. P. Tans, L. S. Waterman, K. W. Thoning, D. R. Kitzis, K. A. Masarie, and N. Zhang *Evidence for interannual variability of the carbon cycle from the National Oceanic and Atmospheric Administration/Climate Monitoring and Diagnostics Laboratory Global Air Sampling Network.* J. Geophys. Res., 1994. **99(D11)**(22): p. 831–22,855.
4. Tans, D.P., *www.esrl.noaa.gov/gmd/ccgg/trends*, NOAA/ESRL.
5. Gribbin, J., *Q is for Quantum - Particle Physics from A to Z*. 1998: Weidenfeld & Nicolson.
6. *Binding Energy of Common Nuclei,* http://www.einstein-online.info/en/spotlights/binding_energy/binding_energy/index.txt.
7. Einstein, A., *Ist die Trägheit eines Körpers von seinem Energieinhalt abhängig? (In German).* Annalen der Physik, 1905(18): p. 639–643.
8. Becquerel, H., *Sur les radiations émises par phosphorescence.* Comptes Rendus Hebdomadaires Des Séances De L'Académie Des Sciences, 1896(122): p. 420-421.
9. Törnebladh, H.R., *The Nobel Prize in Physics 1903 Presentation Speech, Nobel Lectures, Physics 1901-1921*. 1967, Amsterdam: Elsevier Publishing company.
10. Klaproth, M.H., *Chemische Untersuchung des Uranits, einer neuentdeckten metallischen Substanz.* Chemische Annalen, 1789. **2**: p. 387-403.
11. Meitner, L. and O.R. Frisch, *Disintegration of Uranium by Neutrons: a New Type of Nuclear Reaction.* Nature, 1939. **143**(3615): p. 239-240.
12. Hahn, O. and F. Strassmann, *Über den Nachweis und das Verhalten der bei der Bestrahlung des Urans mittels Neutronen entstehenden Erdalkalimetalle (in German).* Naturwissenschaften, 1939. **27**(1): p. 11-15.
13. Anderson, H.L., et al., *The Fission of Uranium.* Phys. Rev., 1939. **55**(5): p. 511-512.
14. Szilárd, L., *Improvements in or relating to the transmutation of chemical elements GB630762*. 1934: British.
15. Anderson, H.L., E. Fermi, and L. Szilárd, *Neutron production and absorption in uranium.* The Physical Review, 1939. **56**: p. 284-286.
16. Fermi, E. *The Development of the First Chain Reacting Pile*. in *Symposium on Atomic Energy and Its Implications*. 1946.
17. Einstein, A. *Einstein's Letter to President Roosevelt*. 1939; Available from: http://www.atomicarchive.com/Docs/Begin/Einstein.shtml.
18. ASME, *SA508 - SPECIFICATION FOR QUENCHED AND TEMPERED VACUUM-TREATED CARBON AND ALLOY STEEL FORGINGS FOR PRESSURE VESSELS*, in *Section II A - Ferrous Material Specifications*. 2000, ASME: Boiler and Pressure Vessel Code.
19. Cottrell, A., *An Introduction to Metallurgy: Second edition*. 1995: The Institute of Materials.
20. Askeland, D.R., *The Science and Engineering of Materials: Third S.I. Edition*. 1996: Nelson Thornes.
21. Bhadeshia, H.K.D.H., ed. *Bainite in Steels: Transformations, Microstructure and Properties*. 2001, IOM Communications.
22. McLean, D., *Mechanical Properties of Metals*. 1962: John Wiley & Sons.

23. Jack, D.H. and K.H. Jack, *Invited Review: Carbides and Nitrides in Steel.* Materials Science and Engineering, 1973. **11**: p. 1-27.
24. Flewitt, P.E.J., *The use of multiscale materials modelling within the UK nuclear industry.* Materials Science and Engineering A, 2004. **365**(1-2): p. 257-266.
25. Odette, G.R., et al., *Cleavage fracture and irradiation embrittlement of fusion reactor alloys: mechanisms, multiscale models, toughness measurements and implications to structural integrity assessment.* Journal of Nuclear Materials, 2003. **323**(2-3): p. 313-340.
26. Odette, G.R., et al., *Nuclear Reactors: Pressure Vessel Steels*, in *Encyclopedia of Materials: Science and Technology*. 2001, Elsevier: Oxford. p. 6369-6376.
27. Little, E.A., *Development of radiation resistant materials for advanced nuclear power plant.* Materials Science and Technology, 2006. **22**(5): p. 491-518.
28. Gurovich, B.A., et al., *Intergranular and intragranular phosphorus segregation in Russian pressure vessel steels due to neutron irradiation.* Journal of Nuclear Materials, 2000. **279**(2-3): p. 259-272.
29. Margolin, B.Z., V.A. Shvetsova, and A.G. Gulenko, *Radiation embrittlement modelling for reactor pressure vessel steels: I. Brittle fracture toughness prediction.* International Journal of Pressure Vessels and Piping, 1999. **76**(10): p. 715-729.
30. Rice, J.R. and J.-S. Wang, *Embrittlement of interfaces by solute segregation.* Materials Science and Engineering: A, 1989. **107**: p. 23-40.
31. Song, S.H., et al., *Dependence of ductile-to-brittle transition temperature on phosphorus grain boundary segregation for a 2.25Cr1Mo steel.* Materials Science and Engineering: A, 2008. **486**(1-2): p. 433-438.
32. Odette, G.R. *Radiation induced microstructural evolution in reactor pressure vessel steels*. in *Materials Research Symposium*. 1995.
33. Lambourne, A., D. Ellis, and T.J. Williams. *Rolls-Royce evidence of late blooming phases*. in *IGRDM 13*. 2006. Tsukuba.
34. Odette, G.R., et al. *Precipitation in Neutron Irradiated Copper-Free RPV Steels*. in *TMS*. 2005. San Francisco.
35. *ASTM E23-07 Standard Test Methods for Notched Bar Impact Testing of Metallic Materials*. 2007, West Conshohocken: ASTM International.
36. McCabe, D.E., J.G. Merkle, and K. Wallin, *An introduction to the development and use of the Master Curve method*. 2005, West Conshohocken: ASTM International.
37. *ASTM E1921-05 Standard Test Method for Determination of Reference Temperature, T_0, for Ferritic Steels in the Transition Range*. 2005, West Conshohocken: ASTM International.
38. Macaulay, D., *The Way Things Work*. 1993, London: Dorling Kindersley.
39. *International Atomic Energy Authority Utility reactor Database* http://www.iaea.org/cgi-bin/db.page.pl/pris.reaopag.htm.
40. *BBC On This Day 17 October - 1956:Queen switches on nuclear power*. Available from: http://news.bbc.co.uk/onthisday/hi/dates/stories/october/17/newsid_3147000/3147145.stm.
41. *Report by HM Nuclear Installations Inspectorate on the results of Magnox Long Term Safety Reviews (LTSRs) and Periodic Safety Reviews (PSRs)*, H.a.S. Executive, Editor. 2000.
42. *U.S. Nuclear Regulatory Commission (NRC) 2007 - 2008 Information Digest (NUREG - 1350 volume 19)*, O.o.t.C.F. Officer, Editor. 2007, U.S. Nuclear Regulatory Commission.

43. *Nuclear Industry Association, Industry Information, UK Nuclear Statistics*. 2009; Available from: http://www.niauk.org/uk-nuclear-statistics.html.
44. *Metalworking: Bulk Forming*. ASM Handbook. Vol. 14A. 2005: ASM International.
45. Anderson, T.L., *Fracture Mechanics; Fundamentals and Applications*. 2005: Taylor & Francis.
46. Rossmanith, H.P. *George Rankin Irwin - The Father of Fracture Mechanics*. in *George R. Irwin Symposium on Cleavage Fracture*. 1997. Idianapolis, Indianna.
47. Fenner, R.T., *Finite Element Methods for Engineers*. 2005, London: imperial College Press.
48. Johnson, H.H. and P.C. Paris, *Sub-critical flaw growth.* Engineering Fracture Mechanics, 1968. **1**(1): p. 3-45.
49. Irwin, G.R. *Plastic zone near a crack and fracture toughness*. in *7th Sagamore Ordnance Material Research Conference*. 1960. Syracuse Research institute.
50. Dugdale, D.S., *Yielding of steel sheets containing slits.* J. Mech. Phys. Solids, 1960. **8**: p. 100-104.
51. *Safety Assesment Principles for Nuclear Facilities*. 2006 Edition, Revision 1, Health and Safety Executive.
52. *U.S. Department of Commerce, National Oceanic and Atmospheric Administration, NOAA Research, Observation Sites* http://www.esrl.noaa.gov/gmd/dv/site/map1.html. 2008; Available from: http://www.esrl.noaa.gov/gmd/dv/site/map1.html.

Chapter B

Fracture Micro-Mechanisms

B Fracture Micro-Mechanisms

Contents

B Fracture Micro-Mechanisms....1
B.1 Ductile Failure....5
B.1.1 Plastic Flow....5
B.1.2 Plastic Instability....10
B.1.3 Micro Void Coalescence....14
B.2 Brittle Fracture....17
B.2.1 Brittle Fracture Mechanism in Low Alloy Steels....17
B.2.2 Factors Affecting Brittle Fracture....27
B.2.2.1 Material Factors....27
B.2.2.2 Geometric Factors....30
B.2.3 Critical Situation for Brittle Fracture....33
B.2.4 Brittle Fracture Modelling....36
B.2.4.1 Early Developments....36
B.2.4.2 The Local Approach to Fracture Modelling....42
B.2.4.3 Statistical Modelling of Single Temperature Scatter....44
B.2.4.4 Relative Temperature Dependence of the Transition Region....46
B.2.4.5 Other Statistical Models of Fracture in the Transition Region....51
B.2.5 Elastic-Plastic Fracture Mechanics and Constraint Correction....54
B.3 Crack Arrest....63
B.3.1 Arrest Toughness Testing and Mechanism....63
B.3.2 Initiation and Arrest Correlations....80
B.3.3 Microarrest....82
B.4 Research Aims and Objectives....86
B.5 Tables....88
B.6 Figures....90

B.7 References.....131

Tables

Table B-1 - Standard Specimen Geometry Constraint Coefficients Established for the Nevalainen and Dodds Trajectories for In-Plane Constraint Loss.....88

Table B-2 - Standard Specimen Geometry Constraint Coefficients Established for the Nevalainen and Dodds Trajectories for Out of-Plane Constraint Loss.....89

Figures

Figure B-1 - Plastic Flow in Ductile Materials.....90

Figure B-2 - Body Centred Cubic Crystal Unit.....91

Figure B-3 - Body Centred Cubic Crystal Directions.....92

Figure B-4 - Stress-Strain Curve for Ductile Materials.....93

Figure B-5 - Dislocation Pile Up at a Grain Boundary.....94

Figure B-6 - Grain Size Effect on the Yield Stress of Typical Low Alloy Steel.....95

Figure B-7 - Sub-grain Formation in Low Alloy Steel.....96

Figure B-8 - Zerilli-Armstrong Yield Stress Model.....97

Figure B-9 - Plastic Instability and Catastrophic Failure.....98

Figure B-10 - Plastic Instability in a Toughness a Specimen.....99

Figure B-11 - Specimen Size requirement for Elastic KIc Measurement.....100

Figure B-12 - Ductile Failure Mechanism (Microvoid Coalescence).....101

Figure B-13 - Microvoid Coalescence Fracture Surface.....102

Figure B-14 - Effect of Inclusion Content on Tensile Behaviour.....103

Figure B-15 - Regions of the Toughness Transition Schematic.....104

Figure B-16 - A Cloud of Defects Contained within the Small Scale Yielding Zone. 105

Figure B-17 - Micro-mechanisms of Cleavage Failure Initiation.....106

Figure B-18 - Comparison of Yield Stress and Toughness Temperature Dependence for Typical A508-3 Material.....107

Figure B-19 - Qiao Grain Boundary Cleavage Model.....108

Figure B-20 - Nil Ductility Temperature Measurement.....109

Figure B-21 - ORNL Extended Database Normalised by 110

Figure B-22 Compact Tension Specimens Used for HSST Programme (1, 2, 4, 6 and 12 inch thick specimens).....111

Figure B-23 - Local Approach Modelling of Fracture.....112

Figure B-24 - Landes and Shaffer Representation of Failure Probability.....113

Figure B-25 - Wallin Extension to Weakest Link Model.....114

Figure B-26 - Effect of Sample Size on the Measured Weibull Modulus for a Known Population.....115

Figure B-27 - Effect of Crack Front Length on Size Corrected Toughness.....116

Figure B-28 - Master Curve Median Temperature Dependence.....117

Figure B-29 - Master Curve Probability Bounds.....118

Figure B-30 - Effect of the Back Wall on the Constraint of Defect.....119

Figure B-31 - Effect of Free Side Surfaces the Constraint of a Defect.....120

Figure B-32 - Toughness Correction Factors as Supplied by Nevalainen and Dodds for a) B×B SE(B), b) B×2B SE(B), c) C(T), and d) C(T) 20% Side Grooved Specimens.....121

Figure B-33 - Effective Thickness Correction Factors as Supplied by Nevalainen and Dodds for a) SE(B) and b) C(T) Specimens.....122

Figure B-34 - Through Wall Temperature Profile and Associated Toughness Behaviour Following a Pressurised Thermal Shock Event.....123

Figure B-35 - Robertson Crack Arrest Specimen.....124

Figure B-36 - Typical Load Time Trace for an Instrumented Charpy Test.....125

Figure B-37 - The Compact Crack Arrest (CCA) Specimen.....126

Figure B-38 - Available Arrest Data Normalised by Arrest Reference Temperature, ...127

Figure B-39 - Initiation and Arrest Toughness Correlation Showing Effect of a) Yield Stress and b) Nickel Content.....128

Figure B-40 - Microarrest Mechanism.....129

Figure B-41 - Results of Microarrest Simulations Showing Specimen Thickness and Reference Temperature Groupings.....130

B.1 Ductile Failure

B.1.1 Plastic Flow

Ductile failure is one of several possible failure modes for low alloy steels and the transition region marks the point where brittle and ductile failure compete as the preferred failure mechanism. Ductile failure inherently implies that the material exhibits noticeable plastic deformation before failure. Plastic flow is possible due to the sliding of crystal planes in metallic materials (see Figure B-1); dislocation mechanics provides a framework for the understanding of plasticity in metallic materials. All low alloy steels are predominantly an iron carbon alloy and obey similar stress strain behaviour; plastic flow induced by shear stresses acting on specific crystal planes, the {110} planes, in the body centred cubic ferritic matrix causing slip [1] (see Figure B-2 and Figure B-3).

Upon loading and up to the yield point the material behaves in an elastic manner and will return to its original form and dimensions once the stress is removed. After the yield point the movement of dislocations within the material will result in permanent deformations once the load is removed (see Figure B-4). Permanent deformation is the result of slip of crystal planes within the material (see Figure B-1). The yield point is controlled by the microstructure of the material; for low alloy steel carbides in a ferritic matrix, and anything that may cause an obstruction to the movement of dislocations, such as coherent carbides, will increase the required shear stress. When dislocations interact with an obstruction the dislocation may move around given the correct conditions; however, at grain boundaries the dislocation is pinned and following dislocations pile up creating a region of stress in the matrix (see Figure B-5).

The effect of grain boundaries on the yield properties of low alloy steel is well established (see Figure B-6) and the famous Hall-Petch relationship between grain size and yield stress provides another control on the yield stress of the material [1-3]. The Hall-Petch relationship, although it appears simple, hides some wonderful insight into the effect of grain boundaries on the movement of dislocations in metallic materials. Grain boundaries provide the ultimate level of resistance to dislocation movement. The disordered nature of the grain boundary and the misorientation angle between grains presents a near impassable barrier to the dislocation. This causes the dislocations to pile up at the grain boundary creating a stress field that will repel further dislocations (see Figure B-5). This affords a strong level of grain boundary strengthening to these materials, and it is in fact easily demonstrated that the yield strength of low alloy steel is highly dependent on the grain size of the material [4].

The Hall-Petch relationship can be expressed simply as:

Equation B-1 $$\sigma_Y = \sigma_0 + \frac{k_y}{\sqrt{d}}$$

where σ_Y = the yield stress of the material [MPa]

σ_0 = the internal resistance to dislocation motion, also known as the friction stress [MPa]

k_y = the materials dependent strengthening coefficient

d = the grain diameter [m]

Anecdotally, it is known that reducing the grain size of a low alloy steel will improve both the yield stress and transition toughness behaviour. There is a limit to the grain boundary strengthening effect but as this occurs at grain sizes of ~100 nm it is far below the expected grain sizes found in low alloy steel forgings, which will be of the order of 10-400 μm. This limit is caused by the reduced difference in the size scale between dislocation equilibrium distances and the grain diameter. At ~100 nm the

dislocation equilibrium distance is approximately equal to the 100 nm grain diameter; at this point the strengthening mechanism is negated as the dislocations can no longer pile up. Despite this limit, grain refinement is one of the most potent methods of improving some of the mechanical properties of a material without adversely affecting others (grain boundary corrosion will be increased due to the increased number of surface breaking grain boundaries; however, this can be mitigated by careful environmental controls).

The microstructure of low alloy steel components is often a complex mixture of carbide containing ferrite that has formed from a number of possible microstructures. It is often found that a grain may contain a number of sub-grains (see Figure B-7). These are areas of microstructure that still share some crystallographic order with the others within the parent grain. These provide some level of strengthening, although not to the same degree as grain boundary strengthening, and it is advantageous to produce a fine sub-structure in a grain. The sub-grain size is dependent on the processing of the material and will often scale with the grain diameter so the sub-grain strengthening effect will be lost in the measurement of the grain strengthening effect; however, for large grained materials this will become the controlling dislocation strengthening mechanism.

The Hall-Petch relationship provides the backbone for a very useful means of estimating the yield stress of a material given very limited information. However the relationship only holds true for materials tested under the same conditions of temperature and strain rate. This limitation can be removed by expansion of the relationship to include the effects of temperature and strain rate; as these models are based on a physical understanding of the flow behaviour of the material this provides confidence that they are applicable to any loading situation. Many constitutive models exist, for example that due to Zerilli and Armstrong [5] model has been demonstrated

to estimate the yield stress of low alloy steels very well [6]. This is due to the fact the mechanism of dislocation movement as a function of temperature and strain rate in any low alloy steel is fundamentally the same; all are essentially modified iron-carbon alloys.

Originally developed to assess the effects of ballistic impacts the Zerilli-Armstrong constitutive model has found favour in the development of dislocation mechanics models as it provides a means to account for both temperature and strain rate effects (see Figure B-8). Two versions exist, one for bcc materials and one for fcc materials. As low alloy steels are bcc materials the bcc relationship is shown below.

Equation B-2 $\sigma_{ZA} = \sigma_G + \frac{k}{\sqrt{d}} + B_0 e^{(-\beta_0 - \beta_1 \ln \dot{\varepsilon})T}$

Athermal terms $= \sigma_G + \frac{k}{\sqrt{d}}$

Thermal terms $= B_0 e^{-(\beta_0 - \beta_1 \ln \dot{\varepsilon})T}$

where σ_{ZA} = Zerilli-Armstrong stress

σ_G = internal resistance to dislocation motion (material constant) [MPa]

k = grain boundary strengthening coefficient (material constant)

d = grain diameter [m]

B_0 = material constant

β_0 = material constant

β_1 = material constant

$\dot{\varepsilon}$ = strain rate [m/m/s]

T = temperature [K]

The model contains athermal and thermal terms. The athermal term appears is identical to the Hall-Petch relationship. As the effects of strain rate and temperature are considered to be inversely proportional, i.e. an increase in temperature has the same effect as decreasing the strain rate, both are included in the thermal section of the relationship. Only five material constants need to be determined for the flow properties of a material over a wide range of temperatures and strain rates to be established.

The athermal terms are effectively microstructure controlled and are dependent on a number of features. The internal resistance to dislocation motion, the σ_G term of the Zerilli-Armstrong relationship accounts for a number of microstructural features: solid solution strengthening, precipitation hardening and point defect formation during neutron bombardment. The grain size strengthening is accounted for by the familiar Hall-Petch term. The thermal terms are still material dependent as the thermal performance will be mostly dependent on the chemistry and processing history of the material; however, these are also dependent on the only external factors, temperature and strain rate.

B.1.2 Plastic Instability

Plastic instability is caused by the development of a fully plastic cross-section in a component. The simplest example is the formation of necking in a tensile test (see Figure B-4). Following loading beyond yield point the entire cross-section becomes plastic, a region of high stress develops in the gauge length due to an inherent or machining defect forming a characteristic neck in this region. Plastic regions can also form in complex component geometries due to under estimation of the loads that will be experienced by the component. This will lead to deformation and distortion of the structure resulting in the structure no longer remaining fit for purpose.

Although failure of the component is not normally the goal of designers, failure through plastic instability is preferable to catastrophic failure due to brittle fracture (see Figure B-9). The conditions for brittle fracture can be estimated, but due to the inherent scatter of material toughness for low alloy steel it is not possible to predict an exact situation that will give rise to brittle failure. When brittle failure does occur there is a reasonable possibility that the component will fail in such a manner as to leave the component in any number of pieces and certainly with at least one major crack. For a nuclear primary boundary component, such as a reactor pressure vessel, any defect that results in the loss of containment is unacceptable.

Failure by plastic instability offers many advantages over brittle failure. Firstly, by the use of accurate stress analysis and material understanding instability can be readily predicted in most cases, as it will occur for the same loading conditions in all instances. The tensile properties of a material can be changed by irradiation or thermal ageing effects and this can lead to further complexity in an analysis. Secondly, the deformations involved with plastic instability may result in the component becoming unfit for purpose; however, the fact that a ligament remains across the damaged area may maintain a pressure boundary. This is essential for

containment of the primary coolant in a light water reactor to prevent a loss of coolant accident.

Plastic instability can be readily designed around for a component by finite element analysis long before production if the mechanical properties of the material from which it is to be made are well understood. This has lead to well designed reactor vessels and primary components with large section thicknesses and as such the author is unaware of any failures due to plastic instability during normal operation. Plastic instability is apparent in other areas of interest to the study of toughness. One area where plastic instability is observed is in test specimens where a small test piece is used to measure the fracture toughness properties of high toughness materials. If the crack depth is too short and the geometry of the specimen is not sufficient to produce a stress intensity factor high enough to cause brittle fracture, plastic collapse is inevitable (see Figure B-10). This can be explained as a development of plasticity from the crack tip to a free surface. Although there is a cut-off point at which brittle fracture cannot be initiated in low alloy steel, the effect of plasticity instability is not as discrete.

In the early days of toughness testing and the creation of the ‘million dollar curve’, so called due to the great cost of early toughness testing, used to develop fracture toughness as a useful tool for the justification of reactor operation, very large test specimens were used to prevent any effect of shear lips on the recorded toughness values [7]. This was done to eliminate the effects of in-plane loss of constraint on the recorded values to establish the lowest possible linear elastic toughness of these materials. By using such large specimens the effect of out-of-plane constraint loss was also mitigated in these testing programmes. Guidelines for specimen sizes are given in ASTM E399 [8] in order to maintain validity and allow comparisons between measurements (see Figure B-11). Developments in the understanding of toughness

measurement have introduced the use of elastic-plastic analysis methods allowing the researcher to use ever-smaller specimens to establish the toughness of modern improved materials. This creates a number of concerns.

The temperature dependence of low alloy steel fracture toughness offers the most obvious demonstration of the loss of constraint in small specimens. When the recorded toughness values for a material begin to diverge significantly from the expected temperature dependence it will become evident that the geometry and size effect of the specimen is influencing measured behaviour. At the point of complete plastic instability, no cleavage results can be obtained and the specimens simply bend to a point where the recording apparatus used is out of the available calibrated range. Before the position of complete plastic instability has been reached, the specimen will begin to lose constraint at lower temperatures, this may go unnoticed by the researcher if the values still fall roughly into the bands of scatter expected in the data.

The absolute effect of plastic instability in these small specimens is currently not taken account of in either ASTM standard method for testing and analysis, E399 [8] and E1921 [9]. A limit load has been applied to censoring of data in the latter, Master Curve method. This limit load is calculated based on the ligament of the specimen used and the yield stress of the material; the calculated value is considered the limit of toughness measurement where small scale yielding conditions will still hold at the crack front. There is much discussion of the correct value for this limit and currently the standard allows significant divergence between the applied load and extent of constraint loss. This is understandable as raising the limit to the required level to guarantee no constraint loss will effectively eliminate small specimens as a viable method of obtaining toughness measurements for modern high toughness materials without exceptionally careful planning of test temperatures. Fortunately, the effect can

be taken into account via fully plastic finite element assessments of standard test specimen geometries [10]. An understanding of this assessment and the application to toughness data will be discussed in a later section.

B.1.3 Micro Void Coalescence

Micro void coalescence is caused by the presence of finally dispersed secondary particles within a ductile matrix allowing plastic flow. This plastic flow causes large deformations, distorting the macrostructure, and hence having a very substantial effect of the microstructure. All low alloy steels contain some form of secondary particles in the form of carbides and despite the most advanced processing methods, many inclusions will remain from the steel making process. During extreme plastic deformation, the material will form a neck at the region of highest stress, this is familiar in tensile specimens specifically designed to fail in the gauge length. The necking process also takes place on a micro-scale between these secondary particles causing a three stage process of initiation, growth and coalescence (see Figure B-12).

Voids form around defects in the matrix, commonly secondary particles and can nucleate from the particle location in two ways dependent on the interfacial strength of the particle to matrix bond. If the bond is weak the particle will debond from the matrix when sufficient stress is applied. The debonded area will often be some fraction of the total interfacial area causing the particle to be visible in the resultant dimple on the fracture surface. This generates a volume unable to support load, which is then expanded during plastic deformation. For strongly bonded particles the local strain at the particle will be sufficient to cause particle fracture before debonding. This also produces a volume unable to support load and generates a small material defect, equivalent to the size of the fractured particle, which is also free to expand during plastic deformation.

Whether a particle debonds or fractures is an energy balance calculation dependent on the fracture strength of the particle and the interfacial energy of the particle-matrix

bond, both of which are very difficult to determine experimentally. Surface energy measurements are very difficult in complex alloys and the fracture strength of a complex intermetallic inclusion is impossible to determine, as it is impossible to scale the inclusion to a suitable size for testing. Although the physical understanding of both mechanisms exists and is theoretically sound [11-12], the energy absorbed by either mechanism is but a small fraction of the overall energy absorbed in the ductile rupture mechanism, and as such is not included in any further analysis or discussion.

There are three steps in the process of ductile rupture of a material illustrated in Figure B-12, initiation, growth and coalescence:

1. Voids form at cracked or debonded particles in the region of highest stress. These initial voids will form on the largest or weakest of the secondary particles; these will commonly be the inclusions formed during the steel making process. These will be widely spaced compared to the microstructure and provide local regions of stress concentrations increasing the rate of plastic flow.

2. The voids continue to grow as the load is increased resulting in local necking between voids. A large amount of local plastic deformation occurs resulting in effects to the macro deformation, which will be discussed below.

3. The stress in the local necks is sufficient to cause particle failure or debonding of the coherent precipitates and carbides in the material. This results in yet further void formation and local necking between these particles. The fracture strength of the matrix material will soon be exceeded in the necked regions causing failure of individual necked regions. As the necks fail the voids coalesce into a single continuous defect in the material causing rupture.

This process produces a very distinctive dimpled fracture surface (see Figure B-13). Large dimples, produced around inclusions may be separated from each other but commonly occur in groups. This is due to the formation of melt defects, or inclusions, in the steel making process that will cluster due to local chemistry differences or segregation. In between the larger dimples, small dimples produced from voids around the precipitates fill the remainder of the surface. At the free surfaces of the specimen failure will occur by means of a fast shear mechanism resulting in distinctive surfaces aligned with the direction of the shear stresses in the component. In total this process absorbs a vast amount of strain energy that is converted into plastic deformation and the creation of new surfaces.

The formation of voids can have an effect on a number of tensile dependent properties. An understanding of the dependence of microstructure on void formation can be used to demonstrate that improved mechanical performance can be obtained from decreasing the inclusion content of a material. For low alloy steels with the same composition and processing route, yet different inclusion content, some key differences can be established in how the steel will perform on the macroscale given limited difference on the microscale (see Figure B-14). For the low alloy steel containing a higher number of inclusions, the yield stress will be reduced due to the reduction in load supporting area. The elongation to failure and reduction of cross sectional area will be greatly reduced by the presence of inclusions, creating many small regions of local necking before one dominant neck forms as opposed to the single dominant neck formed in clean materials.

B.2 Brittle Fracture

B.2.1 Brittle Fracture Mechanism in Low Alloy Steels

The importance of understanding the mechanisms of brittle fracture in low alloy steels cannot be underestimated. The reliance on low alloy steels as the predominant structural metallic material means that the vast majority of major engineering structures are constructed from this material. Catastrophic failure of these structures is unacceptable and it has been demonstrated that a brittle fracture on a large structure can result in the death of many hundreds of people. Much has been learned of the mechanism of brittle fracture from the study of these events, which act as a catalyst to produce tougher steels for use in structures.

Current understanding of the microstructural aspects of brittle fracture and the controlling mechanisms in the initiation of such fractures is such that high toughness materials are readily available. The mechanisms of brittle fracture are similar for a wide range low alloy compositions and are highly temperature dependent. Broadly, temperature dependence can be separated into three very distinct regions, the fully cleavage lower shelf, the transition region, and the fully ductile upper shelf (see Figure B-15). The mechanism of cleavage fracture is believed to be temperature independent, i.e. the same basic principles apply across a wide temperature range from absolute zero to the onset of upper shelf behaviour.

The level of understanding is such that it can be postulated as to the exact mechanism causing brittle fracture, which takes place within the material on a microscale. When a material containing a sharp defect, commonly a fatigue crack, is loaded a region of local plasticity forms ahead of the crack tip. The size of the plastic zone is dependent on the stress intensity factor and yield stress of the material; the

magnitude of the stresses within the zone are proportional to the yield stress of the material.

Within the plastic zone, the material flows by the movement of dislocations. Dislocations move along specific crystallographic planes, {110} in the ferritic matrix and upon reaching a grain boundary become blocked and exert a repulsive force on other dislocations. Certain grains may deform preferentially [13] in the plastic zone due to an effect known as ‘crystal plasticity’. There is limited grain boundary sliding due to secondary particles that pin the boundaries together; hence, a grain may only deform if those surrounding it are sympathetically aligned. The ferrite crystal structure, body centred cubic (BCC), also has anisotropic properties dependent on the differences in packing density on each crystal plane. The closest packed directions, <111>, have a higher Young’s modulus than the loosely packed directions, <100>; 272 GPa and 125 GPa, respectively [14].

A distribution of secondary particles lies within the plastic zone (see Figure B-16), many lie along the grain boundaries of the material, some of the slip bands will be coincident with these particles. Dislocation motion will create a ‘pile up’ at such particles exerting a significant stress in the local area [15]. Second phase particles by acting as barriers to dislocation motion provide significant strengthening to the material; the strengthening effect is proportional to the coherency of the particle with the matrix. Good correlations between the size of carbides and fracture behaviour have been found [16-17] and grain boundary carbides are believed to be the main initiator of brittle fracture in low alloy steels as the slip band length is maximised at the grain boundary and may potentially extend across the entire grain diameter. Temperature will also have an effect on the movement of dislocations through the matrix. At higher temperatures dislocations can move out of plane and around

obstacles in a process of dislocation climb [15]; this reduces the number of particles involved in the fracture process as the temperature increases.

Carbides have very complex structures and are commonly highly coherent with the ferrite matrix. Their composition may also vary across the carbide such that accurate modelling of carbide failure is highly complicated [18].

The stress acting on a particle eventually becomes sufficient to cause it to fracture. Although the particle fails due to an induced stress this step is controlled, from a macro perspective, by the strain induced in the material (see Figure B-17). As described above, a plastic zone is formed ahead of the crack tip allowing local flow of material; within this region dislocations move causing shear stresses to develop at obstacles found at the end of slip-bands.

The micro-crack initiated by the failure of the particle must then be injected into the surrounding matrix. The strong bond between the carbide and the matrix aids in the propagation of the micro-crack during the process of injection into the matrix. The failure of the particle was due to strain; however, there must be sufficient stress to cause fracture of the matrix given the presence of the micro-crack [19]. There is some debate as to whether initiation and injection must happen concurrently [20], or whether the cracked particles still remain a potent initiator causing failure at a higher applied stress. It would be expected that if the events happen concurrently, then the increase in strain rate as the crack traverses the carbide would increase the effective stress (by increasing the inherent lattice friction [21]), and hence, the likelihood of injection.

If the crack is injected and there is sufficient stress to cause fracture of the ferrite matrix then the material will fail on a specific crystal plane, {100}, the ferrite cleavage

plane [1, 21]. The cleavage planes are located on planes of weakness within the bcc crystal, i.e. those with the lowest theoretical strength estimated from atomic arrangement and spacing [1, 21-22]. The crack will propagate across the grain in this plane only resulting in a grain-sized micro-crack in a specific orientation. The crack must then propagate across the first high angle grain boundary encountered; however, there are still several obstructions to the continuation of the fracture process.

The energy released by the failure of a single grain (released energy = strain energy – new surface energy) is very small and it is possible that the surrounding material may be of sufficient toughness to prevent the propagation of the micro-crack [23]. For an arrest event to occur, dislocations must be sufficiently mobile to reach the crack tip before the stress reaches a critical level. The dislocations will then blunt the crack tip reducing the potency of the micro-crack. This is much more likely to happen if the material can be described as heterogeneous at a microstructural level; evidence of non-propagation has been seen in materials that are very heterogeneous [24-25].

This heterogeneity can be caused by either a difference in the microstructure (bimodal grain size, phase constituents, texture effects) [25] or by the presence of highly potent initiators (large cubic particles such as titanium carbo-nitrides) [24] randomly dispersed in the material. Both of the above phenomena lead to small patches, possibly of the order of one-grain diameter, which can initiate brittle fracture. If the initiating grain is surrounded by material that is of sufficiently higher toughness, then the micro-crack will fail to propagate. In reality this is a very rare event, although, by means of controlled heat treatments or poor processing materials can be produced which exhibit the necessary heterogeneity.

Predominantly the failure of the initiating grain is adequate to raise the stresses in the surrounding materials sufficiently to cause failure. The increase in stress around the failed patch causes a cascade failure to begin throughout the material. It is believed that once the expanding cleavage crack front reaches a critical velocity it will run completely through the material, i.e. dislocations are unable to blunt the crack tip leading to auto-catalytic failure. The crack can still be arrested by either removal of the driving force (load) or by a change of material toughness (commonly achieved by grain refinement) though which the crack travels.

Using the lower shelf, the largely temperature independent region A in Figure B-15, as a starting point for discussion it is possible to postulate the mechanisms involved across the complete temperature range of brittle to ductile behaviour. The failure of materials on the lower shelf is signified by the lack of ductile crack extension perceptible on the fracture surfaces, this simplifies the fracture process and results in a cleavage only description of fracture. The absence of ductile behaviour intuitively suggests a fully elastic process; however, plastic flow must occur for brittle fracture to initiate.

On a macroscale, failure on the lower shelf exhibits only small elastic deformations to cause fracture. On a microscale, the movement of dislocations and the resulting plastic deformations initially mitigate the effect of the stress concentration but ultimately cause the failure. The reason for the high toughness of metallic materials compared to ceramics is the ability to accommodate stresses by plastic deformation. As discussed in a previous section, the stresses ahead of a sharp crack tend to infinity at the crack tip when an elastic analysis is applied. Any stress above the yield strength of a metallic material will cause plastic flow. This in effect limits the maximum stresses ahead of a crack tip to 3 – 5 times that of the yield strength of the material [26].

Even at the low absolute temperatures required for lower shelf toughness behaviour, the yield stress of the material is still significantly lower than the (relatively) temperature independent fracture stress. A small scale yielding condition will develop ahead of the crack like defect; however, the plastic zone will be small compared to the length scale required to produce dislocation motion. It would be expected that failure on the lower shelf would be similar to that in ceramics, where failure require stress intensity factors in the order of 1-7 $Mpam^{0.5}$ for silicon carbide and silicon nitride [27]. In ceramics the yield stress is so high in magnitude that the peak stress rises quickly to a point where the fracture stress is exceeded. In low alloy steels the fracture strength is exceeded by the peak stress; however, the magnitude of this stress would be considered enough to cause failure. There are, in fact, two conditions that must be met for brittle fracture to occur, a significant level of stress must be applied over a critical distance ahead of the crack front tip [28].

On the lower shelf the peak stress is large at even low applied loads due to the stress amplification afforded by the sharp defect and high yield stress. However, the distance over which the stress peak acts is narrow and corresponds to a small plastic zone. Failure only becomes possible when both conditions have been met, a high level of stress applied over a significant distance. On the lower shelf, the stress requirement is achieved easily however the distance requirement is only achieved after the application of higher loads.

Early models simply described an instantaneous transition between brittle and ductile behaviour. This is intuitive and is certainly true if the fracture mode is viewed on a decreasing temperature scale where the failure is either ductile or not. A failure event culminating in cleavage failure in the transition range can still absorb large amounts of energy and the temperature range over which this transition occurs is certainly

significant. Failure in the transition region is a competition between brittle and ductile initiation, in which by definition cleavage fracture always intervenes. Failure in this region is also marked by the presence of small scale yielding ahead of the crack tip. The elastic solutions of fracture mechanics imply an infinite stress at the crack tip, this of course is impossible or the material would fail with the slightest application of load.

Failure in the transition region is complex and as yet no model has been proven to capture both the temperature dependence and the inherent scatter of fracture toughness at single temperature measurements [20, 28-33]. The magnitude of the stress developed ahead of the crack tip is dependent on the yield stress of the material; however, this does not capture the temperature dependence exhibited by the toughness of the material. Where the yield stress is decreasing rapidly, the toughness barely increases and where the toughness increases rapidly the yield stress plateaus Figure B-18. This implies that the situation is more complex than the simple critical stress over a critical distance concept that was required on the lower shelf.

The stress state ahead of the crack becomes more complex due to the increased levels of plasticity that occurs at higher temperatures. As plasticity is in abundance the balance has shifted between critical stress and critical distance; a large plastic zone is formed but the stress within it may be insufficient to cause fracture. In order to form a plastic zone the local stresses due to the presence of a stress raising defect must exceed the yield stress of the material. The stresses acting at the particle of interest are dependent on how dislocations move within this plastic zone. On the lower shelf the high magnitude of the peak stresses within a small plastic zone produces a very small process zone limited to the region of the micro-crack created by the particle. The very high hydrostatic stress achieved in the process zone causes

the movements of dislocations to be limited to simple slip only, in the transition region other effects become important.

The larger plastic zone in the transitions leads to a reduction in the magnitude of the peak stresses and as such the dislocations are able to move in more ways than simple slip causing a pile up at the grain boundary. It is entirely possible that the dislocations may dissipate at the micro-crack causing crack blunting; this raises another criterion for failure. The constraint on the micro-crack must be sufficient to prevent blunting of the micro-crack tip. This becomes increasingly difficult as the relative temperature is increased; a particle that may have caused failure on the lower shelf or in the lower transition may not now be involved in the fracture process at all.

For brittle failure to occur, the following criteria have so far been established at the tip of a pre-existing defect:

1. The applied load must be sufficient to generate a peak stress higher than the yield stress of the material creating a plastic zone,
2. The total plastic strain must be sufficient to cause fracture or debonding of a grain boundary particle giving rise to a micro-crack in the material,
3. The peak stress must act over a critical distance large enough to cause the movement of dislocations across a microstructural unit bounded by high angle grain boundaries,
4. Constraint must be maintained at the micro-crack or crack blunting will exclude the particle from further involvement in the fracture process.

In order for the material to fail, the micro-crack must develop and propagate through the material. This presents another obstacle to brittle failure. The micro-crack

encounters a number of barriers in the early stages of development that can arrest further propagation. Firstly, the failure of the matrix must occur and, as can be seen above, this in itself is difficult. Secondly, the expanding micro-crack meets the grain boundary. The grain boundary presents a significant barrier to the cleavage crack that has grown on a single crystal plane. The boundary represents the end of one crystal and the beginning of another; a corresponding misorientation then exists that the cleavage failure must cross.

How a cleavage crack crosses one of these boundaries is often ignored in the development of failure criteria, unsurprising considering the complexity of the situation. A recent model proposed by Qiao [34-35] developed on silicon steels with very large grain sizes offers some explanation for the process of propagation across grain boundaries. It is suggested that when a cleavage crack reaches a grain boundary it is partially injected into the next grain (see Figure B-19). The misalignment between the grain containing the crack and the next can be split into two components, tilt and twist. Tilt is the angle between the cleavage plane of each grain and twist corresponds to the alignment of these planes. The injection does not take place uniformly across the boundary due to the misorientation; the crack is injected across the boundary at coincident points where the cleavage planes cross leaving a distinctive finger type set of features.

At the point of coincidence, the cleavage crack passes easily into the next grain. In between the fingers of cleavage crack extension, the grain boundary remains intact forming a ligament that provides a reduction in the driving force and must fail for the crack to advance. The ligament fails in a ductile manner, a process requiring that the energy released from crack advance is larger than the strain energy required to fail the ligament. This is a significant barrier to crack advance and it is possible that the crack will fail to propagate across the first few boundaries encountered. Once several

grains have failed it is believed that the energy released is sufficient to overcome these barriers and the crack will propagate to failure readily.

The micro-crack propagates towards the macro crack as well as away from it. Once the micro-crack joins with the macro-crack the stress shielding afforded by the remaining ligament is lost. The micro-crack effectively becomes an extension to the macro-crack, now with an atomically sharp point creating stress conditions similar to lower shelf behaviour, failure is almost instantaneous and proceeds at a speed approaching that of sound in the material.

This adds a further two failure criteria:

5. The energy barrier created by a number of grain boundaries must be crossed before the failure becomes auto-catalytic, i.e. the energy released by further crack extension is sufficient to overcome any barrier to propagation,
6. Once the micro-crack propagates back to the macro-crack, catastrophic failure is assured.

From the above criteria it can be seen that just because a particle exists on the grain boundary, does not mean it will cause failure. In fact, even a small stressed volume of steel will contain a large number of potential initiating particles. This means that the critical situation to cause failure, the combination of slip plane, particle size and location, favourably aligned microstructure in both the initiating and surrounding grains, is very rare and requires large applied loads to develop. As brittle fracture is a complex interaction between a large number of perceived controlling material, geometric and loading parameters an understanding of each is required.

B.2.2 Factors Affecting Brittle Fracture

B.2.2.1 Material Factors

B.2.2.1.1 Maximum Local Stress

Elastic analysis methods show that with decreasing crack tip radius, local stresses are unbounded. The high levels of local stress can be attributed to the effect of triaxiality caused by Poisson's shrinkage of the material normal to the applied stress. In actuality, the local stresses are limited by the small amount of plasticity that is induced ahead of the crack tip. The stress state in front of a sharp crack can be estimated by small scale yielding (SSY) finite element simulations and can be shown to be a multiple of the yield stress.

B.2.2.1.2 Slip Band Orientation

During the solidification process grains grow from nucleation sites that are randomly orientated. This texture will then be carried over into the final component if the work applied to the material during the forming process is low. For a rolled plate the level of deformation can be very high and as the material is worked consistently in one direction it develops an underlying texture. The same cannot be said for the majority of heavy section forgings. Although during the forming process some areas may receive large amounts of work, in general the deformation in a heavy section forging is very low compared to a rolled plate. It can therefore be assumed that the randomly orientated grain structure is preserved into the final component.

B.2.2.1.3 Slip Band Length

The length of the slip band is a controlling parameter for the maximum number of dislocations that can pile up, and hence, the magnitude of the opening stress on the

micro-crack The length of the slip band will predominantly be dependent on the grain diameter, however, any secondary particle present on the slip band will act as a barrier to dislocation motion. Secondary particles can be found throughout a grain and it may be possible that the longest slip band in a given grain is actually an inner particle to inner particle length. Recent work has shown that the upper tail of the grain size distribution, and hence slip band length, can be highly detrimental to toughness performance [36], the reasoning for which will be discussed in B.2.3.

The length of a slip band within the material will be directly linked to the grain size of the material. The distribution of particles will likely be consistent between pressure vessel steels, as broadly similar compositions and heat treatments are employed; therefore the likelihood of finding a particle at the end of a long slip band increases with the total available length (grain diameter) i.e. a greater micro-crack opening stress can be exerted in a material with a large grain size. No material is completely homogeneous and the observed variation in grain size will contribute to the noted scatter in measured materials toughness.

B.2.2.1.4 Initiating Particle Type

The type of particle that initiates fracture will control the early stages of the fracture mechanism. If the material contains particles that are large and angular, such as cubic titanium-vanadium carbo-nitrides ([Ti,V – C,N]) or metal oxides, then failure is likely to be initiated by the increase in local stress caused by the presence of a sharp defect. This process requires a much lower applied stress due to the stress raising sharp point of the particle and induces a correspondingly low recorded toughness. Cubic [Ti,V-C,N] and large oxides are melt defects and hence are easily avoided by accurate control during the steel making process. Modern RPV materials should not exhibit inclusion-initiated failure as large and unwanted secondary particles should be

very rare, unless the processing route has been specifically designed to promote their growth or not sufficiently well designed to preclude their presence.

Grain boundary carbides are considered to be the most likely secondary particle to initiate brittle fracture [37]. In low alloy steels, the majority of alloying elements are carbide formers and this can lead to a variety of different morphologies. All are considered brittle and may initiate failure; however, the cohesion of this particle to the matrix depends heavily on the thermal history of the material. A cohesively bonded particle will have an increasing effect on the yield strength of the material but a detrimental effect on the toughness, as the strength of the bond between the particle and matrix increase, the likelihood of particle failure and injection of the micro-crack will also increase.

B.2.2.1.5 Initiating Particle Size

The particle size will also have a direct effect on the fracture process. A larger particle has more chance of being intercepted by a slip band and hence being involved in fracture. The micro-crack formed by the failure/debonding of a large particle will also release more strain energy and hence be preferentially involved in the fracture process [16-17]. If the material has been treated in a way to promote large carbides, carbon will migrate from smaller unstable carbides within the grain to larger more stable carbides at the grain boundary. This effectively increases the slip band length as well as increasing the likelihood that a grain boundary carbide will be at the end of the slip band. Both of these effects will result in reduced toughness.

B.2.2.2 Geometric Factors

B.2.2.2.1 Defect size

The defect size is important in determining the stress intensity factor applied to the material. It is clear that a larger defect creates a larger area though which load cannot be supported, this increases the stress intensity factor at the tip of the defect. The size of the defect is also the dominant factor in determining the level of constraint of the defect. The plastic zone ahead of the crack tip must be constrained for the stresses to reach the highest possible level; this was originally achieved in initiation testing by selecting specimen sizes where the defect depth and ligament were sufficiently larger than the plastic zone size [8]. Modern toughness testing utilises a different approach and hence the constraint on specimen size for plane strain conditions is no longer utilised; specimen size criteria are now calculated on the loading limit based on the yield stress of the material. To ensure a minimum of specimen size/geometry effects of measured toughness the plastic zone is placed in an area as far as possible from any free surface; this is achieved by locating the crack front at a depth equidistant from the top and bottom surface.

If the defect is too shallow or too deep, the plastic zone may ‘escape’ to a free surface. If the plastic zone reaches a free surface the flow of material in this region will relieve the stresses that have developed at the crack tip. There are two possible scenarios: for a shallow crack the zone may jump back to the top surface resulting in crack blunting, or if the plastic zone grows to the back surface then the entire specimen will deform giving rise to general, or large scale, yielding. Escape of the plastic zone is avoided by the use of standard specimen geometries that embed the crack front in the centre of the specimen.

B.2.2.2.2 Defect shape

The shape of the defect can have a similar controlling effect on the potency as the defect size. Crack shapes that diminish the effect of free surfaces, such as a through thickness edge crack, have a much higher stress intensity factor [38]. Notch acuity will also have a large effect on the stress state ahead of a sharp crack for a given defect size. A high level of stress is achieved for a sharp crack compared to a blunted notch due to the stress raising geometry. Again, commonality and standardisation have resulted in comparable measurement for toughness using standard specimen geometries.

B.2.2.2.3 Tri-axial stress state

Within the region of high constraint, a tri-axial stress state is created due to Poisson's contraction of the material normal to the applied load that is constrained by the specimen geometry. By contraction in the out-of-plane direction large stresses are created in the region ahead of the crack tip. This region of high constraint exists across the majority of the crack front; however, at the free surfaces of the specimen the plastic zone can escape, the high stresses are reduced and the plastic zone is distorted.

In reality the reactor pressure vessel is under biaxial loads caused by the hoop and longitudinal pressure stresses; the stress state is further complicated when the size of the defect relative to the structure is considered. Transferability of laboratory measurements to the structure is therefore difficult. Biaxial loading can also be used to alter the tri-axial stress state and hence the level of constraint. Due to the complexities and expense of utilising biaxial loads for materials testing, biaxial tests are rarely performed and the procedure is still in its infancy [39].

To offer a level of conservatism when performing structural integrity assessments, the geometry of test specimens is chosen to provide greater crack tip constraint than can be found in the structure. Laboratory specimens are based on bend stress states that produce higher constraint than the tension loadings often found in structures as the outer surfaces experience much higher stresses in the bend geometry than can be achieved tensile loading only.

B.2.3 Critical Situation for Brittle Fracture

It would be expected that within a material there will be many possible points of initiation; coupling this with the need for a critical situation for fracture gives rise to the inherent scatter exhibited by low alloy steel. Test results are also subject to normal experimental errors but with modern calibration requirements and the accuracy of load and displacement sensors, these errors are considered very small and are commonly ignored. A value of toughness can be reached by several testing methods and also by different analysis routes, in these cases true material differences may not be noticed; however, in all instances the fracture behaviour of the material is believed to be similar.

Looking at each possible situation that may give rise to fracture would, on average, lead to very high toughness values given the number of possible initiators in the material. However, it is believed that just one is responsible for complete failure. The failure emanates from this point which is just one of many thousands of possible sites in a cloud of initiators ahead of the crack tip. The initiator to cause failure is known as the weakest link, as the process is analogous to failure of a chain where once one link fails the chain is unable to support load. The same is assumed of brittle fracture where failure is believed complete on the successful initiation and propagation of a cleavage crack.

The defect to cause failure is the most potent of these initiators and, as has been seen by the high level of toughness achieved by low alloy steels, finding a suitable initiator is difficult. The most potent will be that which has the most favourable parameters for fracture. Due to the large number of controlling parameters and the variation that each can take, it would be expected that the required external load and displacement, and hence recorded toughness, would also vary accordingly. This would produce a wide range of toughness values for the same material, dependent

on the microstructure selected for examination; this is indeed the case for toughness testing of low alloy steels. It is found that the scatter in the toughness values follows a Weibull probability distribution; this distribution can be applied because of the weakest link mechanism believed to take place in the material.

From the assessment of the brittle fracture micro-mechanisms detailed above, it follows that the scatter in measured toughness is a result of the random features of the microstructure. With in the microstructure it is possible to envisage a situation where, by pure chance, a large carbide can be found at the boundary of a large grain with a slip and cleavage plane favourably orientated to the applied load. From the toughness values achieved in pressure vessel steels, it can be suggested that the energy required to drive this failure, even given the favourable situation detailed above, is large. Therefore, only the largest grains within the material should be considered important to the failure mechanism.

The measurement of grain sizes, and their distribution, in low alloy steels is difficult using optical techniques and as such this avenue of research has only recently been followed. The development of electron backscatter diffraction techniques [40] has allowed for high speed and accurate acquisition of grain data. A recent assessment at Rolls-Royce has shown that there is significant promise in this area and good agreement has been found between comparison of grain size distributions and fracture toughness response of low alloy steels [36].

If a distribution of initiators is assumed to lie along a crack front then the recorded toughness value will correspond to the most potent of these initiators. The probability of failure is then not dependent on the average or maximum applied stress to fracture all or a number of the initiators, just the weakest must fail. So although there are many potential initiators in the material, the load required to fail the most potent will

also follow the distribution of the initiators. The scatter in these measurements then comes from the scatter in the most potent of the initiators. By selecting a certain crack front length, many initiators will be assessed and the recorded toughness value corresponding to the most potent; by selecting another crack front of equal length, a new set of initiators will be assessed and the most potent may have a different level of required load to cause fracture. This is found to be the case for toughness measurements of low alloy steel and the scatter of toughness measurements approximately matches the assumed Weibull distribution of initiators [41].

This raises another problem with the assessment of toughness data. The distribution of initiators is based on a per volume basis with the crack front length as a normalising factor; hence the number of sampled initiators is dependent on the load applied, which controls the area of the plastic zone, and the crack front length. It is a reasonable assumption that a larger volume will sample more initiators, increasing the likelihood of finding a potent initiator. This presents a problem in performing an assessment of the toughness of the material, as the toughness established from larger specimens will be lower than that established for smaller specimens. Fortunately the use of a Weibull distribution allow the user to correct for the size based on the assumed distribution of initiators in the material.

By means of the size correction and a good understanding of the stresses in a structure, it is possible to apply the toughness achieved in small specimens to that of a real structure. Without this, the field of fracture mechanics of low alloy steel would be academically interesting but of little engineering applicability.

B.2.4 Brittle Fracture Modelling

B.2.4.1 Early Developments

The modelling of brittle fracture has often been held back by the relative difference between the understanding of the fracture process and an ability to demonstrate the true mechanisms of fracture. This is due to the size scale of the fracture event and speed with which it occurs. Unlike ductile failure, which can be interrupted at any point by simply removing the applied load, once a cleavage crack is running it is very difficult to stop and as such it is hard to perform direct measurements on the process of initiation and propagation of these types of failures. It had long been postulated that defects in the matrix act as initiation sites for cleavage failure.

Smith proposed that the fracture stress was being exceeded due to the presence of sharp defects in the regions ahead of a crack [37]. In modified form this is still the basis of fracture modelling today; an opening stress acting on a small defect, such as a failed carbide, is considered to be the initiation step in brittle fracture. Many attempts have been made to quantify the microstructural effects on toughness but in reality, only qualitative predictions can be made. The failure criteria that must be met for brittle fracture to occur was introduced by from the work of Tetelman et al [19] on the comparisons of fracture strength with brittle behaviour. These three simple criteria hold true today, and are commonly understood to correspond to the three phases of the brittle fracture mechanism; they are:

1. Initiation – a sharp defect must be introduced into the material, such as a micro-crack due to a failed carbide.
2. Injection – there must be sufficient opening stress on the defect to exceed the fracture strength of the material and inject the micro-crack into the surrounding matrix.

3. Propagation – the micro-crack must leave the initiating grain by passing a high angle grain boundary.

These give the starting point for all modelling efforts. The first true attempt at modelling brittle fracture in a using physical quantities obtained from microstructure measurements was the Ritchie Knott Rice model [28]. Combining the fracture criteria of Tetelman et al [19] with an understanding of the fracture process proposed by Smith and a thorough stress analysis produced an effective model for lower shelf behaviour but failed to capture the large upswing seen in toughness measurements. The Ritchie-Knott-Rice model attempted to quantify toughness temperature dependence as a function of the temperature dependence of yield stress relative to fracture stress. It had been established that the fracture stress remained approximately constant for slip-induced cleavage fracture the mechanism of interest for brittle failure; however, the yield stress was known to vary with temperature.

The Ritchie-Knott-Rice model assumes that the injection stage is the critical step in the fracture process. The assumption that the sharp defects are present in the material is a reasonable one; carbides are very brittle and stiff, requiring only the slightest plastic strain to fracture or debond these particles from the matrix creating the sharp defect required for the injection phase [42].

Stress analysis of sharp defects had shown that peak stress was a multiple of the yield stress and the peak stress would, therefore, share the temperature dependence of yield stress. These analyses also showed that the peak stress would exceed the fracture strength of the material at very low applied loads. This created a problem: as the fracture strength was being exceeded the material must fail; this obviously was not the case. To this end Ritchie, Knott and Rice included another criterion that the fracture stress must be exceeded over a microstructurally significant distance ahead

of the crack. It was understood that in order for the cleavage crack to propagate the fracture stress must be exceeded at the first grain boundary encountered. Therefore the fracture stress must be exceeded in two places, the closest grain boundary to the crack tip to initiate fracture and the second grain boundary in order for propagation to occur. As the stress magnification diminishes from the peak stress close to the crack tip, the large applied loads required to exceed the fracture stress at the second grain boundary explain the high toughness achieved in these materials.

It was found that the model worked well on the lower shelf but was unable to capture the temperature dependence of toughness in the transition. This is due to the insensitivity of the yield stress in the temperature range where the toughness is changing most (see Figure B-18). However the Richie-Knott-Rice model did gather together and introduce several important concepts, the most important being the idea of a critical stress over a critical distance; essentially this still holds true and is a useful description of the fracture process.

At this point it is worth discussing the use of ‘nil-ductility temperature’ as a measure of material toughness. Without a good physically based model, the steel industry was left to its own devices; predominantly concerned with the failure of ship and boiler plate, the industry had slowly developed a system of impact testing to establish the toughness properties of steels used for construction of these structures. Originally developed at the beginning of the 20th century, impact testing was used primarily for quality control during steel manufacture. These tests were conducted at room temperature and offered little information for in-service properties of the material. Impact transitions became the norm by the middle of the century and allowed comparison between heats of material. Toughness was still of prime concern and a measure of the nil-ductility temperature (NDT), i.e. the highest temperature at which complete cleavage failure occurs (see Figure B-20), was a useful measure for ship

applications. If the NDT were lower than the possible service temperatures then no brittle fracture would occur; this is essentially designing for the ship structure to remain on the upper shelf in service.

It was not until the advent of fracture mechanics that true toughness information could be gathered and compared. As no physical model existed that could describe the temperature dependence observed in these materials an empirical approach was adopted. It was noted that the relative temperature dependence of the limited number of steels that had been tested thus far was similar and a reference temperature could be used to normalise the values on to one curve. Using the experience of the shipping industry a modified NDT was adopted as the reference temperature used to compare the toughness of different heats of material.

Due to the scarcity of toughness information and ease with which both impact and drop weight-testing information could be gathered a holistic approach to the reference temperature was adopted. The NDT temperature established from drop weight testing would be supported by Charpy impact testing to establish a reference temperature for the heat. The very limited number of toughness tests prevented the use of direct comparisons between toughness, drop weight and impact data and as such the reference temperature nil ductility transition or RT_{NDT} was used for analysis.

The RT_{NDT} is defined as the higher temperature of either:

1. the NDT temperature, or
2. the temperature 33.33 °C below where the Charpy lateral expansion transition exhibits 40 mils (0.016 mm), , and three specimens meet a minimum requirement of 68 J.

Equation B-3 $$RT_{NDT} = Max\{NDT, T_{40} - 33.33\}$$

The nuclear industry required a design curve to demonstrate the safety of the heavy section plates and forgings used for reactor construction. In order to construct a deterministic failure curve, all available toughness data was plotted normalised by the RT_{NDT} reference temperature (see Figure B-21, which includes extra data to that used for the initial determination). The scarcity of toughness data at that time resulted in a large test programme being conducted to provide more data [7], giving rise to the nickname of the ‘million dollar curve’.

The Heavy Section Steel Technology (HSST) programme was developed to assess the fracture toughness of low alloy steels under plane-strain conditions. The high toughness of the A533-B material used for the programme required that very large test specimens be used to maintain plane-strain conditions in accordance with the testing standards of the time, such as ASTM E399 [8]. A special plate, designated HSST-02, was produced such that a small number of 12T compact tension specimens could be tested (see Figure B-22). The scale of these specimens and the likely problems with testing are difficult to comprehend; however, the data generated in this programme form the basis of all toughness modelling.

Plotting all the data together presented a problem; several very low data points stand out against the others, such that the failure curve had to be drawn below these values resulting in a very conservative model for the toughness behaviour of these materials. This became the standard design code for fracture safe structures [43] and is still in use as the basis for design codes in many countries; it has not been until the recent trend of plant life extension that the limitations of this aspect of the design code are truly being felt.

The curve was originally hand drawn as a lower bound to available data and published in the ASME code in 1972 [43]. At this time the Electrical Power Research Institute (EPRI) undertook a large scale-testing programme further to refine the modelling approach and supply much needed data to support the approach. This information was complied and published as the EPRI database [44]. By the end of the 1970's, further assessment had been made on the database resulting in a EPRI special technical report, EPRI SR-719 [45]. This included a mathematical description of the temperature dependence; however, the conversion from imperial to metric units was incorrect. This error was subsequently corrected and the expression, with RT_{NDT} as the normalising temperature, has remained unchanged since acceptance.

Once the method for establishing NDT is understood it becomes obvious why it is not a good measure of the toughness of these materials. The NDT is established by drop weight testing of material, starting at one extreme of temperature and testing until the fracture criteria have been met. The fracture criterion is such that they have little to do with initiation toughness; the criteria are met when the cleavage crack initiated in an as deposited weld bead fails to propagate to either of the two sides of the specimen. As can be seen this test then takes on a very specific meaning. NDT is the temperature at which the material can arrest a running crack within the confines of the specimen; it bears no relationship to the initiation stages of fracture, the property that is trying to be correlated, as a brittle crack starter is designed into the test piece.

Accepted models of toughness behaviour still have a very large empirical element to them; however, they do contain a physical basis for the behaviour that is observed. The measurement of most physical phenomena commonly results in some experimental scatter; the scatter observed in toughness measurements however is inherent to the material and attempts have been made to provide a physical model of the scatter. A natural evolution of the RKR model was to consider a stressed volume

ahead of the crack as opposed to concentrating on the crack plane itself. The 'local approach' to fracture offered some explanation for the scatter observed and is still used by many researchers [30, 46].

B.2.4.2 The Local Approach to Fracture Modelling

The local approach divides the plastic volume ahead of the crack front into a number of distinct elements. Failure in one of these individual elements constitutes failure of the specimen; by using this weakest link approach a Weibull distribution can be used to describe the failure probability of the entire crack front. The so called Weibull stress, σ_w, can be calculated from finite element analysis of the specimen or structure and loading situation

Equation B-4 $$\sigma_w = \left(\sum_{V_p} \sigma_1^{\,m} \frac{\Delta V}{V_0} \right)^{\frac{1}{m}}$$

where V_p = the volume of the plastic zone

σ_1 = the maximum principal stress in an element

ΔV = the volume of element experiencing the principal stress, σ_1

V_0 = a small arbitrary reference volume

m = the inhomogeneity modulus of the Weibull model

The Weibull stress includes the critical stress and distance measure, in this case volume, of the Richie-Knott-Rice model but includes inherent material heterogeneity to describe the scatter obtained from toughness testing. A Weibull distribution is used to model the potency of the initiators in the material and application of the weakest link model means that only the most potent of these need be considered in analysis. The Weibull stress is then the cleavage failure stress of the most potent initiator in

each element. Comparing this to the intrinsic cleavage failure stress of the matrix, σ_u, allows the development of a cleavage failure probability, the cumulative distribution function of which is given below:

Equation B-5 $$P_{failure} = 1 - e^{-\left(\frac{\sigma_w}{\sigma_u}\right)^m}$$

where σ_w = the Weibull stress

σ_u = the cleavage failure stress of the matrix

The local approach provides a means of describing the scatter observed in the measurement of toughness in low alloy steels, though it does have some major drawbacks. The inhomogeneity modulus is a measure of the potency of the initiators in the stressed volume ahead of the crack tip; this will vary with each material. No two materials are alike and as such the distribution of grain boundary carbides, flow stress and grain size will vary. The value of m must then be determined experimentally for each material over a range of temperatures. The number of tests required to establish a good fit of the m value makes this prohibitive, especially for the assessment of irradiated structures where only small volumes of material are available for testing.

If the experimenter has sufficient material to test then it is possible to show that the local approach method provides a very good fit to the data. This is the first model to link a postulated failure mechanism to the observed trends in the recorded data successfully, in this case the weakest link theory of fracture in these materials. However, the model is itself very simple and gives no real indication of the underlying mechanism, just that failure is achieved when an element fails, not the actual micro-mechanisms taking place within that element.

B.2.4.3 Statistical Modelling of Single Temperature Scatter

The local approach represented a significant leap in the understanding of brittle fracture on the microscale; however, the large number of tests required to calibrate the model means that the engineering applicability of the method is limited. As discussed elsewhere in this thesis, availability of material is often limited due to operating conditions or simple material cost. Empirical and physically-informed empirical models have fulfilled this requirement, by removing some or all of the fitted parameters, and in the past three decades become a front-line argument in the safety assessment of components [47-48]. The RT_{NDT} method for toughness prediction has a number of undesirable properties; the most major being the lack of a direct link between RT_{NDT} and measured toughness, the second being that this method does not take account of the inherent scatter observed in the data.

Initially, due to the very limited amount of data available, the observed scatter was believed to be due to normal experimental errors [49]. With the invention of more complicated elastic-plastic toughness measurement techniques it became possible to perform toughness testing on reasonably sized specimens that could be accommodated by most laboratories. As the availability of data increased it became obvious that the scatter was not simply due to experimental error and that a material factor was present. Statistical analysis of a rotor steel data set (see Figure B-24) showed that the J_c data conformed well to a two-parameter Weibull distribution [41]; sparking a more statistical approach to the assessment of scatter, which continues today.

In order to confirm that the scatter was in fact due to a material factor fractographic assessment of the specimens revealed that the distance of cleavage initiation sites from the crack front corresponded well with the measured toughness of the specimen

[50]. The authors, Landes and Shaffer, postulated that the effect was caused by a weakest link mechanism and as such there will be a size effect when comparing data from different specimen sizes. This introduced the concept of size correction by means of the Weibull survivor function (a description of which is given in a later section). This work was the first step in the production of a highly useful and generally applicable modelling approach; however, the work concentrated on J_c, a parameter that is useful in representing energy but has little engineering applicability.

In order for the model to be of use it must be expressed in terms of the elastic-plastic stress intensity factor, K_J, see Equation B-6; this then allows direct comparison of flaws and loading situations as would be found in real components to the model. The early model also had an undesirable mathematical discrepancy, without a lower bounding toughness the model predicted that the toughness of materials could approach zero. Low alloy steels exhibit a lower shelf toughness somewhat higher than zero so the model was not representative. The work of Wallin [51-52] corrects for this by introducing K_{J_c} as the measured parameter, commonly established via J_c, and K_{min} as an absolute minimum value of toughness (see Figure B-25).

Equation B-6: $$K_J = (JE')^{\frac{1}{2}}$$

where: $K_J =$ an elastic plastic stress intensity factor

$J =$ the strain energy release rate calculated via J-integral methods

$E' = E$ for plane stress conditions

$E' = \frac{E}{(1-\nu)}$ for plane strain conditions

The selection of K_{min} is somewhat arbitrary. A value of 20 MPam$^{0.5}$ has been selected for a number of reasons, namely that, to the author's knowledge, no value

has been measured below 20 on steels for which the Master Curve is deemed to be applicable. A statistical estimate of the K_{min} parameter is not possible with any accuracy, as the datum by definition will lie some distance from the data used in its assessment. Wallin gathered together all available data and performed a sensitivity study on the Weibull shape given the selection of a constant K_{min}. It was found that as the number of specimens, and hence accuracy, in a dataset increased, the Weibull shape converged towards a value of 4 [53], showing good agreement with the volume scaling relationship developed as the basis of the Master Curve [49]. A Monte Carlo simulation followed, the famous Wallin funnel diagram (see Figure B-26), which demonstrated that in order to accurately establish the Weibull shape of the parent distribution datasets in the order of 100 specimens or more are required [51].

The Weibull shape and K_{min} can then be considered material independent parameters [49, 51, 54]. Combined with the size correction methodology (which will discussed as part of the development of the model used in this work) proposed by Landes and Shaffer, the work of Wallin provided a very usable method of predicting the scatter in toughness results and allowing comparison between datasets by conversion to a reference crack front length.

B.2.4.4 Relative Temperature Dependence of the Transition Region

The next stage is to account for the temperature dependence of the transition and the measurement of toughness within it. It had been reasoned that the temperature dependence of transition toughness was the same for all low alloy steels since the creation of the limiting curve shown in Figure B-21. The development of the temperature dependence model is not well documented; however, a number of observations make the jump a fairly simple step to make:

- The ASME initiation, K_{IC}, and arrest, K_{IA}, curves offer a simple method of establishing the temperature dependence of the transition. This simple exponential function is easily adapted for other variables.
- With two of the three Weibull parameters, shape and offset, determined only the Weibull scale is free to change. A review of data from early round-robin testing programmes confirmed that the scale and offset of the distribution could reasonably assumed to be temperature independent.

Combining the above into a unified method results in a temperature dependent Weibull scale. The Weibull scale can be easily established for a dataset once the underlying distribution is assumed. For single temperature data, the scale parameter can be resolved by simple rearrangement of the Weibull expression therefore showing that the scale is equivalent to a probability of failure of 63.2 % [55]. This value can be read from a log-log chart or established via the function used for linear regression. The temperature dependence of the Weibull scale parameter is the Master Curve believed to apply to all steels within a range of applicability. The curve can be located on the temperature axis by selection of a reference temperature, much like RT_{NDT}, based on a known value of toughness. Following from empirical observation, there are two parts that the Master Curve attempts to address:

1. The distribution of toughness at a single temperature,

Equation B-7 $$K_{Jc} = K_{min} + Scale\left[\ln\left(\frac{1}{(1-P(x))}\right)\right]^{\frac{1}{4}}$$

where: $K_{min} =$ the threshold toughness value, 20 Mpam$^{0.5}$

$Scale =$ the temperature dependent Weibull Scale

$P(x) =$ the failure probability of interest

2. The relative temperature dependence of the scale of the distribution used to describe the scatter

Equation B-8 $$Scale = 11 + 77e^{0.019(T - T_0)}$$

where: $T =$ the absolute temperature (in °C)

$T_0 =$ the reference temperature (in °C)

The Master Curve has now been widely adopted by the fracture community as a useful tool in the estimation of transition toughness behaviour. The Master Curve is based on a number of assumptions that allow it to be used for a wide range of materials. The assumptions are:

1. All ferritic steels share the same failure mechanism in the transition region.
2. Failures conform to the weakest link model
3. All ferritic steels exhibit the same relative temperature dependence in the transition region.
4. Small scale yielding conditions exist across the entire crack front length.
5. The lower limit of toughness is material and temperature independent.

By making these assumptions it is possible to take a similar approach to that of the 'million dollar curve', except here the toughness data themselves are used to calculate the reference temperature. In order to do this, the data must first be size corrected to a convenient crack front length, the mathematics and physical reasoning for this are explained elsewhere within this work (see C.3.2); Figure B-27 graphically shows the effect of the size correction on postulated failure probabilities. This allows data to be plotted on the same toughness axis knowing that they are equivalent, i.e. a toughness measurement on a larger specimen will be equivalent to a higher measurement on a smaller specimen, plotting uncorrected data therefore does not

allow for direct comparison of different materials. As the relative temperature dependence and scatter is fixed the data can be used to establish a reference temperature, T_0, for the material.

In the context of the Master Curve method, the reference temperature, T_0, has a very specific meaning: *it is the temperature at which the median toughness of the material for a 25 mm defect is equivalent to 100 MPam$^{0.5}$*. This mathematically corresponds to a balance point in the median toughness when alternative exponential coefficients are considered (see Figure B-28). Applying this method to the original million dollar curve data clearly removes the outlying points from the plot, providing increased confidence and a large reduction in conservatism compared to the NDT methods used previously. Bar some exclusions for particularly low or high strength materials [9] the Master Curve appears to hold true for a large number of materials in a variety of conditions. Due to the adoption of maximum likelihood methods the transition behaviour of a material can be established with known uncertainty from a very small number of tests, as few as six valid results.

The Master Curve estimates the scatter of toughness across the temperature range as a change in the scale parameter of a 3-parameter Weibull distribution as a function of temperature, normalised by T_0. The shape and offset parameters of the Weibull distribution are assumed to be the same for all applicable materials, this assumption can be made on the premise that the fracture mechanism for all ferritic steels is the same.

The idea proposed by Smith [37] of fracture nucleated at grain boundary carbides suggests two controlling mechanisms, the distribution of initiators ahead of the crack and the opening stress on the micro-crack due to dislocation motion. It is believed that, as there are numerous such potential sites of initiation in all low alloy steels a

suitable initiation site will always be found. The opening stress is controlled by dislocation motion in the material; as all low alloy steels behave as a modified iron carbon matrix, the movement of dislocations will be similar for all. The variation in absolute temperature dependence between heats can then be postulated as microscopic effects on the movement of dislocations within these materials.

The Master Curve is also a fully probabilistic method; a series of representative probability bounds is given in Figure B-29. Those wishing to use it for deterministic analysis are required by definition to use the value of the lower limit. This of course is unacceptable and the use of the Master Curve for risk informed or fully probabilistic analysis is highly beneficial compared to the ASME Code method using NDT outlined above. Here a reasonably low probability of failure can be used as the ‘below all points’ design curve with the knowledge that the master curve is applicable through life. Using the Master Curve method certainly has advantages over the ASME Code method, but it still contains some hidden flaws.

It has been observed that the Master Curve is excessively conservative in the lower tail. The Master Curve is believed to capture the distribution of initiation toughness well, i.e. the required stress intensity factor to meet the three criterion of Tetelman et al [19]. In reality it only captures the first two stages of failure: initiation and injection. At higher values of stress intensity factor the conditions for the third, propagation, will be met instantaneously. At low applied stress intensity factors the propagation criterion may not be met resulting in a non-propagation micro-crack event; the term ‘micro-crack arrest’ or ‘microarrest’ has been adopted as a name for the phenomenon.

This effect is very difficult to quantify, as it would require measurement of arrest behaviour on the microscale, a method for which has yet to be determined in

predominantly homogeneous and tough material. Evidence of these arrest events can be found in the study of poor toughness materials showing heterogeneity on the macro scale. A measurement of the micro arrest toughness of the material is beyond the ability of current experimentation techniques; however, it was proposed by Williams et al [23] that the macro arrest toughness could be used as a surrogate for the arrest properties on the micro scale. Following the work of Wallin on an arrest master curve it became apparent that the initiation and macro arrest distributions overlapped. By comparing a randomly generated initiation value to a randomly generated arrest value, it was possible to build up a record of failure and microarrest against temperature. Williams et al demonstrated that this showed better agreement with observed trends in the lower tail; a detailed description of this method is given in section B.3.3.

B.2.4.5 Other Statistical Models of Fracture in the Transition Region

A number of other statistical models of fracture are presented in the literature. These offer alternative methods to those described above for the prediction of transition toughness fracture behaviour. Models fall broadly into two disciplines, those based on physical measurement and those based on stress analysis. The RKR model [28] already discussed epitomises the physical measurement group through grain size dependence, although more modern models also exist, such as the Ortner-Hippsley model [32] which uses fractrographic measurements to estimate toughness.

The alternative approach is based on a stress model of the geometry considered and the discretisation of the volume ahead of the crack front. Here a set of criteria are assessed by the model, commonly the comparison of the local stress to fracture stress for the element. As probabilistic methods came to the fore, the fracture criteria have been randomly sampled from assumed distributions. A number of methods have been proposed for this model type. The Beremin model [30] being the first,

which has then been modified and extended in a number of models such as that proposed by Bordet [56-57] and the Unified Curve method [58-59].

The WST model [29, 60] bridges the gap between the two methods by using a physical measure, in this case initiating particle size. All of these models make assumptions over which is the controlling parameter for fracture, and in many cases a number of the model parameters cannot be measured and must be assumed. All of these models assume a much simplified stress state ahead of the macro-crack and do not take account of crystal plasticity effects. Other models have attempted to circumvent these simplify assumptions by assessing the interactions of dislocations and initiating particles. Of most promise are those proposed by PEAI [61], extending the dislocation pile-up assessment of Yokobori [62], and that due to Noronha and Ghoniem [63-65], building on the crack tip shielding assessment of Roberts [66-67] . If these models prove successful it will demonstrate a complete understanding of the fracture process; however, they are not yet capable of truly capturing the absolute temperature dependence and scatter of transition toughness behaviour, it is expected to be several years before these models are fully applicable.

The physically-informed empirical approach adopted by the Master Curve is very successful and high applicable, but in some instances it has been found to be too simple. The complex macro-structures of some steels means that a region of homogeneous material from which enough specimens can be taken for a toughness determination may not exist. In these instances, the statistical nature of the Master Curve network can be exploited, allowing assessment of varied microstructures in one dataset [68]. A set of empirical rules have also been proposed to identify when a material shows excessive homogeneity, the SINTAP procedure [69]. This provides some level of protection against optimistic toughness assessments.

In all assessment methods and toughness models the crack front is idealised to a straight, planer defect. In the real world cracks can come in manner of shapes but the most common is semi-elliptical fatigue crack which emanates from an initiation point. The stress state of this crack continuously changes along a curved crack front, complicating the statistical assessment of fracture as the driving force is not uniform in the potential fracture process volume. For an irradiated vessel or quench rate affected material, the mechanical properties of the material (including fracture resistance) varies as a function of depth, yet further complicating any assessment. A method has been proposed to deal with these effects but is yet to achieve standardisation or safety application [70].

Moskovic [71-72] has developed a competing-risk analytical model of fracture toughness properties in the transition temperature regime. This model requires complex statistical and probabilistic analysis. Experimentally, a knowledge of the ductile tearing prior to cleavage failure is required; this model is therefore difficult to apply in all circumstances to literature information where only minimal test measurements are supplied.

B.2.5 Elastic-Plastic Fracture Mechanics and Constraint Correction

Linear-Elastic Fracture Mechanics (LEFM) solutions are based on the assumption that the defect exists in a semi-infinite plate or structure, or that the structure is so large that the stress state ahead of the notch is unaffected by the presence of free surfaces.. In reality the material behaves in a manner similar to this ideal as long as elastic conditions are maintained. As has been seen the plastic flow of metallic materials very quickly creates a complex stress situation ahead of a crack front effectively creating an escape route for the build-up of high stress states toward free surfaces. This loss of constraint is effectively a problem of transferability, or how much belief can be put in the toughness values established with small specimens compared to large structures? The early developments in the toughness testing of materials used specimens of sufficient size to create a pseudo-elastic stress state in the specimen; the specimen size has reduced significantly with the adoption of J-integral as a more realistic measure of applicable toughness.

The high toughness of modern materials precludes the use of pseudo-elastic specimens as they would simply be too large to test except at very low and structurally irrelevant temperatures, both for economic and production reasons. However, the use of small specimens creates a significant problem for the accurate measurement of toughness, namely the loss of constraint giving rise to an over estimation of the unaffected toughness of the material. In a small specimen, it would be expected that significant bending or deformation of the specimen; could take place before cleavage failure of the specimen, in fact the high loads required to cause cleavage failure in these high toughness materials will often cause extensive plastic deformation at relevant temperatures. This is an effect of the presence of the specimen back wall, interfering with the development of the tri-axial stress state.

Figure B-30 Shows the effect of a close back wall on the peak and mean stresses in an idealised ligament.

The stress and strain distribution in material ahead of a sharp defect can be characterised, via the Westergaard functions [73], using only K, the stress intensity factor, for linear-elastic materials. When large scale plastic deformation occurs, K can no longer be used to characterise the stress and strain state ahead of the crack tip and the alternative J-integral method must be used. J is used in the same manner as K, i.e. J can be used to characterise the stresses and strains ahead of sharp crack in a material exhibiting plastic deformation. However, the solutions are more complex and were developed independently by Hutchinson [74], and Rice and Rosengren [75]. and are therefore known as the HRR solutions. These solutions still assume that the region of high stress is small compared with the size of the structure, i.e. the geometry is under ‘small-scale yielding conditions’, the plastic zone is constrained by the surrounding elastic material, and a high level of stress triaxiality is maintained ahead of the crack.

In finite size geometries such as fracture mechanics specimens, the plastic zone can become a significant proportion of the uncracked ligament. Under such circumstances the level of triaxiality can reduce; particularly in tension specimens, or specimens containing shallow cracks. In both cases, plastic flow occurs towards the specimen boundary in an unconstrained manner and a low condition of constraint is generated ahead of the crack. By comparison, in a bend geometry the plasticity is constrained by the way plasticity develops. The strain fields form in logarithmic spirals which fall back and across the crack plane, therefore the plastic strain remains relatively low while the hydrostatic stress remains high, i.e. a condition of high constraint is maintained at the crack tip.

Under low constraint conditions, a single parameter such as K or J cannot characterise the stress and strain state adequately and a second parameter is required. Two approaches are widely used.

First, the elastic K-T solutions [76-77] provide a measure of the normal stress in the crack front plane (T-stress is the stress acting perpendicular to the applied load and parallel to the crack front) and recently the elastic-plastic J-Q methodology [10, 78-81] has further increased the accuracy of simulations. The Q parameter is not a true measure of an individual stress tensor but is a measure of the difference between the high constraint stress state, e.g. from the HRR solutions, and the true state of stress, e.g. established from finite element simulations of the cracked geometry of interest [82-83].

There are two possible approaches that can be taken to assess the effect of constraint loss in these specimens: an elastic-plastic analysis of the stresses in a given geometry, or an assessment of the distribution of prospective initiation events ahead of the crack front, a local approach method. The stress analysis is by far the simpler of the two approaches and will be dealt with first.

It has long been realised that the semi-infinite plate solutions of fracture mechanics do not completely capture the stress state in a small specimen. Initially concern comes from the stress generated along the length of the crack front due to Poisson contraction. At the specimen centre the contraction creates a stress acting parallel to to the crack front, the deformation is contained affording a high hydrostatic stress (plane strain) This stress acts against the sides of the specimens, which as free surfaces, are unable to support the load (plane stress) and cause the stress to dissipate requiring more load to be applied to achieve an equivalent stress at the crack tip as if the dissipation had not occurred (see Figure B-31).

The J-integral is used as a measure to establish the size over which large deformations occur. The stress acting along the normal to the applied load can then be established and applied to give the triaxiality that is achieved a short distance from ahead of the crack front. The effect of increasing applied load against the actual stresses ahead of the crack front can then be established. This gives a characteristic driving force curve, the ‘trajectory’, for the loading conditions evaluated. In order to establish an empirical trajectory the material must be tested in various loading conditions and geometries to give various constraint levels [84]. If accurate trajectories are required the shear number of specimens that must be tested becomes impractical, if this is coupled with the observation that the shape of the trajectory may be temperature dependent then this method seems even less attractive; fortunately there is an alternative, the use of elastic-plastic finite element modelling.

The basis of the local approach to fracture is that a cloud of initiators exists in the material. If the failure criteria for these defects is postulated, it is possible to calculate the volume of material ahead of a crack tip that meets these criteria for a given loading situation. The failure criteria from previous sections can be simplified to effectively one simple criterion for this type of analysis, the local stress must exceed some critical value for failure to occur. This accommodates both requirements for a plastic zone; the critical stress will certainly be higher than the yield stress giving rise to a plastic area ahead of the crack tip, and a sufficiently large peak stress to cause cleavage failure.

Crack tip stress modelling and the local approach can be combined by using the J-Q trajectories to calculate the stresses in the test piece, which in turn can be used to calculate the stressed volume meeting the failure criteria. This method has been applied with great effect in the work of Nevalainen and Dodds [10, 85]. Their work

simplifies the process further by calculating the ratio of the applied load to that which is available in the specimen for fracture. This difference is not just caused by the in-plane constraint loss caused by the sides of the specimens, the back wall also has a large effect and, depending on the specimen geometry, may be dominant. The presence of the back wall and side faces causes the small scale yielding conditions to be violated at even modest applied loads and as such both in-plane and out-of-plane constraint must be modelled accurately to produce a good scaling model.

This gives a modified stress field ahead of the crack tip. The Master Curve assumes that the shape and size of the plastic zone ahead of the crack tip is constant along the crack front length. It can be seen that this is not the case and that the size varies according to the presence of side grooves and the relative crack front length (see Figure B-32). This gives rise to a stressed volume ahead of the crack tip which bears little resemblance to the idealised volume assumed by the master curve method. To correct for this Nevalainen and Dodds recommend the use of an effective crack front length (see Figure B-33), easily calculated from the stressed volume divided by the maximum cross-sectional area of the volume.

The curve shape of each of the scaling models, each one particular to a specimen geometry, is consistent with a short region of proportionality before each breaks away from the 1:1 line signifying a loss of constraint. The curves have therefore been modelled in two sections:

$J_{avg}/b\sigma_0 \leq$ limit of proportionality, $J_0/b\sigma_0 = J_{avg}/b\sigma_0$

$J_{avg}/b\sigma_0 >$ limit of proportionality, $J_0/b\sigma_0 = f\left(J_{avg}/b\sigma_0\right)$

where $f\left(J_{avg}/b\sigma_0\right)$ takes the form:

Equation B-9
$$f\left(J_{avg}/b\sigma_0\right) = \begin{matrix} b_0\left(J_{avg}/b\sigma_0\right)^{\frac{1}{4}} + \\ b_1\left(J_{avg}/b\sigma_0\right)^{\frac{1}{2}} + \\ b_2\left(J_{acg}/b\sigma_0\right) + \\ b_3\left(J_{avg}/b\sigma_0\right)^2 \end{matrix}$$

The ratio of effective to actual crack front length is approximated by a decaying exponential function and is also a function of the applied load expressed in terms of a J-integral: Assessment of Equation B-9 reveals that, as the expression contains a squared function, the trajectory will therefore be parabolic. This can be accommodated in assessments via the introduction of two potential censoring limits to coincide with the toughness at the limit of proportionality, $K_{J_c\,elastic}$, or at the maximum value of the trajectory, $K_{J_c\,\max}$, i.e. $max\left[f\left(J_{avg}/b\,\sigma_0\right)\right]$.

Equation B-10
$$\frac{B_{eff}}{B_i} = d_0 + d_1 e^{\frac{d_2 J_{avg}}{b\sigma_0}}$$

The failure criteria selected by Nevalainen and Dodds for use in the local approach aspects of the model is very simple. Failure will only initiate in regions of high stress where $\sigma_1/\sigma_0 \geq \sim 3$. Selecting this stress contour also defines the scaling model for J-integral. By adopting this criterion the work of Nevalainen and Dodds provides a simple method for establishing the actual toughness of a material:

1. Correct applied load to true load to cause fracture, effectively the load contributing to fracture neglecting specimen bending, using toughness scaling model (Equation B-9).
2. Correct specimen thickness to a measure of the stressed volume ahead of the crack tip (Equation B-10).

A set of constraint correction coefficients for standard specimen geometries is given in Table B-1 and Table B-2.

From this work it is possible to calculate the load limit of a specimen for a given level of constraint loss. The load limit formula provides a means of establishing if a critical loss of constraint has been reached:

Equation B-11 $$b \geq \frac{MJ_{avg}}{\sigma_0}$$

where b = the ligament width, i.e. $b = W - a$

M = in plane deformation factor

J_{avg} = the externally applied load expressed as a J-integral

Initial recommendations in the Nevalainen and Dodds paper where for no or limited constraint loss; however, this proved to be so restrictive that a large number of test results are censored. The level of constraint loss is controlled by the selection of an appropriate value of M in Equation B-11, the current recommended value in the E1921 standard is 30 [9], but some researchers have recommend values as high as 200 for SE(B) specimens to maintain a high level of constraint [84, 86]. A more reasonable balance was achieved by allowing a small constraint loss for a valid test has been adopted; this may have been an error and has resulted in a missed opportunity in the understanding of toughness data. The effect of constraint correction on toughness data will be reviewed in results of a database analysis in a later section. By simply selecting a limiting value the constraint correction has become partially excluded from current standard practice in the assessment of toughness data. It must be noted that even the modest application of load to a small

specimen will produce constraint loss and hence an over measurement of the true toughness of the material may result.

The effect of constraint loss is also dependent on the hardening behaviour of the material. A material with a more pronounced hardening response will maintain a higher level of constraint following plastic deformation and as such different trajectories are recommended for different hardening responses. The Ramberg-Osgood model [87] of tensile behaviour provides a convenient method of defining the strain hardening behaviour of a material using the following expression.

Equation B-12 $$\varepsilon = \frac{\sigma}{E} + K\left(\frac{\sigma}{E}\right)^{n}$$

Where K and n are material dependent variables. The expression can be rewritten to replace K with a yield stress dependent term further increasing the applicability of the equation for use with low alloy steels.

Equation B-13 $$\varepsilon = \frac{\sigma}{E} + \alpha_{RO}\frac{\sigma_0}{E}\left(\frac{\sigma}{\sigma_0}\right)^{n}$$

where α_{RO} = a material dependent factor

n = the strain hardening exponent

σ_0 = the yield stress of the material

The value of α_{RO} is commonly selected to correspond to the 0.2 % plastic strain offset, or 0.2% proof stress. The strain hardening exponent, n, provides a simple description of the strain hardening behaviour and is commonly approximated to 10 for low alloys steels, although it can be measured directly by fitting to tensile data.

A more complex method of constraint correction can also be generated using the local approach method defined above. Recent work by Petti and Dodds [80, 88-90] on the comparison of constraint loss between specimen geometries has produced yet further simplification to the process of applying a constraint correction. These recent methods, based on the local approach, provide simple trajectories that are applied as easily as those contained within the earlier work of Nevalainen and Dodds. As the local approach is adopted, the trajectories are dependent on the Weibull modulus, m, which requires calibration to the material. As this requires calibration for different material conditions, including irradiation, it is currently precluded from becoming a readily applicable method.

B.3 Crack Arrest

B.3.1 Arrest Toughness Testing and Mechanism

Compared to the mechanisms of ductile and brittle fracture, the available information in the literature on crack arrest is limited. The following is a description of the reasons for interest in this topic and the historical development of arrest testing which has played a crucial role in the development of fracture micro-mechanisms. Firstly, what constitutes a crack arrest event must be defined.

Crack arrest is the prevention of a fast running cleavage failure from further propagation; essentially the brittle failure is arrested and as such the component although heavily damaged, may still offer some level of structural integrity. Arrest first became of concern when the production of all welded ship hulls resulted in dramatic and catastrophic failures [91], such as those of the Liberty ships discussed in a previous section. The all welded construction affords a complete and continuous structure through which a fast running crack could progress unhindered. Previously, ships where constructed from riveted plates; this offered protection from complete failure in two respects. First, the plates are not fusion joined and as such are separate and distinct from each other so a running crack must re-initiate in each successive plate. Secondly, the method of hot rivet joining creates a residual compressive stress in the plates that it joins; this may be sufficient to reduce the crack driving force to low enough levels that the brittle failure propagation is halted.

Arrest toughness properties are particularly relevant to large welded structures such as ships where post weld heat treatment is difficult or can be demonstrated as uneconomical. The structure is therefore predominantly made up of two microstructures: the wrought plates used for construction and the fusion

microstructures of welds that join the plates. The microstructure of the plates can be controlled effectively and the mechanical properties will be consistent and easily determined. The weld microstructures will be complex in comparison and prediction of the mechanical properties, especially cleavage toughness, will be associated with significant scatter above that observed for wrought materials. The probability of creating local brittle zones within an industrial welding process is considered high and as such must be assumed to exist in a structure as large as a ship where there may be several hundred metres of welds.

With the acceptance of a probabilistic view of cleavage fracture it is therefore obvious that the brittle fracture resistance of the weld may be insufficient. This creates a problem when assessing the structure from a cleavage initiation standpoint; the likelihood of generating a cleavage failure is so high that a brittle fracture prevention argument is easily overcome. Here arrest toughness comes to the aide of the structure and the metallurgist generating the assessment. Acknowledging that brittle failure is a distinct possibility, if it can be demonstrated that the failure can be contained locally and not propagate throughout the structure then the safety of the structure can be assured.

Originally the cost of steels with high enough arrest toughness properties were prohibitive and this held back the use of all welded construction for a number of years. As steel making techniques improved to the extent where suitable steels, with low residuals and good mechanical properties, can be expected at economically viable costs, the shipping industry has moved to all welded construction. The driving force for developments and understanding in arrest toughness has now switched from the shipping industry to the nuclear industry. Arrest, in general, will not be invoked as a supporting argument to a safety case within the UK regulatory environment and is currently of little importance in the development of incredibility of

failure arguments. However, with the current generation of plants reaching the end of design life and undergoing plant life extension activities, arrest may once again come to the fore as a required avenue of research. In addition, the intended design lives of new build plants and future designs may have to rely on arrest arguments in order to achieve a justifiable plant life of up to 80 years.

Arrest has predominantly remained a purely empirical avenue of research compared with the initiation of brittle fracture and as such little development has been made in the development of physical or physically informed models. Testing has progressed through large laboratory tests to structurally representative experiments, and finally, small-scale laboratory tests, which provide good correlations to the large scale testing methods. Testing methods will be discussed in this work out of chronological order; i.e. structurally representative tests will be considered first, then the testing scale will be reduced to the point where valuable arrest information can be gained from small test specimens. The difficulties of establishing the arrest toughness of a material will be discussed at suitable opportunities throughout the following interpretation of arrest testing.

To demonstrate that arrest events can happen under the loading conditions achieved in a pressurised water reactor, structurally representative tests were conducted [92-94]. These commonly involved recreating pressurised biaxial loading conditions, as found in operation, into cylindrical large scale test pieces containing defects. The profile and depth of these defects was controlled and intended to represent the worst possible defect that could exist in a reactor pressure vessel; in actuality these defects will most likely be far more potent than any that exist in an operational reactor just to get brittle fracture to initiate. The test is then intended to establish if the initiated brittle fracture will run to completion.

The stress state in the test vessel can be achieved in one of two ways. The most dramatic is the spinning cylinder test, which introduces a mixture of radial, hoop and longitudinal stress by spinning a vessel [95] with a representative thickness a considerable number of revelations per minute. An alternative method, adopted for thin walled structures such as pipeline sections, is to use gas or liquids to create an internal pressure [96]. The methods can also be combined in a number of ways producing the most representative test of conditions during a worst case loading situation for a reactor vessel; a loss of coolant accident. The thermal stress generated during one of these events is considerable and may initiate a brittle failure (see Figure B-34).

The thermal stress and reduction in material temperature for this event will be attenuated through the wall thickness. This provides the possibility for crack arrest on two fronts: the driving force is being reduced as the crack propagates from the inner to the outer wall, and the absolute toughness of the material improves with increasing temperature and thus depth in the vessel wall. Both these effects independently could cause arrest of the fast running crack; the combination of both effects certainly lends confidence to an arrest event occurring. This provides a certain level of justification for undertaking such large-scale and expensive testing programmes.

The parameters of these experiments cannot be controlled to the same extent as laboratory tests, requiring that a large number of sensors are used to establish material response. Temperature gradients are measured with embedded thermocouples to ascertain the effect of low temperature coolant injection into the vessel. Strain gauges are used to establish the development of strain fields around the defects and on the expected crack path. Acoustic emission is used to record crack run-arrest events to provide an indication of the development of the crack throughout the experiment.

These tests afford proof-of-principle that arrest can happen under loading conditions consistent with that found in operation of structurally critical components. However, these structural representative experiments offer little information to help understand the arrest mechanism; for example, the presence of such a complicated mix of changing loading conditions and material properties through the vessel wall during a simulated pressurised thermal shock event makes it impossible to determine specifically why the crack arrested. Large-scale laboratory tests offer more control over the conditions of any experiment and, as will be discussed later, the size of such specimens resolves a particular issue with stress wave reflection.

Large laboratory tests offer an element of control that cannot be obtained with empirical or component tests. As opposed to empirical testing these experiments are not intended to produce a replication of a complete failure event, i.e. initiation of brittle fracture and possible crack arrest under expected loading conditions. Large scale laboratory tests are intended to measure the crack arrest properties of the material only. This requires that steady state crack propagation is created in the specimen; this in turn requires suitably large specimens to provide a long crack path within which to test.

The first of these tests to become widely used was the Robertson crack arrest test [97]. Here a plate of the material of interest is welded to other plates top and bottom such that a load can be applied evenly along the long edges of the specimen (see Figure B-35). This is intended to create a uniform driving force across the entire specimen. A running brittle fracture is introduced by using an impact to the side of the specimen, which contains a brittle starter notch. The result of this test is simply pass or fail; however, there are a few conditions on the validity of the measurement. The

most important of these validity conditions is how far the crack jumps during a run-arrest event.

Stress waves are introduced into the sample due to the impact and release of strain energy at the initiation of brittle fracture [91, 98-99]. The stress waves radiate out from the initiation site and the propagating crack and are reflected at the specimen boundaries; if the waves return to the advancing crack front the interaction may be sufficient to cause crack arrest. Once the stress wave passes, brittle fracture may re-initiate causing a series of run-arrest events, easily detectable by acoustic emission. The validity criterion then becomes a measure of the distance that the crack runs before arrest; the crack must grow far enough from the point of initiation such that it can be considered a running crack, but not so far that the arrest event will be caused by a reflected stress wave.

Initially the temperature of the tested plate was uniform allowing only the measurement of crack arrest temperature in a similar method to nil-ductility temperature (as discussed in an earlier section, and to be revisited in this section). A single test simply provides information if a running crack will arrest at the test temperature chosen; this, unsurprisingly, is a very expensive way to determine the temperature related arrest properties. A development of the wide plate test is to introduce a temperature gradient across the specimen width [100]; cold at the point of initiation and hot on the opposing flank of the specimen. The likelihood of an arrest event is increased significantly, therefore reducing the economic cost of each test series.

By using a temperature gradient across the specimen the point of arrest can be used to calculate the temperature at which the crack arrested. This creates results across a wide temperature range for a limited number of large scale tests, increasing the

economy and usefulness of such testing. The introduction of a temperature gradient removes the arrest/no-arrest nature of the testing therefore allowing the temperature dependent properties of arrest toughness to be explored. The output from such testing is still defined as the temperature at which arrest will occur, and is commonly designated the crack arrest temperature (CAT) [91].

An alternative approach to generating sufficient data for the construction of arrest temperature relationships is to use small test pieces. These methods introduce a fast running cleavage crack but the specimens are of insufficient size to allow development of steady state propagation. The loading conditions in test specimens are also different to the structure due to constraint loss. It is plausible that the structure may have a linear elastic response at a temperature which coincides with ductile and arrest behaviour in the specimen; as such care must be taken in the direct application of arrest properties established from these tests.

The results of three simple testing procedures have been found to correlate well with the CAT as established by larger empirical testing procedures. The first of these approaches to be considered here, drop weight testing [101], is a direct measurement of crack propagation. As discussed in an earlier section of this work, the output of a drop weight test is a simple arrest/no-arrest at a given temperature. The NDT as established by this method shows a good correlation to the CAT from large scale arrest tests, with the inclusion of a margin to take account of the difference in constraint between the specimen sizes [102].

Another alternative to the measurement of arrest toughness directly is the correlation of CAT to other mechanical properties, predominantly from fracture surface features following impact testing. A development of the drop weight test is the drop weight tear test [103]. This utilises a larger specimen thickness than the requirement for drop

weight testing (19 mm compared to 16 mm) and a shallow pressed notch as a crack starter. An impact to the specimen causes fracture and the surfaces are assessed for the ratio of shear to cleavage surface area; the test is then repeated over a range of temperatures to establish the fracture appearance transition. It is found that a good correlation exists between the 75% shear fracture appearance transition temperature (FATT) and the CAT established from larger tests [96].

The final empirical correlation method is to use a similar approach to drop weight tear testing but applied to the fracture surfaces generated from Charpy impact testing. The commonality of the Charpy impact test means that this approach is much more easily adopted, as it does not require bespoke test equipment. The information generated by Charpy testing can also be used for other purposes, namely, specification acceptance requirements and quality control; therefore, a significant number of Charpy tests have been performed. This approach is not without faults as the issues of specimen size are exaggerated by the use of yet smaller specimens.

The fracture surfaces can be assessed in a similar way to drop weight tear testing and a fracture appearance transition created. Correlations to a number of different shear fracture percentages have been proposed, but the most promising has been for 50% shear FATT [102]. These correlations show significant scatter, the primary cause for which is believed to be the fact that the material may show brittle crack propagation in fracture mechanics testing at temperatures which would be considered upper shelf for Charpy impact. This difference is due to the way in which the Charpy test is performed, as a complete simulation of a failure event containing both initiation and propagation to failure.

Comparison of absorbed energy from Charpy impact testing to arrest properties yields further difficulties. The energy absorbed during an impact test is a combination

of the initiation and propagation stages. The high quality and low inclusion content of modern materials requires a large amount of energy to initiate the failure; however, once the cleavage crack is running it absorbs a very small amount of energy. The initiation and propagation stages can be separated by instrumented Charpy testing. A considerable amount of information about material behaviour can be established from the load-time trace of an instrumented Charpy test (see Figure B-36). The different stages of initiation and propagation are clearly visible on the load-time trace, allowing distinctions between energy absorption for each stage. Successful correlations have been made between the temperature dependence of energy absorption following a brittle event and the CAT [91].

A more direct approach to establishing the crack arrest properties of materials is to measure the arrest toughness in fracture mechanics type tests. These are analogous to initiation fracture toughness testing, utilising similar sized specimens and loading conditions. The use of fracture mechanics to assess the arrest event provides transferability to different crack depths and applied loads such that the potential for arrest can be calculated. A number of different testing geometries have been utilised; however, only one has been standardised by ASTM, the compact-crack arrest test [104].

The compact-crack arrest specimen shares a number of similar features with the other arrest tests discussed above; however, the brittle failure is initiated not by an impact but by a steadily increasing load in the material. A starter notch with a non-heat treated weld is opened by a wedge and the crack opening displacement is monitored (see Figure B-37). The arrest toughness is then established from the opening displacement at the point of arrest.

Of great importance to the fracture mechanics testing of arrest properties is the length that the crack runs before arrest and the path that is taken. The crack must grow a suitable distance to be considered a running crack, a feature that cannot be achieved in the smaller empirical test specimens outlined above. If the crack diverges significantly from the original fracture plane then the use of simple fracture mechanics, assessing against defect depth and applied load only, cannot be performed. The compact-crack arrest test geometry was chosen for standardisation as it increased the likelihood of maintaining a straight crack path while offering sufficient crack jump lengths [105].

The use of side grooves is also permitted to help maintain a straight crack path and the creation of plane-strain conditions across the advancing crack front length. Side grooves will also decrease the likelihood of crack tunnelling due to ductile tearing at the surfaces of the specimen; this would slow the crack advance significantly at the specimen surfaces and may lead to an incorrect measure of the bulk properties.

By measuring the crack opening to calculate arrest toughness the value is considered to be quasi-static, as it is for initiation toughness testing, as no information about the propagation of the crack is required. In reality, the arrest toughness corresponds to a dynamic process and as such a further parameter needs to be considered, the dynamic stress intensity factor [91, 99]. It can be shown that the dynamic stress intensity factor and the static value of arrest toughness are equivalent at the point of arrest; however, preceding and following the arrest event the two can differ widely.

The dynamic stress intensity factor is affected by the reflection of stress waves in the material. As discussed previously for large scale testing, a requirement for the validity of the test is that returning stress waves do not interact with the advancing crack

front. In this instance the reflection of stress waves has a very large effect on the dynamic stress intensity factor experienced at the crack tip, causing large fluctuations in the stress intensity factor following an arrest event. This can lead to a number of crack jumps until the stress waves dissipate. If the crack front arrests before the stress waves return then the arrest toughness can be established from the static value; if the arrest is caused by stress wave interaction it is not possible to determine the loading conditions and hence no arrest toughness data are afforded.

The testing methods outlined above do not provide a physical reasoning for arrest to occur; arrest is a material response to the presence of a fast moving cleavage crack and as such the propagation of such cracks must be considered. The mechanisms of cleavage propagation have not been explored as extensively in the literature as the mechanisms of cleavage initiation; this is most likely due to the fact that once a cleavage crack has initiated the component will, by most definitions, fail. Some experimental programmes have attempted to assess the controlling factors of crack propagation and the resulting fracture surfaces.

A number of significant features exist on fracture surfaces that have formed during steady state propagation; some are dependent on the speed with which the crack progresses, others on the heterogeneity of the material. First to be considered are the characteristic river patterns that are seen on most cleavage fracture surfaces. These patterns are in fact small ligaments which failure in a ductile manner between primary cleavage cracks that radiate from the point of initiation; this can be used to aid finding the point or region of initiation on a test specimen.

When a cleavage crack has more material in which to propagate such that a steady state velocity is achieved, a number of river patterns combine to form chevron markings. This produces a series of ‘V’ shaped features on the fracture surface, the

root of which points towards the initiation site. It has been suggested that these markings are created by re-initiation of the cleavage failure ahead of the primary crack front caused by stress waves emanating from the advancing crack front; in this way the crack front progresses by a stop-start mechanism [106-107]. The reason for the characteristic ‘V’ shape of such makings is due to the location of the re-initiation points; these will preferentially occur at the centre thickness of the component or specimen due to the increased constraint in this region compared to the surfaces.

If the crack accelerates beyond steady state growth the crack front will move with sufficient speed to interact with the shear stress waves that precede it. When this occurs, the direction of maximum stress experienced by the crack front will no longer coincide with the applied load and the crack will branch in alternative directions influenced by the shear stress [108]. This is unlikely to occur in the specimen sizes used for laboratory experiments but can be clearly seen in a number of failures in large components. For low crack velocities the radial shear stress is comparable to static conditions resulting in a planar crack front.

Another feature commonly noted on cleavage cracks is surface roughness. It would be expected that cleavage failure should result in a macroscopically smooth surface as the energy absorption of such failures is negligible and they occur nearly instantaneously. It is often found that the crack path of the cleavage failure is anything but direct. This could be due to a number of factors. The crack front roughness appears to be a direct result of the speed with which the crack front is moving. In the early stages of propagation the crack front appears smooth, as the crack accelerates towards steady state propagation the surface roughness increases until a chevron pattern appears; the crack then branches and a similar cycle is repeated [109]. The roughness is believed to be caused by the interlinking of small areas of cleavage failure due to micro cracks which initiate ahead of the growing

crack front; these failures occur at different heights compared to the crack front and the resulting coalescence via shearing of the remaining ligament results in a roughening of the surface [99, 110-111].

Arrest of a fast moving crack may happen in a number of ways depending on the external forces and the materials capacity to arrest. The most obvious way to arrest a crack is removal of the driving force; however, this is only a viable option in a limited number of circumstances. One possible instance would be for a through-wall defect in a gas containing pressure vessel; the escape of the gas may be sufficiently rapid to lower the internal stresses and halt crack advance, although a considerable distance may have been covered in this time. For the majority of defects, the load cannot be removed quickly enough to prevent complete failure of the component.

The driving force can also be reduced, or even reversed, by the presence of reflected stress waves within the material. These cause arrest by interacting with the applied stress field and are the reason for such difficulties in establishing valid arrest toughness measurements. No advantage of this process can be taken in safety assessments of components due to the highly complex nature of the stress state and stress wave propagation that result; these cannot be readily predicted and therefore cannot be used for assessment. Also, many structures are of sufficient size that by the time a reflected stress wave has returned to the crack front the defect will be very large. The stress wave may also only delay the propagation momentarily and once the wave has passed, cleavage failure may re-initiate, or the reflected wave may reinforce and increase the applied loads at the crack tip.

A considerable number of material factors will affect the propagation and arrest of cleavage crack. First, as the crack moves from one grain to the next it must change direction to the cleavage plane of the second grain before it can proceed. The

propagation model proposed by Qiao [34-35] and discussed in a previous section provides a plausible explanation for how this may occur. Each propagation event may use a small amount of the available strain energy; this can result in arrest in the very early stages of propagation if the energy barrier is too high or may help to slow the crack upon interaction with an area of largely mis-orientated grains.

Second, the mesoscale of the material microstructure needs to be considered. Despite manufacturers best efforts, no material produced in tonnage quantities, such as the raw products used for pressure vessel construction, are completely homogeneous. Local variations in the materials capacity to resist crack propagation can be expected, and in fact certain regions may not cleave at all, everything else being equal. This creates a number of ligaments behind the advancing crack front which act as energy sinks, using up the strain energy which could otherwise be used to drive the crack front [112].

Arrest at the nanoscale is believed to be due to the movement of dislocations ahead of the propagating cleavage failure [61]. If dislocations can move to blunt the micro-cracks that form ahead of the main crack front then the conditions for cleavage failure as explored in a previous section cannot be met and the material will deform by ductile mechanisms. This requires that the dislocations can move quickly enough to blunt the micro defect before the dynamic stress intensity factor reaches a sufficient level to initiate failure.

From this review it can be established that a propagating cleavage crack may arrest in two ways:

(i) The driving force available for crack propagation is reduced to the point where there is insufficient strain energy available to cause re-initiation

ahead of the main crack or injection into surrounding grains. This could be achieved by the removal of the applied load or by the creation of ductile ligaments and surface features in the wake of the advancing crack front.

(ii) The cleavage crack encounters regions of high toughness material which arrest the crack completely. Here the crack may encounter a change in material type such as moving from a weld to a plate and the increased toughness afforded by the improved microstructure of the plate is sufficiently tough to completely resist further propagation.

The parameters that control arrest toughness are broadly similar to those that control initiation as the propagation of a cleavage crack may be viewed as a number of discontinuous initiation events. Again, these can be split between material and geometric factors as per the initiation mechanism.

a) Material Factors

a. Maximum Local Stress

The maximum local stress will not only be dependent on the static yield stress of the material, but will be greatly affected by the velocity of the crack. As the crack travels faster, the strain rate ahead of the crack will increase causing a rise in the effective yield stress of the material. As discussed earlier, the interaction with the shear stress waves emanating from the crack front cause a change in the direction of principal stress and as such the situation is further complicated.

b. Grain Boundary Mis-orienation

The crack path on a micro-scale will be determined by the cracks ability to propagate from one grain to the next. The energy required to inject the crack from a failed grain into the surrounding microstructure is determined by the mis-orientation angle between the grains. A high mis-orientaion angle may require that the crack diverts around specific grains in order to progress.

c. Micro-crack Initiation

Once a steady state propagation rate is reached, the initiation properties of the material are once again important. In this case, however, the dynamic loading situation will affect the creation of micro-cracks by increasing the effective stress. The size, morphology and volume density of initiating particles remains important to determine the potency of such initiators and therefore the crack path within the material.

b) Geometric Factors

a. Defect Depth

The depth of the defect, or depth the crack has grown from an original defect, will control the crack velocity that has been achieved. A short crack jump will not reach a steady state growth rate so may be stopped more readily than for a crack front which has reached a higher velocity, accelerated by the release of strain energy.

b. Component Design

The design of the component will be highly significant to the development of crack arrest. If the component is of continuous design, as in a complete cylinder or welded ship hull, the crack can travel large distances before interaction with reflected stress waves can take place.

From the above, a number of important differences to initiation can be obtained. First, the measured arrest properties of the material will be more dependent on the average or best properties of the bulk material, not on the assessment of one weakest link or the local properties. Second, there is no size effect in the measurement of arrest properties as the sampling of different volumes will not affect the outcome of the test; again the average or best properties are considered, the likelihood of sampling the average is not increased with specimen size. These suggest that the scatter of arrest toughness data will be less than that for initiation.

The successful modelling of arrest toughness data has been limited. The amount of data available for fracture mechanics arrest measurements is very limited compared to the large number of tests that have now been conducted for initiation assessments. Only two models have achieved some level of acceptance: a model developed at the Oak Ridge National Laboratory (ORNL) [113], and the Arrest Master Curve as developed by K. Wallin [114-115]. Both models use a log-normal distribution to describe the scatter about a median value that has similar temperature dependence to the median initiation toughness. The distinction between the models is the use of different philosophies for the normalisation temperature.

The updated model proposed by ORNL uses RT_{NDT} as a normalising temperature for crack arrest data. However, recent assessments of the proposed model have shown that RT_{NDT} may not have been utilised as the sole normalising temperature for

assessment of the database used for establishing the model parameters [116] and as such this model cannot be used for further assessments in this work. The Arrest Master Curve uses a similar procedure to the Master Curve to establish a reference temperature based on the dataset being assessed. This method is more mathematically and physically robust and has received further assessment in the literature.

The Arrest Master Curve model proposed by Wallin includes a similar expression (see Equation B-14) to that which defines the bounds of the Master Curve, utilising $T_{K_{Ia}}$ as the reference temperature. A similar definition of the Master Curve reference temperature, T_0, is used to define $T_{K_{Ia}}$ as the temperature at which the median arrest toughness is equal to 100 MPam$^{0.5}$. The scatter is modelled by the log-normal distribution such that the standard deviation is constant; this maintains the same level of proportional scatter across the temperature range. The standard deviation has been assumed to be 18% for all materials.

Equation B-14 $$K_{Ia(med)} = 30 + 70e^{\left[0.019\left(T - T_{K_{Ia}}\right)\right]}$$

Application of the assumed model parameters to selective available data has been highly successful (see Figure B-38) and provides the current best estimate of arrest toughness properties of low alloy steels.

B.3.2 Initiation and Arrest Correlations

The correlation between the initiation and arrest toughness properties of low alloy steels has received less discussion in the literature than may have been expected. Only recently has the link between initiation and arrest been explored empirically [114-115], and little discussion has been made on the reason for the correlation

between these parameters. Again, the work of Wallin has been key to providing an empirical model of this relationship.

The model proposed by Wallin is based on an empirical data fitting exercise, which revealed a number of important points about the relation between initiation and arrest toughness (see Figure B-39). Following investigations of the arrest toughness and the successful application of an Arrest Master Curve, the next obvious step was to compare the reference temperatures established from each Master Curve model. A correlation seemed likely as the same temperature dependence coefficient, $0.019(T - T_0)$, could be applied with success in both models.

The first point to note is that the difference between the initiation and arrest reference temperatures decreases with increasing initiation reference temperature, or from a physical standpoint the arrest toughness of the material is more representative of the poorest initiation properties that can be achieved. Further work on the correlation revealed that the relationship was also dependent on yield stress of the material, this is apparent from an understanding of both physical processes. The yield stress will have a controlling effect in both mechanisms; the maximum principal stress for initiation and the ability to move dislocations to cause arrest will both be dependent on the yield behaviour of the material.

The model has also been developed to include the effect of nickel on the correlation. Addition of a single high nickel material (~2.5 wt% Ni), the datum from which lay well away from the initial model, demonstrated that nickel has a substantial effect on the relationship between initiation and arrest that was not captured by the difference in yield stress. At present, an understanding of why steels of this type produce such good transition toughness is not complete and requires significant further work. The

inclusion of nickel effects generates the most recent correlation model (see Equation B-15).

Equation B-15 $$T_{KIa} - T_0 = \exp\left[5 - \frac{T_0 + 273}{136.1} + \frac{\sigma_{y(RT)}}{660.3} - \left(\frac{\text{Ni wt\%}}{2.5}\right)^{2.91}\right]$$

It should be noted that there is significant scatter on the proposed correlation especially at lower reference temperature values. There are very limited data, compared to initiation, to establish a model of the arrest properties of materials; a rigorous assessment may not yet be possible with the limited number of data points currently available. The controlling parameters of initiation and arrest may, broadly speaking, be similar but subtleties are yet to be understood and the correlation requires more consideration before a fully quantitative physical model is available.

Recent work by Marjorie EricksonKirk has suggested that the physical basis for a correlation between initiation and arrest is due to a universal hardening curve [61]. This concept is based on an understanding of the flow properties of the material, and hence the dislocation movement of the material. In this work, EricksonKirk suggests that initiation and arrest are simply changes in the interaction of the loading condition with the universal hardening curve of the material. This work is yet to be validated but is promising as an explanation for both the uniform temperature dependence of initiation and arrest, and the correlation between them.

B.3.3 Microarrest

It was noted that the initiation and arrest distributions actually overlapped by varying degrees dependent on reference temperature; therefore, it was conceivable that run-arrest could occur in a single material without changing the loading condition (removal of driving force). From a macroscopic point of view this could be considered

a homogeneous event; the cleavage failure initiates in the same material that causes arrest. On a microscale, no material is homogeneous and combined with an observation of fewer failures than expected in the lower tail of the initiation distribution gave rise to the ‘Microarrest’ concept of fracture.

Microarrest proposes that the interaction of the initiation and arrest distribution can cause the non-propagation of cleavage fracture following failure of the first few grains at the site of initiation (see Figure B-40). This is commensurate with the different stages of cleavage failure discussed in a previous section; in fact, from a mechanistic point of view, there are two stages at which the local arrest properties, or local ability to deform as oppose to cleave, can result in non-propagation of the cleavage failure. First, the micro-crack initiated in the secondary particle has to be injected into the surrounding matrix; this requires that the local material cleaves and as such the micro-crack may fail to propagate if the surrounding material is suitably tough. Secondly, the micro-crack must propagate from the first few grains into the surrounding material; this is required to release the strain energy that will drive the cleavage crack through the material. If the material can absorb the necessary strain energy by deforming plastically and blunting the progressing crack front, then arrest will occur.

The mechanism of microarrest has therefore been postulated for many years; however, a formal link between the processes and the effect of arrest on the measurement of toughness has only been made recently. The work of Williams et al [23] gives the results of Monte Carlo simulation of the effect of arrest on initiation toughness, utilising both the initiation and arrest Master Curves proposed by Wallin and the correlation described above. The basic premise of the Micro Arrest model is the use of the macro arrest toughness to describe the arrest properties of the material on the microscale.

If it were possible to measure the arrest toughness and the initiation toughness of the same material, the way in which the properties are measured will be distinctly different. The initiation toughness will be a sample of the initiators in the material, the most potent of which corresponds to the measured value. If it were possible to measure the same crack front length for arrest toughness a single measurement will also be achieved, but this will equate to an average or best of the arrest properties of the material. The work of Williams et al [23] accounts for this in simulations by sampling the arrest toughness only once for a given crack front, and sampling the initiation toughness repeatedly until the arrest toughness is bettered and failure of the virtual specimen is declared .

The simulation was conducted to allow direct comparison to a database of toughness measurements. Each data point in the database was simulated many times in order to establish a parent distribution of toughness values which could have been achieved from testing of the same material, in the same condition and geometry as physically measured. The resultant parent distribution can then be compared to the database of known values to assess the suitability of the model, the results of which were very encouraging. A number of hypotheses of the model were tested and found to be in good agreement with the database.

As there is no effect of specimen size on the arrest toughness of a material, the Microarrest model hypothesises that the effect will be greatest on larger crack front lengths. Essentially, the statistical size correction that applies to initiation will result in a decrease of the expected toughness for long crack front lengths; the arrest toughness is not reduced and as such the relative difference between the initiation and arrest distribution is reduced, resulting in more microarrest events. The second hypothesis is that high T_0 materials exhibit more micro arrest events due to the

diminishing difference between the initiation and arrest distributions as the initiation toughness decreases. The database can then be portioned into a number of subsets that should exhibit slightly different measured toughness in the lower tail of the distribution.

Williams et al divided the database into low and high crack front lengths (< and > 90 mm) and low and high T_0 (< and > -70 °C). This created four subsets of the database, which were anticipated to exhibit differing effects of microarrest on the data. It was found in all instances that the number of actual data points below prescribed toughness bounds more closely matched the predictions of the Micro Arrest model than the Master Curve (see Figure B-41). This result supports that the Micro Arrest model, and the assumed underlying physical description of the fracture process, warrants further investigation.

B.4 Research Aims and Objectives

A strong and widely adopted theory for the brittle fracture mechanisms of low alloy steels in the transition region exists; however, the speed with which this mechanism operates and the stochastic nature of the initiation point makes direct measurement of the process practically impossible. The fracture process is believed to be made up of three critical steps: particle fracture, matrix injection and crack propagation. Different physical models place emphasis on different stages of the fracture assuming that either the preceding steps have occurred and that the remaining stages will happen. The most successful and robust approach to this problem has been the adoption of physically-based empirical models, such as the Master Curve method. These have been shown to be robust for application to a wide range of low alloys steels and require on a small level of calibration to each material.

A better position has been reached for the assessment of fracture toughness models as it is now possible to confirm or challenge the assumptions of empirical models by comparison of statistical fits to a large database. Compared to the original toughness modelling assessments, there is now a wealth of toughness data with which to compare modelling approaches. This large amount of data allows meaningful comparison between the predictions of a model and the actual data population. This method of database inference is a very powerful technique; the data population represents the real world with minimal interpretation, therefore a model based on this approach will be highly representative of the true failure mechanisms.

An improved toughness model is required to demonstrate physical understanding of the fracture process such that it can be applied in situations which require extrapolation outside of the current data population. This situation is likely to become

more common with extended operational lifetimes of current fleet of utility power reactors.

The following investigation aims to provide an accurate description of fracture toughness in the transition regime, particularly in the lower bounds. The approach uses database inference to assess modelling assumptions and establish corrections to the established model.

B.5 Tables

Table B-1 - Standard Specimen Geometry Constraint Coefficients Established for the Nevalainen and Dodds Trajectories for In-Plane Constraint Loss

Specimen Type	Side Groove	a/W	B/W	Limit of Proportionality	b_0		b_2	b_3	$Max(J_{avg}/b\sigma_0)$
[#]	[%]	[mm/mm]	[mm/mm]	[#]	[#]	[#]	[#]	[#]	[#]
SE(B)	0	0.5	1	0.008	-0.03645	0.215608	-0.06064	-0.56486	0.15565
SE(B)	0	0.5	0.5	0.00706	-0.04732	0.265808	-0.17953	-0.50544	0.13144
C(T)	0	0.5	0.5	0.012	-0.04699	0.25299	-0.02889	-0.70659	0.16685
C(T)	20	0.5	0.5	0.012	-0.03418	0.196496	0.094021	-0.96813	0.15846

Table B-2 - Standard Specimen Geometry Constraint Coefficients Established for the Nevalainen and Dodds Trajectories for Out of-Plane Constraint Loss

Specimen Type	Side Groove	a/W	B/W	d_0	d_1	d_2
[#]	[%]	[mm/mm]	[mm/mm]	[#]	[#]	[#]
SE(B)	0	0.5	1	0.63	0.27	-160
SE(B)	0	0.5	0.5	0.45	0.45	-200
C(T)	0	0.5	0.5	0.47	0.43	-140
C(T)	20	0.5	0.5	0.5	0.3	-100

B.6 Figures

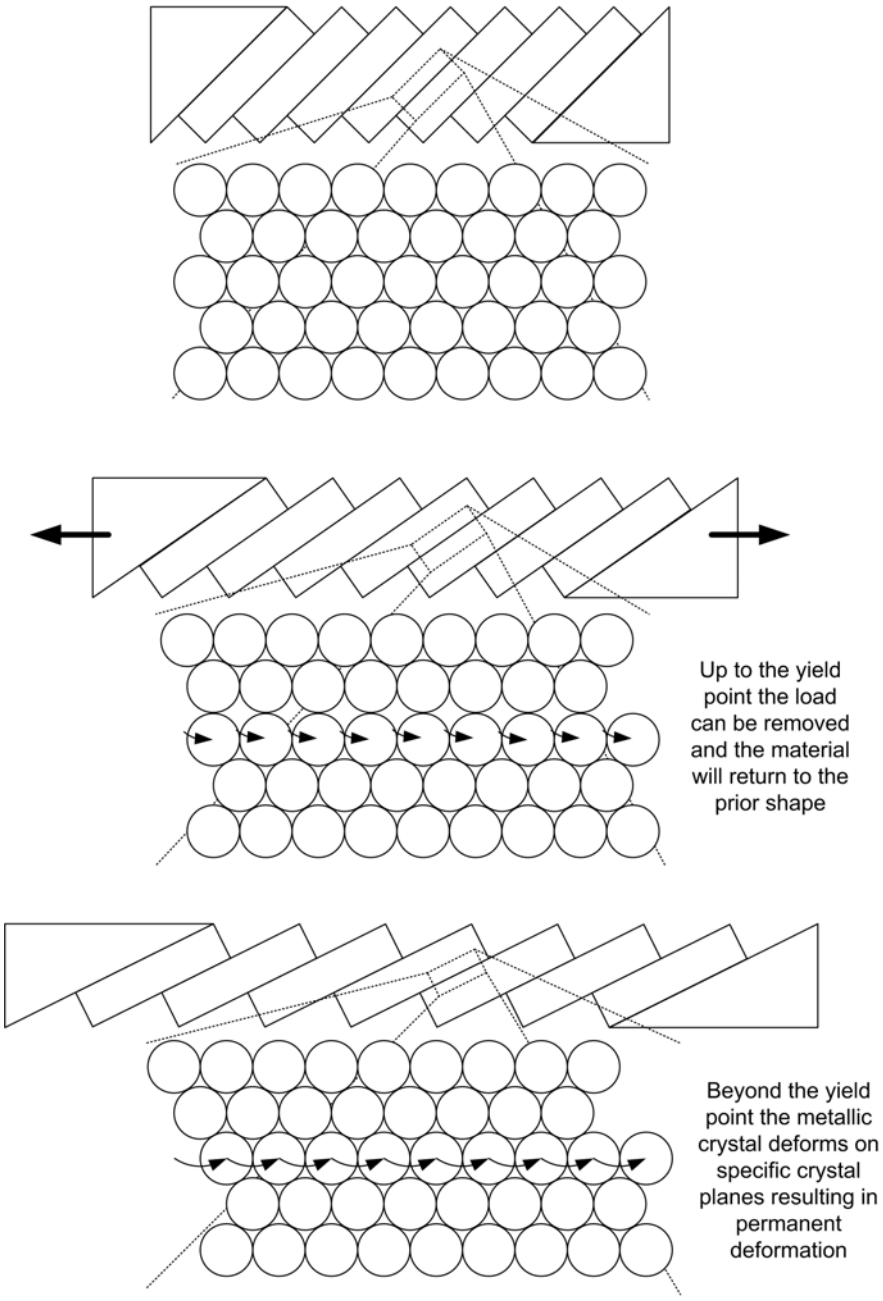

Figure B-1 - Plastic Flow in Ductile Materials

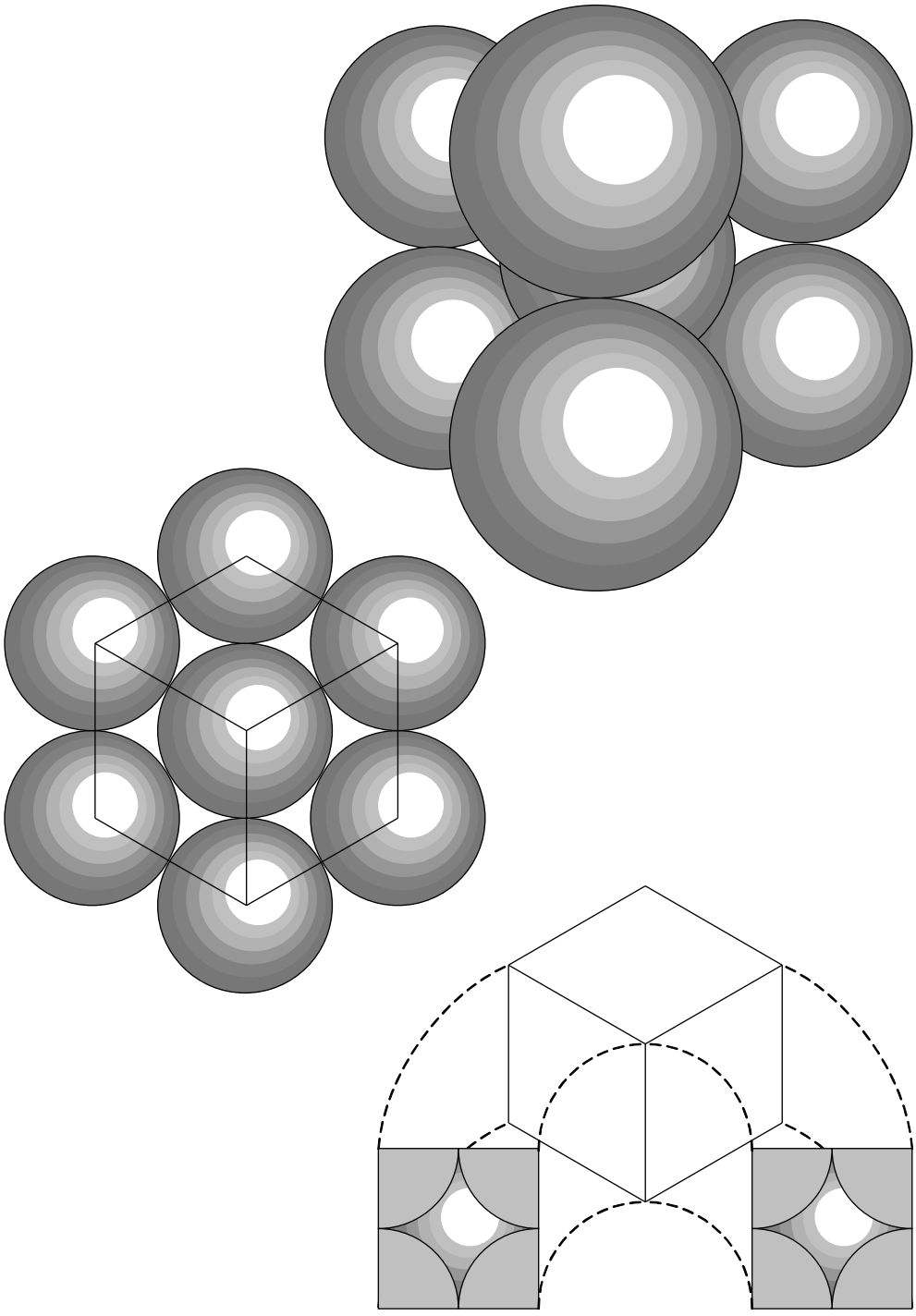

Figure B-2 - Body Centred Cubic Crystal Unit

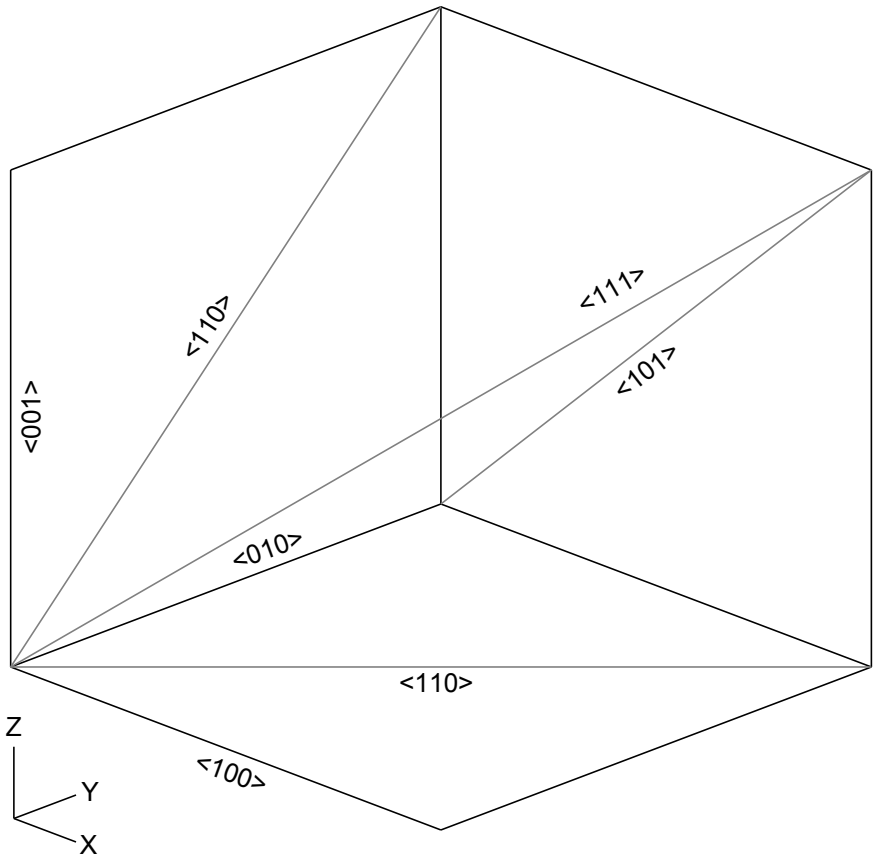

Figure B-3 - Body Centred Cubic Crystal Directions

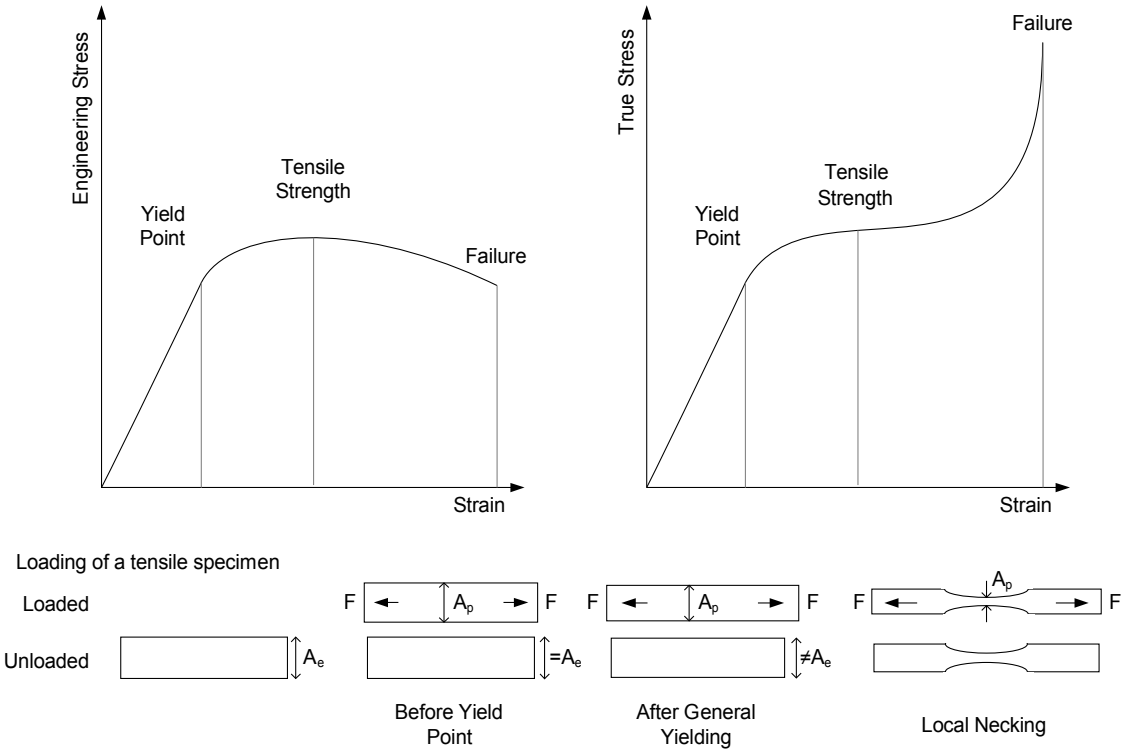

Figure B-4 - Stress-Strain Curve for Ductile Materials

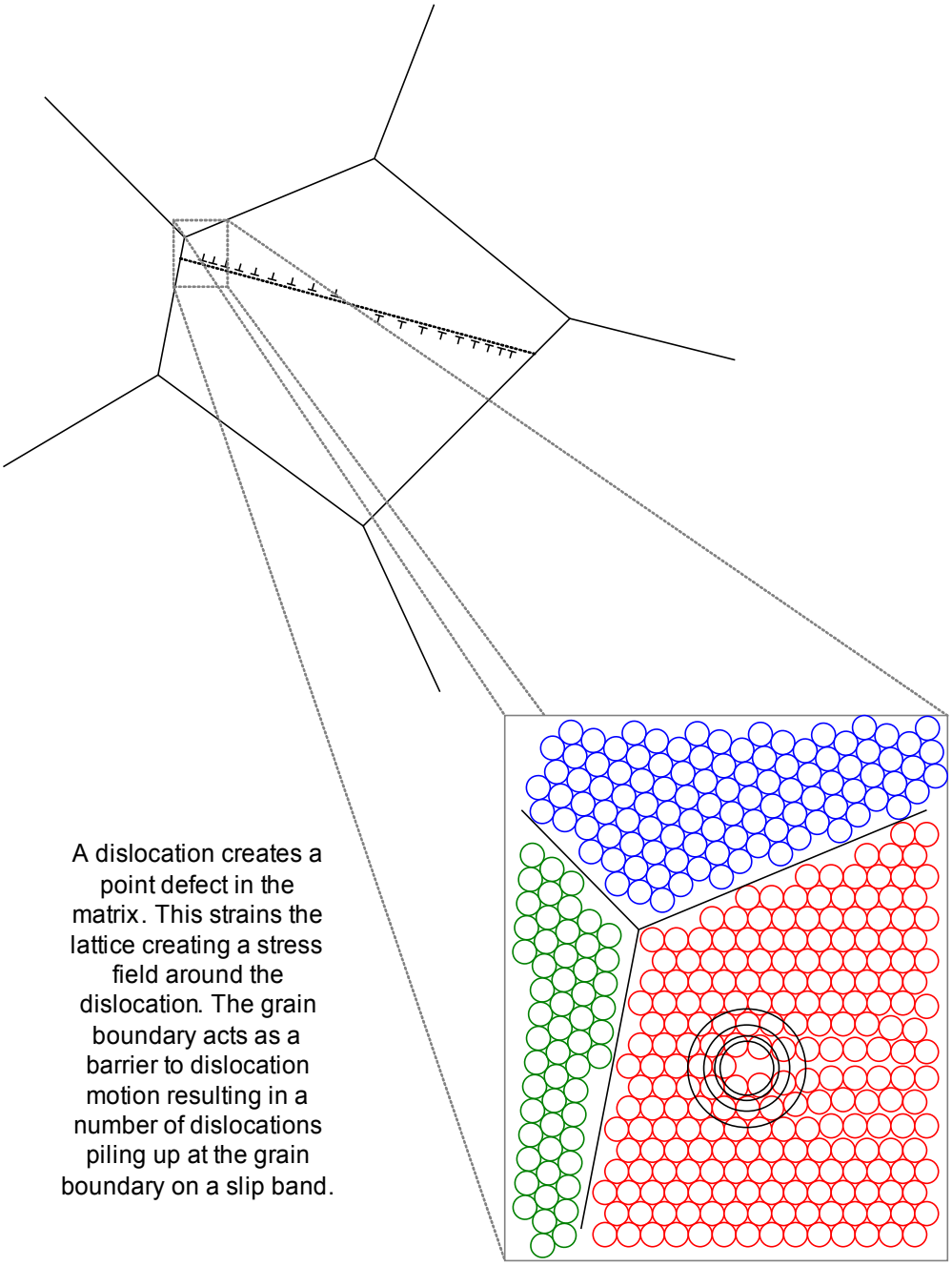

A dislocation creates a point defect in the matrix. This strains the lattice creating a stress field around the dislocation. The grain boundary acts as a barrier to dislocation motion resulting in a number of dislocations piling up at the grain boundary on a slip band.

Figure B-5 - Dislocation Pile Up at a Grain Boundary

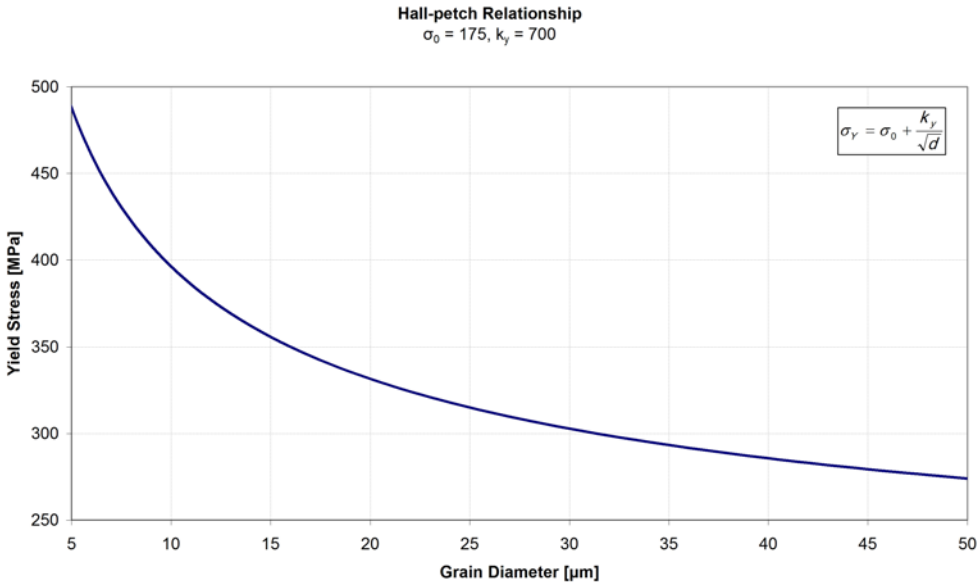

Figure B-6 - Grain Size Effect on the Yield Stress of Typical Low Alloy Steel

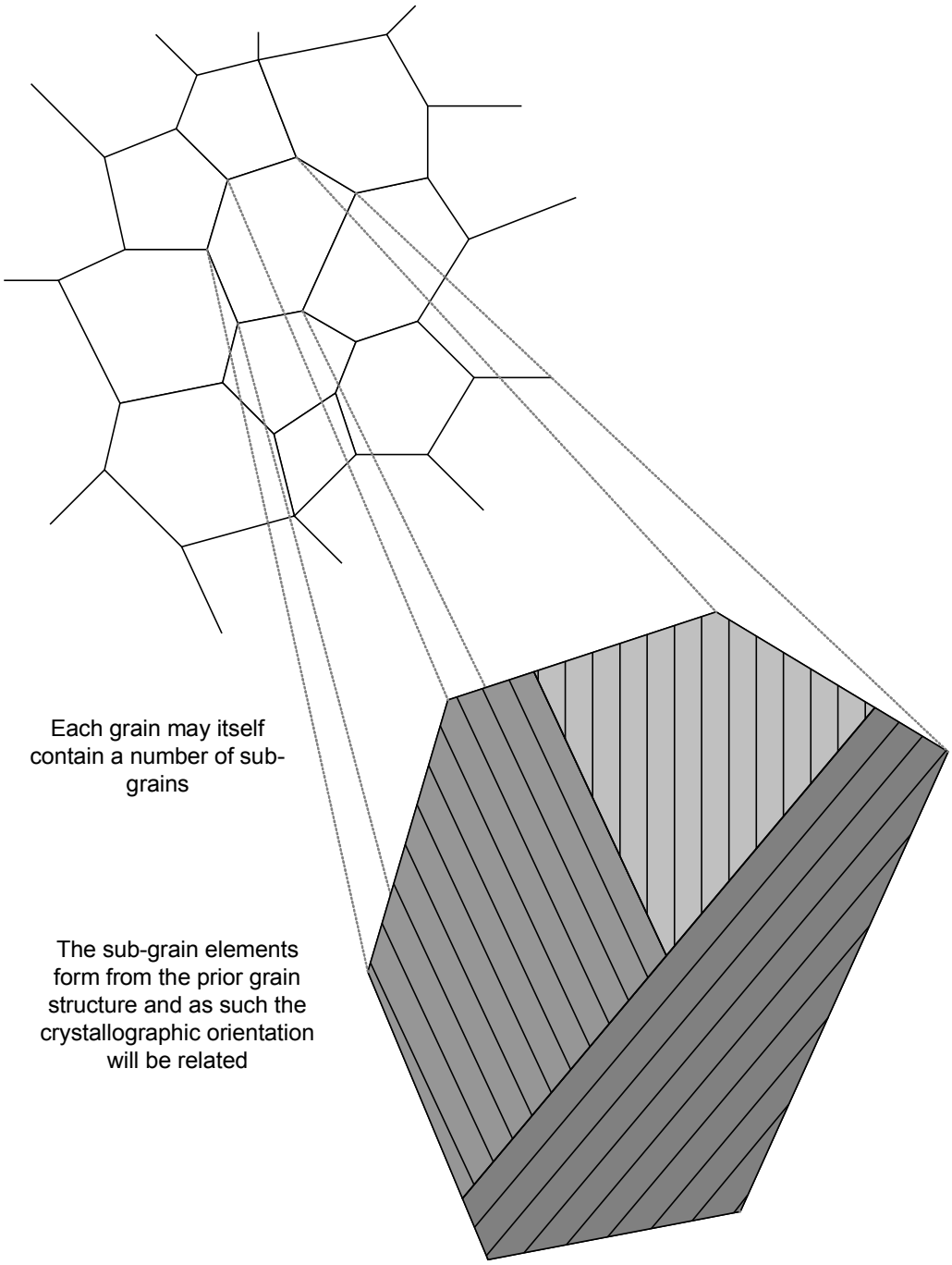

Figure B-7 - Sub-grain Formation in Low Alloy Steel

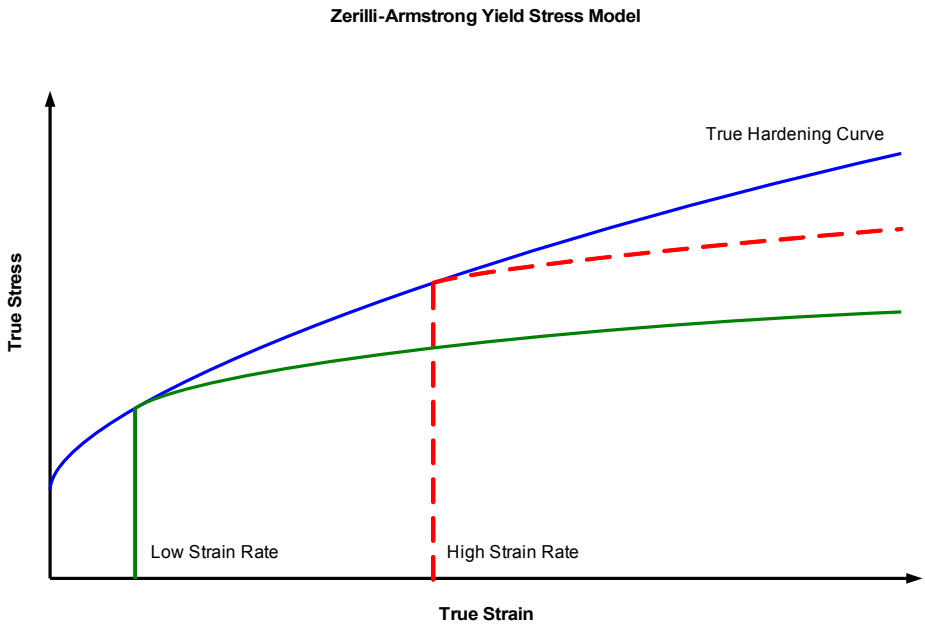

Figure B-8 - Zerilli-Armstrong Yield Stress Model

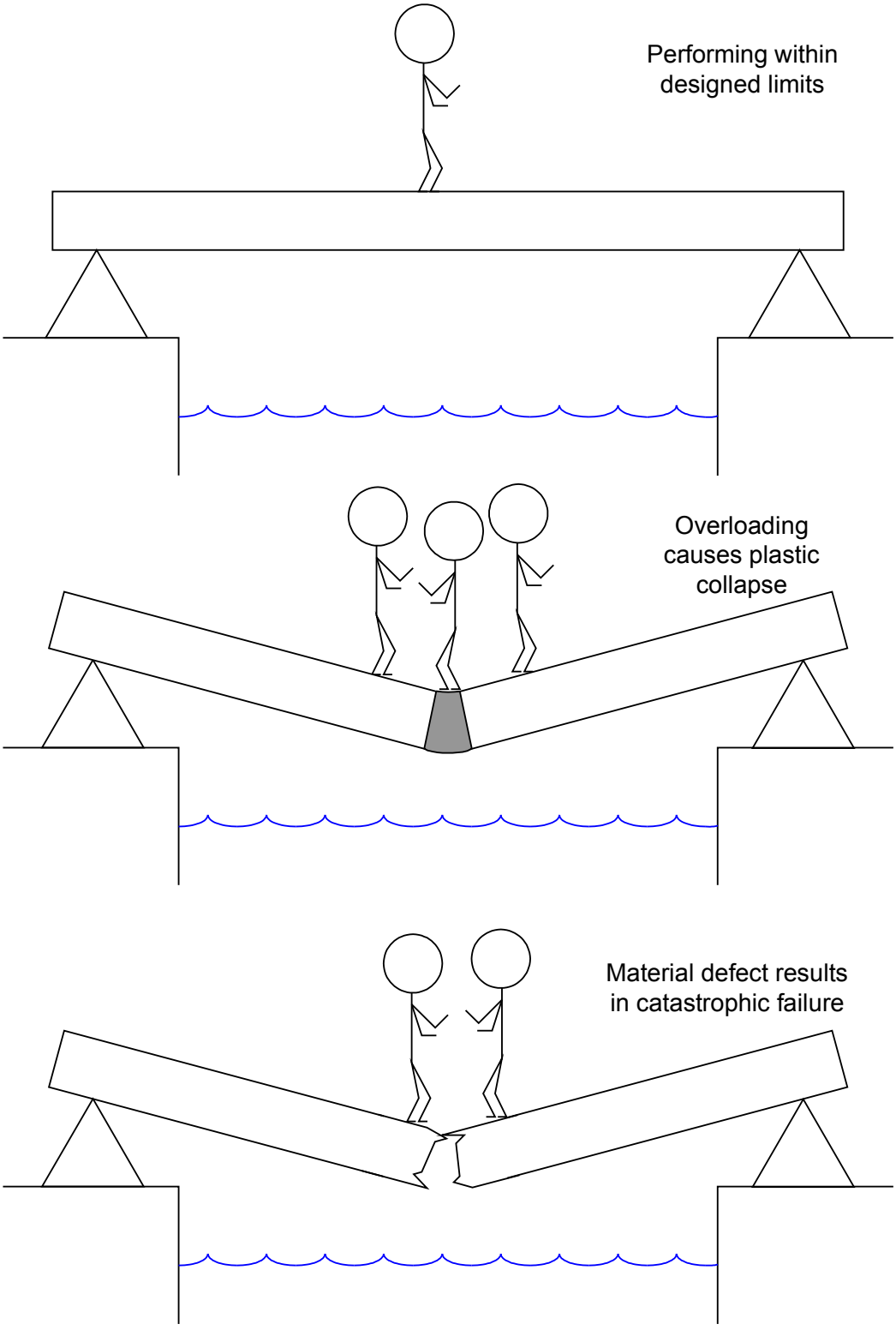

Figure B-9 - Plastic Instability and Catastrophic Failure

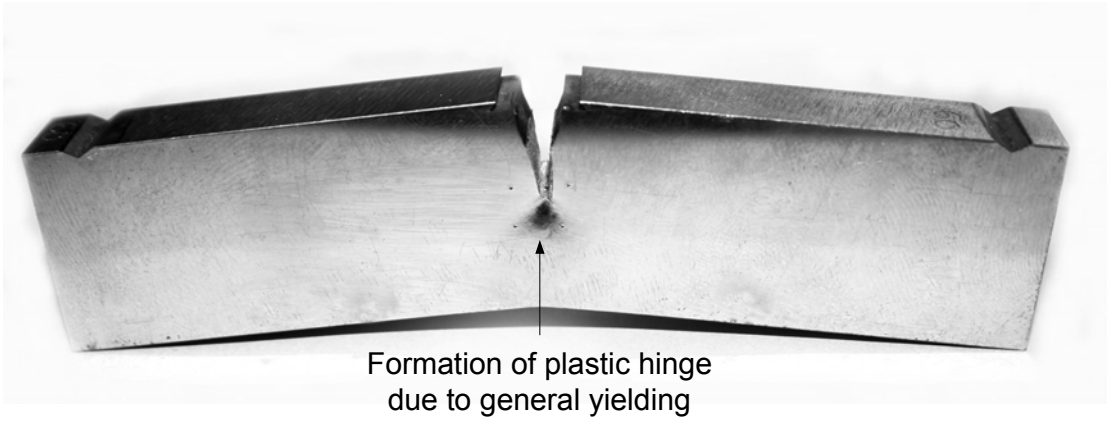

Figure B-10 - Plastic Instability in a Toughness a Specimen

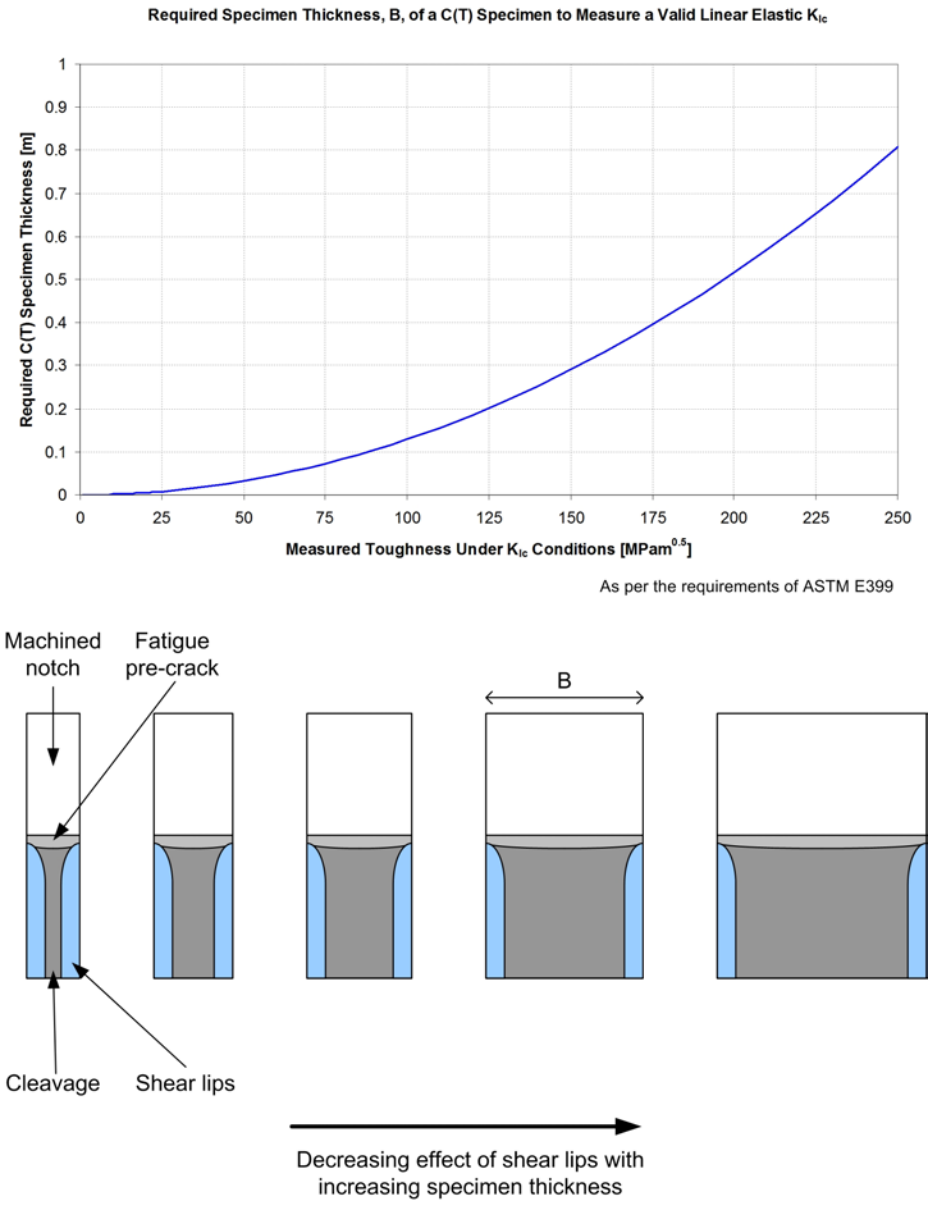

Figure B-11 - Specimen Size requirement for Elastic K_{Ic} Measurement

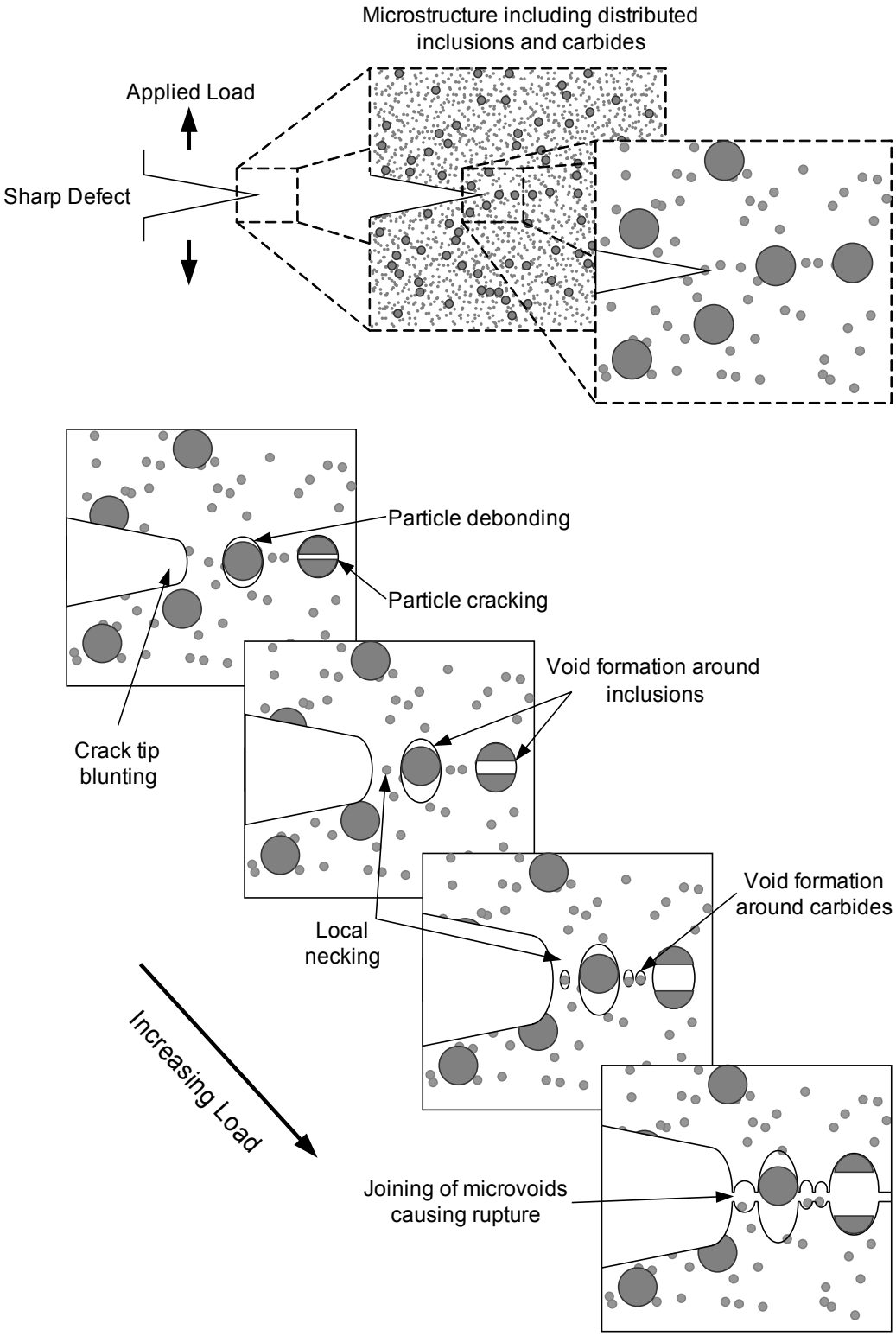

Figure B-12 - Ductile Failure Mechanism (Microvoid Coalescence)

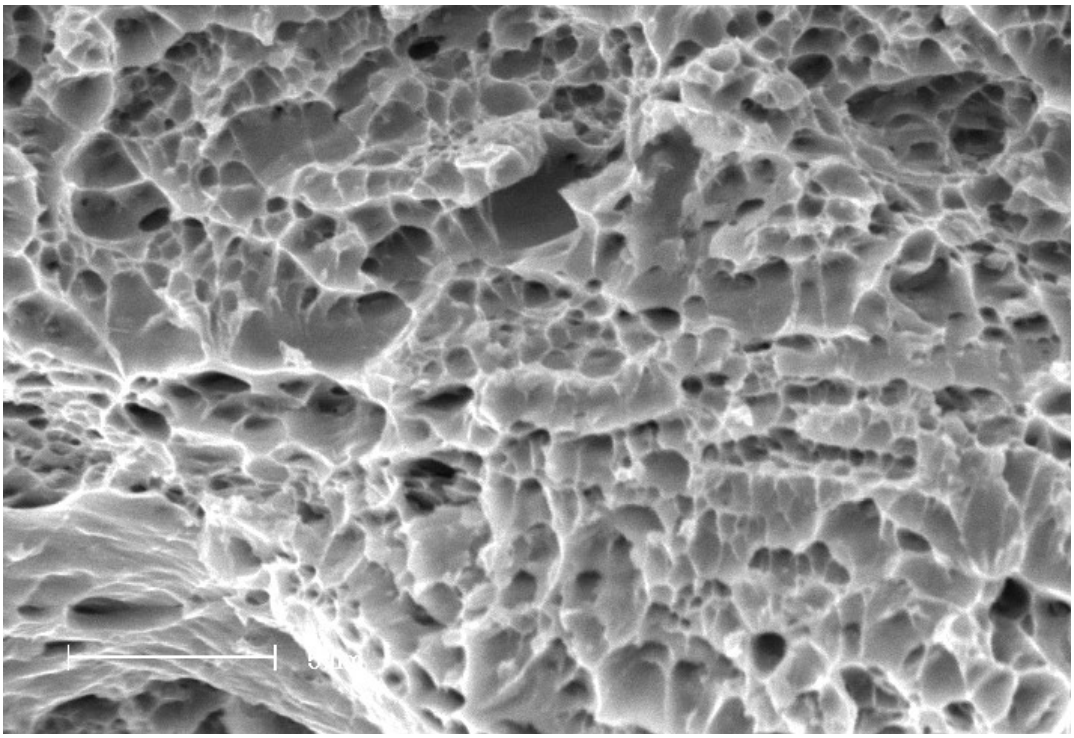

Figure B-13 - Microvoid Coalescence Fracture Surface

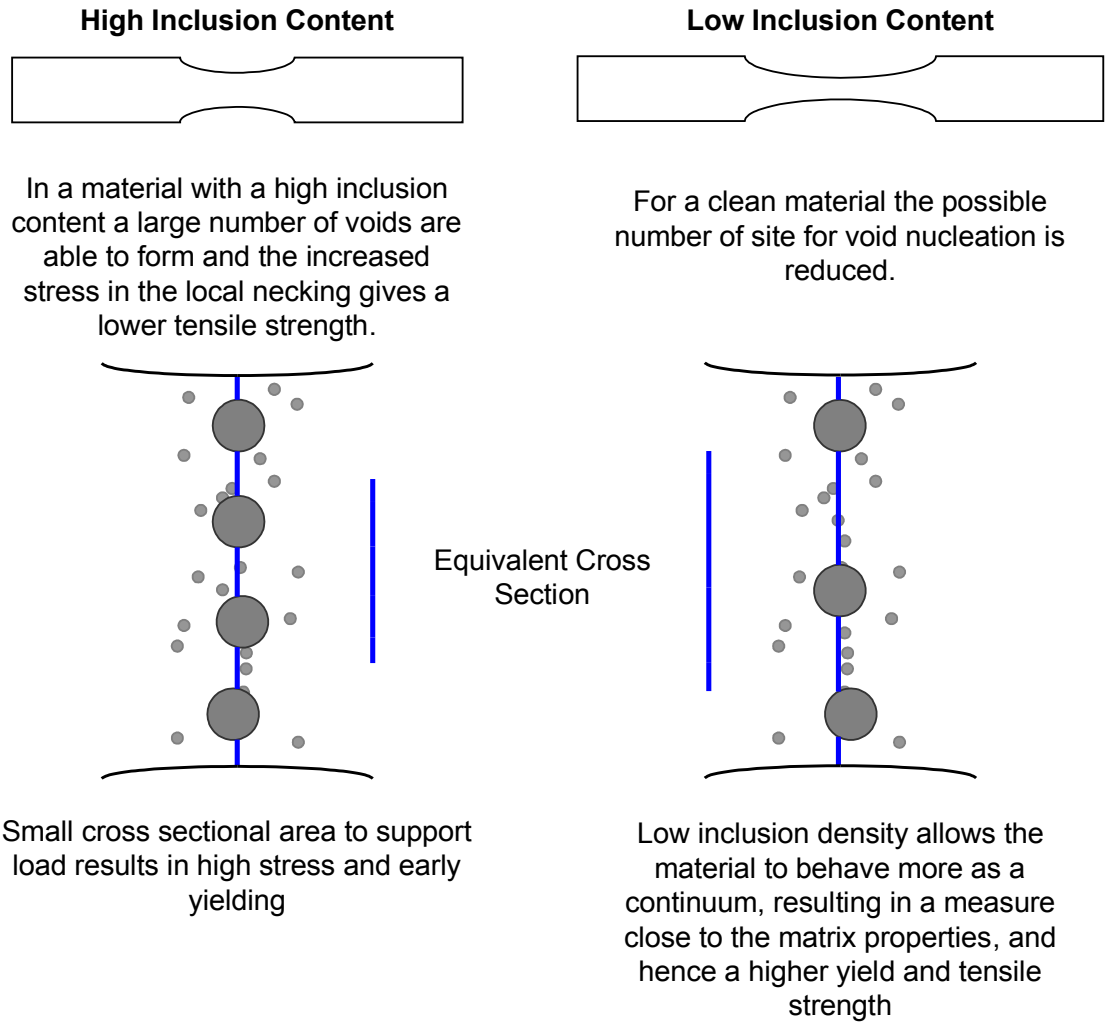

Figure B-14 - Effect of Inclusion Content on Tensile Behaviour

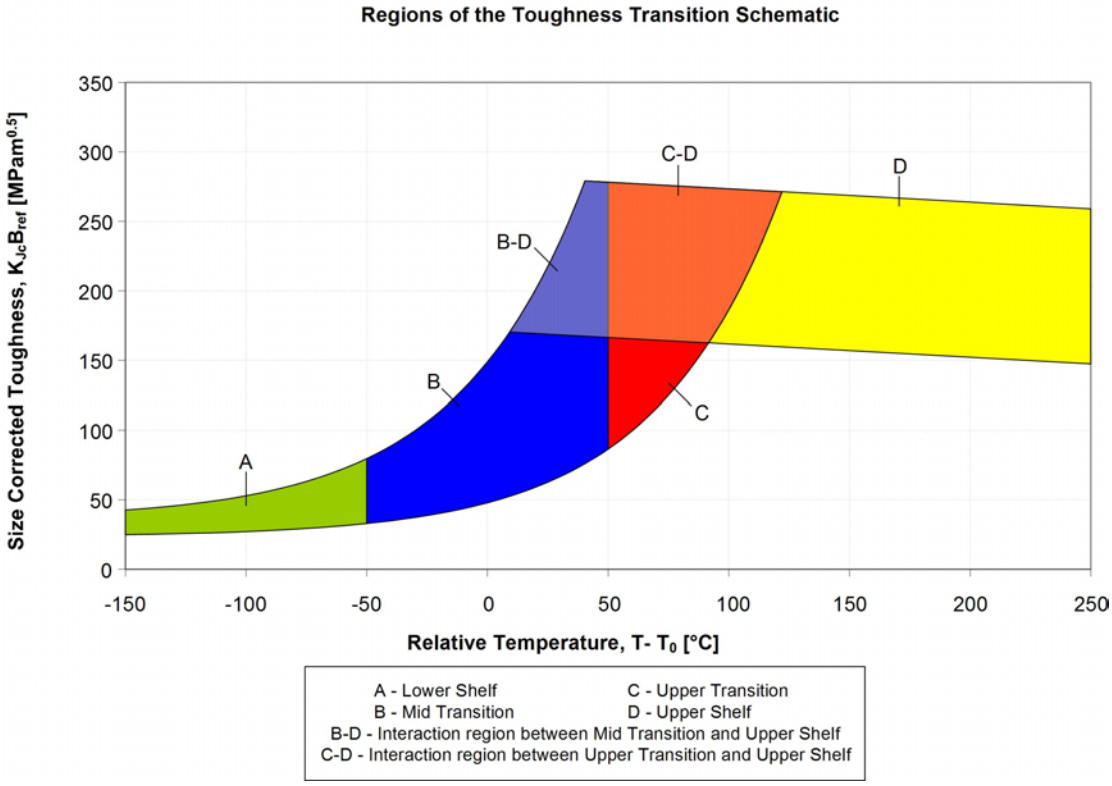

Figure B-15 - Regions of the Toughness Transition Schematic

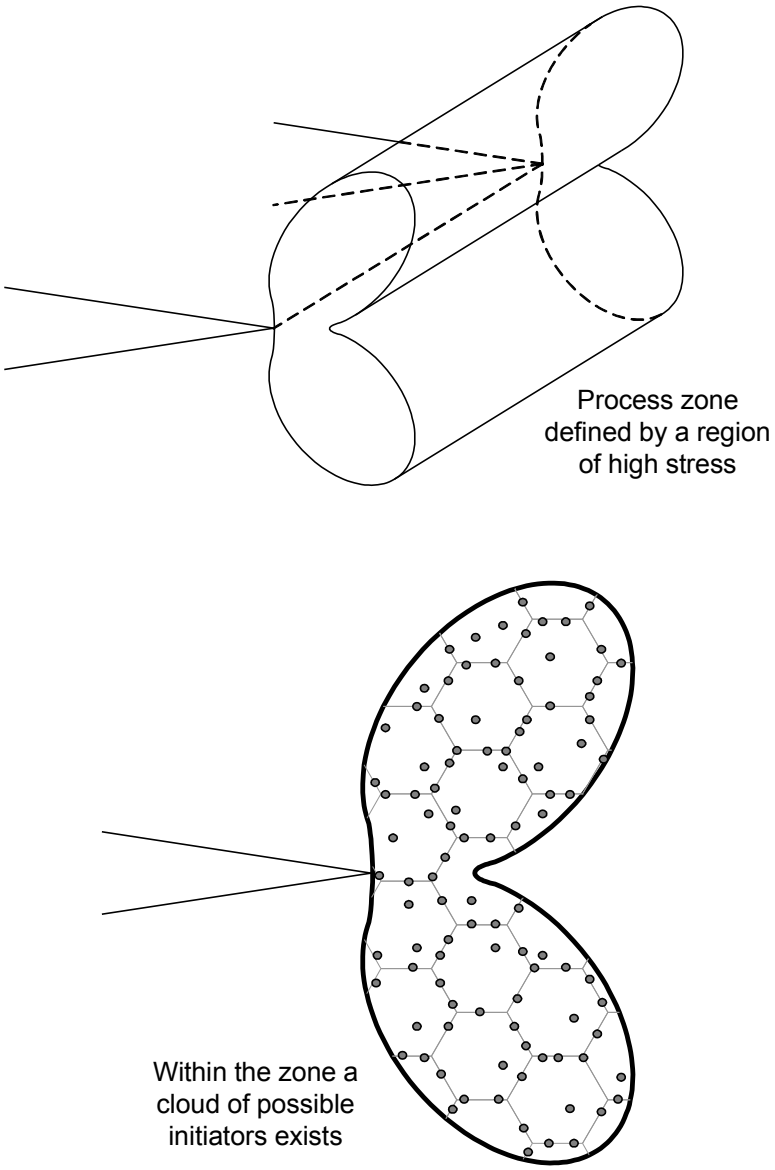

Figure B-16 - A Cloud of Defects Contained within the Small Scale Yielding Zone

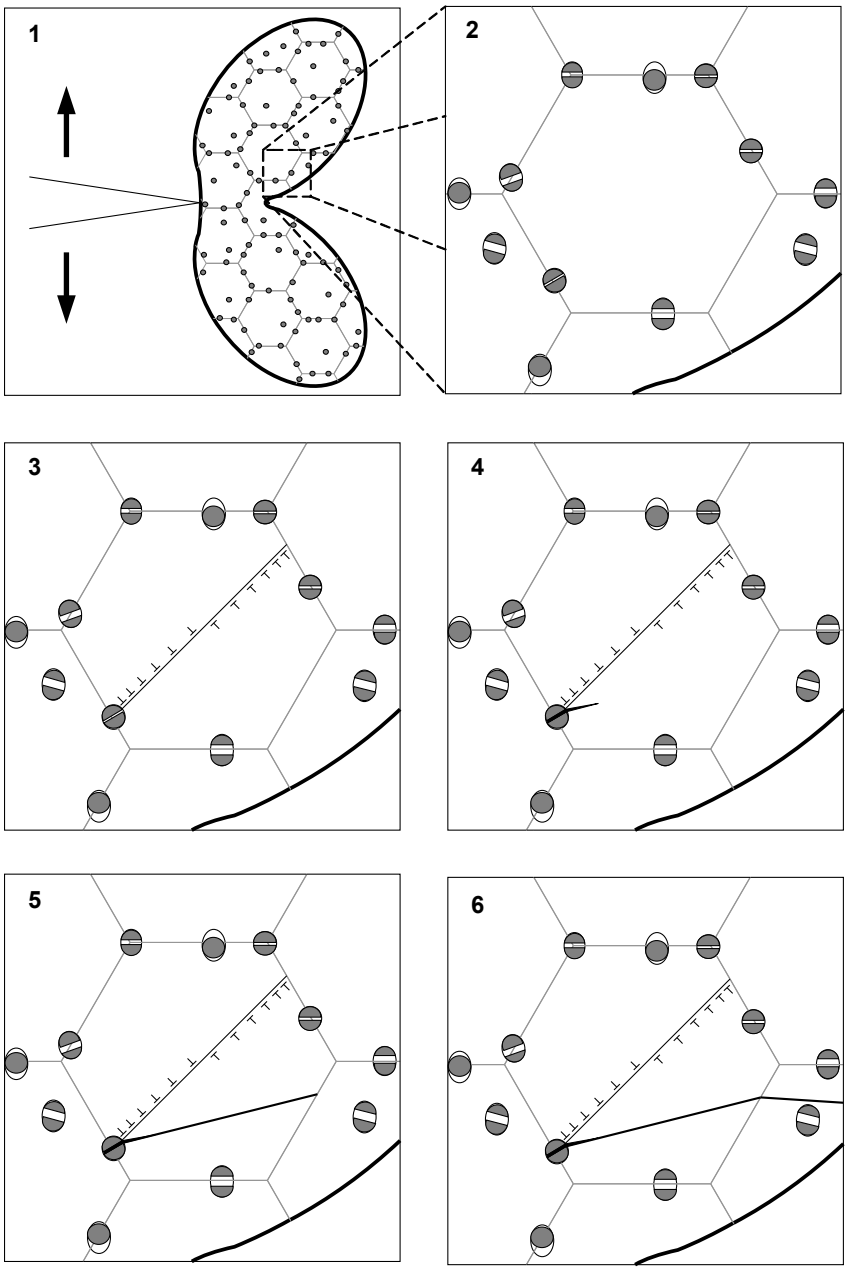

1. Formation of plastic zone ahead of macro-crack tip
2. Debonding and particle fracture forming a number of micro-cracks
3. A slip band terminates at the micro-crack generating an opening stress
4. The micro-crack is injected into the matrix
5. The micro-crack rapidly extends to the opposite grain boundary
6. The micro-crack is injected into the neighbouring grain and re-initiates on the new cleavage plane

Figure B-17 - Micro-mechanisms of Cleavage Failure Initiation

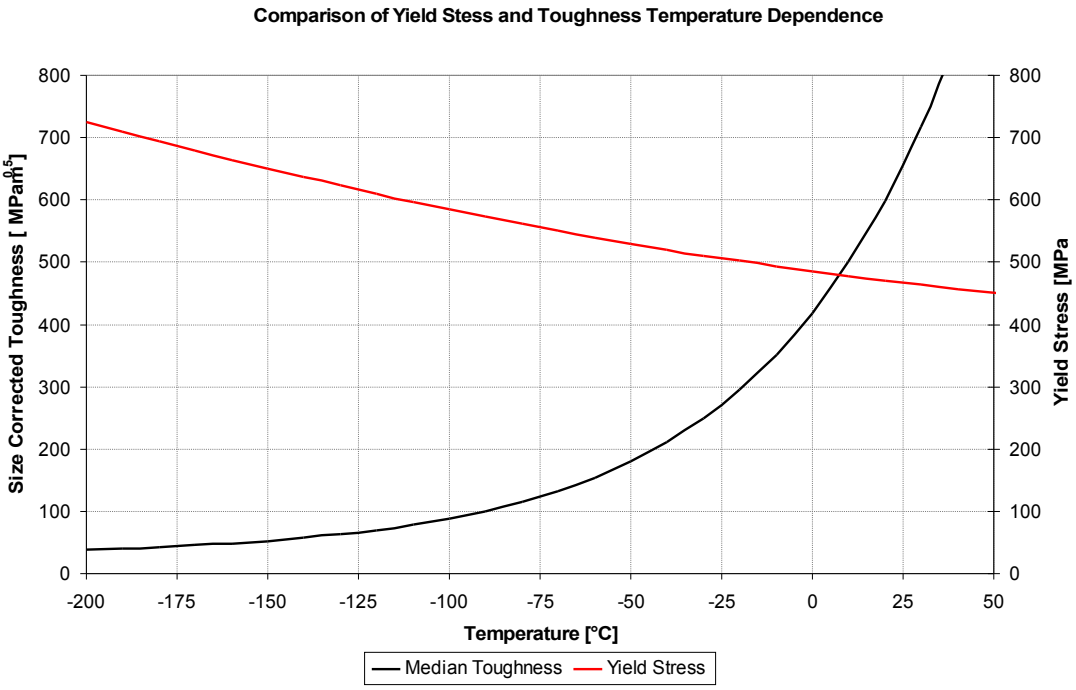

Figure B-18 - Comparison of Yield Stress and Toughness Temperature Dependence for Typical A508-3 Material

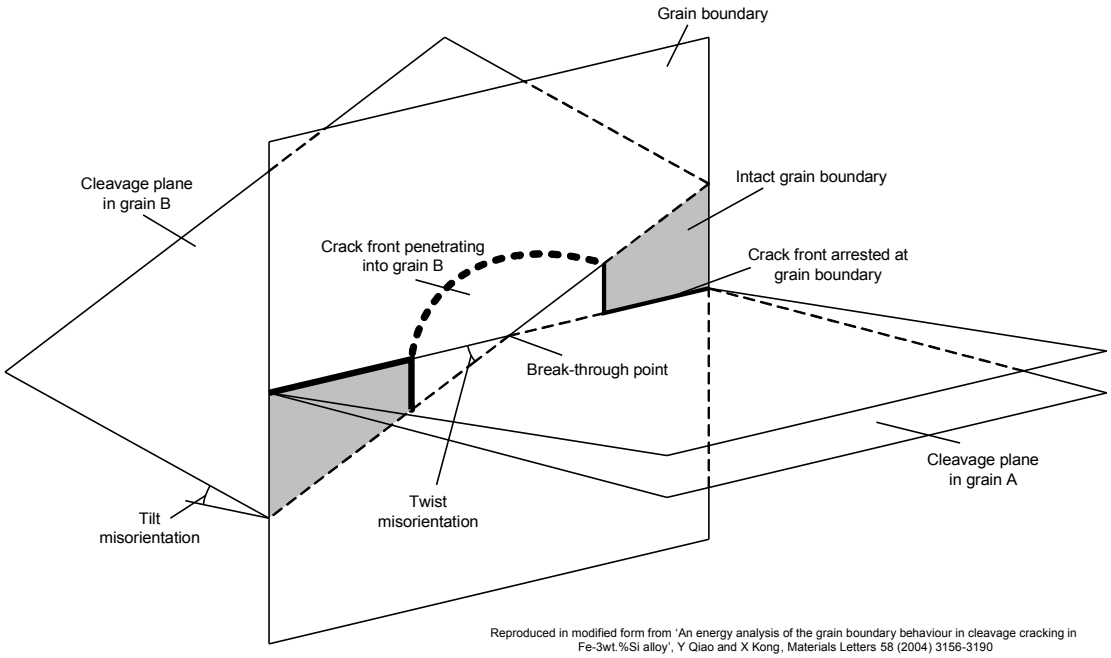

Figure B-19 - Qiao Grain Boundary Cleavage Model

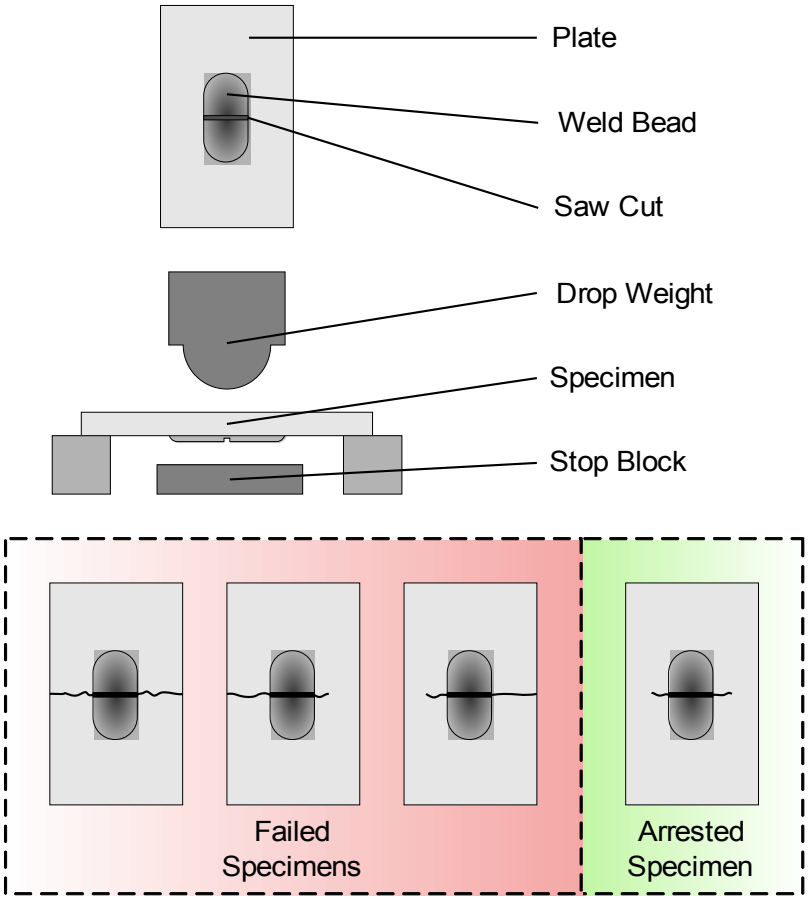

Figure B-20 - Nil Ductility Temperature Measurement

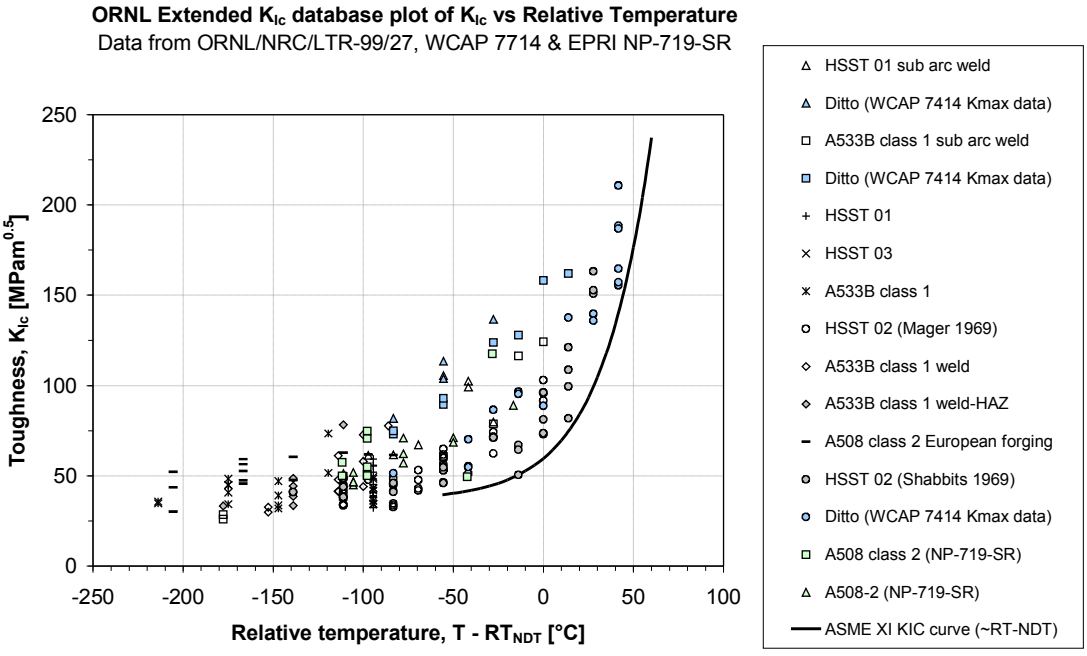

Figure B-21 - ORNL Extended Database Normalised by RT_{NDT}

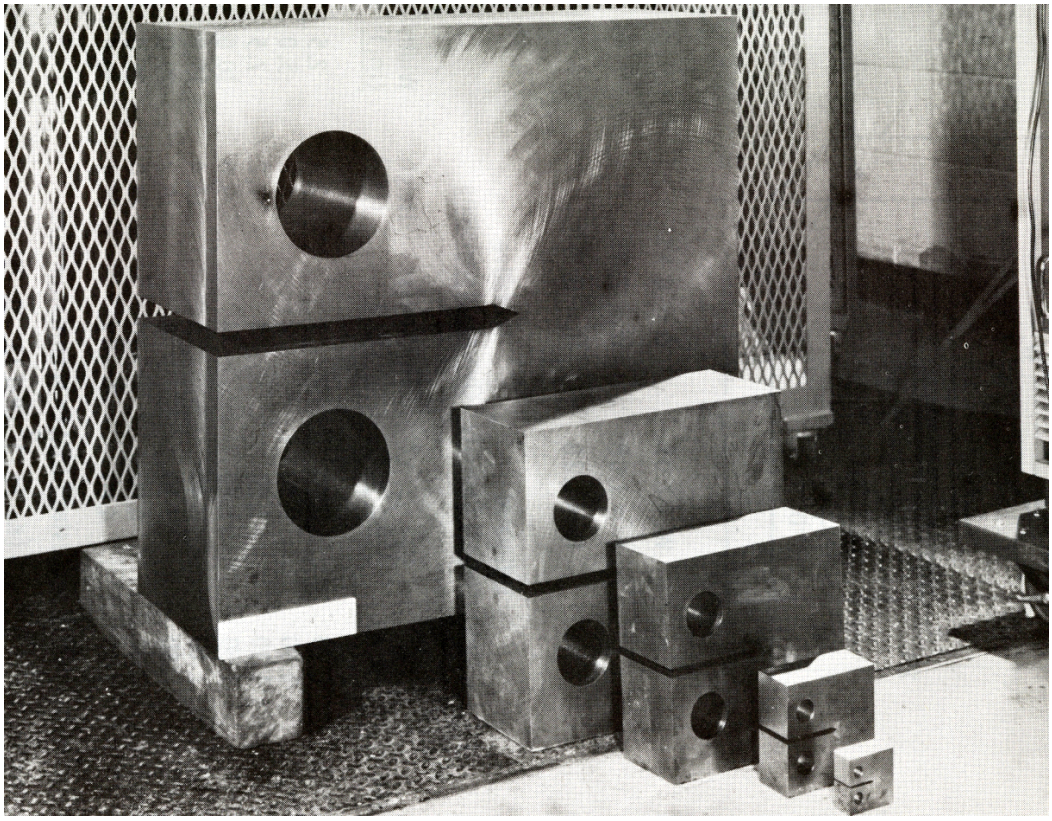

(Image taken from [7])

Figure B-22 Compact Tension Specimens Used for HSST Programme (1, 2, 4, 6 and 12 inch thick specimens)

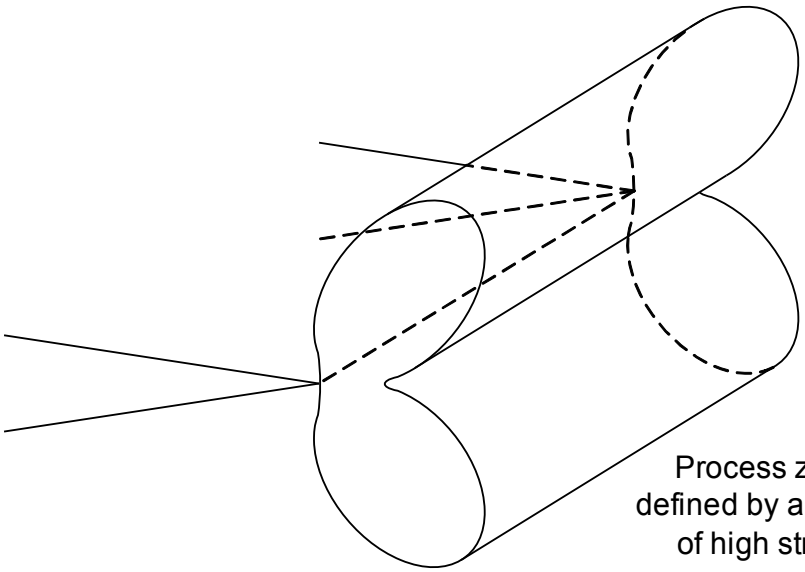

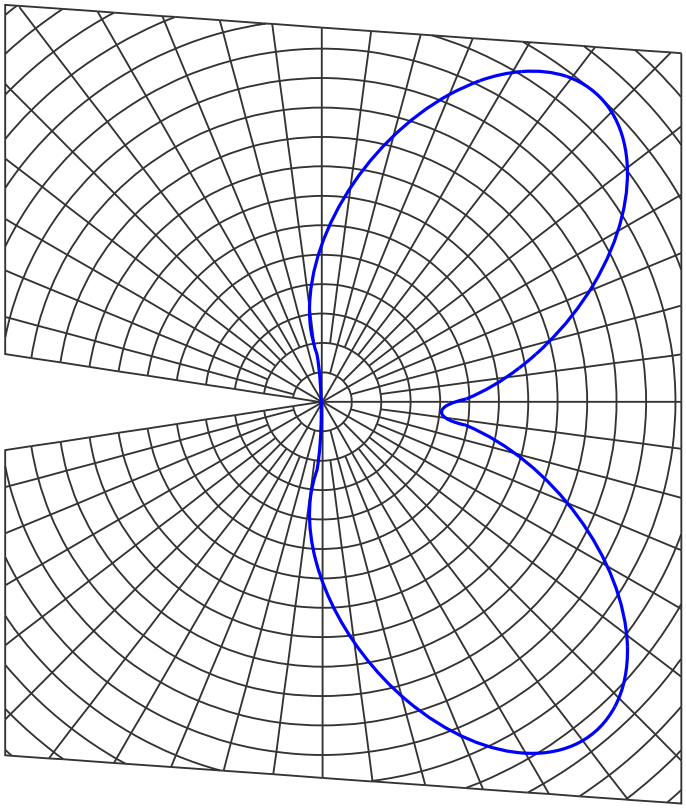

This region can be defined as a number of elements

These elements have a probability of failure ascribed to them and the stress can then be calculated from finite element simulations

Figure B-23 - Local Approach Modelling of Fracture

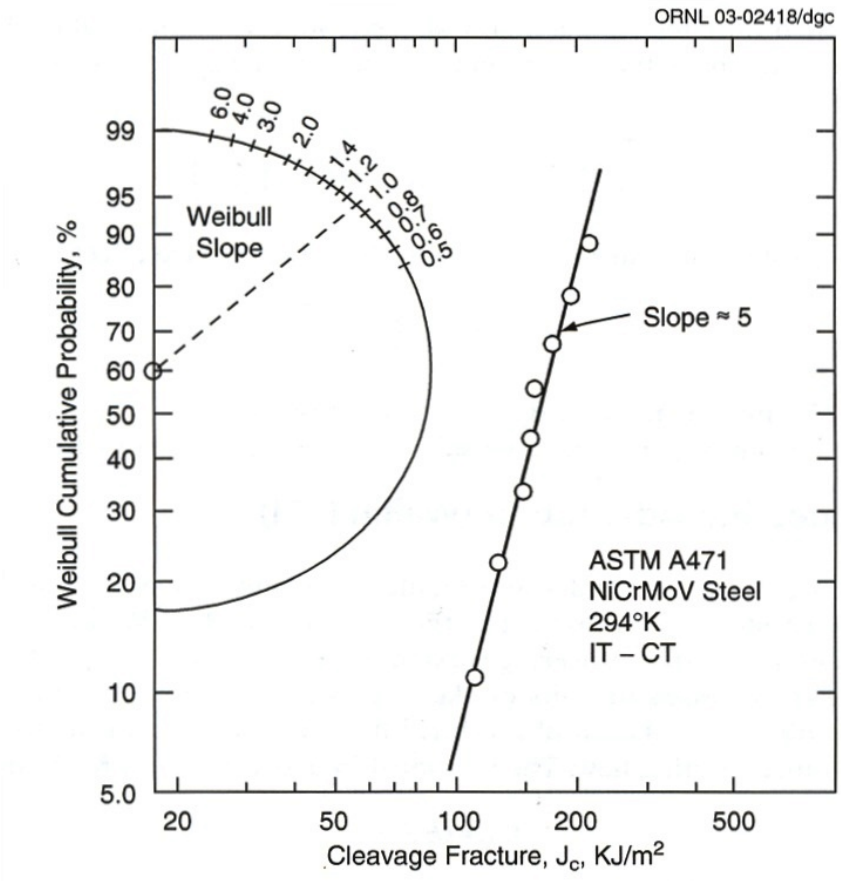

After McCabe et al [49]

Figure B-24 - Landes and Shaffer Representation of Failure Probability

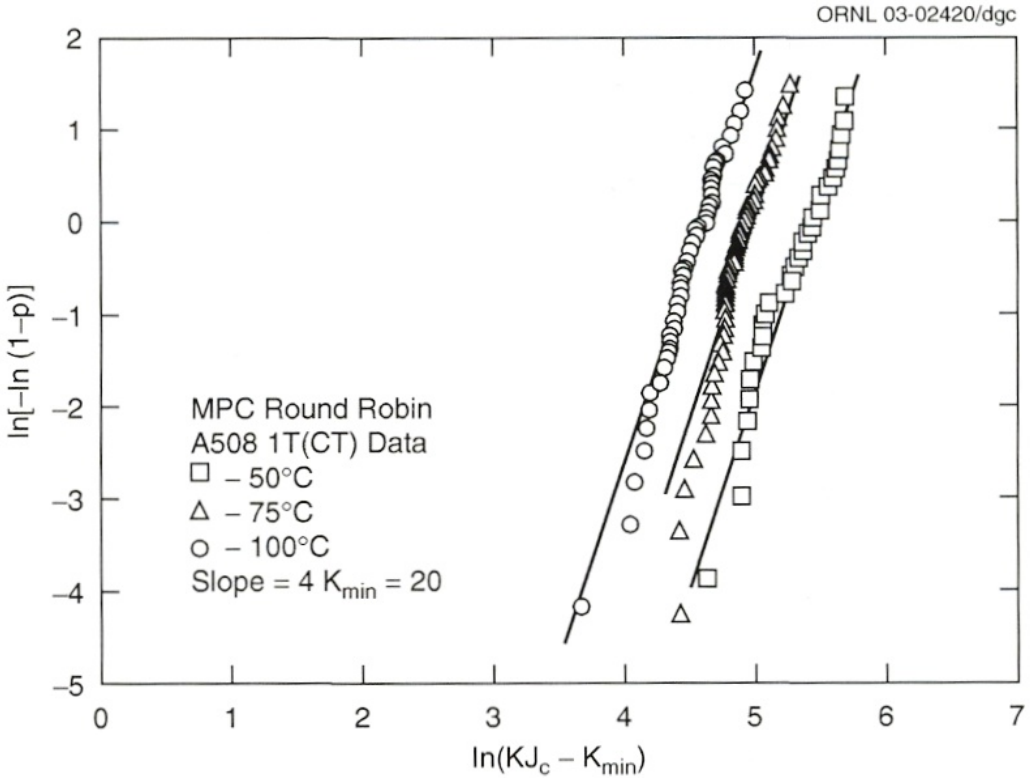

After McCabe et al [49]

Figure B-25 - Wallin Extension to Weakest Link Model

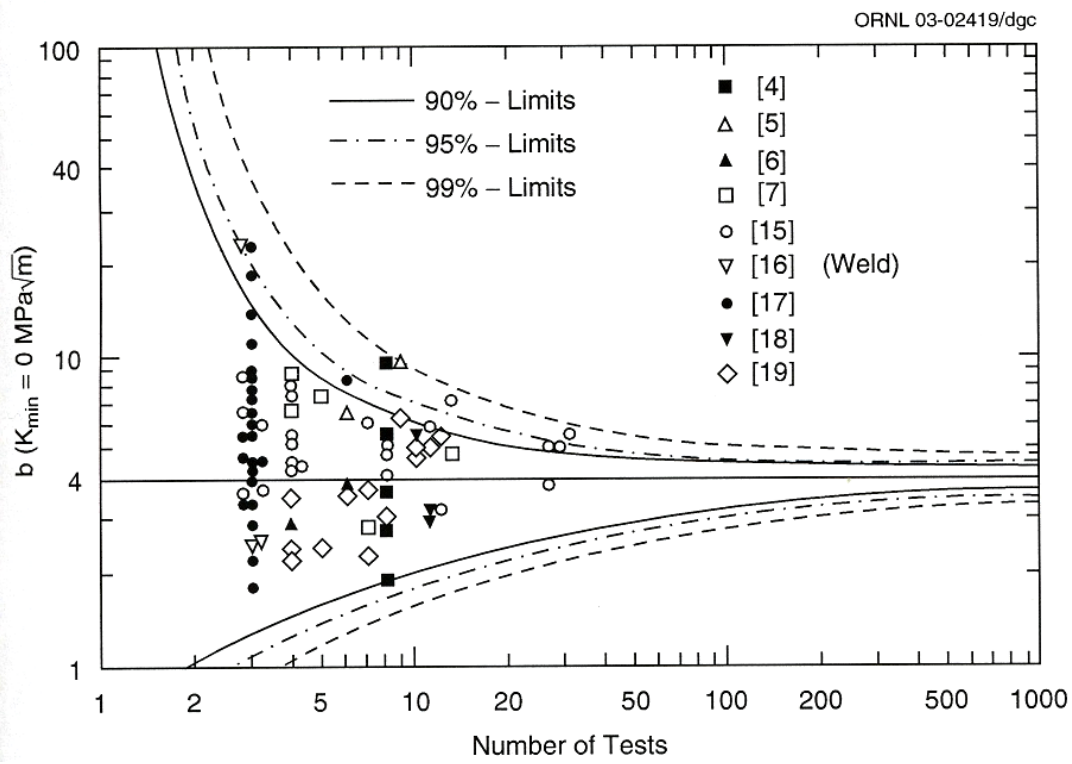

After McCabe et al [49], the identifying numbers can be found in [51]

Figure B-26 - Effect of Sample Size on the Measured Weibull Modulus for a Known Population

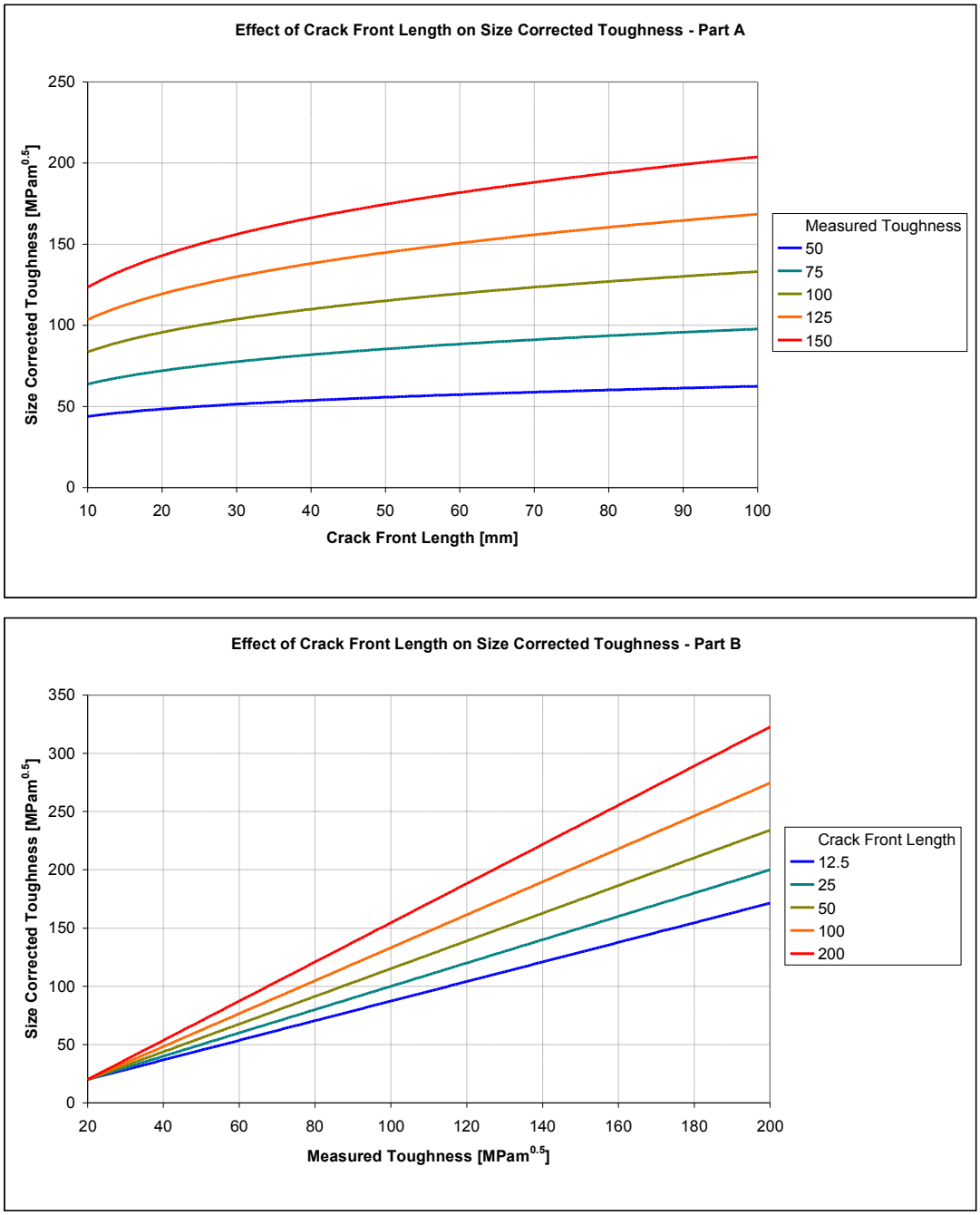

Figure B-27 - Effect of Crack Front Length on Size Corrected Toughness

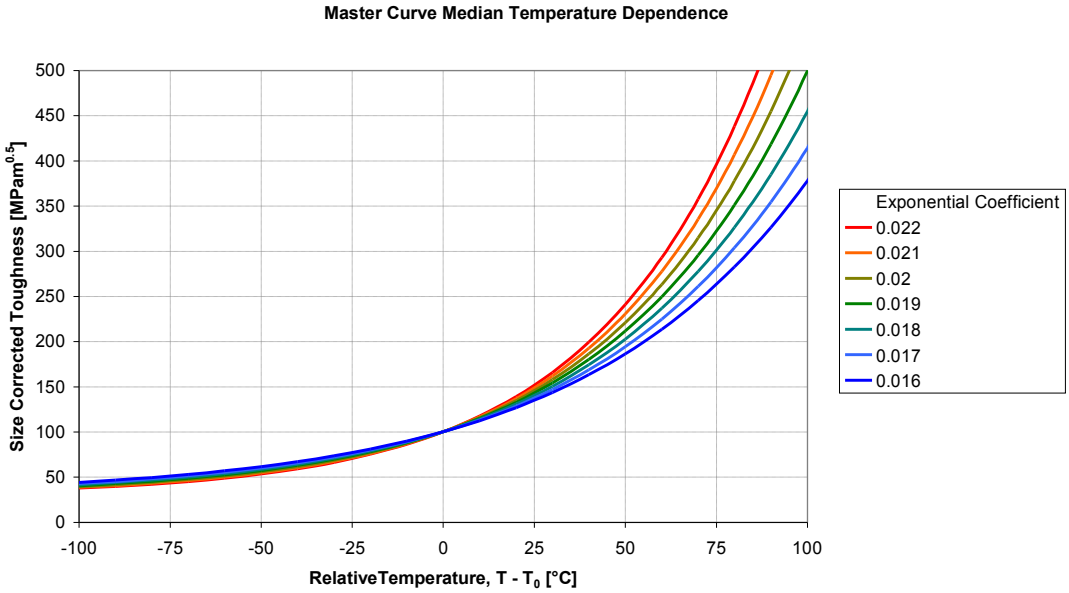

Figure B-28 - Master Curve Median Temperature Dependence

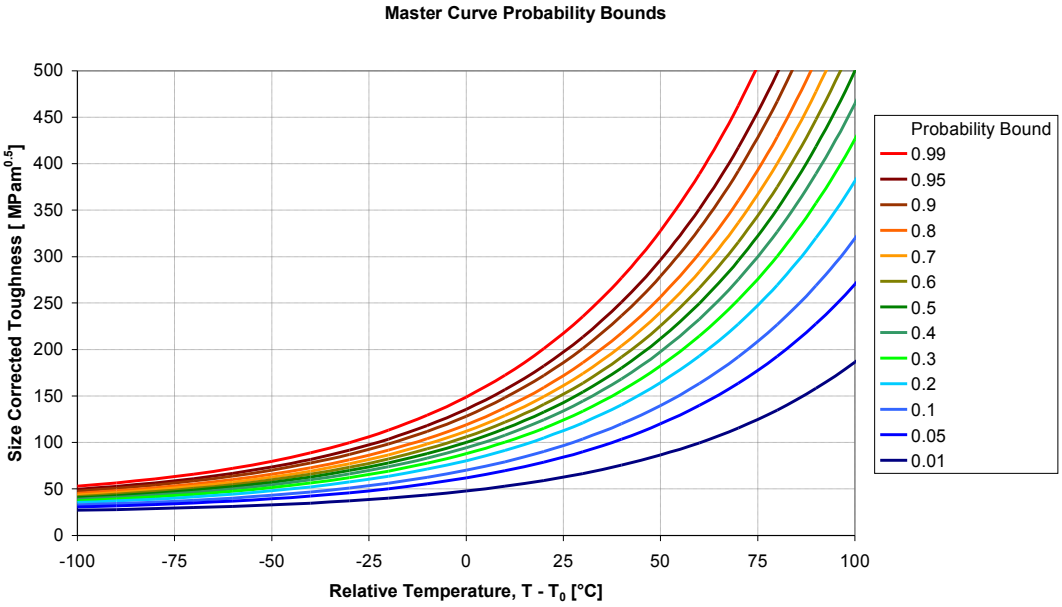

Figure B-29 - Master Curve Probability Bounds

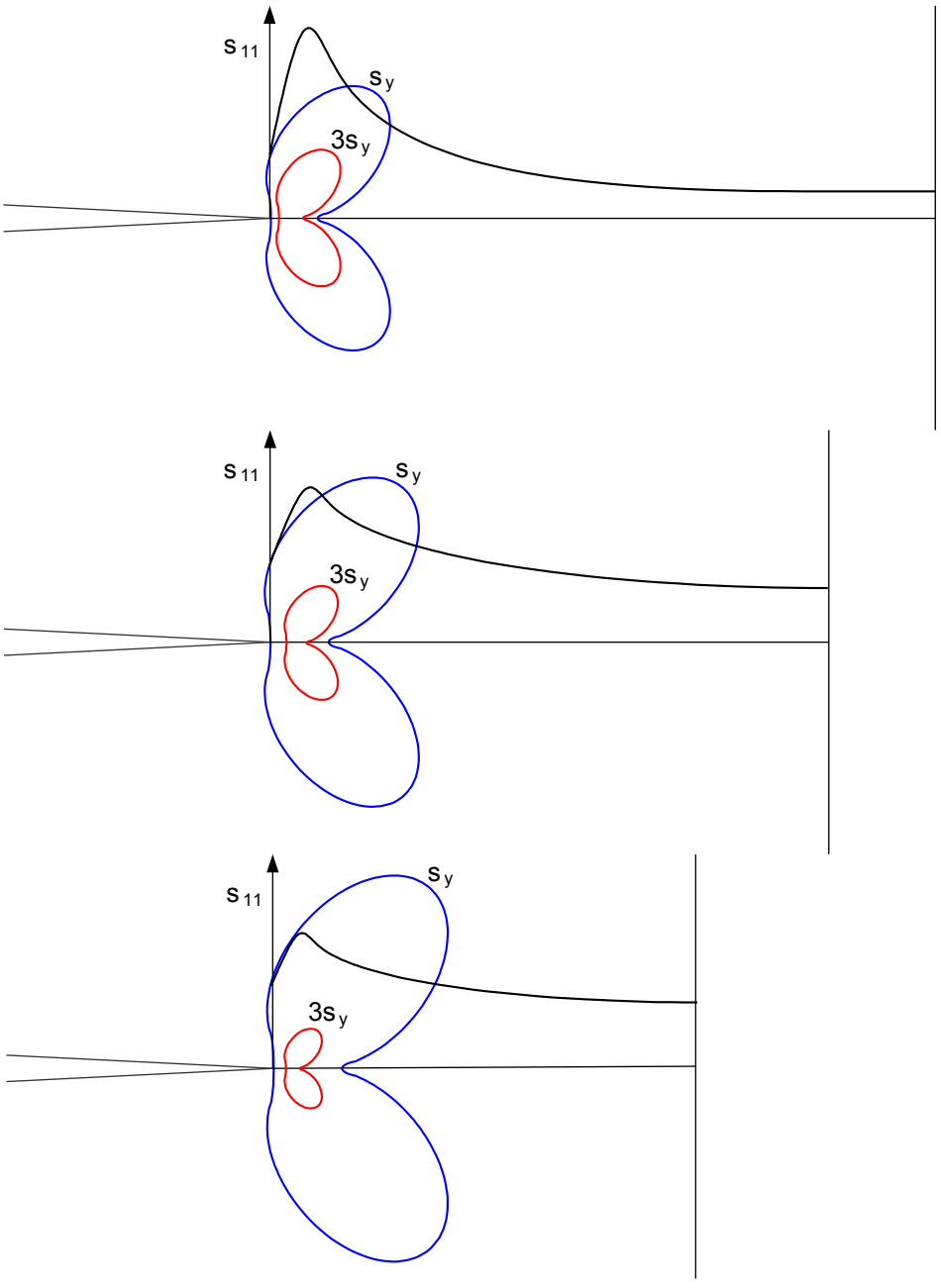

Figure B-30 - Effect of the Back Wall on the Constraint of Defect

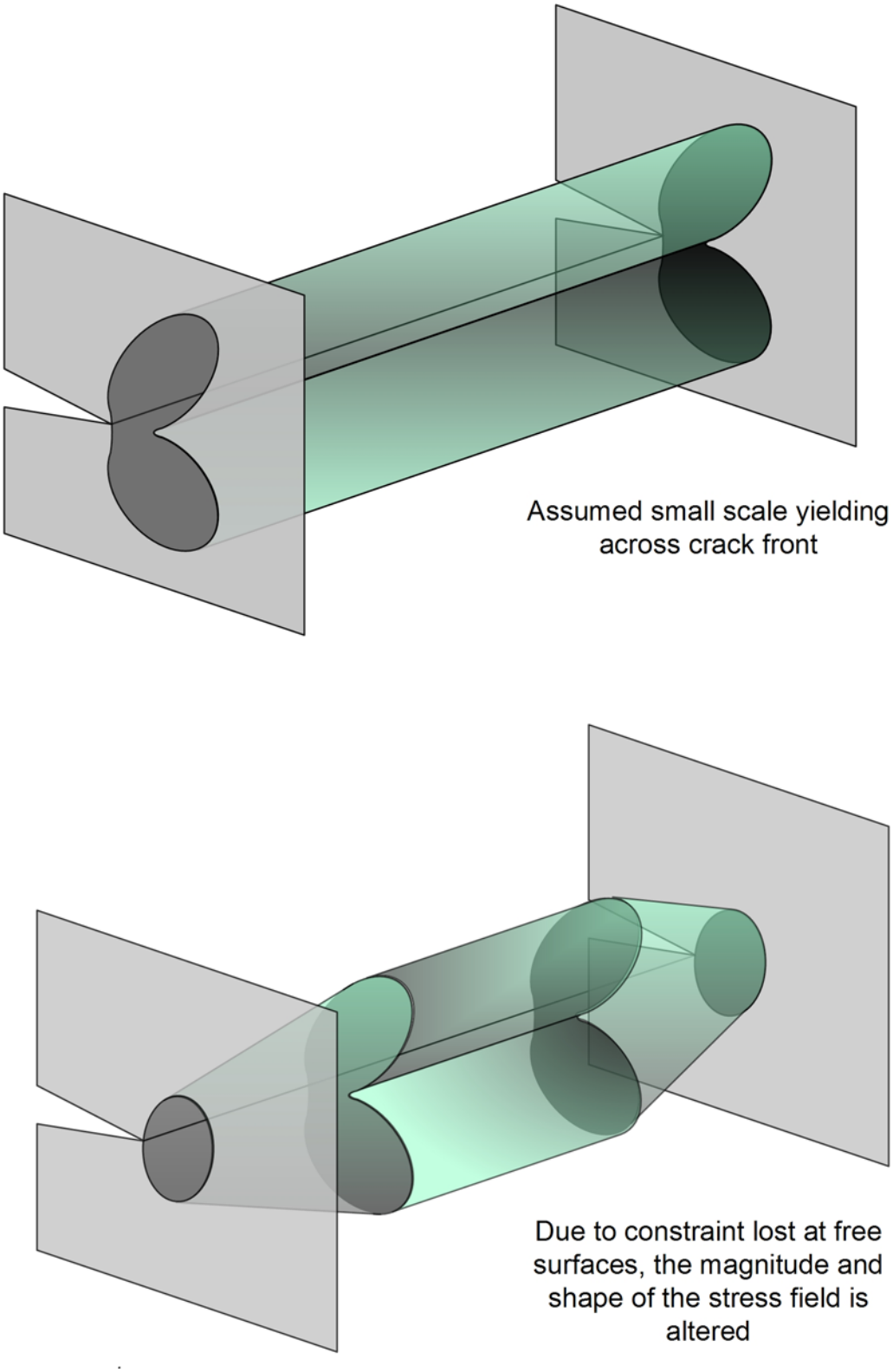

Figure B-31 - Effect of Free Side Surfaces the Constraint of a Defect

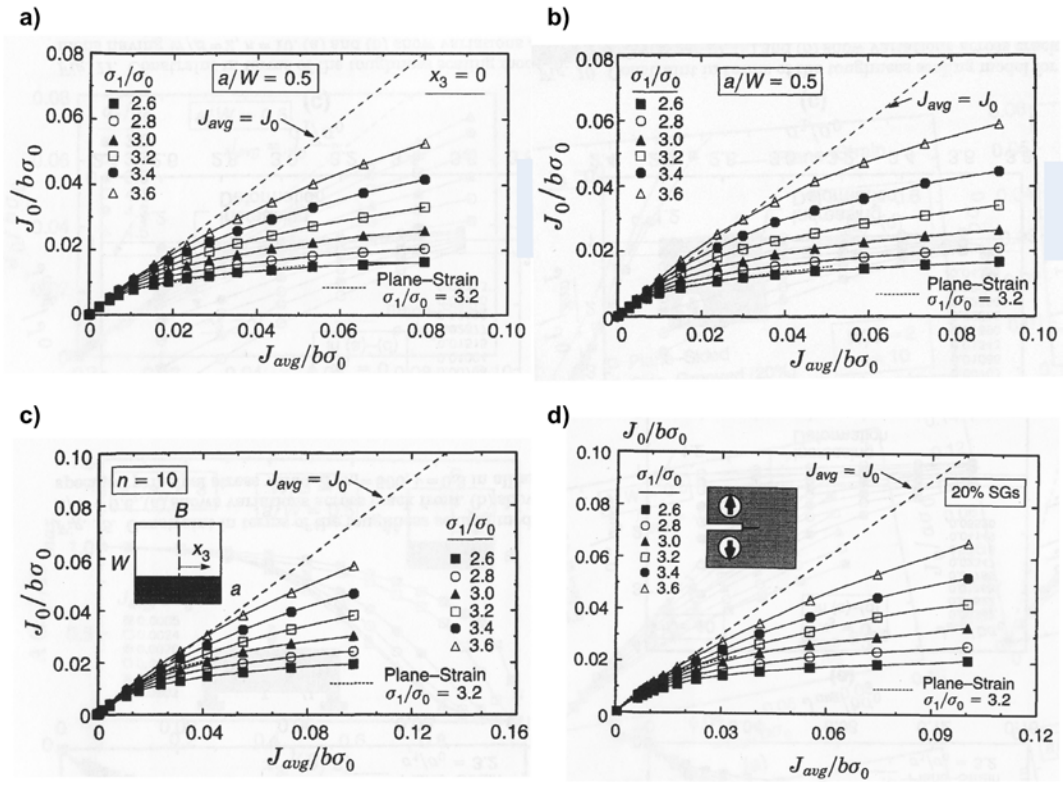

After Nevalainen et al [85]

Figure B-32 - Toughness Correction Factors as Supplied by Nevalainen and Dodds for a) B×B SE(B), b) B×2B SE(B), c) C(T), and d) C(T) 20% Side Grooved Specimens

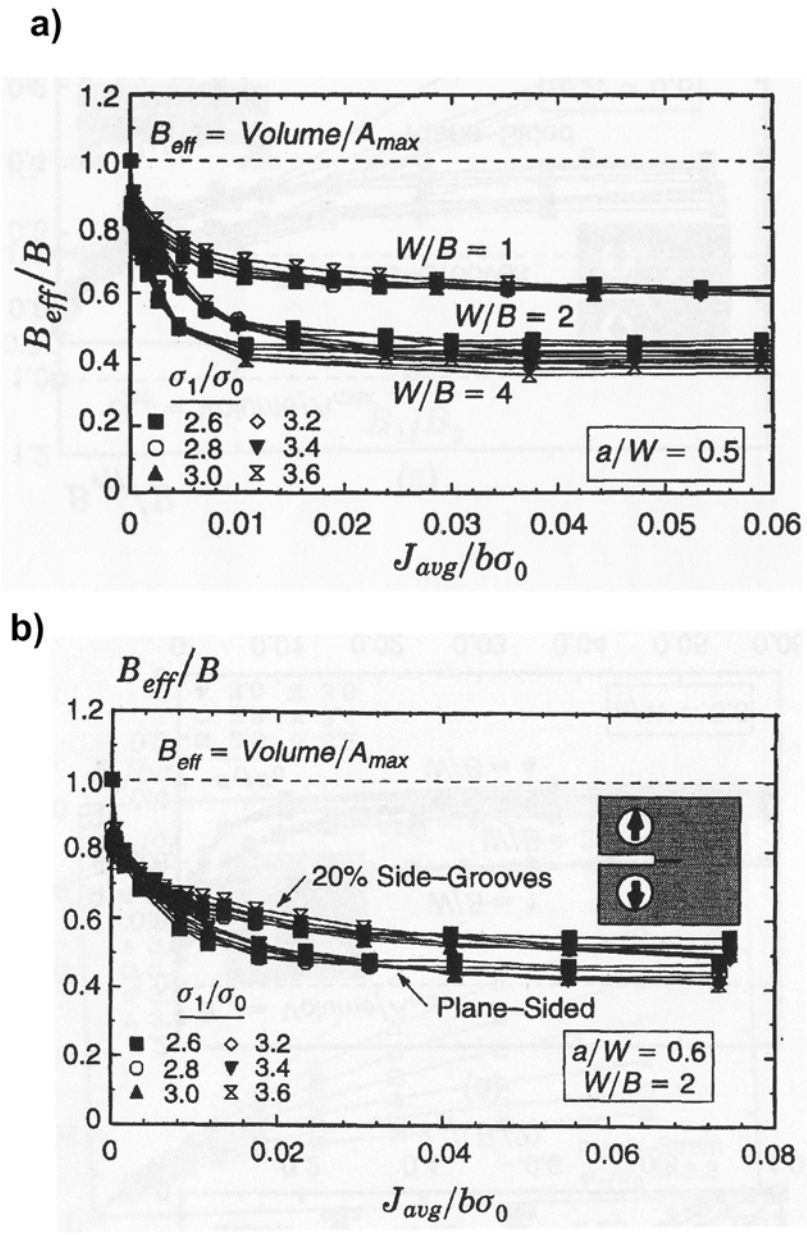

After Nevalainen et al [85]

Figure B-33 - Effective Thickness Correction Factors as Supplied by Nevalainen and Dodds for a) SE(B) and b) C(T) Specimens

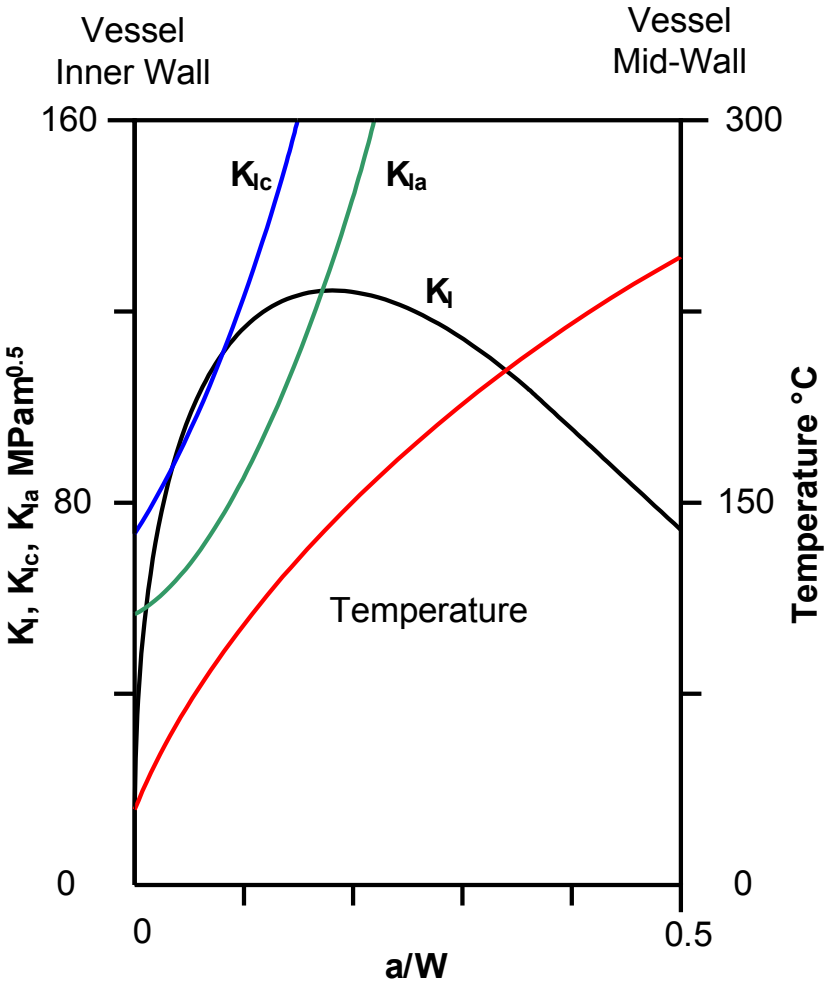

After Cheverton et al [92]

Figure B-34 - Through Wall Temperature Profile and Associated Toughness Behaviour Following a Pressurised Thermal Shock Event

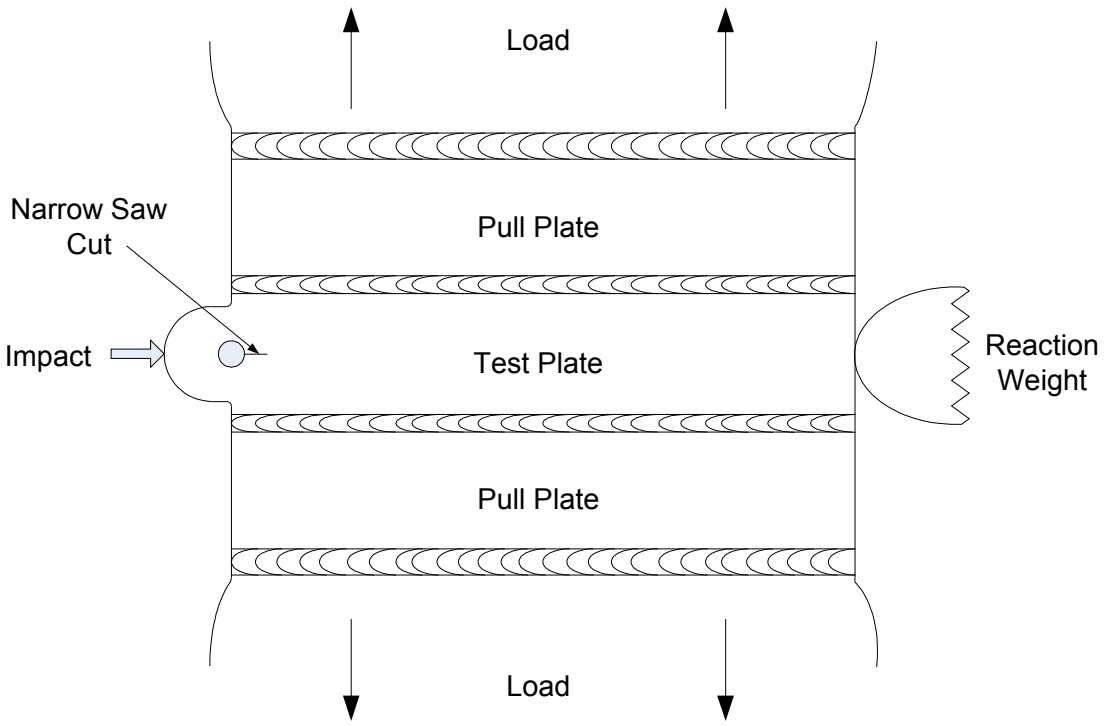

Figure B-35 - Robertson Crack Arrest Specimen

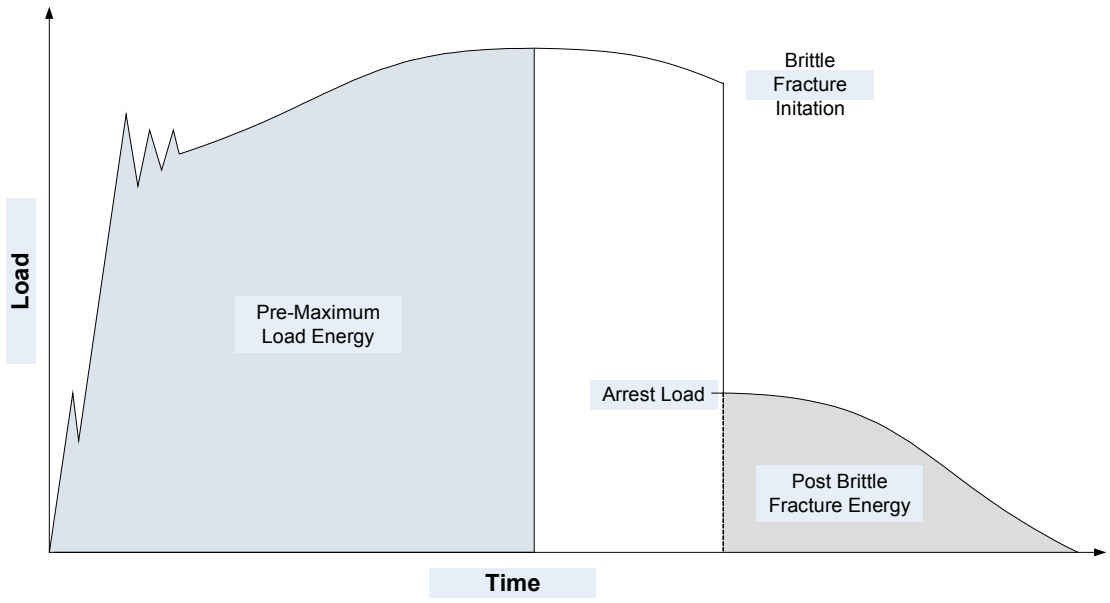

Figure B-36 - Typical Load Time Trace for an Instrumented Charpy Test

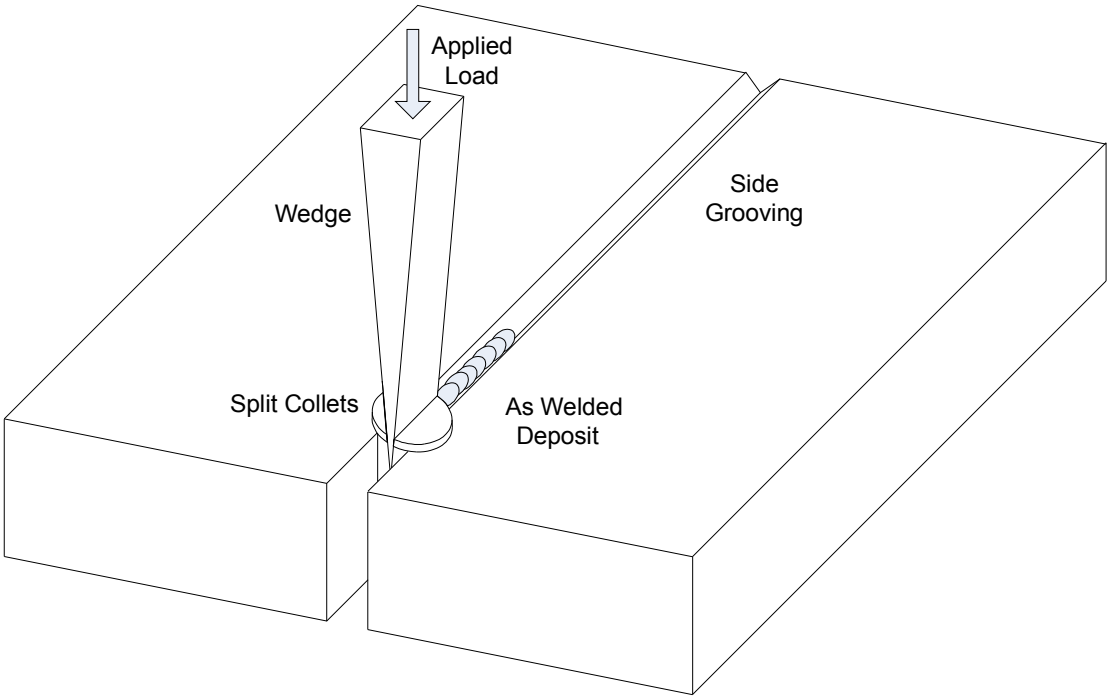

Figure B-37 - The Compact Crack Arrest (CCA) Specimen

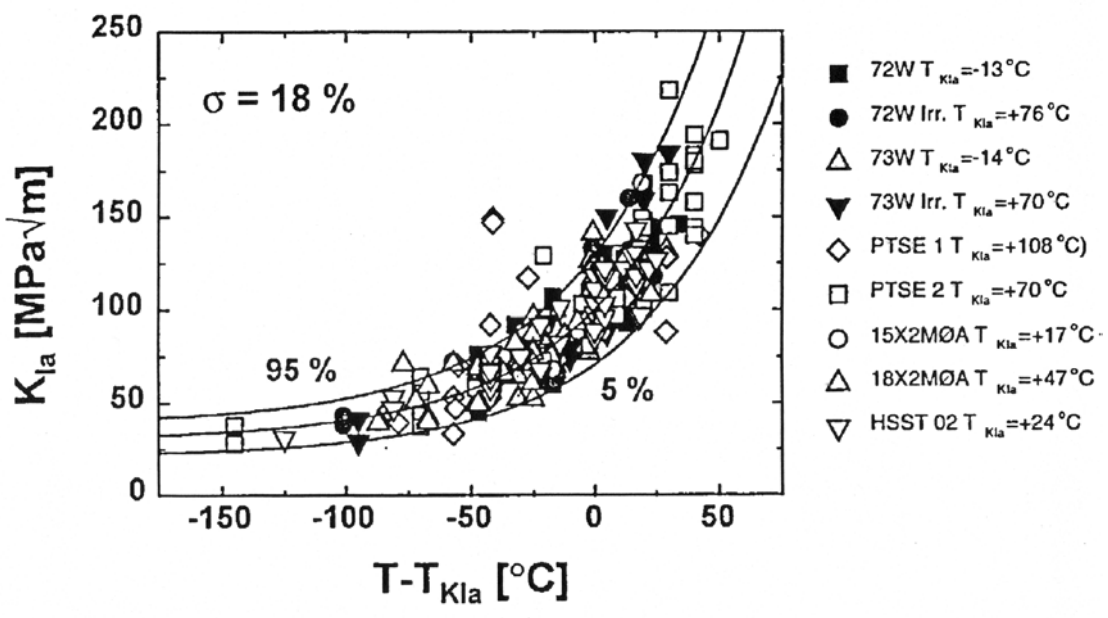

After Wallin [115]

Figure B-38 - Available Arrest Data Normalised by Arrest Reference Temperature, $T_{K_{Ia}}$

a)

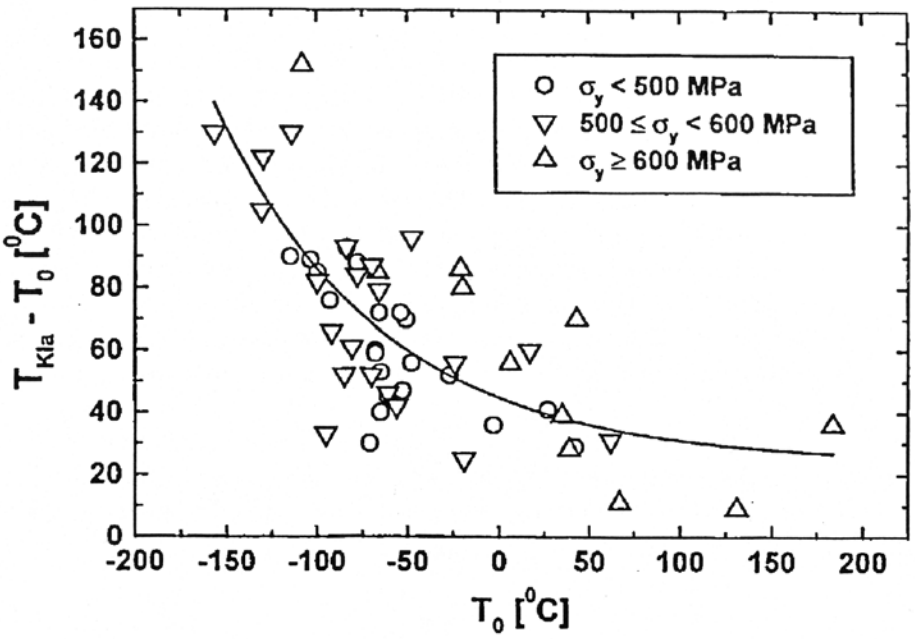

b)

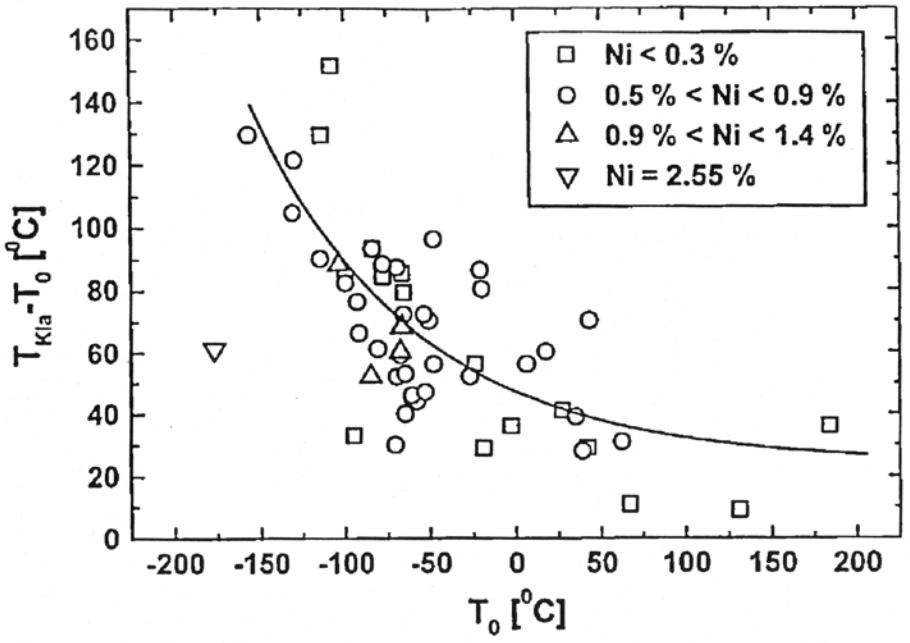

After Wallin [115]

Figure B-39 - Initiation and Arrest Toughness Correlation Showing Effect of a) Yield Stress and b) Nickel Content

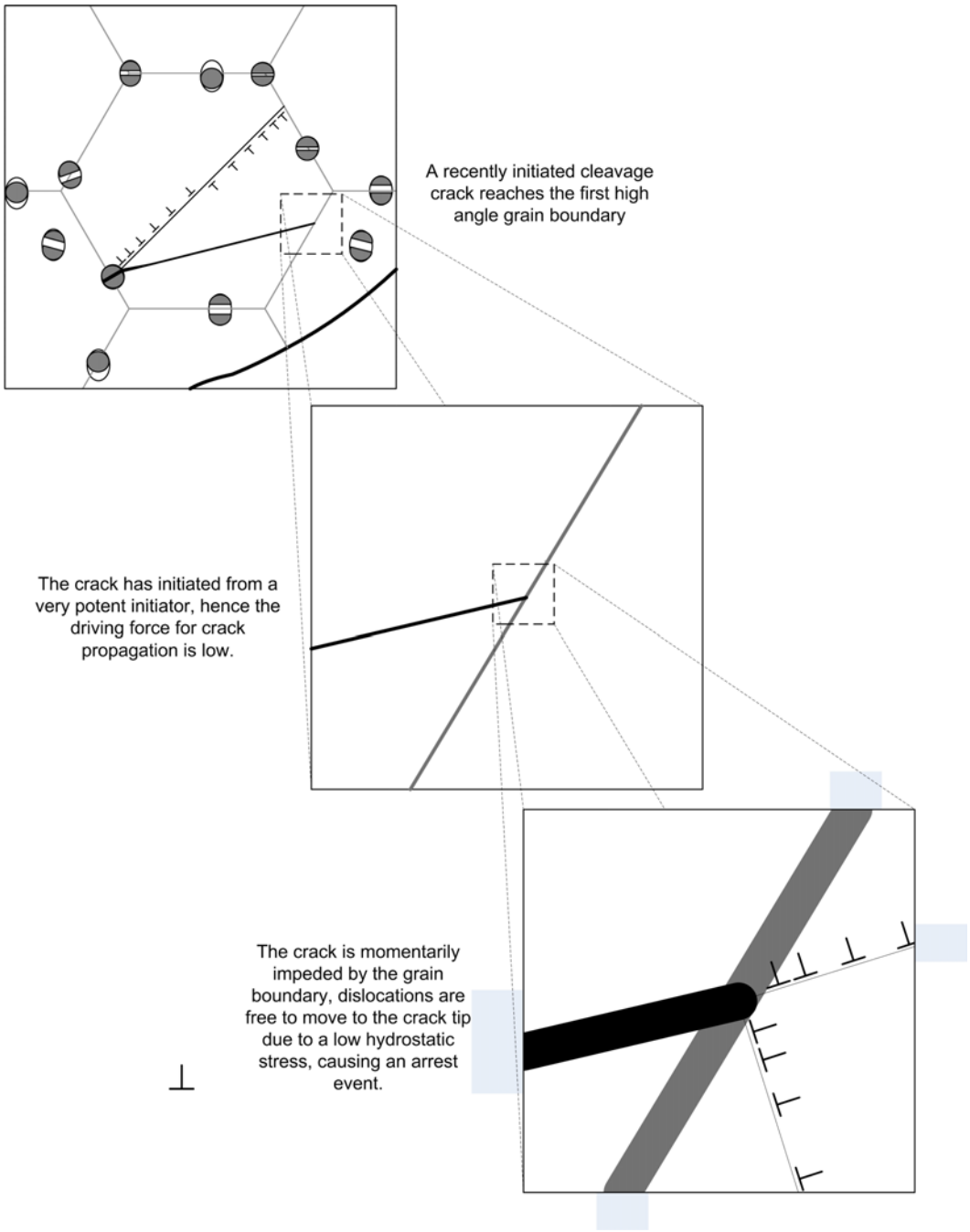

Figure B-40 - Microarrest Mechanism

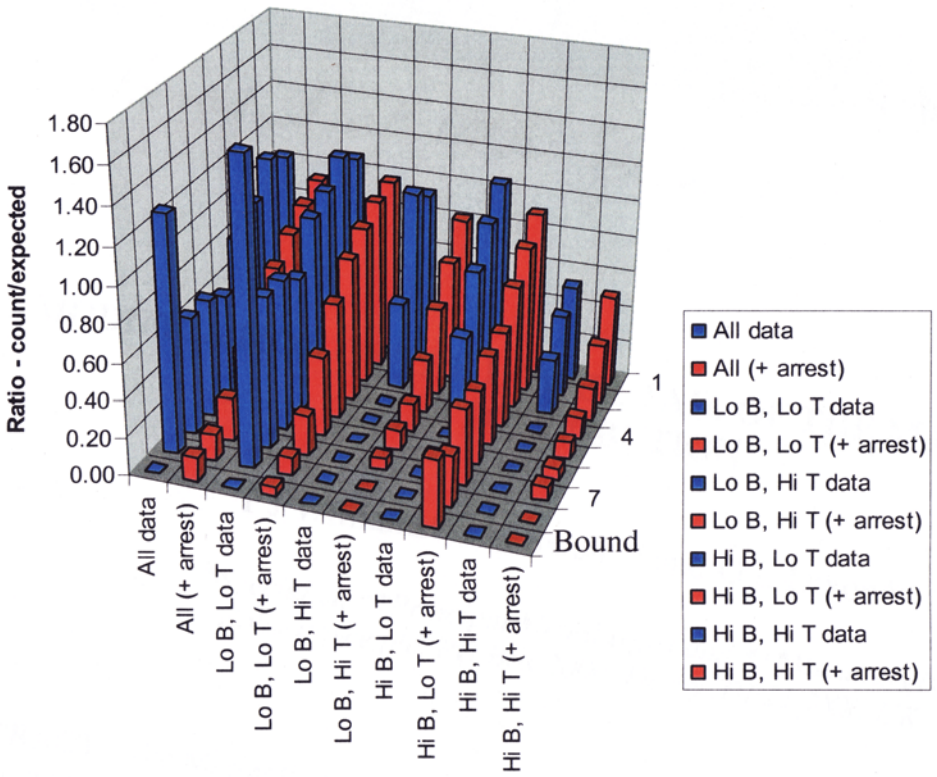

After Williams et al [23]

Data divided into subsets based on low and high crack front lengths
(Lo B, <90 mm and H B, >90 mm) and low and high T_0 (Lo T, <-70 °C, and H T, > -70 °C)

Figure B-41 - Results of Microarrest Simulations Showing Specimen Thickness and Reference Temperature Groupings

B.7 References

1. Cottrell, A., *An Introduction to Metallurgy: Second edition*. 1995: The Institute of Materials.
2. Hall, E.O., *The Deformation and Ageing of Mild Steel: III Discussion of Results.* Proceedings of the Physical Society, 1951. **64B**(9): p. 747-753.
3. Petch, N.J., *The Cleavage Strength of Polycrystals.* Journal of the Iron and Steel Institute, 1953. **173**: p. 25.
4. Askeland, D.R., *The Science and Engineering of Materials: Third S.I. Edition*. 1996: Nelson Thornes.
5. Zerilli, F.J. and R.W. Armstrong, *Dislocations-mechanics-based constitutive relations for dynamics calculations.* Journal of Applied Physics, 1987. **61**: p. 1816-1825.
6. Wagenhoffer, M., *Modelling the transition region fracture behaviour of ferritic steels*. 2002, University of Maryland.
7. Wessel, E.T. *Linear Elastic Fracture mechanics for Thick-Walled, Welded Steel Pressure Vessels: Material Property Considerations*. in *Symposium on Fracture Toughness Concepts for Weldable Structural Steel*. 1969. Risley: United Kingdom Atomic Energy Authority.
8. *ASTM E399-06 Standard test method for Linear-Elastic Plane-Strain Fracture Toughness K_{Ic} of Metallic Materials*. 2006, West Conshohocken: ASTM International.
9. *ASTM E1921-05 Standard Test Method for Determination of Reference Temperature, T_0, for Ferritic Steels in the Transition Range*. 2005, West Conshohocken: ASTM International.
10. Nevalainen, M. and R.H. Dodds Jr, *Numerical investigation of 3-D constraint effects on brittle fracture in SE(B) and C(T) specimens.* International Journal of Fracture, 1995. **74**(2): p. 131-161.
11. Anderson, T.L., *Fracture Mechanics; Fundamentals and Applications*. 2005: Taylor & Francis.
12. Janssen, M., J. Zuidema, and R.J.H. Wanhill, *Fracture Mechanics*. 2004: Spon Press.
13. Taylor , G.I., *Plastic Strain in Metals.* Journal of the Institute of Metals, 1938. **62**: p. 307-324.
14. Hutchinson, W.B. *Texture Without Tears*. in *SMEA 2006*. 2006.
15. Weertman, J. and J.R. Weertman, *Elementary Dislocation Theory*. 1964, New York: Macmillan.
16. Bowen, P., S.G. Druce, and J.F. Knott, *Effects of microstructure on cleavage fracture in pressure vessel steel.* Acta Metallurgica, 1986. **34**(6): p. 1121-1131.
17. Bowen, P., S.G. Druce, and J.F. Knott, *Micromechanical modelling of fracture toughness.* Acta Metallurgica, 1987. **35**(7): p. 1735-1746.
18. Jack, D.H. and K.H. Jack, *Invited review: Carbides and nitrides in steel.* Materials Science and Engineering, 1973. **11**(1): p. 1-27.

19. Tetelman, A.S., T.R. Wilshaw, and C.A. Rau Jr, *The critical tensile stress criterion for cleavage.* The International Journal of Fracture Mechanics, 1968. **4**(2): p. 147-157.
20. EricksonKirk, M., M. Wagenhoffer, and P.T. Williams, *PEAI End of Year Report.* 2008.
21. McLean, D., *Mechanical Properties of Metals*. 1962: John Wiley & Sons.
22. Umeno, Y., *Ab initio DFT Study of Ideal Strength of Crystal and Surfaces in Covalent Systems*, in *Materials Research Society*. 2008.
23. Williams, T.J., D.I. Swan, and G. Dixon, *Modification of the lower tail of the Master Curve distribution*, in *IAEA Specialist Meeting*. 2004: Moscow.
24. Lambert, A., et al., *Application of acoustic emission to the study of cleavage fracture mechanism in a HSLA steel.* Scripta Materialia, 2000. **43**(2): p. 161-166.
25. Milne, I., *Failure of a rock crusher*, D. Cogswell, Editor. 2007.
26. Dugdale, D.S., *Yielding of steel sheets containing slits.* J. Mech. Phys. Solids, 1960. **8**: p. 100-104.
27. SHIH, T.T. and J. OPOKU, *APPLICATION OF FRACTURE MECHANICS TO CERAMIC MATERIALS - A STATE-OF-THE-ART REVIEW.* Engineering Fracture Mechanics, 1979. **12**: p. 479-498.
28. Ritchie, R.O., J.F. Knott, and J.R. Rice, *On the relationship between critical tensile stress and fracture toughness in mild steel.* Journal of the Mechanics and Physics of Solids, 1973. **21**(6): p. 395-410.
29. Wallin, K. and A. Laukkanen, *New developments of the Wallin, Saario, Törrönen cleavage fracture model.* Engineering Fracture Mechanics, 2008. **75**(11): p. 3367-3377.
30. Beremin, F.M., *A local criterion for cleavage fracture of a nuclear pressure vessel steel.* Metallurgical Transactions A, 1983. **14A**: p. 2277-2287.
31. Noronha, S.J., J. Huang, and N.M. Ghoniem, *Multiscale modeling of the brittle to ductile transition.* Journal of Nuclear Materials, 2004. **329-333**(Part 2): p. 1180-1184.
32. Ortner, S.R. and C.A. Hippsley, *Two component description of ductile to brittle transition in ferritic steel.* Materials Science and Technology, 1996. **12**(12): p. 1035-1042.
33. Margolin, B.Z., et al., *Development of Prometey local approach and analysis of physical and mechanical aspects of brittle fracture of RPV steels.* International Journal of Pressure Vessels and Piping, 2007. **84**(5): p. 320-336.
34. Qiao, Y. and A.S. Argon, *Cleavage cracking resistance of high angle grain boundaries in Fe-3%Si alloy.* Mechanics of Materials, 2003. **35**(3-6): p. 313-331.
35. Qiao, Y. and A.S. Argon, *Cleavage crack-growth-resistance of grain boundaries in polycrystalline Fe-2%Si alloy: experiments and modeling.* Mechanics of Materials, 2003. **35**(1-2): p. 129-154.
36. Cogswell, D., *The effects of microstructure on the mechanical properties of A508-3 heavy section forgings.* Nuclear Future, 2009. **5**(3): p. 138-144.
37. Smith, E., *The spread of plasticity between two cracks.* International Journal of Engineering Science, 1964. **2**: p. 379-387.
38. King, J.E. and J.F. Knott, *The effects of crack length and shape on the fracture toughness of a high strength steel 300m.* Journal of the Mechanics and Physics of Solids, 1980. **28**(3-4): p. 191-200.

39. Taylor, N. and K.F. Nillson, *Transferability of Laboratory Fracture Data to Safety Assessment of Postulated Defects in Critical NPP Components.* Strength of Materials, 2004. **36**(1): p. 42-46.
40. Randle, V., *Recent Developments in Electron Backscatter Diffraction*, in *Advances in Imaging and Electron Physics*, W.H. Peter, Editor. 2008, Elsevier. p. 363-416.
41. Landes, J.D. and D.H. Shaffer, *Statistical Characterization of Fracture in the Transition Region*, in *Fracture Mechanics Twelfth Conference, ASTM STP700*. 1980, American Society for Testing and Materials. p. 368-382.
42. McMahon Jr, C.J. and M. Cohen, *Initiation of cleavage in polycrystalline iron.* Acta Metallurgica, 1965. **13**(6): p. 591-604.
43. *ASME Boiler and Pressure Vessel Code Section III, Appendix G: Protection against non-ductile failure*, American Society of Mechanical Engineers.
44. Server, W. and W. Oldfield, *Nuclear Pressure Vessel Steel Data Base EPRI NP-933*. 1978, Electric Power Research Instituite.
45. *Flaw evaluation procedures: ASME Section XI, EPRI SR-719*, T.U. Marston, Editor. 1978, Electric Power Research Institute.
46. Fontaine, A., E. Maas, and J. Tulou, *Prevision of the cleavage fracture properties using a local approach: application to the welded joint of a structural C-Mn steel.* Nuclear Engineering and Design, 1987. **105**: p. 77-81.
47. Kirk, M. and M. Mitchell, *Potential roles for the Master Curve in regulatory application.* International Journal of Pressure Vessels and Piping, 2001. **78**(2-3): p. 111-123.
48. Wallin, K., *Statistical re-evaluation of the ASME KIC and KIR fracture toughness reference curves.* Nuclear Engineering and Design, 1999. **193**(3): p. 317-326.
49. McCabe, D.E., J.G. Merkle, and K. Wallin, *An introduction to the development and use of the Master Curve method*. 2005, West Conshohocken: ASTM International.
50. Landes, J.D. and D.H. Shaffer, *Effect of Section Size on Transition Temperature Behaviour in a Structural Steel*, in *ASTM STP833*. 1984, American Society for Testing and Materials. p. 659-678.
51. Wallin, K., *The scatter in KIC-results.* Engineering Fracture Mechanics, 1984. **19**(6): p. 1085-1093.
52. Wallin, K., *The size effect in KIC results.* Engineering Fracture Mechanics, 1985. **22**(1): p. 149-163.
53. Wallin, K. *Statistical modelling of fracture in the ductile-to-brittle transition region*. in *Defect Assessment in Components - Fundamentals and Applications, ESIS/EGF9*. 1991. London: Mechanical Engineering Publications.
54. Wallin, K., *Master curve analysis of the "Euro" fracture toughness dataset.* Engineering Fracture Mechanics, 2002. **69**(4): p. 451-481.
55. Lawless, J.F., *Statistical Models and Methods for Lifetime Data*. 1982, New York: Wiley.
56. Bordet, S.R., et al., *A new statistical local criterion for cleavage fracture in steel. Part I: model presentation.* Engineering Fracture Mechanics, 2005. **72**(3): p. 435-452.
57. Bordet, S.R., et al., *A new statistical local criterion for cleavage fracture in steel. Part II: application to an offshore structural steel.* Engineering Fracture Mechanics, 2005. **72**(3): p. 453-474.

58. Margolin, B.Z., et al., *A new engineering method for prediction of the fracture toughness temperature dependence for RPV steels.* International Journal of Pressure Vessels and Piping, 2003. **80**(12): p. 817-829.
59. Margolin, B.Z., et al., *Prediction of the dependence of KJC(T) on neutron fluence for RPV steels on the basis of the Unified Curve concept.* International Journal of Pressure Vessels and Piping, 2005. **82**(9): p. 679-686.
60. Törrönen, K., et al., *Evaluation of the effect of metallurgical variables on materials behaviour and reference curves.* International Journal of Pressure Vessels and Piping, 1984. **15**(4): p. 251-269.
61. EricksonKirk, M., *Development of a Theoretically-based Statistical Model of Transition Toughness Distribution*. 2005, Phoenix Engineering Associates: Sykesville.
62. Yokobori, T., et al., *Non-linear interaction between main crack and near-by slip band.* Engineering Fracture Mechanics, 1975. **7**(3): p. 377-388.
63. Noronha, S. and N. Ghoniem, *Dislocation simulation of brittle-ductile transition in ferritic steels.* Metallurgical and Materials Transactions A, 2006. **37**(3): p. 539-544.
64. Noronha, S. and N. Ghoniem, *Modelling the brittle–ductile transition in ferritic steels: dislocation simulations.* International Journal of Mechanics and Materials in Design, 2008. **4**(1): p. 1-12.
65. Noronha, S. and N. Ghoniem, *Modelling the brittle–ductile transition in ferritic steels. Part II: analysis of scatter in fracture toughness.* International Journal of Mechanics and Materials in Design, 2008. **4**(1): p. 13-20.
66. Roberts, S.G., A.S. Booth, and P.B. Hirsch, *Dislocation activity and brittle-ductile transitions in single crystals.* Materials Science and Engineering: A, 1994. **176**(1-2): p. 91-98.
67. Roberts, S.G., *Modelling crack tip plastic zones and brittle-ductile transitions.* Materials Science and Engineering A, 1997. **234-236**: p. 52-58.
68. Viehrig, H.-W., M. Scibetta, and K. Wallin, *Application of advanced master curve approaches on WWER-440 reactor pressure vessel steels.* International Journal of Pressure Vessels and Piping, 2006. **83**(8): p. 584-592.
69. Pisarski, H.G. and K. Wallin, *The SINTAP fracture toughness estimation procedure.* Engineering Fracture Mechanics, 2000. **67**(6): p. 613-624.
70. Wallin, K., *Use of the Master Curve methodology for real three dimensional cracks.* Nuclear Engineering and Design, 2007. **237**(12-13): p. 1388-1394.
71. Moskovic, R., *Fracture toughness and crack growth resistance of pressure vessel plate and weld metal steels.* Engineering Fracture Mechanics, 1988. **30**(6): p. 839-861.
72. Moskovic, R. and P.L. Windle, *Suggested procedures for the analysis of multi-specimen fracture toughness test data.* Engineering Fracture Mechanics, 1988. **31**(2): p. 221-235.
73. Westergaard, H.M., *On the resistance of ductile materials to combined stresses in two or three directions perpendicular to one another.* Journal of the Franklin Institute, 1920. **189**(5): p. 627-640.
74. Hutchinson, J.W., *Plastic stress and strain fields at a crack tip.* Journal of the Mechanics and Physics of Solids, 1968. **16**(5): p. 337-342.
75. Rice, J.R. and G.F. Rosengren, *Plane strain deformation near a crack tip in a power-law hardening material.* Journal of the Mechanics and Physics of Solids, 1968. **16**(1): p. 1-12.
76. Fett, T., *A compendium of T-stress solutions*. 1998.

77. Wallin, K., *Quantifying Tstress controlled constraint by the master curve transition temperature T0.* Engineering Fracture Mechanics, 2000. **68**(3): p. 303-328.
78. Bass, B.R., et al., *Fracture assessment of shallow-flaw cruciform beams tested under uniaxial and biaxial loading conditions.* Nuclear Engineering and Design, 1999. **188**(3): p. 259-288.
79. Kirk, M.T., *The second ASTM/ESIS Symposium on Constraint Effects in Fracture; an overview.* International Journal of Pressure Vessels and Piping, 1995. **64**(3): p. 259-275.
80. Petti, J.P. and R.H. Dodds, *Constraint comparisons for common fracture specimens: C(T)s and SE(B)s.* Engineering Fracture Mechanics, 2004. **71**(18): p. 2677-2683.
81. Faleskog, J., *Effects of local constraint along three-dimensional crack fronts--a numerical and experimental investigation.* Journal of the Mechanics and Physics of Solids, 1995. **43**(3): p. 447-465.
82. O'Dowd, N.P. and C.F. Shih, *Family of crack-tip fields characterized by a triaxiality parameter--I. Structure of fields.* Journal of the Mechanics and Physics of Solids, 1991. **39**(8): p. 989-1015.
83. O'Dowd, N.P. and C.F. Shih, *Family of crack-tip fields characterized by a triaxiality parameter--II. Fracture applications.* Journal of the Mechanics and Physics of Solids, 1992. **40**(5): p. 939-963.
84. Rathbun, H.J., et al., *Influence of statistical and constraint loss size effects on cleavage fracture toughness in the transition--A single variable experiment and database.* Engineering Fracture Mechanics, 2006. **73**(1): p. 134-158.
85. Nevalainen, M. and R.H. Dodds Jr, *NUREG/CR-6317 Numerical Investigation of 3-D Constraint Effects on Brittle Fracture in SE(B) and C(T) Specimens*, O.o.N.R. Research, Editor. 1996, U.S. Nuclear Regulatory Commission.
86. Rathbun, H.J., et al., *Influence of statistical and constraint loss size effects on cleavage fracture toughness in the transition - A model based analysis.* Engineering Fracture Mechanics, 2006. **73**(18): p. 2723-2747.
87. Ramberg, W. and W.R. Osgood, *Description of stress-strain curves by three parameter. Technical Note No. 902*. 1943, National Advisory Committee For Aeronautics: Washington DC.
88. Petti, J.P. and R.H. Dodds, *Coupling of the Weibull stress model and macroscale models to predict cleavage fracture.* Engineering Fracture Mechanics, 2004. **71**(13-14): p. 2079-2103.
89. Petti, J.P. and J.R.H. Dodds, *Ductile tearing and discrete void effects on cleavage fracture under small-scale yielding conditions.* International Journal of Solids and Structures, 2005. **42**(13): p. 3655-3676.
90. Petti, J.P. and R.H. Dodds, *Calibration of the Weibull stress scale parameter, [sigma]u, using the Master Curve.* Engineering Fracture Mechanics, 2005. **72**(1): p. 91-120.
91. Wiesner, C.S. and B. Hayes, *A review of crack arrest tests, models and applications*. 1995, The Welding Institute.
92. Cheverton, R.D., et al., *Application of crack arrest theory to a thermal shock experiment*, in *STP 711*. 1980, American Society for Testing and Materials. p. 392-421.
93. Cheverton, R.D., et al., *Fracture mechanics data deduced from thermal shock and related experiments with LWR pressure vessel material.* Journal of Pressure Vessel Technology, 1983. **105**: p. 102-110.

94. Cheverton, R.D. and D.G. Ball, *The role of crack arrest in the evaluation of PWR pressure vessel integrity during PTS transients.* Engineering Fracture Mechanics, 1986. **23**: p. 71-80.
95. Stumpfrock, L., et al., *NESC-II Final Report - Brittle crack initiation, propagation and arrest of shallow cracks in a clad vessel under PTS loading*. 2003, Institute for Energy.
96. Fearnehough, G.D., D.W. Jade, and R.T. Weiner. *The arrest of brittle fracture in pipelines*. in *Practical application of fracture mechanics to pressure vessel technology*. 1971. London: Institute of Mechanical Engineers.
97. Robertson, T.S., *Propagation of brittle fracture in steel.* Journal of the Iron and Steel Institute, 1953. **175**: p. 361-374.
98. Kamath, M.S., *Crack propagation and arrest Part 1 - Wide plate crack arrest studies and the empirical test of Pellini and others.* The Welding Institute Research Bulletin, 1980(January): p. 14-25.
99. Kamath, M.S., *Crack propagation and arrest Part 2 - Dynamic aspects, mechanisms and the static LEFM approach.* The Welding Institute Research Bulletin, 1980(July): p. 193-203.
100. De Wit, R., S.R. Low, and R.J. Fields, *Wide plate crack arrest tesing: Evolution of experimental procedures*, in *STP 969*. 1988, American Society for Testing and Materials. p. 679-690.
101. *ASTM E208-91 Standard Test Method for Conducting Drop-Weight Test to Determine Nil-Ductility Transition Temperature of Ferritic steels*. 1991, West Conshohocken: ASTM International.
102. Smedley, G.P., *Prediction and specification of crack arrest properties of steel plate.* International Journal of Pressure Vessels and Piping, 1989. **40**: p. 279-302.
103. *ASTM E436-91 Standard Test Method for Drop-Weight Tear Tests of Ferritic Steels*. 1991, West Conshohocken: ASTM International.
104. *ASTM E1221-88 Standard Test Method for Determining Plane-Strain Crack-Arrest Fracture Toughness, K_{Ia}, of Ferritic Steels*. 1988, West Conshohocken: ASTM International.
105. Crosley, P.B. and E.J. Ripley, *A compact specimen for plane strain crack arrest testing.* Journal of Testing and Evaluation, 1980. **8**: p. 25-31.
106. Kies, J.A., A.M. Sullivan, and G.R. Irwin, *Interpretation of fracture markings.* Journal of Applied Physics, 1950. **21**(July): p. 716-720.
107. Irwin, G.R. and J.A. Kies, *Fracturing and fracture dynamics.* Welding Journal, 1952: p. 95-100.
108. McClintock, F.A. and S.P. Sukhatme, *Travelling cracks in elastic materials under longitudinal shear.* Journal of the Mechanics and Physics of Solids, 1960. **8**: p. 66-75.
109. Robertson, T.S. *Experimental techniques developed in investigations into high speed yield in brittle fracture*. in *IMechE Conference*. 1957. London.
110. Pratt, P.L. and T.A.C. Stock, *The distribution of strain around a running crack.* Proceedings of the Royal Society, 1965. **285**(1400): p. 73-82.
111. Tipper, C.F., *The study of fracture surface markings.* Journal of the Iron and Steel Institute, 1957. **185**(January): p. 4-9.
112. Hoagland, H.G., A.R. Rosenfield, and G.T. Hahn, *Mechanisms of fast fracture and arrest in steels.* Metallurgical Transaction, 1972. **3**(January): p. 123-136.

113. Bass, R., P.T. Williams, and C.E. Pugh, *An updated correlation for crack-arrest fracture toughness for nuclear reactor pressure vessels.* International Journal of Pressure Vessels and Piping, 2005. **82**: p. 489-495.
114. Wallin, K., *Application of the master curve method to crack initiation and crack arrest.* International Journal of Pressure Vessels and Piping, 1999. **393**: p. 3-9.
115. Wallin, K., *Correlation between static initiation toughness K_{Jc} and crack arrest toughness*, in *Fatigue and Fracture Mechanics: 32nd Volume ASTM STP 1406*, R. Chona, Editor. 2001, American Society for Testing and Materials: West Conshohocken. p. 17-34.
116. Swan, D.I., *Applicability of ORNL Arrest Model*, D.J. Cogswell, Editor. 2009.

Chapter C

Statistical Assessment of a Fracture Toughness Database

C Statistical Assessment of a Fracture Toughness Database

Contents

C Statistical Assessment of a Fracture Toughness Database....1
C.1 Interrogation of a Large Toughness Database....4
C.2 Establishing a Valid Reference Temperature....5
C.3 Toughness Database Assessment Methods....13
C.3.1 Weibull Distribution....13
C.3.2 Size Correction....15
C.3.3 Data Censoring....20
C.3.4 Maximum Likelihood Methods....21
C.3.4.1 Formation of Maximum Likelihood Equation....21
C.3.4.2 Maximum Likelihood Estimator....25
C.3.4.3 Error Estimates (Minimum Variance Bound)....27
C.3.5 Goodness of Fit Test....31
C.4 Probability Bounds....34
C.5 Toughness Database Analysis and Results....38
C.6 Discussion....54
C.6.1 Database Inference....54
C.6.2 Master Curve Weibull Shape Sensitivity Study....55
C.6.3 Micro Arrest Modified Master Curve....59
C.6.4 Constraint Corrected Master Curve Weibull Shape Sensitivity Study....62
C.6.5 Micro Arrest Extension to Constraint Corrected Model....67
C.6.6 General Concerns....72
C.7 Recommendations for Processing Data....75
C.8 Conclusions....78

C.9 Further Work.....80

C.10 Figures.....84

C.11 References.....113

Figures

Figure C-1 - Relative Proportions of a) Product Form and b) Irradiation Conditions..84

Figure C-2 - Simplified Representation of Size Correction.....85

Figure C-3 - Right Censoring of Lifetime Data.....86

Figure C-4 - Typical Parabola of Log Likelihood Function.....87

Figure C-5 - Typical Likelihood Surface for 2 Parameters.....88

Figure C-6 - Effect of Dataset Size on the Single Temperature Error Function.....89

Figure C-7 - All ASTM 1921-05 Data Normalised by Reference Temperature, ...90

Figure C-8 - Histogram of Actual to Expected Data for All ASTM E1921-05 Data Normalised by Reference Temperature, ...91

Figure C-9 - Effect of Weibull Shape on the Appearance of the All ASTM E1921-05 Data Histogram.....92

Figure C-10 - Effect of Scale Temperature Dependence on the Appearance of the All ASTM E1921-05 Data Histogram.....93

Figure C-11 - Effect of Weibull Shape on the Goodness of Fit Parameter, , for a Weibull shape modified ASTM E1921-05 model for a) 100 bins, and b) 50 bins.....94

Figure C-12 - Shape Optimised Model for All Data Normalised by Reference Temperature, ...95

Figure C-13 - Histogram of Actual to Expected Data for Shape Optimised Model.…96

Figure C-14 - Effect of Applying Micro Arrest Concept to ASTM E1921-05 Model.…97

Figure C-15 - Constraint Corrected Model for All Data Normalised by Reference Temperature, ...98

Figure C-16 - Histogram of Actual to Expected Data for Constraint Corrected Model 99

Figure C-17 - Effect of Weibull Shape on the Goodness of Fit Parameter, , for a Weibull shape modified Constraint Corrected model for a) 100 bins, and b) 50 bins 100
Figure C-18 - Shape Optimised Constraint Corrected Model for All Data Normalised by Reference Temperature, ... 101
Figure C-19 - Histogram of Actual to Expected Data for Shape Optimised Constraint Corrected Model..... 102
Figure C-20 - Effect of Varying Arrest Model Parameters on the Goodness of Fit (χ2 Probability) for the Shape Optimised Constraint Corrected Model..... 103
Figure C-21 - Effect of Varying Arrest Model Parameters on the Goodness of Fit (χ2 Probability) for the Shape Optimised Constraint Corrected Model for a) below , and b) above..... 104
Figure C-22 - Comparison of Low and High Temperature Ranges, Each Normalised by Maximum Value..... 105
Figure C-23 - Comparison of Arrest Distribution Parameters..... 106
Figure C-24 - Histogram of Actual to Expected Data for Micro Arrest Modified Shape Optimised Constraint Corrected Model..... 107
Figure C-25 - Failure Tolerance Bounds Predicted from the Micro Arrest Constraint Corrected Model for Typical A508-3 in the Start of Life Condition..... 108
Figure C-26 - Failure Tolerance Bounds Predicted from the Micro Arrest Constraint Corrected Model for Typical A508-3 in the End of Life Condition..... 109
Figure C-27 - Failure Tolerance Bounds Predicted from the Micro Arrest Constraint Corrected Model for Typical A508-3 Following Extended Irradiation..... 110
Figure C-28 - Histogram of All Below Reference Temperature Data Vs Expected for the Microarrest Constraint Corrected Model..... 111
Figure C-29 - Histogram of All Above Reference Temperature Data Vs Expected for the Microarrest Constraint Corrected Model..... 112

C.1 Interrogation of a Large Toughness Database

The database used in this investigation was originally provided to Rolls-Royce Nuclear Materials and Chemistry Support by Mark EricksonKirk of the United States Nuclear Regulatory Commission as part of an information exchange. The size of the database has since been significantly increased by the author to include propriety information available to Rolls-Royce. The database contains 8184 data points for 258 materials in 102 irradiation conditions. Figure C-1 details the relative proportions of product form and irradiation conditions for the database.

The database assessment has taken approximately two man-years of effort to complete and has broadly fallen into two stages. First, twelve months effort for database cleaning and building the calculation engine to allow rapid assessment of the database; the early stages of development of the calculation spreadsheet are detailed in the appendices. Second, a further twelve months effort has been required to fully develop the statistical and micro-mechanism assessments of the models employed.

Available models, such as those adopted or assumed in the Master Curve framework and the Micro-arrest description of fracture, suggest fixed values for key variables. This investigation goes further by assessing the physical implications of changing these variables to establish a truly robust method, both mathematically rigorous and mechanistically sound, which can be used to provide a highly accurate and verified model of toughness behaviour of low alloy steels in the transition region.

C.2 Establishing a Valid Reference Temperature

A number of methods exist for calculating the reference temperature, T_0, of a material. All, however, rely on the assumed probability distribution of the Master Curve and maximum likelihood estimation of the unknown parameters. The first and simplest method to be used was the single temperature technique. Tests are often performed as replicates to measure the scatter for the same testing conditions, i.e. temperature, specimen geometry, loading rate, etc. Assessing these data against a known distribution is the most straightforward approach to establishing the reference temperature. The Master Curve prescribes the parameters of the failure distribution and we can compare the results from testing against the known distribution using maximum likelihood methods, literally maximising the chance that given the current data the estimate is the most likely value of the parameter of interest.

These solutions can often be complex and cannot be solved analytically, fortunately, the mathematics become simpler as the relative temperature, $T - T_0$, is constant for all specimens; closed form solutions can be created to solve for relative temperature using partial differential equations [1-2]. In graphical terms, the relative temperature is adjusted until the data produces the best possible fit to the Master Curve distribution by moving it parallel to the temperature axis. The error on this estimate is readily established from the maximum likelihood procedure and also has a closed form solution. This solution can be reworked to provide the number of specimens required to achieve a certain level of error in the estimate, as the error contains the relative temperature term the error function itself has temperature dependence. This requires the use of a different number of specimens to reach a required level of error at different temperatures. Although not explicitly stated in the standard (ASTM-E1921 [3]) it is possible to demonstrate that the acceptable error

used for the standard is 10.5 °C, to follow convention, the error is then reported to the nearest whole number.

This allows the user to establish the number of specimens required to produce a T_0 that meets the validity requirement. The numbers of valid tests required is startling, as low as six. Considering that from these tests the probability of obtaining any toughness over a 100 °C temperature interval is readily established. In reality, such a small number of tests are rarely conducted unless the available material volume is very limited. The chance of generating an invalid test result is also greatly increased by testing at higher temperatures where constraint effects and the onset of ductile tearing begin to play a more significant role in the recorded toughness and specimen behaviour.

The single temperature technique is useful for assessing small datasets and establishing a good understanding of the basic mathematics of the Master Curve; however, the testing of material for large components will often involve multiple temperatures and a much larger number of tests. This provides the researcher with a better appreciation for the material; by testing at a number of temperatures, any unexpected trends are readily apparent and outlying data points readily identified for further investigation. The trade-off for this more visually pleasing assessment of the data is an increase in mathematical complexity. Closed form solutions to establish the reference temperature and error no longer exist, and the problem must be solved numerically. This is not a great hardship as most data analysis and spreadsheet software packages include some form of numerical solver, given the correct inputs they provide highly accurate solutions, several orders of magnitude better than are required for assessment.

While the mathematics becomes more complex, working from first principles makes use of the same formulae used for the single temperature assessment; they do however, quickly become much more sizeable as the terms cannot be equated and removed. The error function is no longer a simple relative temperature dependent function as each test temperature in the dataset will be different and the simple methods employed before cannot be used in exactly the same way. The ASTM E1921 standard [3] (hereafter labelled as the 'Standard'), requires that the data used to calculate the reference temperature must lie within the relative temperature range of $-50 \leqslant T - T_0 \leqslant 50$ °C. It is not possible to know if all data will lie within this range before testing, although it is possible to estimate the reference temperature from Charpy data and this can provide guidance on the temperature range to utilise for testing.

Following this initial estimation of T_0, it is possible that some of the data may lie outside the limits defined above; the relative temperature estimate then needs to be remade with the outliers excluded. This process may need to be repeated several times to establish a truly valid T_0; in some cases the estimate will alternate between two values where a data point is removed and then included by the fluctuation. For these data sets, it is evident that the more conservative value must be chosen, i.e. the higher of the two T_0 values. The estimate of T_0 will be as accurate using this method as the equations are the same; hence the multi temperature method can be applied to both replicate and temperature variable datasets.

This raises some problems on how to establish the validity of a reference temperature. The method used for the single temperature technique was to establish how many valid tests results are required to meet a predetermined uncertainty in the T_0 estimate. This could be done because of the closed form solutions but we no

longer have these for the multi temperature method. The approach adopted by the Standard maintains the simplicity of the single temperature technique by partitioning the data into relative temperature bands. Each band has a factor dependent on the number required to achieve a valid single temperature T_0, so for a band requiring six tests to produce a valid T_0, the factor is 1/6. By simply multiplying the number of valid tests in each band by the scoring factor and summing across all bands one can say that the calculated reference temperature is valid if the total score is more that 1, i.e. the uncertainty will be better than or equal to that which could be achieved with the single temperature technique. This requirement can result in datasets being declared 'invalid' when they could provide useful data, this will discussed later in this section.

The Master Curve method is simply a mathematical approach to the estimation of toughness and it can be misused or misinterpreted just as simply. The Standard provides a rigorous and essentially foolproof way of calculating a T_0 figure for a dataset. However, little guidance is provided on what is a self-similar data set and what material types the Master Curve can reasonably be applied to. As such the Master Curve has been applied to data that bear no resemblance in material type and form for which the Master Curve was verified against or intended to mode [4]. The grouping of data from various sources and even the misinterpretation of data from within a single component can generate errors in the T_0 estimate. It must be remembered that T_0 is the result of a mathematical fit to a dataset; if the dataset contains a variety of materials, a valid T_0 will likely result, but which would be entirely inappropriate for use in safety assessments.

In order to prevent the use of a non-conservative T_0 for a dataset that may contain heterogeneous data, the SINTAP [5-7] method has been developed. This was

method was used in early versions of the database assessment to aid database cleaning exercises; a flow chart describing its use can be found in the appendices. This gives a three-stage process to assess the heterogeneity of the data used to establish a reference temperature. The stage 1 value is equivalent to the E1921 value and as is calculated using the multi-temperature technique outlined in the Master Curve standard. This becomes the benchmark value for comparison to the stages 2 and 3 values. The stage 2 values are calculated by censoring the higher recorded toughness values to produce a conservative estimate based on the lower recorded toughness values. The SINTAP process is as follows:

1. A suitable test temperature can be established either from previously obtained toughness data for the material or from the Charpy 28 J temperature.

2. Stage 1. The generated data are used to calculate a reference temperature using either the multi or single temperature methods as per ASTM E1921. This is used as a benchmark for comparison to the other stages below.

3. Stage 2. All values above the median probability line, effectively the upper tail of the distribution, are censored and the reference temperature recalculated. By censoring the data back to the median any excessively high data points caused, for example, by the loss of constraint or inclusion of heterogeneous data do not have a controlling effect on the resultant reference temperature. An iteration is then performed by censoring all data that lie above the new median and the reference temperature is again recalculated; this may need to be completed several times until an unchanging reference temperature is established.

4. Stage 3. Remembering that the reference temperature is simply a mathematical fit, it is possible to estimate a reference temperature for each data point. By taking the maximum T_0 estimate from a dataset it is possible to assess the homogeneity of the dataset, and hence the homogeneity of the material used for assessment. In this case the poorest material is used to establish if heterogeneous data has been used. As a general rule, data would not be expected to lie beyond the 2 and 98 % for datasets containing less than 50 specimens; any values lying beyond these limits warrant further investigation. It must be remembered that due to the inherent scatter in toughness measurement it is entirely possible to obtain what appears to be heterogeneous data from a homogeneous material.

5. The various reference temperatures generated by the SINTAP method need to be compared and a value selected for use in safety assessments. The down selection process involves comparison first between the stages 1 and 2 values, the higher of which is used for further assessment. Comparing the resultant value to the maximum of stage 3 reference temperature gives an indication of the heterogeneity of the data. If the stage 3 value is at least 8 °C higher than the stage 1 or 2 value then the data can be considered heterogeneous and the stage 3 value should be used.

The SINTAP method does not guarantee a conservative reference temperature for the material; this can only be achieved by testing a very large number of specimens and in some cases this may be necessary. The procedure makes the best use of the data available and helps to preclude the use of optimistic reference temperatures in safety assessment. The inherent scatter in toughness measurement makes it difficult to be definitive about any calculations based on these datasets; it must always be

remembered that an excessively low toughness value can always occur, but it is highly unlikely.

It was mentioned early in this section that using a modified single temperature method to establish validity for multi temperature data was not ideal. In reality the method used by the E1921 Standard is conservative if the correct data is used and easy to apply. It is a good engineering solution to what can be a complex mathematical problem and by taking the difficult stages, the double differentiation of the likelihood expression to establish the error function, out of the process, the prospect of errors is greatly reduced. This, of course, is highly advantageous for a standardised analysis method where it is certainly preferable for the values produced by any research or test house to be the same given the same data; however, this can result in data not being accurately assessed. In particular, the SINTAP procedure removes consideration and quantification of errors for simplification of the process, removing a very powerful element of the assessment method.

The error in a maximum likelihood estimate is readily calculable and it is regrettable that it is not more widely used. The estimate of a variable is obtained by equating a partial differential of the likelihood function to zero, the error is simply the double differential at the same point. Difficulty in the derivation of the formulae used in the Master Curve and the solving of maximum-likelihood equations that may not have a closed form solution have resulted in a much simplified approach being adopted in the Standard. Due to this, the use of the simplified engineering approach can result in a reference temperature being declared ‘invalid’ when in reality it is perfectly within acceptable limits.

The error generated from the likelihood approach is also the true error in that estimate. This does raise the question of what is a valid reference temperature?

Again, we must remember that the reference temperature is a mathematical fit to data; any generated reference temperature could be used in assessments as long as the associated error is known. This of course moves away from the reason for having a standard method for the assessment of toughness data, i.e. to provide a simple and clear approach that can be readily followed and applied. The method of using the error to assess the validity of the reference temperature is simple and prevents the use of data with excessive error for safety assessment.

The statistical nature of the Master Curve enables the use of probabilistic methods for structural integrity safety assessments. Using the error generated using the pseudo single temperature method is overly conservative and suitable for deterministic approaches; however, excessive conservatism is not required when performing probabilistic analysis. In fact the goal is to represent reality as closely as possible. The use of an accurate error established directly from the likelihood function could provide improvements to the predicted failure rate and prolong plant lifetimes.

C.3 Toughness Database Assessment Methods

C.3.1 Weibull Distribution

The Weibull distribution [8-9] is one of several extreme value distributions and is commonly used in lifetime analysis. Extreme value distributions are used to assess the maximum or minimum obtained in a random sample from a population. The Weibull distribution was originally developed following lifetime analysis of mechanical and electrical components but has since been used for many varied purposes, such as the strength of spaghetti strands [10] or pharmaceutical testing [2]. Commonly used for assessing lifetimes of populations, the Weibull distribution is highly flexible and transferable to any number of situations. The mathematics of the Weibull distribution make it somewhat easier to manipulate than the Normal distribution; the probability and cumulative distributions can be easily established by knowing the other via differentiation or integration, respectively. The Weibull distribution also has a definite left hand limit whereas the normal distribution has none, essentially the normal distribution has the possibility of generating a negative value, and this is undesirable when assessing a number of physical phenomena.

The mathematics of the Weibull distribution is considered simple as the probability and cumulative density functions are readily obtained by differentiation and integration, respectively of the other function. This makes it possible to easily establish a maximum likelihood procedure containing censored data, a topic that will be discussed later and will be shown as highly important in the development of toughness modelling. The Weibull distribution is available in two forms, a two-parameter and a three-parameter description. Both versions contain the shape and scale functions. As stated earlier, the distribution is very flexible and can take any number of ‘shapes’ dependent on the shape variable; for a shape value of 4 the

distribution resembles a Normal distribution, while for a shape value of 1 the exponential distribution is created. The scale variable simply controls the fit of the function generated by the shape value to accommodate any magnitude of input data. The 3-parameter model also includes an offset value; as not all physical phenomena conveniently begin at a zero datum, the offset value allows the whole distribution to be shifted along the x-axis while maintaining the mathematical properties of the distribution.

The 2-parameter Weibull Distribution is given below. Equation C-1 describes the probability density function, PDF, and Equation C-2 describes the cumulative probability density function, CDF.

Equation C-1
$$P(x;\alpha,\beta) = \frac{\beta}{\alpha}\left(\frac{x}{\alpha}\right)^{\beta-1} e^{-\left(\frac{x}{\alpha}\right)^{\beta}}$$

Equation C-2
$$F(x;\alpha,\beta) = e^{-\left(\frac{x}{\alpha}\right)^{\beta}}$$

where α = Weibull Scale parameter

β = Weibull Shape parameter

The 3-parameter Weibull Distribution is given below. Equation C-3 describes the probability density function, and Equation C-4 describes the cumulative probability function.

Equation C-3
$$P(x;\alpha,\beta,\gamma) = \frac{\beta}{\alpha}\left(\frac{x-\gamma}{\alpha}\right)^{\beta-1} e^{-\left(\frac{x-\gamma}{\alpha}\right)^{\beta}}$$

Equation C-4
$$F(x;\alpha,\beta,\gamma) = e^{-\left(\frac{x-\gamma}{\alpha}\right)^{\beta}}$$

where γ = Weibull Offset parameter

As discussed in a previous section the Weibull distribution is used to model the toughness of low alloy steels (LAS) in the Master Curve method. A cloud of possible initiators lies ahead of a crack tip; as only the most potent is considered by the weakest link method, the most potent initiator is essentially sampled from all possible initiators. The Weibull distribution affords a means of assessing the most potent of these initiators when a weakest link model is assumed for failure. The true benefit of the Weibull distribution comes from the use of the survivor function discussed below. This describes the probability of survival as opposed to the probability of failure and is easier to manipulate. The survivor function can be used to describe the size effect of toughness measurement in LAS.

C.3.2 Size Correction

The size effect exhibited by LAS is due simply to the change in sampled volume ahead of a crack tip. The likelihood of finding a highly potent initiator is increased in a larger sampled volume. The beauty of the approach taken to size correction adjustment is that the underlying distribution of initiators in a material does not need to be established; however, a comparison can be made between the known distributions of toughness values for a certain length of crack front.

Size correction is inherent in the Master Curve method as it follows directly from weakest link theory and the mathematics of the Weibull distribution. Weakest link theory states that the component can be broken down into discrete blocks, i.e. we can test a crack front and obtain a toughness value, if we could then break the crack front into smaller sections and retest taking the lowest value from the smaller blocks would be equivalent of the value from the large block. Following from this understanding a method for size correction of toughness data can be established.

A crack front length in a component can be described as a collection of shorter crack fronts in each block of the component. As failure of one block will cause catastrophic failure, in order for the component to survive, all blocks must survive. If the probability of failure in each block is independent and equal, a key assumption for the adoption of the Weibull distribution, then a crack front length size correction can be established as follows.

To simplify the situation and ease the understanding of the development process, an assumption can be made that the component can be divided in 4 blocks. The probability of failure, $F(x_{1block})$, is known from experiment and is modelled well by the Weibull distribution.

Equation C-5 $F(x_{1block}) = 1 - S(x_{1block})$

where $S(x_{1block}) =$ the probability of survival for one block

As the blocks are independent of each other, the probability of failure for the component can be established by multiplication of the probability of survival for each block (see Figure C-2).

Equation C-6 $F(x_{4blocks}) = 1 - S(x_{4blocks})$

Equation C-7
$$\begin{aligned} S(x_{4blocks}) &= S(x_{1block}) \times S(x_{1block}) \times S(x_{1block}) \times S(x_{1block}) \\ &= S(x_{1block})^4 \end{aligned}$$

Equation C-8 $F(x_{4blocks}) = 1 - S(x_{1block})^4$

To generalize for any number n blocks in a component the following expression can be formed.

Equation C-9 $$F(x_{component}) = 1 - S(x_{1block})^n$$

From this foundation, the standard Master Curve size correction expressions can be established. However, instead of using blocks to describe the component the crack front length, following the description of the fracture process zone, can be used to determine the stressed volume ahead of the crack. For a crack front length, B_i, the probability of failure is known and is assumed to follow a three parameter Weibull distribution. Replacing the generic terms of Equation C-3 and Equation C-4 with those specific to toughness analysis the following expressions are established

Equation C-10 $$F(B_i) = 1 - e^{-\left(\frac{K_{B_i} - K_{min}}{\alpha}\right)^{\beta}}$$

where $K_{\min} \equiv \gamma$, the Weibull Offset parameter

Equation C-11
$$S(B_i) = 1 - F(B_i)$$
$$= e^{-\left(\frac{K_{B_i} - K_{min}}{\alpha}\right)^{\beta}}$$

By utilising and modifying Equation C-9 it is possible to calculate the probability of failure for any length, for example a reference length B_0.

$$F(B_0) = 1 - S(B_i)^n$$
$$1 - S(B_0) = 1 - S(B_i)^n$$

Equation C-12 $S(B_0) = S(B_i)^n$

where n = number of lengths with a known probability of failure, $\equiv \frac{B_i}{B_0}$

Equation C-13 $S(B_0) = e^{-\left(\frac{K_{B_0} - K_{min}}{\alpha}\right)^{\beta}}$

Equation C-14 $S(B_i) = e^{-\left(\frac{K_{B_i} - K_{min}}{\alpha}\right)^{\beta}}$

Equation C-12 to Equation C-14 can be combined and evaluated to bring the $\frac{B_i}{B_0}$ exponent within the Weibull expression.

Equation C-15

$$\begin{aligned} S(B_0) &= S(B_i)^n \\ e^{-\left(\frac{K_{B_0} - K_{min}}{\alpha}\right)^{\beta}} &= \left(e^{-\left(\frac{K_{B_i} - K_{min}}{\alpha}\right)^{\beta}}\right)^{\frac{B_i}{B_0}} \\ &= e^{-\frac{B_i}{B_0}\left(\frac{K_{B_i} - K_{min}}{\alpha}\right)^{\beta}} \\ &= e^{\left(\frac{(K_{B_i} - K_{min})\left(\frac{B_i}{B_0}\right)^{\frac{1}{\beta}}}{\alpha}\right)^{\beta}} \end{aligned}$$

The numerators of the exponent on each side of the above expressions can be extracted from the above equation and equated.

Equation C-16 $$K_{B_0} - K_{min} = \left(K_{B_i} - K_{min}\right)\left(\frac{B_i}{B_0}\right)^{\frac{1}{\beta}}$$

Equation C-17 $$K_{B_0} = K_{min} + \left(K_{B_i} - K_{min}\right)\left(\frac{B_i}{B_0}\right)^{\frac{1}{\beta}}$$

Equation C-18 $$K_{B_i} = K_{min} + \left(K_{B_0} - K_{min}\right)\left(\frac{B_0}{B_i}\right)^{\frac{1}{\beta}}$$

Equation C-17 and Equation C-18 are very useful for quick calculations from one crack length to another; however, they provide little insight into why the size correction can be universally applied. Alternatively, the survivor expression for B_i can be manipulated further into another useful form.

Equation C-19
$$S(B_i)^n = e^{\left(\frac{(K_{B_i}-K_{min})\left(\frac{B_i}{B_0}\right)^{\frac{1}{\beta}}}{\alpha}\right)^{\beta}} = e^{-\left(\frac{[K_{B_i}-K_{min}]}{\left(\frac{\alpha}{\left(\frac{B_i}{B_0}\right)^{\frac{1}{\beta}}}\right)}\right)^{\beta}}$$

This is the survivor function for a modified Weibull distribution using the same shape and location as before but the scale parameter has been altered by the size correction ratio. The distribution parameters are then insensitive to the manipulation for size correction, which makes this approach mathematically simple to apply, such that the size correction can be used at any number of stages in the Master Curve method. This makes it possible to interchange when the size correction is applied in any assessment method, something that can become confusing and as such the author will highlight when a size correction is applied to data.

C.3.3 Data Censoring

It is often the case in lifetime studies that the component may survive longer than the duration of the test (see Figure C-3), this is also known as right censoring. This presents a problem for the researcher, as although it is known that the component could survive beyond the duration it is unknown when or whether that particular specimen will have eventually failed. Although the exact value of the failure is unknown, the point at which it was still functioning is known. Commonly when performing any experiment, some specimens will not terminate within the measuring limits of the test. Before the introduction of data censoring, this would have frequently resulted in the data being excluded from further analysis, however useful statistical information can be taken from this null result if the underlying probability distribution is known or can be assumed. In this way, all information from an experimental programme can be used in the analysis of the results. The above is true when conducting toughness testing.

In a test specimen, as the load is incremented, the applied stress intensity factor is limited by the geometry of the specimen. At some point during loading, the specimen will lose constraint resulting in gross plastic deformation of the specimen. The specimen can be said to have survived the test without failing. The specimen's ability to maintain a high constraint region is known from finite element modelling and a non dimensional measure of constraint, M, can be used as a censoring parameter [11-12], i.e. if the load and specimen geometry combine to give a value below, in this case, a pre-chosen M value, then the datum will be censored. In this case, it will only be known that the specimen survived past a particular loading point, and hence stress intensity factor, at the chosen censoring M value. Any number of validity criteria can be applied to the data as a means of censoring test results.

For example, consider a small (10 × 10 mm) three-point bend specimen, SE(B), tested in the upper transition region. In this region it is highly likely that the specimen will lose constraint resulting in the formation of a plastic hinge as opposed to brittle failure. This will result in a number of possible censored values depending on which criteria are applied. If the underlying failure distribution is assumed then this datum can still be used. From the cumulative distribution, it is possible to estimate the probability that a datum will lie beyond the measuring limit and hence the proportion of specimens that will survive past this limit can be predicted.

C.3.4 Maximum Likelihood Methods

Maximum likelihood methods are a very powerful way of estimating variables for probability distributions. Superficially, the procedure appears slightly backwards in that the data are used to assess an estimate of the variable rather than estimating the variable directly from fitting of the data, but in fact the method is very robust. By using estimated values for a variable it is possible to calculate the likelihood that the dataset of interest could be generated. In order to assess the suitability of the estimated variable, the likelihood expression must first be formed. This must include the probability distribution of interest and any censoring parameters.

C.3.4.1 Formation of Maximum Likelihood Equation

A maximum likelihood expression can be formed to estimate the parameters of a probability distribution. Censored data can also be included due to the use of the survivor function and the right censoring concept outlined above, i.e. if the specimen survives the test the researcher can still take useful statistical information that can be used in maximum likelihood estimates.

There are two possibilities when performing a toughness test: the specimen may fail in a brittle manner, or the specimen may survive the test by either failing past a pre-set limit or not failing at all for a number of reasons. Where the specimen fails and no limits are reached, then the probability of this failure can be estimated from the assumed toughness distribution.

Equation C-20 $P(Failure) = P(x)$

Where the specimen fails beyond a limit or survives the test then the probability that the failure lies beyond the measuring limit can be estimated

Equation C-21 $P(Failure) = P(x > limit)$

These can be combined into a joint expression that estimates the probability of failure at any x.

Equation C-22 $P(Failure) = P(x)^{\delta} P(x > limit)^{1-\delta}$

where $\delta = 1$ for uncensored data, i.e. $x < limit$

$\delta = 0$ for censored data, i.e. $x > limit$

For uncensored data Equation C-22 simply reverts to Equation C-20. For censored data, Equation C-22 reverts to Equation C-21.

Equation C-23

$$\begin{aligned} P(Failure)_{\delta=1} &= P(x)^{\delta} P(x > limit)^{1-\delta} \\ &= P(x)^{1} P(x > limit)^{0} \\ &= P(x) \end{aligned}$$

Equation C-24

$$\begin{aligned} P(Failure)_{\delta=0} &= P(x)^{\delta}\, P(x > limit)^{1-\delta} \\ &= P(x)^{0}\, P(x > limit)^{1} \\ &= P(x > limit) \end{aligned}$$

Applying the above method to brittle fracture initiation testing a modified version of Equation C-22 can be used to describe the probability of fracture.

Equation C-25 $P(Failure) = P(K)^{\delta}\, P(K > K_{Jc_{limit}})^{1-\delta}$

where $\delta = 1$ for uncensored data, i.e. $K < K_{Jc_{limit}}$

$\delta = 0$ for censored data, i.e. $K > K_{Jc_{limit}}$

$K_{Jc_{limit}}$ = value of toughness corresponding to the censoring condition

By making the assumption that failure in the transition is initiation controlled, i.e. controlled by weakest link statistics, Equation C-25 can be re-written to produce the probability of failure for any tested value.

Equation C-26 $P(initiation|K) = P(initiation_K)^{\delta}\, P(initiation_{> K_{Jclimit}})^{1-\delta}$

Equation C-27 $$P(initiation_K) = \frac{\beta}{\alpha}\left(\frac{K - K_{min}}{\alpha}\right)^{\beta-1} \exp\left[-\left(\frac{K - K_{min}}{\alpha}\right)^{\beta}\right]$$

Equation C-28 $$P(initiation_{> KJclimit}) = \exp\left[-\left(\frac{K - K_{min}}{\alpha}\right)^{\beta}\right]$$

Equation C-29

$$P(initiation|K) = \left(\frac{\beta}{\alpha}\left(\frac{K - K_{min}}{\alpha}\right)^{\beta-1}\exp\left[-\left(\frac{K - K_{min}}{\alpha}\right)^{\beta}\right]\right)^{\delta} \times \left(\exp\left[-\left(\frac{K - K_{min}}{\alpha}\right)^{\beta}\right]\right)^{1-\delta}$$

$$= \left(\frac{\beta}{\alpha}\left(\frac{K - K_{min}}{\alpha}\right)^{\beta-1}\right)^{\delta}\exp\left[-\left(\frac{K - K_{min}}{\alpha}\right)^{\beta}\right]$$

where K = measured K if $K < K_{Jclimit}$ (uncensored), or

$K = K_{Jclimit}$ if $K > K_{Jclimit}$ (censored)

Equation C-29 can be formed into a likelihood expression.

Equation C-30

$$L = \prod_{i=1}^{N}\left(\frac{\beta}{\alpha}\left(\frac{K - K_{min}}{\alpha}\right)^{\beta-1}\right)^{\delta}\exp\left[-\left(\frac{K - K_{min}}{\alpha}\right)^{\beta}\right]$$

This expression can be computationally difficult to calculate due to the accuracy available to computers. By taking the natural logarithm of the expression the value of the numbers used during calculations is greatly increased by converting the multiplication to addition, as the product quickly becomes exceedingly small.

Equation C-31

$$\Omega = \sum_{i=1}^{N}\log\left(\left(\frac{\beta}{\alpha}\left(\frac{K_i - K_{min}}{\alpha}\right)^{\beta-1}\right)^{\delta}\exp\left[-\left(\frac{K_i - K_{min}}{\alpha}\right)^{\beta}\right]\right)$$

$$= \sum_{i=1}^{N}\delta\log\left(\left(\frac{\beta}{\alpha}\left(\frac{K_i - K_{min}}{\alpha}\right)^{\beta-1}\right)\log\left(\exp\left[-\left(\frac{K_i - K_{min}}{\alpha}\right)^{\beta}\right]\right)\right)$$

$$= \sum_{i=1}^{N}\delta\log(\beta) - \delta\beta\log(\alpha) + (\beta - 1)\log(K_i - K_{min}) - \left(\frac{K_i - K_{min}}{\alpha}\right)^{\beta}$$

The above expression can be used to find an estimate for any variable in the equation. The value, which has the highest likelihood of being a true estimate of a variable, will correspond to the highest value of Ω . A plot of Ω vs any variable will give a parabolic curve (see Figure C-4), the peak of which corresponds to the highest likelihood estimate for the variable.

C.3.4.2 Maximum Likelihood Estimator

There are a number of methods for solving maximum likelihood equations which are simply a function of the variable of interest. These can be maximised successfully by various methods. Commonly the estimate of a variable is made by differentiating the log likelihood function with respect to the variable and equating this to zero. This can be performed for all variables, leading to a series of equations which must be solved simultaneously. These systems can be highly complex and difficult to solve; the above log likelihood expressions have three variables requiring three equations to solve the system. These variables may also be dependent on others, such as α is dependent on reference temperature in the Master Curve method. An estimate for reference temperature is simply an expression of the log likelihood differentiated with respect to reference temperature.

Often the partial derivatives are highly complex, however, the use of the Weibull distribution again simplifies the process. The partial derivatives for this system can at least be formed and as such can be solved as a set of simultaneous equations. The partial derivatives for the three parameters are given below.

Equation C-32
$$\frac{\partial \Omega}{\partial \beta} = \sum_{i=1}^{N} \frac{\delta}{\beta} + \log(K_i - K_{\min}) - \left(\frac{K_i - K_{\min}}{\alpha}\right)^{\beta} \log\left(\frac{K_i - K_{\min}}{\alpha}\right) - \delta \log(\alpha)$$

Equation C-33 $$\frac{\partial \Omega}{\partial \beta} = \sum_{i=1}^{N} \frac{\left(K_i - K_{\min}\right)\left(\frac{K_i - K_{\min}}{\alpha}\right)^{\beta - 1}\beta}{\alpha^2} - \frac{\delta\beta}{\alpha}$$

Equation C-34 $$\frac{\partial \Omega}{\partial K_{\min}} = \sum_{i=1}^{N} \frac{\left(\frac{K_i - K_{\min}}{\alpha}\right)^{\beta - 1}\beta}{\alpha} - \frac{\beta - 1}{K_i - K_{\min}}$$

The three variables may be fixed if the distribution is known, as is the case with the Master Curve method; the shape and offset are fixed, to 4 and 20 respectively, and the scale is free to vary but the value is constrained to follow a function dependent on T_0, or relative temperature, of the material. This function describes the relative and absolute temperature dependence of the Master Curve. As only the scale of the distribution changes with temperature the Master Curve maintains mathematical simplicity across the entire recommended temperature range. The equation itself is very simple, comprising an athermal term and a thermal term, including the temperature dependence variable of 0.019. This variable controls the severity of the transition.

Equation C-35 $$\alpha = 11 + 77e^{0.019(T - T_0)}$$

When the above is input into the maximum likelihood expression only one derivative remains, which can be expressed as a function of T_0. The derivative of interest is given below.

Equation C-36 $$\frac{\partial \Omega}{\partial T_0} = \sum_{i=1}^{N} \frac{5.852e^{0.019(T_i - T_0)}\left(K_i - 20\right)^4}{\left(11 + 77e^{0.019(T_i - T_0)}\right)^5} - \frac{5.852\delta e^{0.019(T_i - T_0)}}{11 + 77e^{0.019(T_i - T_0)}}$$

The maximum of Ω is then easily found by equating $\frac{\partial \Omega}{\partial T_0}$ to 0 and including the summation required for the maximum likelihood estimation, this gives the common form of solution found in E1921.

Equation C-37 $$\sum_{i=1}^{N} \frac{e^{0.019(T_i - T_0)}(K_i - 20)^4}{\left(11 + 77e^{0.019(T_i - T_0)}\right)^5} = \sum_{i-1}^{N} \frac{\delta e^{0.019(T_i - T_0)}}{11 + 77e^{0.019(T_i - T_0)}}$$

Solving for T_0 must be completed by numerical methods, but as these are available in most spreadsheet and statistical software packages, it is considered trivial to solve the above and produce an estimate of the reference temperature for the dataset. The situation becomes much more complex when free fitting of all variables is conducted. Here the problem becomes multi dimensional and difficult to visualise; for a single variable the data can be plotted on a simple x-y plot (see Figure C-4), for two variables a third dimension must be employed (see Figure C-5), for three dimensions a hypercube must be used. As can be seen, it becomes impossible to represent the data on a standard plot and purely numerical techniques must be used to solve the system. Fortunately, the numerical solvers included in most software packages are capable of solving for several variables if the expressions are given in a suitable format for the software to compute.

C.3.4.3 Error Estimates (Minimum Variance Bound)

Maximum likelihood estimators have two further desirable features, one of which is paid for by an inbuilt bias in the estimate. This bias is a problem often overlooked and for the purpose of this work will also be overlooked as the bias is removed by choosing even modest sample sizes. The bias does, however, give a very useful

property to a maximum likelihood estimate, that of invariance. This provides a level of freedom in the way the analysis can be conducted. The invariance is the reason that the reference temperature could be estimated directly although the variable is not a parameter of the Weibull distribution, i.e. assessing for the peak in the likelihood can be performed by using either the scale variable directly or something on which it depends; both will yield the same estimate.

The second desirable feature of maximum likelihood estimators is the ease with which the error on that estimate can be determined. It can be shown that the variance of the estimate is a function of the second differential of the likelihood function with respect to the variable of interest [1]. Taking the estimate of T_0 as a specific example we obtain:

Equation C-38

$$Variance(T_0) = -\frac{1}{\partial^2\Omega / \partial T_0^2}$$

Equation C-39

$$Error(T_0) = \sqrt{-\frac{1}{\partial^2\Omega / \partial T_0^2}}$$

Equation C-40

$$Variance(T_0) = -\sum_{i=1}^{N} \frac{1}{\frac{8.562\delta e^{0.038(T_i - T_0)}}{\left(11 + 77e^{0.019(T_i - T_0)}\right)^2} - \frac{0.111\delta e^{0.019(T_i - T_0)}}{11 + 77e^{0.019(T_i - T_0)}} - \frac{42.807e^{0.038(T_i - T_0)}(K_i - 20)^4}{\left(11 + 77e^{0.019(T_i - T_0)}\right)^6} + \frac{0.111\delta e^{0.019(T_i - T_0)}(K_i - 20)^4}{\left(11 + 77e^{0.019(T_i - T_0)}\right)^5}}$$

Evaluating this expression results in a function that is unwieldy at best and open to a number of possible errors in application of the formula. It was understandable that this process was not adopted in the E1921 Standard but because of this a general understanding of the mathematics that power the Master Curve method has been lost. Instead, a step function based on the single temperature method has been applied to produce a notional acceptance criterion. In reality, this is based on the error function, Equation C-39. If this is applied to the single temperature technique then it is possible to work backwards to the number of specimens required to meet this estimate. This is effectively the dataset size requirement published in the Standard.

Using the single temperature method outlined in the Standard allows the use of the closed form solution for establishing the reference temperature of the material; i.e. it is possible to equate the derivative to zero and solve the equation analytically. The second differential of the likelihood function for the single temperature method can be simplified considerably [13] to produce the expression shown below:

Equation C-41
$$\frac{\partial^2 \Omega}{\partial T_0^{\,2}} = \left(\frac{4 \times 77 \times 0.019 e^{0.019(T - T_0)}}{(11 + K_{\min}) + 77 e^{0.019(T - T_0)}} \right)^2 \sum_{i=1}^{N} \delta_i$$

The error of this estimate is considerably easier to obtain than that of the full expression (Equation C-40) as can be seen below:

Equation C-42

$$Error(T_0) = \sqrt{-\frac{1}{\partial^2\Omega / \partial T_0^2}}$$

$$= \sqrt{-\frac{1}{\left(\frac{4 \times 77 \times 0.019e^{0.019(T-T_0)}}{(11+K_{\min})+77e^{0.019(T-T_0)}}\right)^2 \sum_{i=1}^{N}\delta_i}}$$

$$= \frac{(11+K_{\min})+77e^{0.019(T-T_0)}}{4 \times 77 \times 0.019e^{0.019(T-T_0)}} \sqrt{\frac{1}{\sum_{i=1}^{N}\delta_i}}$$

Equation C-43

$$Error(T_0) = \frac{\phi}{\sqrt{\sum_{i=1}^{N}\delta_i}}$$

where ϕ is used in lieu of β, the variable name adopted in ASTM E1921

Equation C-44 $\phi = \dfrac{(11-K_{\min})+77e^{0.019(T-T_0)}}{4 \times 77 \times 0.019e^{0.019(T-T_0)}}$

Equation C-42 can be plotted for various dataset sizes and it soon becomes clear how the values supplied in the tables of the Standard for the required number of specimens in a relative temperature range have been established (see Figure C-6). The number of valid specimens required simply conforms to the number required to equal or better an error of 10.5 °C in the estimate of T_0. This may result in useful data being thrown out, as it is possible with the multi-temperature method to achieve better errors with fewer valid specimens. If the error is calculated rigorously by assessing the second differential of the likelihood function at the peak the true error in the estimate can be obtained. This produces more valid data and also reduces the error applied when conducting safety assessments.

There is a much simpler process to determine both the maximum likelihood estimate and the error on that estimate. By simply taking the values of the likelihood function

in a step wise fashion it is possible to produce both the differential and the second differential using very simple gradient expressions.

Equation C-45
$$\frac{d\Omega(x)}{dx} = \frac{\Omega(x+\delta x) - \Omega(x-\delta x)}{2\delta x}$$

Equation C-46
$$\begin{aligned}\frac{d^2\Omega(x)}{dx^2} &= \frac{d}{dx}\left(\frac{\Omega(x+\delta x) - \Omega(x-\delta x)}{2\delta x}\right)\\ &= \frac{1}{\delta x}\left(\frac{\Omega(x+\delta x) - \Omega(x)}{\delta x} + \frac{\Omega(x) - \Omega(x-\delta x)}{\delta x}\right)\\ &= \frac{\Omega(x+\delta x) - 2\Omega(x) + \Omega(x-\delta x)}{\delta x^2}\end{aligned}$$

This numerical procedure is more computationally intensive than the direct evaluation afforded for single temperature techniques; however, the approach is easier to apply and a more simple solving method can be adopted.

C.3.5 Goodness of Fit Test

In order to establish if changes to the Master Curve model are actually making improvements to the fit obtained with a large database a goodness of fit test is required. Many candidate goodness of fit tests exist, but due to the large number of data points in the assessed database, one based on binning the data is preferred. A modification of the χ^2 test allows assessment of a model compared to a histogram of the experimental data [1]. This is ideal for this application as it is easy to determine the probability of failure associated with a toughness value at any temperature in the transition region. This allows the creation of a histogram of the data binned by the probability of failure; we can then assess the number obtained in a bin versus the

number expected. A very simple formula can then be used to assess the χ^2 parameter.

Equation C-47 $$\chi^2 = \sum_{i=1}^{N} \frac{(y_i - f(x_i))^2}{f(x_i)}$$

where y_i = the actual number of events in bin i

$f(x_i)$ = the predicted number of events in bin i

The χ^2 probability can then be calculated using standard tables; the degrees of freedom used for the calculation are simply the number of bins in the histogram minus the number of fitted parameters, which will commonly only be one, the reference temperature, T_0. It should be spelt out that a high χ^2 probability does not prove that a model is a good fit to the data, it is the probability that a model that genuinely describes the data would give a value of χ^2 as large, or indeed larger, than the one calculated. In effect, it reinforces a hypothesis that a model fits the data well and applies a score to that level of fit, i.e. for χ^2 values equal to the number of degrees of freedom the model has a high probability of being an accurate description of the data. For very large χ^2 values the model may still be incorrect the user has just been 'unlucky' with the data.

The mathematics of the χ^2 distribution make it obvious when a correct fit has been obtained; as will be seen later, small changes in the χ^2 value can equate to large

changes in the χ^2 probability. A very low value of χ^2 can often be interpreted as an incorrect model. A low χ^2 value would imply that the variability of the data is lower than would be expected from random variation. This may happen when the data being assessed are in some way dependent on the parameter attempting to be fitted or the data have been generated using the distribution used to describe them. This will be avoided in this work as the data being assessed are from experimental measurements.

C.4 Probability Bounds

The inherent scatter in toughness measurements presents a problem for the application of defect tolerance design to structures; how can the scatter be taken into account in a manageable and safe manner? Prior to the advent of the Master Curve, the fitting of a lower bounding curve to all available data mitigated the scatter; this eventually evolved into the ASME Code design curve and this is still in wide use today as a requirement for the demonstrable safety of many plants. The lower bounding curve, and the associated method to draw the curve, is deemed conservative for all material of a similar condition, i.e. of similar composition and strength levels. The use of a deterministic lower bounding curve suffers from a risk that applies to all deterministic methods; new data may contradict the curve by lying below it.

As data have been added to the world knowledge of toughness results, it has become apparent that the ASME method and the associated lower bound curve may not apply in all cases. The addition of a dataset of HSST material (HSST-02 plate) has resulted in a data point lying very close to the supposedly limiting design curve [14]. This of course raises a number of concerns about this method, namely is the method conservative? The use of probabilistic methods and the associated statistically based bounds therefore becomes preferable and it is of no surprise that more recent methods have adopted this approach. With widespread adoption of the Weibull probability distribution to describe brittle fracture a simple method is now available to accommodate scatter.

Again, the analytical nature of the Weibull distribution greatly simplifies the mathematics of any manipulation. As the cumulative and probability density functions can both be represented as simple algebraic expressions, the equations can be

readily modified to provide probability bounds. These bounds can then be used either, as comparisons to plotted data or for full probabilistic assessments. The Master Curve method provides a highly suitable framework on which to base a probabilistic assessment method and will be used as an example of the use of Weibull based probability bounds.

Firstly, an estimate of the value of toughness for a given probability must be created. This can be done by rearrangement of the three-parameter Weibull cumulative probability function already established as a suitable description of the brittle fracture process.

$$P(x) = 1 - e^{-\left(\frac{x-\gamma}{\alpha}\right)^{\beta}}$$

Equation C-48

$$x = \gamma + \alpha\left[\ln\left(\frac{1}{1-P(x)}\right)\right]^{\frac{1}{\beta}}$$

where $x =$ a random variable

$\alpha =$ the Weibull Scale

$\beta =$ the Weibull Shape

$\gamma =$ the Weibull Offset or Threshold

By replacing the generic parameters with the notation specific to the Master Curve, a familiar expression from the ASTM Standard is generated.

Equation C-49

$$K_{Jc} = K_{min} + \left(11 + 77e^{0.019(T-T_0)}\right)\left[\ln\left(\frac{1}{1-P(x)}\right)\right]^{\frac{1}{4}}$$

Using the above equation, it is possible to estimate the size corrected toughness, with associated probability bounds, for the relative temperature range selected by the user. The Standard recommends application limited to a relative temperature range of $-50 \le T - T_0 \le 50$ °C, however this limit is arbitrary as the changes between failure mechanisms are not so clearly defined. Initial assessment of the database showed that this range could be increased slightly to encompass more data and improve the accuracy of reference temperature estimates' therefore, in this work a range of $-60 \le T - T_0 \le 60$ °C has been selected. This expression provides a very convenient method for defining the scatter to be used for probabilistic assessment mathematically; for example the expression for the 50% probability bound is simply:

Equation C-50

$$\begin{aligned} K_{Jc50\%} &= K_{min} + \left(11 + 77e^{0.019(T-T_0)}\right)\left[\ln\left(\frac{1}{1-0.5}\right)\right]^{\frac{1}{4}} \\ &= 20 + \left(11 + 77e^{0.019(T-T_0)}\right)\left[\ln\left(\frac{1}{1-0.5}\right)\right]^{\frac{1}{4}} \\ &= 20 + \left(11 + 77e^{0.019(T-T_0)}\right)[0.693]^{\frac{1}{4}} \\ &= 20 + 0.912\left(11 + 77e^{0.019(T-T_0)}\right) \\ &= 20 + \left(10.032 + 70.224e^{0.019(T-T_0)}\right) \end{aligned}$$

Which upon rounding to the nearest integer gives the expression described as the Master Curve.

Equation C-51 $K_{Jc50\%} = 30 + 70\exp\left[0.019\left(T - T_0\right)\right]$

The above method can be applied to any chosen probability in order to gain an appreciation of the temperature dependence of the selected bound. The concern that the next dataset to be generated will disprove the curve is now removed or at least heavily mitigated. The lowest probability bound, i.e. $P\left(K_{Jc}\right) = 0$, results in a

temperature independent lower bounding, K_{min} . The merits of a lower bounding K_{min} are discussed elsewhere. This, of course, presents a problem for deterministic assessment as in this case a $P(K_{Jc}) = 0$ is implied by the assessment. This is not acceptable; low alloy steels are chosen for high integrity applications due to the very high toughness levels that can be achieved at very modest material cost.

Selection of the $K_{Jc0\%}$ line would result in the use of a very unusual toughness curve, one in which there is no transition region. This would require all designs of pressure vessels to remain on the ductile upper-shelf through life, something that may not be achievable for cases where irradiation damage has resulted in toughness property shifts. In this case, a compromise must be made between the absolute demands of the deterministic methods and the realism offered by the probabilistic approach.

Calculating any probability bound is mathematically simple; however, selecting which bound to use for a deterministic equivalent of the ASME design curve is non-trivial. It has been shown that although the analysis methods are different the 5 % Master Curve bound is broadly equivalent to the ASME K_{Ic} curve with some small differences in the temperature dependence[15]. This has helped in the adoption of the Master Curve as an analysis method for utility reactor plant safety assessments, albeit with a margin applied to the reference temperature to insure conservatism.

C.5 Toughness Database Analysis and Results

To test if the Master Curve is a true representation of toughness behaviour two methods can be employed: a) a physical assessment of the underlying models; this provides confidence in the application of the model away from established limits imposed by the requirement of remaining within the confines of the data used to fit the model, b) the second approach is to assess the quality of fit to a large database of known results. This empirical approach offers an alternative view; by using the data to establish what differences must be made in the model accurately to fit the database it may be possible to establish the effects of physical phenomena on toughness. It would be preferable to have a very large amount of data to provide the best possible fit for the model parameters, hundreds of thousands of points would give a great deal of confidence in any proposed changes. In reality, the number of toughness tests conducted worldwide on low alloy steel is probably less than 15,000; this means that any database used for fitting represents one roll of the dice and although it may offer insight and increase confidence it will not be a definitive proof of any model.

The toughness database used in this analysis is an extended version of the EPRI database compiled by Mark Kirk during his employment at Westinghouse. The database relates to materials applicable to RPV steels and has been slowly added to over the years to include the vast majority of data in the public domain. The current author has extended this further to include the proprietary data of Rolls-Royce PLC and, due to this, the data cannot be presented in tabulated form. The data can be described in a number of ways but it is prudent to have an understanding of the different product forms that make up the database. The database is predominantly made up of wrought materials; this includes forgings and plates, mostly of the A533-B and A508-3-1 specifications, and comprises 83.3 % of all data. The next

most numerous product form in the database are welds, comprising 16.3 %. The remaining 0.4 % is made up of casting and heat affected zone material. The database also contains a significant proportion of irradiated data; in fact the irradiated data comprise 22.9 % of the total.

In order to make useful sense of the toughness data it must first be divided into subsets. A reference temperature only has meaning if it applies to one material, mixing data sets results in a heterogeneity that can be dealt with but the process is complex and is simply not needed if the source of the data is well established. As the database is well catalogued, it was possible to create subsets based on the following conditions:

- Material

  This is the production lot, or heat, of the material and, as such, materials with different chemistries and thermal histories are separated from each other.
- Irradiation condition

  The irradiation condition is a highly important factor. The same materials may well be irradiated to different levels of embrittlement; this will affect the mechanical properties of the material.
- Orientation

  It is well known that the forging of low alloy steel can introduce anisotropy into the material. Common practice is to test at the worst possible orientation, however, a number of testing programmes have looked at orientation effects and these data are still of use.

The above defines the tensile properties of the material, which have either been established directly by measurement or, where this has not been undertaken an

average value from the appropriate material specification has been applied. The remaining factors used to define the subsets are based on the experimental procedures used to determine the toughness of the material.

- Specimen geometry

  It has been established in previous sections that the specimen geometry may have an effect on the recorded toughness value due to constrain effects. Certainly the toughness established with different specimen types are known differ.

- a/W, defect depth

  It has long been known that shallow defects exhibit a higher toughness than would be expected from application of deep defect data to their analysis. This is due to constraint loss at the surface that cannot currently be accurately modelled and as such only deep defect data are of interest.

- Loading rate

  The loading rate can have a marked effect on the tensile properties of a material. Much research has been conducted on the toughness of LAS subjected to high loading rates to simulate ballistic impacts and shock loads. The effect of dynamic data on the recorded toughness is yet to be modelled in such a way that it can be compared to pseudo-static data and as such must be separated.

It is mathematically possible to calculate a reference temperature for any of the subsets, but in order to take useful information from the analysis, a certain amount of filtering is required. This eliminates datasets that do not conform to a set of criteria based on the dataset selection method above plus one mathematical constraint. All possible materials are considered and no subset is filtered based on the material,

irradiation condition and orientation. The specimen geometry is also not used for filtering as all toughness data within the database have been measured using specimens of standard geometry for which compliance functions are known. Only deep notch specimens, those with an a/W between 0.4 and 0.6 are used in the production of a valid reference temperature. All dynamic data are also excluded from further analysis as they cannot be corrected or compared directly to static measurements.

The mathematical requirement comes from the maximum likelihood procedure used to estimate the reference temperature. In the E1921 Standard a set of lookup tables is used to assess the error in the T_0 estimate and if a critical value of error, 10.5 °C, is bettered or matched then the reference temperature is considered 'valid'. By adopting a more complete approach to maximum likelihood estimation it is possible directly to determine the error in any estimate. To follow convention, it has been decided that the same validity criterion should be used for all assessments. This allows the definition of an exact meaning of a reference temperature calculated from this database as:

The reference temperature, T_0, estimate of a self-consistent dataset of toughness measurements of the same material and irradiation condition, evaluated in the same orientation and specimen type under static loading conditions, providing the validity condition has been met.

Following calculation of the reference temperature for each subset and filtering on the above criteria allows a plot to be generated of 4431 data points, divided into 211 subsets on a chart of size corrected toughness vs. relative temperature (see Figure C-7). If we overlay the 1, 5, 50, 95 and 99 % failure probability curves from the

Master Curve method, it is possible to gain a visual representation of how the Master Curve estimates the toughness of these materials. It can be seen that from a purely visual perspective the data broadly lie between the 1 and 99 % bounds and follows the temperature dependence of the Master Curve across a wide temperature range.

It is not until a histogram of the actual number of data points versus expected number per probability bound is plotted that the differences between the predictions from the Master Curve and the recorded data become apparent (see Figure C-8). By grouping the data into probability bounds, it is possible to assess how the data conforms to the probability distribution and selected parameters across the entire temperature range of the Master Curve. If the data follow the model exactly the number of data points in each bin will closely match that predicted by the model. Generally a one to one ratio of expected to actual number of data points exists across the vast majority of the probability distribution. There are two exceptions, at both tails of the distribution. At the lower tail there are fewer data points than expected, while at the upper tail there are far more data than expected.

The effects at the lower tail are believed to be independent of initiation toughness and controlled by the arrest properties of the material and will be modelled separately. The upper tail will be dependent on initiation if the data are truly cleavage only. The amount of data in the 99 – 100 % bound far exceeds the model prediction. This bin effectively captures all data from the temperature dependent 99 % to infinity band, so a larger number of data in this bin than expected suggests that the model is not capturing the upper tail correctly. This of course could not be a failing of the physical model, but the data to which it is being compared with may be dependent on other processes and therefore the assumptions of the model are incorrect or faulty.

Application of the goodness of fit test outlined in a previous section shows that the model does not represent the data, an insignificant χ^2 value of ~0 is has been calculated from the histogram shown in Figure C-8. The very low probability of fit is being dominated by the effects of the tails but also subtly affected by a general trend that can be observed on the histogram. Excluding the tails the height of the histogram shows a gradual change from under estimation to over estimation across the range of probability bounds.

A sensitivity study was conducted on the Weibull shape parameter and the temperature dependence of the scale parameter. The results of this analysis are summarised in Figure C-9 and Figure C-10. It was discovered that the shape parameter controlled curvature of the histogram, while variation of the temperature dependent scale parameter altered the gradient of the histogram. The effect of Weibull shape is shown in Figure C-9, where an inflection can be seen by the selection of a low and high Weibull shape, 2.5 and 5.5, respectively. For low values of Weibull shape (shallow peaked distribution) more data than expected lie within the central region of the distribution; for high values of Weibull shape (steeply peaked distribution) more data than expected lie at the tails of the distribution. Figure C-10 shows the effect of altering the exponential coefficient of Equation C-50. Using values far from the specified 0.019 have a similar effect, whether the difference is positive or negative the effect is the same; a concave shape appearance of the histogram results

From this brief study it was apparent that the Weibull shape had the greatest effect on the dissimilarity between the plateau of the histogram and a uniform horizontal line. As shown in a previous section, it is possible to manipulate the Master Curve to

change any constant to an alternative value and maintain the mathematical framework and solving techniques.

As the Weibull shape is easily modified and carries some physical meaning, it was selected as the subject of a parametric study. A simple optimisation procedure was used to estimate the Weibull shape parameter producing the best fit to the data established using the χ^2 goodness of fit test. Following initial investigations, it was established that the goodness of fit improved at Weibull shapes of less than 4. The Weibull shape was then varied between 2.5 and 4 using a step size of 0.05, with the χ^2 value calculated for histograms of both 100 and 50 bins, the results of which are given in Figure C-11.

Assessment of the effect of Weibull shape on the χ^2 value and associated probability for 100 bins shows two distinct peaks; only one peak exists on the assessment of 50 bin data. By using a histogram with discrete bounds, the calculated χ^2 value output produces a distinctly stepped function. As discussed elsewhere, a small change in the χ^2 value can result in large change in the χ^2 probability; this effect is obvious in these results, making the selection of the best model parameters less difficult. The 50 bin data analysis is not as affected by the movement of data between discrete bounds and therefore shows only one peak, which coincides with the lower peak on the 100 bin plot. Although the high peak on the 100 bin plot gives a better goodness of fit the presence of only one peak for the 50 bin analysis cannot be ignored and hence a Weibull shape parameter of 3.5 is believed to be the most appropriate parameter to use with this model.

Figure C-12 and Figure C-13 demonstrate the effect of using the shape optimised parameters against all data for size corrected toughness vs. relative temperature and the histogram of probability bands, respectively. Visually the plot of size corrected toughness vs. relative temperature looks similar between the E1921 and shape optimised versions. The histogram of actual to expected data is also very similar, however, the plateau across the mid range of probability bands has levelled and the peak at the 99 – 100 % bin has reduced slightly but is still by far the most prominent feature on the plot.

The χ^2 goodness of fit test allows quantification of the suitability of the model to the data by the use of the χ^2 probability distribution. Although greatly improved over the goodness of fit offered by the basic model assumed by the ASTM E1921-05 method when 100 bins are considered, a probability of 2.02×10^{-4} for the optimised model versus 6.23×10^{-14} for the E1921-05 model, would still be considered poor. For an engineering assessment, a probability of greater than 5% is commonly considered to indicate the model represents the data. As can be seen, there is still large scope for improvement.

An initial assumption of this work was that the Micro Arrest concept of fracture would provide an acceptable model upon application to the basic E1921-05 model. The Micro Arrest model, as described in a previous section, has been applied to the data and the goodness of fit assessed using similar methods to the above. In this instance a Weibull shape parameter of 4 has been used, not the optimised Weibull shape parameter established above as it was believed that this may offer sufficient improvement to the goodness of fit. The histogram of 100 bins for the application of the Micro Arrest concept is shown in Figure C-14.

The histogram shows that the Micro Arrest concept, as applied here, using the macro established arrest toughness distribution has a very large effect on the lower tail of the failure distribution. The model has switched from an under estimation of the number of data points found in the lower tail, to an overestimation. The χ^2 value has increased accordingly to 527 and the associated probability has decreased markedly to 1.21×10^{-59}.

The Weibull shape of 4 is established from the scaling of the stressed volume ahead of a crack front to the stress intensity factor. This is an indisputable fact, but does rely on a key assumption: the same stress condition exists along the crack front length. Deviation from the value of 4 signifies that the model is not accurately modelling the data and as the Weibull shape has a large effect on the size correction used in the Master Curve then the size correction is also not capturing reality correctly. A reduction in the Weibull shape suggests that the true crack front length required for calculation is shorter that the specimen width, it is well known that free surface effects at the edge of toughness specimens will affect the stress state causing relaxation. Which results in a reduction of the stressed volume at the free surfaces and as such only small scale yielding conditions exist in the centre of the specimen.

Generally, constraint loss in the specimens used to generate toughness data is a concern. The large number of data points lying in the >99 % bound suggest that it is much more common than would be expected. On this basis, the current trend of using smaller and smaller specimens to generate toughness data can often result in higher than expected toughness being achieved in testing. The use of smaller specimens also raises a problem that may be hidden in the data; constraint loss begins at surprising low levels of loading in small specimens and the slight increase in toughness for limited constraint loss is not readily apparent and may just be

assumed to be part of the scatter. The fact that, with the exception of the upper and lower tails, the histogram is very flat across the central section, means 90 % of the data are modelled correctly and, as such, this may not be a problem; however, 10 % of the data is still obviously being modelled incorrectly and this is certainly significant.

The data are censored by the use of the limit load; based on finite element modelling of the loss of constraint in standard specimens, the limit load is a compromise between accuracy and having sufficient data to use for assessment. The limit load is selected to be a limit to the loss of constraint before the data generated must be censored; the difficulty is in selecting the correct limit. Setting the limit too low will result in the vast majority of data being labelled as beyond the limit load, reducing the overall confidence in the approach. This is especially true in the upper transition where the high toughness levels achieved require higher loads to cause cleavage failure will almost definitely be above the limit load for all but the largest of specimens. The use of small specimens puts yet further pressure on the selection of the limit load; such specimens may deviate from the high constraint condition at very modest loads well into the middle to lower transition.

The Master Curve is a cleavage only model, which requires the assumption of small scale yielding across the entire crack front. The sides of the surfaces act as free surfaces with stress dissipation obviously having an effect on the upper tail of the data, and due to the presence of smaller specimens in the database any recorded toughness value may be elevated. It is thus conjectured that the constraint loss is causing a major discrepancy between the data and the model. If the recorded toughness data can be accurately adjusted then it will be possible to find the true parameters of the initiation toughness distribution.

Nevalainen and Dodds proposed a set of constraint corrections based on finite element modelling of standard specimen geometries combined with a very simple criterion to describe the volume of interest ahead of the crack front. These corrections make it possible to correct for both in and out of plane constraint by simple mathematical expressions correlating applied load to the actual stress intensity experienced at the notch root, via the elastic-plastic J integral. Corrections are provided for both the measured toughness and the specimen width. From these assessments, it is possible to see that the shape of the plastic zone in the material is far from uniform for both plane and groove sided specimens. This demonstrates that the Master Curve assumption of Small Scale Yielding (SSY) across the entire crack front is correct to a point; however, the toughness measured using this assumption may over estimate the true loading conditions causing fracture of the specimen.

Using the constraint corrections proposed by Nevalainen and Dodds [11-12] developed in B.2.5, it is possible to make simple corrections to the input data that, in turn, can be used in the Master Curve framework. These modifications can be applied to the database with the addition of the expressions given in a previous section to the database spreadsheets. Unfortunately the limited number of corrections given in the paper means that non-standard test piece geometries cannot be assessed. The number of datasets lost is in fact only a small proportion of the total data; the vast majority of researchers refrain from using non-standard geometries so that test data can be easily compared without having to give consideration to geometry effects.

Applying the Nevalainen and Dodds corrections to the database and recalculating the reference temperatures shows some very promising results (see Figure C-15). The overall plot of size corrected toughness vs. relative temperature exhibits a markedly reduced degree of scatter when compared to Figure C-7 and Figure C-12. The large

number of outliers above the 99 % bound has been greatly reduced, with the behaviour in the upper transition bears little resemblance to that for the uncorrected assessment. The data for the uncorrected model show a distinct trend of 'kicking-up' away from the probability bounds suggesting that the Master Curve is highly conservative in these regions. Application of the constraint correction modifies the data in this region closely to match the lower probability bounds. The data is grouped around the median and predominant lie within the 1 and 99 % probability bounds; this inspires confidence that the modification is performing well throughout the temperature range and for all specimen sizes. The largest toughness values have been reduced by almost a factor of two.

The histogram of actual to expected data (see Figure C-16) shows one major improvement over the uncorrected database; the number of data residing in the upper tail matches much more closely to the model predictions. The removal of this peak demonstrates that loss of constraint is the primary cause for the increased number of data points falling beyond the 99 % bound within the temperature range considered, $-60 \le T - T_0 \le 60$ °C. The lower tail is unaffected by the constraint correction as the loads on the specimen will cause either little or no loss of constraint and the reduction in ratio of actual to expected number of data points seen for the uncorrected dataset is maintained. The values obtained from the χ^2 goodness of fit test are also encouraging.

The χ^2 value using a Weibull shape of 4 has reduced to 145 with an associated probability of 1.81×10^{-3} for a 100 bin assessment. This is an order of magnitude improvement, in terms of χ^2 probability, compared to the shape optimised E1921-05 model and several orders of magnitude better than the basic E1921-05 model;

however, this is still lower than the 5% bound required to establish the model as an appropriate and applicable fit to the data.

The histogram does show a definite curvature. As established earlier, an incorrect Weibull shape parameter causes this curved shape; the concave shape of the histogram implies that the current Weibull shape is too low, i.e. the data are more closely grouped than the distribution used to model it. A further sensitivity study was performed on the effect Weibull shape had on the goodness of fit of the constraint corrected model; in this instance, the histogram shape suggested that the Weibull shape may be larger than 4 and, as such, a range of 3 to 4.5 was selected in the further analysis. Initially a step size of 0.05 was utilised; however, it was found that further resolution was required in the shape range of 4 to 4.5 and the step size was decreased to 0.025 for this range. The results of the sensitivity study are shown in Figure C-17.

Again, selection of the optimal parameters is made difficult by the multiple peaks that occur due to the stepped output function of the χ^2 value. Four peaks can be seen on the 100 bin plot, all corresponding to high levels of goodness of fit; all have a probability higher than the 5% deemed to provide a good level of fit, with two lying above 30%. As previously, the output for 50 bins can be used to aide in the decision of optimal parameters. Only one of the peaks with a probability value higher than 30% has a corresponding peak in the 50 bin output; as such, a Weibull shape of 4.35 was selected the optimal parameter for this model. Figure C-18 and Figure C-19 demonstrate the effect of using the shape optimised parameters against all data for size corrected toughness vs. relative temperature and the histogram of probability bands, respectively.

The shape optimised constraint corrected model produces a very high level of fit compared to the shape optimised E1921-05 model; a χ^2 value of 104 with an associated probability of 0.358 is achieved. This value suggests that the shape optimised constraint corrected model is highly applicable to the data and offers a realistic interpretation of the distribution of toughness values in the mid transition. There is still; however, a noticeable over prediction of the number of data points that would be expected in the lower tail of the distribution. As the lower probability bounds are of great importance in safety assessments, a further sensitivity study was conducted on the Micro Arrest concept.

As established in a previous section, use of the macro parameters for the arrest Master Curve causes an overestimation of the Micro Arrest effect on the failure probabilities. As the parameters for the arrest distribution have no effect on the reference temperature, these can be changed without re-running of the database and as such, a wider range and a higher resolution can be considered. Following initial, low resolution trials, it was established that the parameters, denoted A for the relative temperature independent variable and B for the dependent variable (values of 30 and 70, respectively, are prescribed by the Arrest Master Curve), would lie in a range of $0 < A < 50$ and $0 < B < 100$. This matrix was assessed with a grid resolution of 1 × 1, i.e. 5000 combinations have been assessed, and the 100 bin χ^2 value recorded and the associated probability calculated.

The results of this trial are shown in Figure C-20. It was hoped that a single region of high goodness of fit would be achieved via the application of the Micro Arrest model, as can be seen from the contour plot, a family of solutions provide an improved fit compared to the constraint corrected shape optimised model to the database. This is believed to be due to the use of the histogram for establishing the goodness of fit; the

entire temperature interval is considered as one. As such, a Micro Arrest modification that provides an improved fit to data in the lower temperature range may have no effect on the higher temperature range but will still provide an improved overall fit.

To ascertain a single set of model parameters that could be applied to a both low and high temperature ranges, the sensitivity study was repeated for two relative temperature ranges using the reference temperature to define the interval. The results of these studies are shown in Figure C-21. As would be expected, the lower temperature range favours the temperature independent parameter due to the relative temperature independence of data in this region compared to the rapidly increasing higher temperature range. It is apparent from this assessment that a region of high level of fit exists for both the low and high temperature ranges in the upper left quadrant of the parameter space.

This has been confirmed by multiplying the probabilities of the low and high temperature ranges and normalising to the maximum value (see Figure C-22). This plot clearly shows that only a small range of the values considered for A and B can be applied successfully to both temperature ranges. The optimal parameters established from the normalised plot are in good correlation to those obtained directly from the goodness of fit to all data; A value of 8 and B values of 81. These parameters corresponding to the highest level of fit have been selected as the optimal model parameters. A visual comparison of the median arrest toughness estimated by these parameters and that of the Arrest Master Curve is shown in Figure C-23.

A histogram of the Micro Arrest modified shape optimised constraint corrected model is shown in Figure C-24. This demonstrates the very high level of fit achieved, when

assessed using the χ^2 method; a χ^2 probability of 0.565 is realized, suggesting that the proposed model is highly accurate representation of the database.

C.6 Discussion

C.6.1 Database Inference

The way in which model parameters have been estimated is, to the author's knowledge, a novel approach for the field of transition toughness. Sufficient data exist that model assumptions can be tested and extensions and modifications to these models explored; in this sense, a large and properly cleaned database is an invaluable tool. The method used to establish model parameters as described earlier uses the data to establish model parameters by the use of sensitivity studies and statistical testing; this in reality, is an extended form of data fitting.

The process employed in this work of back fitting model parameters has highlighted a number of key points about the estimation of transition toughness. Each will be discussed in turn below. The basic Master Curve model has become the framework for a number of extension and modifications to a weakest link description of fracture. This work set out to ascertain not only optimised parameters for models, but by understanding the significance of the implications to the underlying physical description of changing these parameters, a more complete understanding of the micro-mechanism can be gained.

All fitting methods rely on the quality of the data being used to establish the model as being adequate for the purpose. The data used in this work have been checked thoroughly for unusual data points and the data used for calculations has been grouped and filtered to remove non-static testing conditions and materials that are known to show failure mechanisms other than trans-granular cleavage failure as laid out in Chapter B. One general concern is that the data, in some yet unknown way, do not reflect the failure mechanisms or the true material behaviour. If this is the case,

all transition toughness models can be described as inaccurate and this would have far reaching implications for the safety assessments of many structures.

The developments in transition toughness modelling established in the previous sections on database assessment will be discussed in order, beginning with the sensitivity study conducted on the basic mathematics of the Master Curve. The reasoning for the avenue of investigation followed, constraint correction coupled with a micro arrest description of the fracture process will be examined, culminating in what the author believes to be an accurate description of brittle fracture behaviour in the mid-transition region and where this description may also be lacking.

The definition of reference temperature validity in this work has also been taken to mean the literal mathematical definition of a limit of error or uncertainty in the estimated value. The pseudo-single temperature method adopted in the E1921 Standard is understandable due to the complexity of the full expression required to establish a true error estimate of the reference temperature. The E1921 Standard must be simple to follow and reproducible; however, by adopting this approach the reasoning behind the validity criteria becomes lost and those capable of applying the mathematics in full may come under unwarranted scrutiny. By using the error figure from maximum likelihood estimates of the reference temperatures all suitable datasets are considered in these studies, thereby making use of as much information as possible from the available data.

C.6.2 Master Curve Weibull Shape Sensitivity Study

The majority of Master Curve parameters were established through data fitting (lower bounding toughness, K_{min}, and temperature dependence) or set by physical understanding to appropriate values. Since the initial model was developed, the Weibull shape has taken on a physical meaning and is crucial to the weakest link

description of fracture and the crack front length scaling model. The shape parameter is used in two stages of the modelling procedure: first, the shape is used in the size correction then, secondly, the shape is used to define the distribution or scatter of toughness data.

In order to assess the effect of changing the Weibull shape the reference temperature estimates of the entire database have to be recalculated for each selected value. This is a laborious and time consuming process if conducted manually; an Excel macro was written to automate this task and was extensively checked on a number of smaller subsets of the database before being applied to all data. This automation has allowed the extensions to the Master Curve to be pursued in this work; without it, the number of calculations required would have not been possible in a reasonable time-frame.

Despite the very large number of calculations involved in this sensitivity study, the useful output is to establish that the Weibull shape used by the Master Curve does not provide the best description of the toughness database utilised in this investigation. The value established as providing the best fit is found to be 3.5. Due to the physical importance of this variable and that a value of 4 is crucial to the toughness and size scaling models assumed by the Master Curve, a number of points of discussion are raised about these assumptions and the implications to the understanding of the fracture process zone specifically.

Two underlying assumptions of the Master Curve method and the associated mathematics used to describe the fracture process may be responsible for a change in the Weibull shape from the theoretically derived value to the optimised value found in this investigation of 3.5. The first is due to an over-simplification of the process zone of fracture, the assumption of SSY across the entire crack front, and the second

is more fundamental to the selection of a three-parameter Weibull distribution and the variation in parameters this may cause.

The assumption of SSY across the entire crack front length is an over-simplification of the fracture process zone. It has long been known that the edges of the specimen do not have the same level of crack tip constraint as the centre due to the escape of plasticity at free surfaces. The original size requirements for K_{Ic} testing were to control the effect of free surfaces on the measured resulting toughness value, by stepping too far from this specimen size requirement without accounting completely for the difference in size and toughness scaling has caused this understanding to be lost or misinterpreted.

The assumption of SSY across the entire crack front is simply untrue provides an explanation for the difference in Weibull shape by shortening the crack front length involved in the fracture process and hence reducing the stressed volume. A move to smaller specimens accentuates the constraint loss effect by yet further reducing the crack front length involved in the fracture process.

In order to achieve the same level of toughness for a shortened crack front length the Weibull shape must be decreased. This can be established from simple rearrangement of the size scaling model utilised by the Master Curve.

Equation C-52

$$K_{min} + \left(K_{Measured} - K_{min}\right)\left(\frac{B_{gross}}{B_0}\right)^{\frac{1}{\beta_{gross}}} \equiv K_{min} + \left(K_{Measured} - K_{min}\right)\left(\frac{B_{true}}{B_0}\right)^{\frac{1}{\beta_{true}}}$$

where B_{gross} = actual specimen thickness

B_{true} = crack front length corresponding to reduced stressed volume

Equation C-53

$$\left(\frac{B_{gross}}{B_0}\right)^{\frac{1}{\beta_{gross}}} \equiv \left(\frac{B_{true}}{B_0}\right)^{\frac{1}{\beta_{true}}}$$

In order to maintain the same scaling relationship for a reduced crack front length the Weibull shape must be decreased.

Equation C-54

$$\left(\frac{B_{gross}}{B_0}\right)^{\frac{1}{\beta_{gross}}} \equiv \left(\frac{\downarrow}{B_0}\right)^{\frac{1}{\downarrow}}$$

The question of why this has not been noted in the open literature is intriguing. It is conceivable that visual assessment of a dataset against Master Curve bounds has not produced a graphical representation that would cause concern. The difference between a Weibull shape of 4 and 3.5 would be imperceptible to the naked eye when comparing a scattered set of data points to continuous bounds; a statistical analysis is required to show such a difference.

The other difference is due to the selection of a three-parameter Weibull distribution. As discussed in a previous section, the addition of the lower bounding toughness parameter, K_{min}, is physically justified as ferritic steels exhibit a toughness lower-shelf; therefore, assuming a non-zero baseline for transition toughness is physically justified. This is also, of course, acceptable from a mathematical treatment of the data. Any distribution can be applied to the data, deciding which is appropriate to model the underlying mechanisms is important to the researcher.

The weakest link description of fracture can be followed through mathematically to arrive at a two-parameter Weibull distribution. This distribution has a Weibull shape of 4 as described by the toughness scaling model employed by the Master Curve and has a zero lower bound, i.e. a very low positive toughness can be generated. The addition of a non-zero lower limit has a minor implication for the assessment of a dataset. By effectively decreasing the range of the distribution by including an offset, the model must conform by becoming truncated. This requires that the Weibull shape be increased by a very small amount to accommodate the decreased data space. This difference, of course, acts in an opposing direction to the current optimisation, but will be revisited later in this discussion.

C.6.3 Micro Arrest Modified Master Curve

The intention of this part of the investigation was to assess the suitability of the Micro Arrest model to the database. In order to establish an accurate basis for an extension of the Master Curve model, such as the Micro Arrest description of fracture, the initiation model must be highly accurate and, at this point in the discussion, it is improved but not yet the best estimate. A full review of the application of Micro Arrest to the database will be given in later section of this discussion (C.6.5); however, there are specific points that should be noted when comparing the Micro Arrest model as assumed in this work to that in the literature to the philosophy of establishing the model parameters by back fitting that has been employed in this work.

The model from the literature uses simulation to generate a series of results that could have been produced from the same materials as tested, i.e. the dataset used to establish the reference temperature for a material is simply one throw of the dice. If the material is tested again, there is no guarantee that the same toughness values would be measured; however, the reference temperature can be estimated with a degree of certainty from maximum likelihood methods. This simulation approach

allows the creation of millions of virtual data points, each of these will have gone through a cycle of random sampling – in this case the initiation and arrest toughnesses are sampled and compared, if the initiation value is higher then it is recorded as a failure and the cycle begins again. If the arrest is higher than the initiation, then the initiation toughness is re-sampled until a failure is recorded.

The 'virtual' database of toughness values can then be compared to an actual database of toughness values. The results of this analysis have been very encouraging, and this could be for a number of reasons: first, the Micro Arrest description of fracture is accurate; secondly, the results are showing improvement by virtue of the fact that the distribution of predicted toughness values is being reduced. The method adopted for this work is different from the above in one key aspect; the database is used to establish the correct model by direct application of a prospective model and statistically assessing the quality of fit. As such, the Micro Arrest model has been applied with a subtle but crucial difference. The model as described in the literature assumes that the macro established arrest properties apply throughout the material of interest; this equates to sampling only one arrest toughness for a number of initiation events. This mimics the reality of arrest testing, where one arrest value will be established for a specimen, and initiation testing, where only one value of initiation will be obtained.

There is simply nothing else that in the context of a description of arrest on the micro-scale can be done with the recorded macro arrest and initiation values and as such the Micro Arrest concept as applied in the literature is in a number of ways correct and certainly merits further investigation. The concept that initiation behaviour must be bounded by arrest affords several ways to interpret the data and is also highly applicable to any debate on the lower bounding toughness, K_{min}. The idea

that an essentially temperature dependent lower bound can be established from macro measurements is appealing from the point of view of both probabilistic and deterministic assessments.

The model as applied in this work is equivalent to re-sampling the arrest toughness for each initiation toughness, i.e. the arrest properties required are those in the surrounding grains of the initiation site, not the average or best performing microstructure for arrest in the material. The difference between the micro and macro descriptions of arrest will be discussed in a later section (C.6.5) as it is more pertinent to an understanding of the complete derived model. This method is more applicable than the simulation method described above as the interaction of the arrest and initiation distributions can be calculated analytically; the probability that an arrest event will happen is simply the probability that the arrest toughness is higher than the initiation toughness.

The difference in modelling philosophies has generated a difference between the results of this work and that of previous studies of Williams et al [16]. It was hoped that application of the Micro Arrest model would be sufficient to produce a much-improved goodness of fit of the overall model to the database. The results show that application of the Micro Arrest model using the macro arrest distribution as established from the arrest Master Curve and the philosophy of apply arrest at the micro level as described above gives rise to an over-estimation of the Micro Arrest effect. The lower tail of Figure C-14 shows that more data points have been altered by the application of Micro Arrest than are required, hence more data lies below the 5% than would be expected from the model. As stated earlier, in order to establish the true effect of the micro arrest mechanism on the transition toughness of low alloy steel the initiation model must be of the highest possible quality.

C.6.4 Constraint Corrected Master Curve Weibull Shape Sensitivity Study

As stated above, the assumption of the Master Curve model that small scale yielding exists along the entire crack front is incorrect. In order to obtain truly representative toughness values, all effects of using specimens that simply cannot maintain constraint for high toughness materials must be taken into account. The most complete model for taking account of these effects is the Nevalainen and Dodds constraint correction [11-12]; this yields vast improvements to the goodness of fit of the Master Curve model to the database. Application of this model correction rectifies the faulty assumption of the Master Curve.

The constraint correction model changes the specimen size and toughness scaling relationships by generating a corrected measured toughness and effective crack front length using a method described in B.2.5. Both of these parameters can then be used as direct replacements in the standard Master Curve method. The constraint correction must be applied in its entirety or it will provide incorrect or misleading values of true measured toughness. The toughness, calculated via J-integral, is calculated as the true loading contributing to fracture experienced by the material at the crack tip, not the measured toughness obtained from experimental sensors. The volume scaling relationship is more complicated and requires brief discussion.

The volume scaling relationship proposed by Nevalainen and Dodds is very similar to the basic Master Curve; failure will initiate within a region ahead of the crack front, the volume of which is proportional to the applied stress intensity factor or J-integral. In the Master Curve method, this volume is not defined; for a scaling relationship the size of the volume is not important just that the relationship between relative volume change and toughness be known. This is one of the many reasons that the Master

Curve is easy to apply. Calculating the volume is straightforward once the stress contour which defines this region is known; however, defining which stress contour controls fracture is very difficult.

The Nevalainen and Dodds model requires that the volume of interest be calculated. This follows from local approach modelling that a suitable multiple of the yield stress be chosen; a value of around three is commonly used. As the Nevalainen and Dodds model normalises the scaling relationship using the yield stress, the exact value chosen for the stress contour is not as important as it first seems [17]. This normalisation procedure increases the applicability of the model by using a commonly available material parameter, yield stress, as an input to the correction. In effect, a similar situation to the basic Master Curve model exists; the ability to define the true process volume is not as important as knowing the scaling relationship between the applied load and measured toughness.

The size scaling relationship used by the Nevalainen and Dodds correction is also a simplification of the result from the finite element simulations. By describing an effective thickness calculated from the sampling volume the process is simplified greatly but this may in fact be an oversimplification. The volume encompassed by the stress contour of interest may afford a better description, but again this introduces another parameter that must be known (which multiple of yield stress should be used to define the contour) in order to apply the model, which at the present time cannot be established. This is worthy of further examination but will require a fully validated physical model of the brittle fracture process to define the process volume.

The difference associated with the small change in Weibull shape from 4 to 4.2 when the constraint correction is applied in the analysis of the database may be a direct result of this simplified approach to size scaling. A simple reworking of Equation C-53

can be conducted, establishing that a difference of approximately 5% is required in the value of B_{eff} used for toughness calculations to provide a Weibull shape of 4. However, this is only one of a number of possible explanations for the observed difference.

As discussed above, the inclusion of a lower bound into the Weibull distribution may have affected the Weibull shape required to model the data correctly. The curtailing of the lower tail requires that the Weibull shape be increased slightly to accommodate the tighter distribution of data. This difference would not be discernible to the naked eye on a probability plot, but is apparent from a review of the way the data would be clustered. In reality, the difference of including a lower limit or not to the where the data actually lie is unimportant. The development of a lower bounding toughness is more important for the application of such models in safety assessments and is therefore a highly desirable trait of the Master Curve approach.

The data lend support to a lower bound by the simple fact that the data do not lie below the ascribed lower bound defined in the Master Curve method, i.e. 20 MPam$^{0.5}$. The probability of obtaining a data point that approaches the lower bound value is incredibly low considering either a two or three parameter Weibull distribution (the P_f of a two parameter distribution at T_0 for a value of 20 MPam$^{0.5}$ is 0.00266). The likelihood of generating any data in this region is therefore incredibly slight but may occur in the future with yet further test results. The inclusion of a lower bounding value at present makes little difference to the analysis conducted and therefore the increase in Weibull shape estimate is unlikely to be caused by the inclusion of a lower bound.

The most likely cause of this difference is the constraint correction model used within the Nevalainen and Dodds model. It has been noted that within the mid-transition region considered in this investigation, in the upper range of both temperature and toughness this area of the plot is sparsely populated when compared to the uncorrected data (see Figure C-12 and Figure C-18). In the upper transition region beyond that used for data fitting, the effect is more apparent. The paucity of data in this area indicates that the correction model is over adjusting the data to lower values than would be expected from the weakest link description.

The Nevalainen and Dodds model is for correction of large scale yielding only and does not take account of another very important mechanism in this region; the development of ductile tearing before brittle failure. This was explored in earlier work by Tang, Dodds and Anderson [18] and offers a highly plausible explanation for the effects in the data seen here. High values of measured toughness are also associated with significant ductile tearing preceding fracture. Ductile tearing affects the fracture process in a number of ways. First, the creation of ductile fracture surfaces requires lots of energy in terms of both local plastic deformation and surface energy. Second, on the length scales considered here the ductile crack initiates ahead of a severely blunted notch; the sharp ductile tear increases constraint resulting in an increased stressed volume per applied external load.

The modelling process becomes further complicated when the sampled volume is considered. Initially, the stressed volume forms ahead of a very sharp fatigue crack; the volume grows with the increased application of external load until the loading limit of the specimen is exceeded with the application of further external load barely affecting the stress volume. Upon initiating ductile tearing a sharp defect is reintroduced into the material causing the stressed volume to grow yet again. Compared to the stationary fatigue crack used to create the initial stressed volume,

the ductile tear is mobile, progressing into the material as the applied load is increased. The volume sampled by the defect is then proportional to the level of ductile tearing and the load achieved at failure.

All of the above results in an increase in the true toughness measured by the specimen or, in simple terms, the inclusion of ductile tearing will result in higher values of constraint corrected toughness, and thereby repopulating the sparse area of the plot. This avenue of research appeared to be abandoned in the mid 1990s and, unfortunately, was not followed up therefore the complete descriptions of specimen loading as afforded by Nevalainen and Dodds do not exist. This would be a highly profitable area for further work and resolve a key issue with the application of the Master Curve; the use of a cleavage only model to describe data affected by ductile tearing.

The current description of the range controlled by mid-transition (cleavage only) behaviour is temperature based, i.e. $-50 \leq T - T_0 \leq 50$ °C. A visual review of the data compared to the Master Curve shows that this is a reasonable approach; only when the data are examined for physical effects on the model does it become apparent that this may just be happenstance. The physical effects of constraint loss and ductile tearing appear to be balanced such that a cursory review of the model shows that it is acceptable; only a full statistical analysis as conducted here can reveal that effects of constraint loss are more pervasive than originally considered.

Unfortunately the full effect of combining ductile tearing with constraint loss cannot be applied to the toughness database without rerunning the finite element simulation used to determine the effect on the stressed volume ahead of the crack tip. The groundwork for such simulations has been largely conducted in the literature but

would require significant academic input and time to realise. As such the constraint corrected model, as used in this investigation, is believed to provide a suitable cleavage only model for the assessment of the postulated Micro Arrest affect on data in the lower tail of the distribution. The effects of ductile tearing can be resolved by the censoring of data to a suitable bound of the upper shelf toughness; however, it is noted that a model of upper shelf toughness requires considerably more investigation before even a semi-empirical model can be established.

Again, the use of maximum likelihood methods allows the development of complex censoring criteria and censoring limits for a number of parameters can be considered; these will be explored in a later section on recommended ways to process data to ensure that an accurate description of the data is realised.

Another important material assumption of the Nevalainen and Dodds correction is the application of the Ramberg-Osgood model of tensile behaviour. For this work, a hardening exponent of 10 has been applied to all materials, as this is believed to be broadly applicable to low alloy reactor pressure vessel steels. A suite of solutions for different hardening exponents would increase the accuracy of the method but would require that more material information be established for materials contained within the database; this is simply not possible without access to archive materials. The intention is to make the overall model as broadly applicable as possible while retaining a reasonably accurate description of the failure process and as such selection of a hardening exponent of 10 is a sensible compromise.

C.6.5 Micro Arrest Extension to Constraint Corrected Model

Following work on application of the Micro Arrest model to the basic Master Curve model, it was concluded that the macro arrest distribution as a surrogate for arrest on the microscale was an over estimation. This was not surprising, as the arrest

properties as measured in macro testing are not entirely applicable on the microstructural level. By considering what happens in an arrest test (see B.3), it is possible to establish that the measured value of a macro arrest test is a measurement of the best arrest properties of that material; or, the reverse of the weakest link theory of brittle fracture.

As a fast moving cleavage crack propagates through a material certain regions may resist propagation more than others; for instance, regions of fine-grained material increase the grain boundary density and therefore the number of deviations and re-initiations that crack must complete to propagate. In heterogeneous materials, one component may also simply be ‘too tough’ for cleavage failure at the test temperature, creating a ductile bridge across the crack front. These regions will act as barriers to the propagation of the crack front and may possibly lead to outright arrest if the crack has insufficient energy to cross or progress around one of these regions. The crack is therefore arrested at the microstructure offering the highest propagation resistance in the material and the measure of arrest toughness taken corresponds to upper tail of the arrest distribution of the material. It then follows that the macro distribution is a highest extreme value of the micro distribution.

Arrest on the microscale, or micro non-propagation, cannot therefore be controlled by the macro measured distribution. The micro arrest distribution must have a similar range to the macro distribution but be more tightly distributed at lower values. Again, the database has been used to infer the properties on the microscale by assessment of the goodness of fit of a model to the database. The model used does not require re-running of the database to establish reference temperatures for each change of the Micro Arrest model parameters, allowing much quicker progress to be made on the effect of changing these parameters on the resultant goodness of fit.

In principle, it should be possible to establish the Micro Arrest model parameters from a knowledge of the other distributions; i.e. the failure distribution is a combination of the initiation and arrest distributions, if two are known the third can be calculated. In reality, this is a very complex statistical problem and there is currently no direct solution for the model parameters. Instead the parameters have been established by a sensitivity study on the parameters of the log normal distribution used to describe arrest behaviour.

The choice of optimised parameters, and the reasons for leaving some parameters unchanged, require discussion. First, the unchanged parameters have been left at specific values, as it is believed that these are physically important. As discussed above, it is the belief of the author that the macro measured arrest distribution is directly related to the micro arrest distribution considered here. Therefore the temperature dependence of both the macro and the micro distributions will be similar, hence the value controlling relative temperature dependence, 0.019, remains unchanged. An assumption, however, is made on the scatter of the micro arrest distribution. As no direct measurement of the micro arrest distribution is currently possible, the scatter cannot be established; the same scatter of 18% is then assumed to apply to both distributions.

Secondly, the optimised parameters show a number of interesting features that correspond well with an understanding of the fracture process. Figure C-23 demonstrates the temperature dependence of the optimised Micro Arrest Master Curve is more severe than the Arrest Master Curve; this matches theoretical expectations by increasing the overlap of arrest and initiation as relative temperature increases. Arrest is essentially the interaction of a ductile process impeding cleavage failure and therefore requires thermal energy to allow dislocation movement. The optimised parameters also afford only a small to negligible effect on data in the lower

half of the relative temperature range considered in this investigation; this also corresponds well to theoretical understanding as the likelihood of arrest at low relative temperatures is believed to be limited.

Of concern is the use of the Wallin T_0 to $T_{K_{Ia}}$ correlation utilised in the literature Micro Arrest model [16] for a modified arrest distribution and also employed in this work. This relationship was established by data fitting to a database of initiation and arrest reference temperatures and therefore is fitted to macro arrest data. As yet, a testing method has not been devised which will accurately establish the arrest toughness of a material on a microscale and as such the micro arrest toughness cannot be measured and modelled in the same manner as macro arrest properties. It is therefore impossible to establish the same type of empirical correlation between initiation and micro arrest properties.

Following the logic that macro arrest properties represent the strongest link, or the highest extreme value, of the micro arrest properties, then the above concern can be mitigated. The correlation that applies to a referencing value on the macro distributions will also apply to the correlation between macro and micro distributions, albeit to a different, but corresponding, reference value for the micro distribution. For example the macro distribution is referenced to an arrest toughness of 100 MPam$^{0.5}$, this will correspond to an arrest toughness in the modified best fit distribution of 89 Mpam$^{0.5}$, established by addition of the A and B model parameters (8 and 8, respectively). Essentially a further expression is subsumed into the correlation to accommodate the difference in the macro and micro arrest distributions. A similar definition to $T_{K_{Ia}}$ can be created to correspond to the temperature at which the median micro arrest toughness is 89 Mpam$^{0.5}$, to be known as $T_{K_{Ima}}$.

The combination of constraint correction and a modified micro arrest model produces an incredibly high χ^2 probability value, suggesting that the data are well represented by the applied model. This implies that the Master Curve model as it exists in the ASTM standard is broadly applicable but the use of small specimens requires further consideration before they are used for safety critical applications or the resulting measured toughness values can be corrected to true toughness values via use of the a constraint correction method. The method explored here has been found to be highly effective for cleavage only data; however, where ductile tearing effects may be prevalent, the correction method will generate overly conservative values.

The failure distribution, P_f, of the data can therefore be established using the optimal parameters and input values established above for the initiation distribution, P_I, and the micro arrest distribution, P_{MA}, in the following expressions:

Equation C-55
$$P_I = 1 - \exp\left[- \left(\frac{K_{J_0 B_{eff}} - K_{min}}{11 + 77 \exp[0.019(T - T_0)]} \right)^{4.35} \right]$$

Equation C-56
$$P_{MA} = \frac{1}{0.18\sqrt{2\pi}} \exp\left[- \frac{\left(\ln\left(K_{J_0 B_{eff}}\right) - \ln\left(8 + 81 \exp\left[0.019\left(T - T_{K_{iam}}\right)\right]\right)\right)^2}{0.0648} \right]$$

Equation C-57
$$P_f = P_I . P_{MA}$$

The above expression can also be used to estimate bounds to the failure distribution. As the arrest distribution is described by a log-normal distribution the failure bounds cannot be calculated analytically; however, a simple spreadsheet can be created utilising a numerical solver to establish the bounds of the failure distribution with ease. Examples of the failure probability bounds for a typical ASTM A508 type

material in start and end of life conditions is given in Figure C-25 and Figure C-26, respectively. An extreme situation of an extended irradiation is given in Figure C-27 more easily to show the differences between the small effect of micro arrest in the start of life condition and the effect of smaller difference between initiation and arrest.

The elastic and maximum values established from the constraint correction are also shown is these plots, these can be used to help define test programmes by selecting temperature ranges which limit the expected loss of constraint and improve the likelihood of cleavage failure by selection of a test temperature lower than the corresponding bound of interest. The probability bounds and the specimen measurement limits are size and specimen geometry dependent and should be established for the defect size and loading condition of interest to allow accurate predictions of failure probabilities.

C.6.6 General Concerns

Despite the clear statistical results of this investigation, a number of concerns remain with the assessment of the toughness database and the micro-mechanisms of failure assumed by the models employed. First, the data within the database used to test these assumptions may bias the optimised distribution parameters..

The database has been considered as a single entity for the purpose of assessing the assumptions of the Master Curve and the associated extensions and modifications pursued in this investigation. One key assumption is that the failure mechanisms of low alloy steels are essentially the same for a range of compositions and processing histories that produce a ferritic microstructure. It has been noted in other work that the Master Curve has been applied to a relatively limited set of data and this investigation is constrained by that fact; the model is semi-empirical and

therefore application to materials outside the current knowledge base is not recommended without demonstration of compatibility.

When the Micro Arrest modified shape optimised constraint corrected model is considered, comparison of the histograms for data that fall below (see Figure C-28) and above (see Figure C-29) the reference temperature shows a few key differences. First, the lower temperature range data correspond very well to the model, as shown by the low χ^2 value and high corresponding probability (104.042 and 0.371, respectively). The higher temperature range shows the model has deficiencies, especially for data in the upper half of the distribution, $P(failiure) > 50\%$. The model considered in this work does not take account of ductile tearing, which would be prevalent in this region. Utilising a large scale yielding only correction model has resulted in an over correction of these data causing more data to fall in the centre of the estimated distribution. The proportion of data above the reference temperature is approximately half the database, 2492 points or 50.4 % of all valid data and, as such, the effects of ductile tearing should be considered as a high priority for further work.

The failure mechanism of these materials is assumed to be the same; however, there may be subtleties in the behaviour between materials that at present cannot be accommodated in the empirical model discussed above. The database used for data fitting in this investigation contains a significant number of dataset from high nickel (>1 wt%) materials. It would appear that these materials have a different temperature dependence than the standard Master Curve; the transition region is over a shorter range for these materials, therefore the temperature dependence is increased. These materials have increased hardenability over lower nickel counter parts creating a finer microstructure.

It is possible that the finer structure will have an affect on the relative temperature dependence of these materials. The above observation is consistent with this experimental work and it is conceivable that the materials used to establish the original Master curve parameters were all of a similar grain size. This is a good example of the fact that the Master Curve framework and the underlying assumption of a weakest link failure mechanism is correct but the parameters themselves may be more material dependent than first realised.

The inclusion of the high nickel data may have biased the results of this investigation but this is believed to have been a minimal effect or it would be evident from the statistical assessment of the data. A difference, however, is noted between the lower and upper half of the relative temperature range considered in this investigation. This is most likely due to the inclusion of the high nickel data in this investigation; the higher levels of nickel suppress the ferrite nose during heat treatment giving a fine lath and packet structure. It should be remembered that this work is an assessment of the broad applicability of the Master Curve and the modifications created during this investigation and all available data has been used.

C.7 Recommendations for Processing Data

As a result of this investigation, the follow recommendations are made in order to create highly accurate estimations of the cleavage failure probability of low alloy steels exhibiting a toughness transition and within the specified strength limitations of ASTM E1921-05 the following procedure should be followed.

1) Fracture toughness testing of the material should be performed to ASTM E1921-05 using a standard specimen geometry for which a Nevalainen and Dodds constraint correct exists. The largest possible test specimens should be tested in the lower half of the relative temperature range to reduce the effects of constraint loss.
2) The measured toughness, K_{Jc}, should be converted to a true toughness, K_{J_0}, utilising the appropriate large scale yielding correction parameters given in Table B-1. The expressions are given below:

   $J_{avg}/b\sigma_0 \leq$ limit of proportionality, $J_0/b\sigma_0 = J_{avg}/b\sigma_0$

   $J_{avg}/b\sigma_0 >$ limit of proportionality, $J_0/b\sigma_0 = f\left(J_{avg}/b\sigma_0\right)$

   where $f\left(J_{avg}/b\sigma_0\right)$ takes the form:

$$f\left(J_{avg}/b\sigma_0\right) = \begin{array}{l} b_0\left(J_{avg}/b\sigma_0\right)^{\frac{1}{4}} + \\ b_1\left(J_{avg}/b\sigma_0\right)^{\frac{1}{2}} + \\ b_2\left(J_{acg}/b\sigma_0\right) + \\ b_3\left(J_{avg}/b\sigma_0\right)^2 \end{array}$$

   Where the value of $J_{avg}/b\sigma_0$ is beyond the peak of the function to provide $J_0/b\sigma_0$, the value will be censored to the maximum value of $J_0/b\sigma_0$.

3) The gross specimen thickness, B_i, should be corrected to an effective thickness, B_{eff}, using the appropriate correction parameters given in Table B-2. The expression is given below:

$$\frac{B_{eff}}{B_i} = d_0 + d_1 e^{\frac{d_2 J_{avg}}{b\sigma_0}}$$

4) $K_{J_0 B_{eff}}$ should be size corrected utilising the effective thickness to generate $K_{J_0 B_0}$, which is used in subsequent calculations. The expression is given below:

$$K_{J_0 B_0} = K_{min} + (K_{J_0 B_{eff}} - K_{min}) \left(\frac{B_{eff}}{B_0} \right)^{\frac{1}{4}}$$

5) The initiation reference temperature should be calculated by maximising Equation C-31 with respect to T_0 with the following parameters:

   a. $K_{\min} = 20$

   b. $\alpha = 11 + 77 \exp[0.019(T - T_0)]$

   c. $\beta = 4.35$

   d. censor data beyond $Max(J_{avg} / b\sigma_0)$

6) The appropriate arrest reference temperature, T_{Klam}, can then be calculated using the following expression:

$$T_{Klam} - T_0 = \exp\left[5 - \frac{T_0 + 273}{136.1} + \frac{\sigma_{y(RT)}}{660.3} - \left(\frac{\mathrm{Ni}_{wt\%}}{2.5} \right)^{2.91} \right]$$

7) The failure probability bounds can be estimated using a spreadsheet containing a simple numerical solver that accounts for specimen size and geometry, which computes the appropriate level of $K_{J_0 B_0}$ for a required probability bound of P_f ; the initiation and arrest probabilities distributions are given below:

$$P_I = 1 - \exp\left[- \left(\frac{K_{J_0 B_{eff}} - K_{min}}{11 + 77 \exp\left[0.019\left(T - T_0\right)\right]} \right)^{4.35} \right]$$

$$P_{MA} = \frac{1}{0.18\sqrt{2\pi}} \exp\left[- \frac{\left(\ln\left(K_{J_0 B_{eff}}\right) - \ln\left(8 + 81 \exp\left[0.019\left(T - T_{K_{Iam}}\right)\right]\right)\right)^2}{0.0648} \right]$$

$$P_f = P_I . P_{MA}$$

C.8 Conclusions

Statistical modelling of the transition toughness behaviour of low alloy pressure vessel steels has been conducted to establish if the current Master Curve approach for the generation of failure probability bounds in this region is applicable and accurate. Two additions to the Master Curve modelling approach have been considered to improve the accuracy and provide insights into the fracture process. A number of key points can be concluded from this examination:

1. The goodness of fit of the basic Master Curve model, as found in ASTM E1921-05, to a substantial toughness database is statistically poor, i.e. the established χ^2 probability is less than 0.05. The calculated value is in-fact ~0.
2. Improvements can be made to the goodness of fit of the Master Curve model by application of an optimised Weibull shape parameter of 3.5, highlighting an incorrect assumption of through thickness small scale yielding of the crack front.
3. Application of the Nevalainen and Dodds constraint correction to data before use in a Master Curve framework greatly improves the quality of fit by mitigating the faulty assumption of small scale yielding across the entire crack front.
4. Further improvements can be made to the goodness of fit with application of an optimised Weibull shape of 4.35 in the constraint corrected mode. This implies that the assumed shape of the small scale yielding used for toughness and size-scaling relationships requires further work.
5. Application of the modified Microarrest model is found to improve the goodness of fit yet further. The new parameters of the arrest model

correspond well to an understanding of the likely interaction between initiation and arrest.

6. The model is found to be lacking in regions of significant ductile tearing prior to cleavage failure and further work to understand the effects of tearing on fracture toughness measurements is strongly recommended.

C.9 Further Work

The results of this work demonstrate that the Master Curve framework, though not the assumptions and chose parameters, is a highly accurate description of the transition toughness of a broad range of low alloy steels. As determined by the analysis of a large database, the goodness of fit can be improved even further by the application of constraint correction and the Micro Arrest concept, pursued in this work by the application of a microscale arrest distribution, which can be established from the macro arrest properties of the material. However, a number of issues need to be resolved to yet further improve the understanding and physical relevance of the model. First, the statistical model requires further refinements.

The reason for the optimised Weibull shape of 4.35, as opposed to that predicted from theory of 4, has not be definitively established in this work. A number of explanations have been explored in the discussion of these results; the quantitative difference caused by these effects need to be explored. Fundamental to an understanding of the application of a weakest link model is the inclusion of the offset parameter. As stated previously, the inclusion of an offset parameter, K_{min}, affects the distribution in a very subtle way and this requires further work to establish if a non-zero value is physically justified. As K_{min} lies at the edge of the distribution in a region where there are very few data to allow testing of any hypothesis, it is difficult to determine if an offset is required at all or what value it should take. A complete statistical analysis of the effect of an offset could be conducted using simulation methods.

Another explanation for the discontinuity between the theoretical and optimised Weibull shape may be due to physical effects that are not taken account in the

current model. It could simply be that the increased complexity of the constraint corrected scaling model has resulted in mathematical changes to failure distribution assessed in this work. A review of small scale yielding within the constraint correction should reveal if the difference is purely geometric, i.e. the change in the shape of the small scale yielding zone due to large scale yielding changes the size scaling relationship from K^4 to $K^{4.35}$.

The effect of ductile tearing prior to cleavage failure is currently ignored in the model. This, of course, needs to be resolved before a non-conservative model of the mid and upper transition can be proposed. As seen in the results, application of a large scale yielding correction model only results in over correction of the data that would be affected by pre-cleavage crack extension; essentially all data that lie in the interaction zone between upper shelf behaviour and the transition. This zone extends well into the transition region beyond the arbitrary relative temperature cut off designed to limit the effects of crack extension on the data. If a truly cleavage only model is required, a further censoring limit of a suitable probability bound of the upper shelf could be extended to the mid transition; this requires knowledge of the upper shelf toughness properties of a material, so at present cannot be applied to the current database.

The effect of ductility can also be accounted for by modelling the effect that the growing ductile crack has on the stress state ahead of the advancing crack tip. Initial research in this area has shown that pre-cleavage crack extension increases the constraint and therefore the true toughness at the crack tip compared to the current corrected value. This would repopulate the region affected by ductile tearing on the plot of all data vs relative temperature. Establishing the true effect of pre-cleavage crack extension on the measured values of toughness is complex, both

philosophically and scientifically, and requires significant further work to understand how this can be quantified and applied.

A model of the effect of ductile crack extension on fracture requires detailed measurements of fracture surface topography to establish the necessary input parameters. The pre-cleavage crack extension measurements available in the literature are of variable, and quite often, insufficient quality. A widely accepted method is yet to be adopted to distinguish between the stretch zone caused by crack tip opening displacement and the ductile tear preceding fracture. A full review of available techniques is required to establish a best practice method for future assessments, such that sufficient data can be established in a systematic and standardised manner to truly explore the difference between the effect of the stretch zone, which controls the cleavage only toughness, and the ductile tear, which controls the additional toughness afforded by the pre-cleavage crack extension.

An area of improvement for the optimisation of the statistical model will be to use maximum likelihood as the comparative measure of goodness of fit. The use of χ^2 has been very profitable; however, a number of undesirable features stem from its use, namely, the stepped output function of χ^2 value against the fitted parameter. This prevents the use of numerical optimisation techniques and forces the user to resort to sensitivity studies to established optimal parameters; numerical optimisation would allow the development of accurate predictions of the optimal parameters. As discussed previously, maximum likelihood methods are very powerful but require that a likelihood function be formed. The combination of a Weibull and Log-normal distributions in the failure distribution means that the likelihood function is highly complex and as yet has not been developed. This requires knowledge of probability

theory and statistics far beyond the author's ability and will require significant academic input to overcome.

The second major area of further work is the development of a proof of principle of the Micro Arrest concept beyond the statistical modelling adopted in this work. This is very difficult due to the rarity of such events and a full experimental procedure is yet to be developed. A simple test of the hypothesis would be the creation of a material at the extreme of the current database that should demonstrate a high overlap between initiation and arrest distributions. An assessment of the correlation shows that this material should have a high reference temperature and nickel content, and a low yield stress. Experience of these materials dictates that this would be a difficult material to produce as high nickel content is commonly associated with good toughness and tensile properties.

An alternative is the production of a steel within which the phase proportions of tempered martensite and bainite can be controlled and suitably mixed. It would be expected that failure would initiate in the bainitic region and arrest in the martensitic. The initiation and arrest properties of each phase could be measured individually to provide baseline data to establish the level of overlap between each distribution. The phase proportions can then be varied to affect the probability of microarrest events and test hypotheses on the predicted number of events for given conditions. Consideration of the location of microarrest events shows that these may not occur on the final crack plane and a suitable method of in-test detection, such as acoustic emission, should be employed to enable a test to be stopped and the microarrest events examined.

C.10 Figures

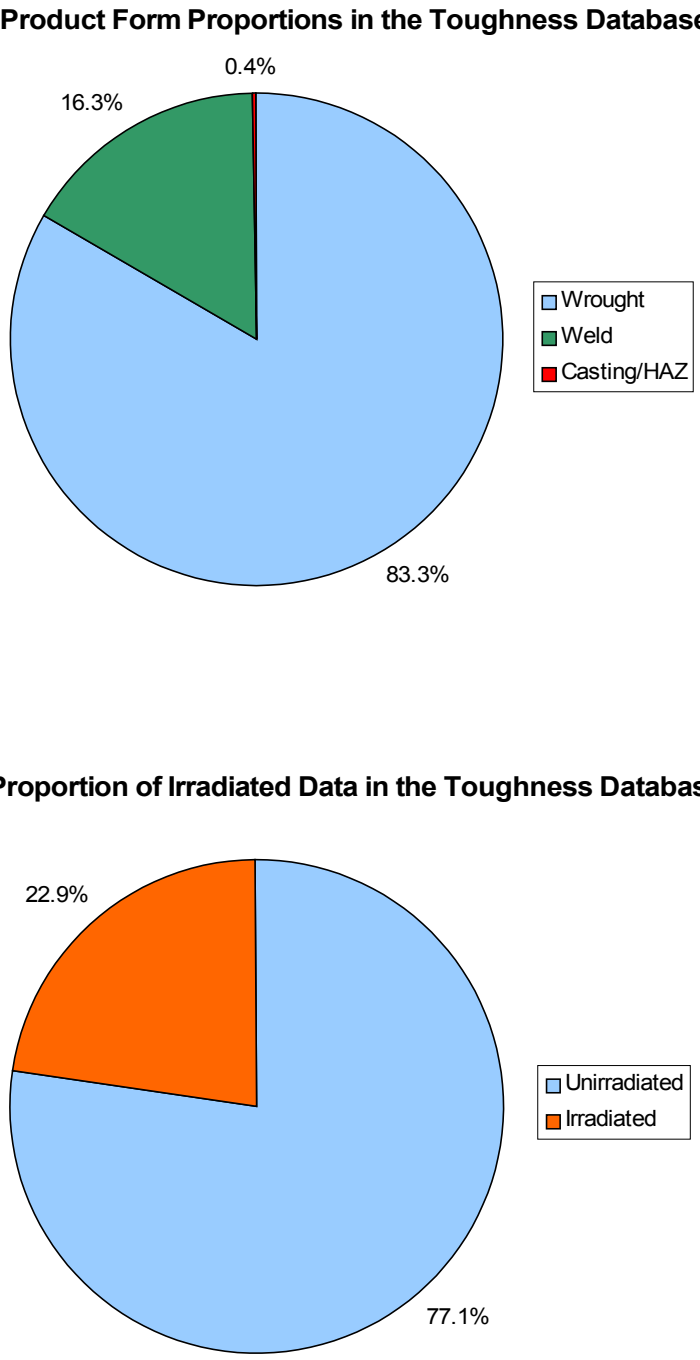

Figure C-1 - Relative Proportions of a) Product Form and b) Irradiation Conditions

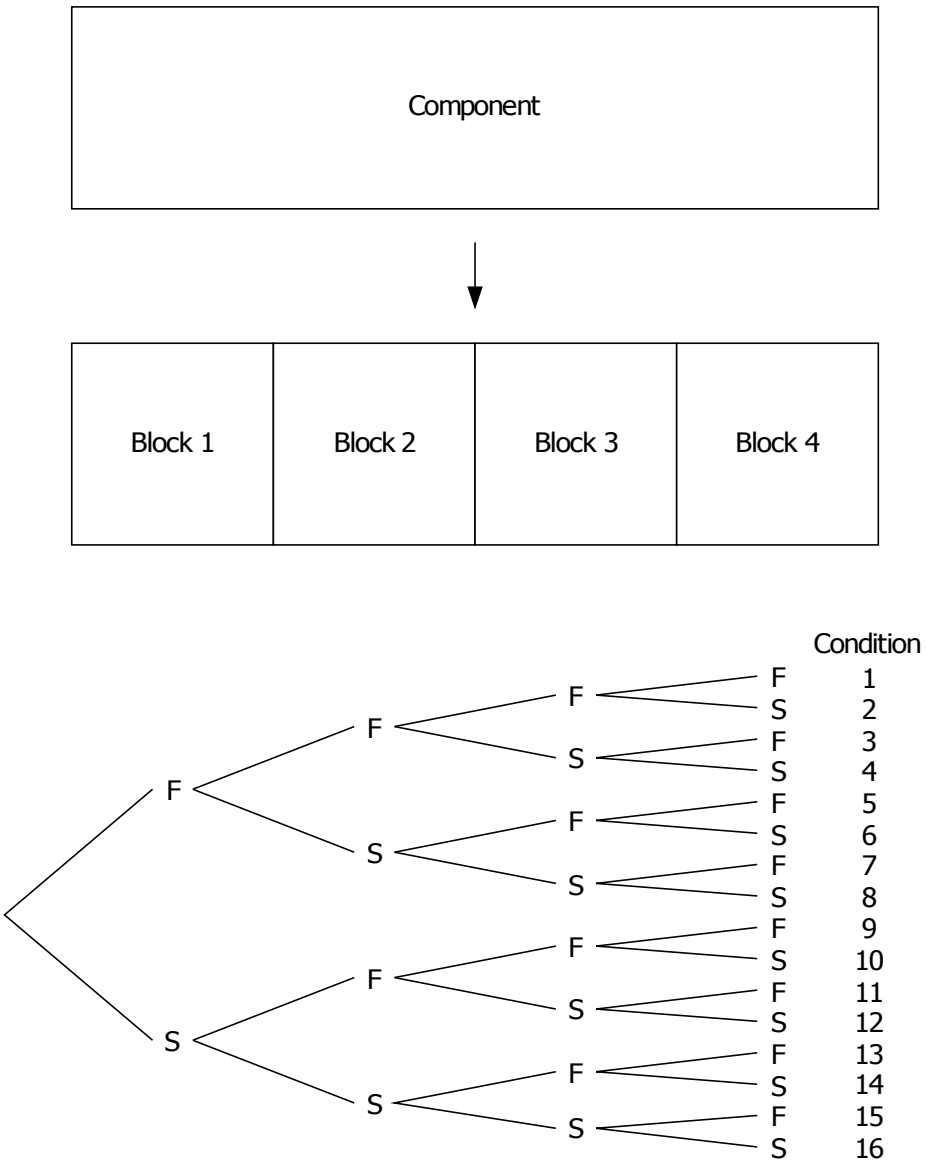

Condition 16 is the only condition in which the component will survive.

Figure C-2 - Simplified Representation of Size Correction

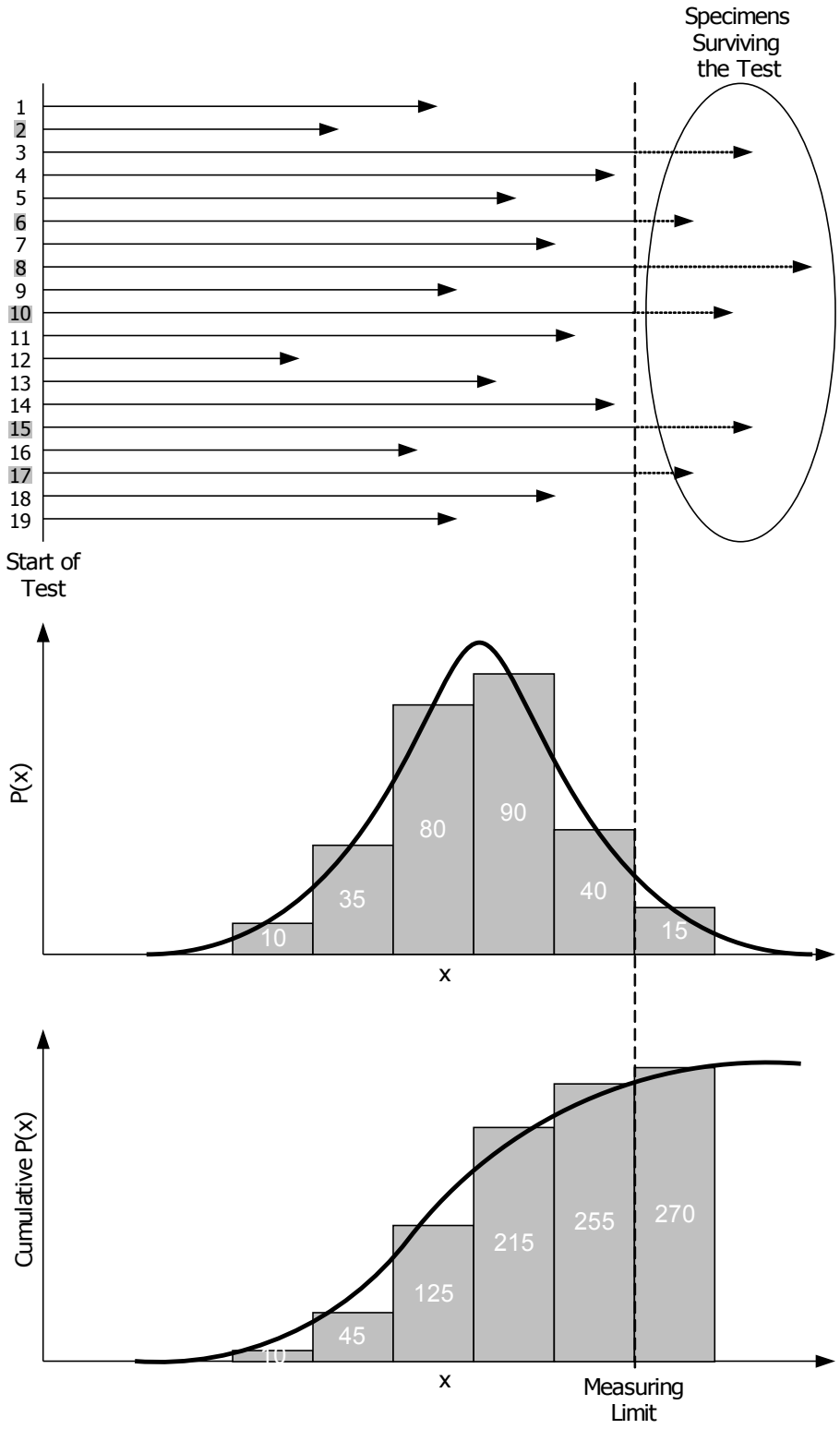

Figure C-3 - Right Censoring of Lifetime Data

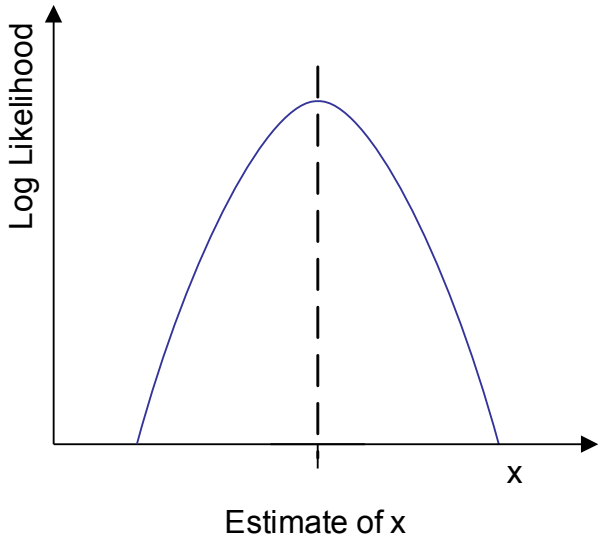

Figure C-4 - Typical Parabola of Log Likelihood Function

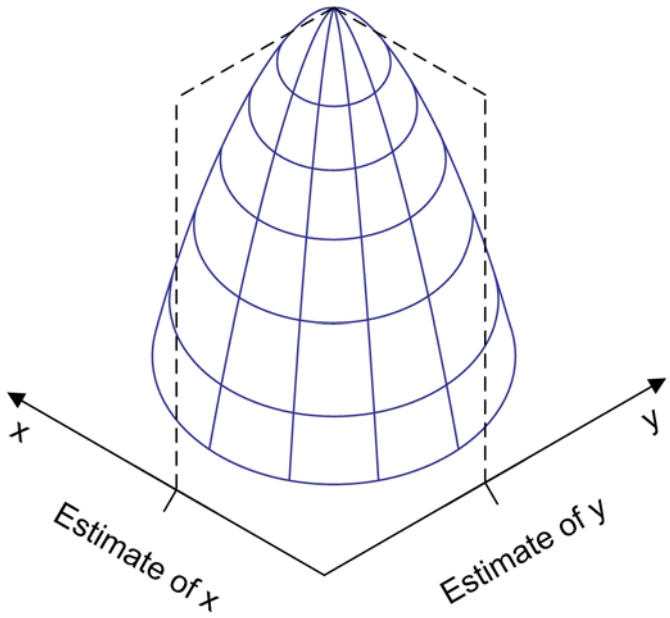

Figure C-5 - Typical Likelihood Surface for 2 Parameters

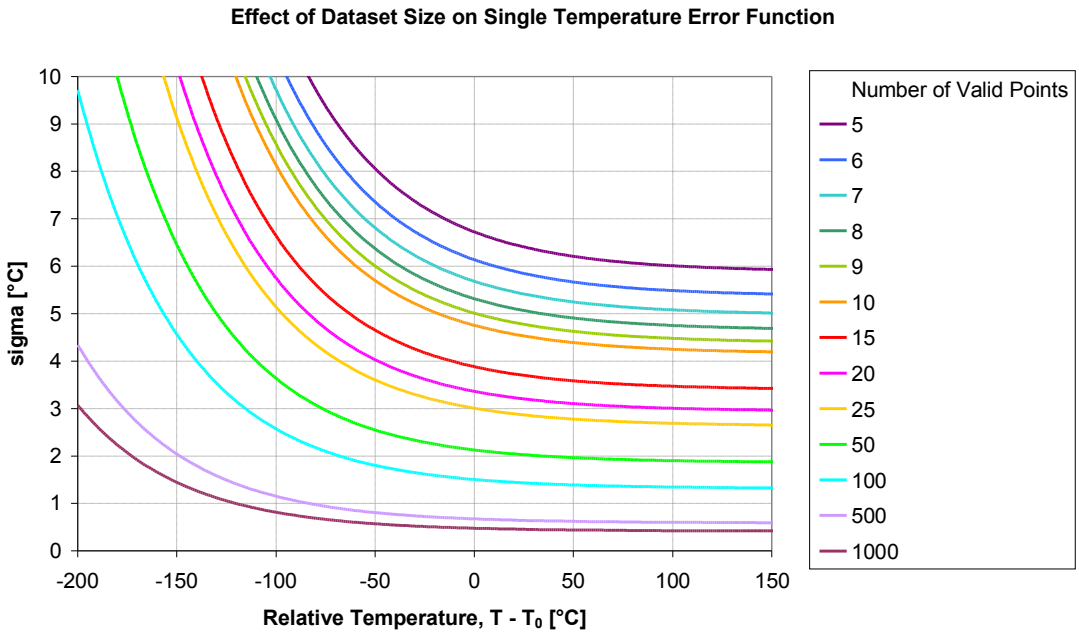

Figure C-6 - Effect of Dataset Size on the Single Temperature Error Function

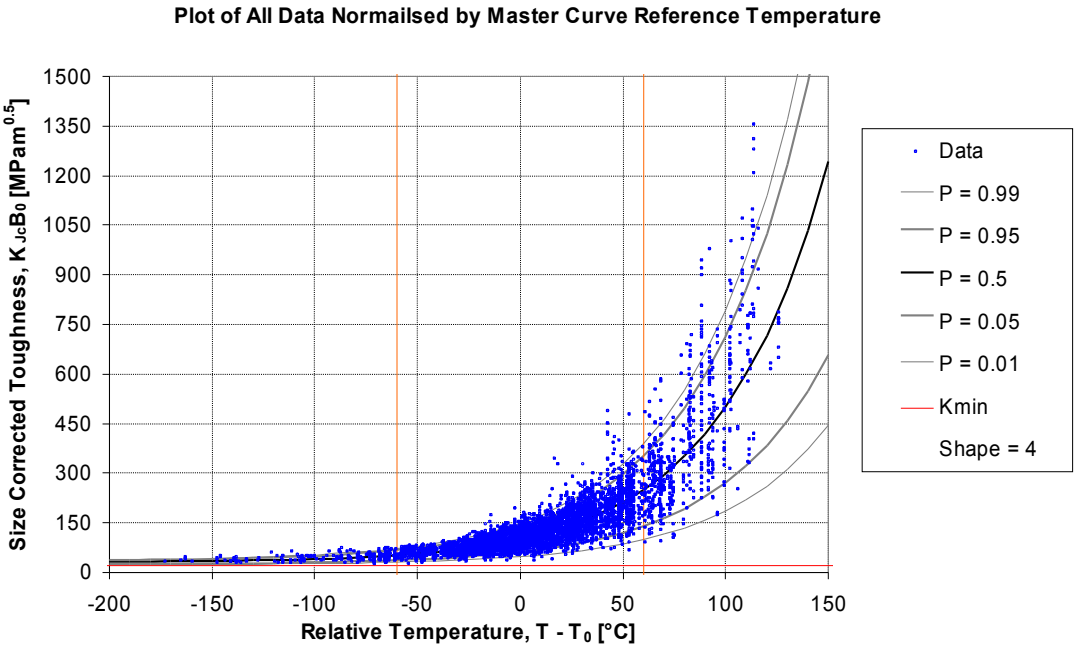

Figure C-7 - All ASTM 1921-05 Data Normalised by Reference Temperature, T_0

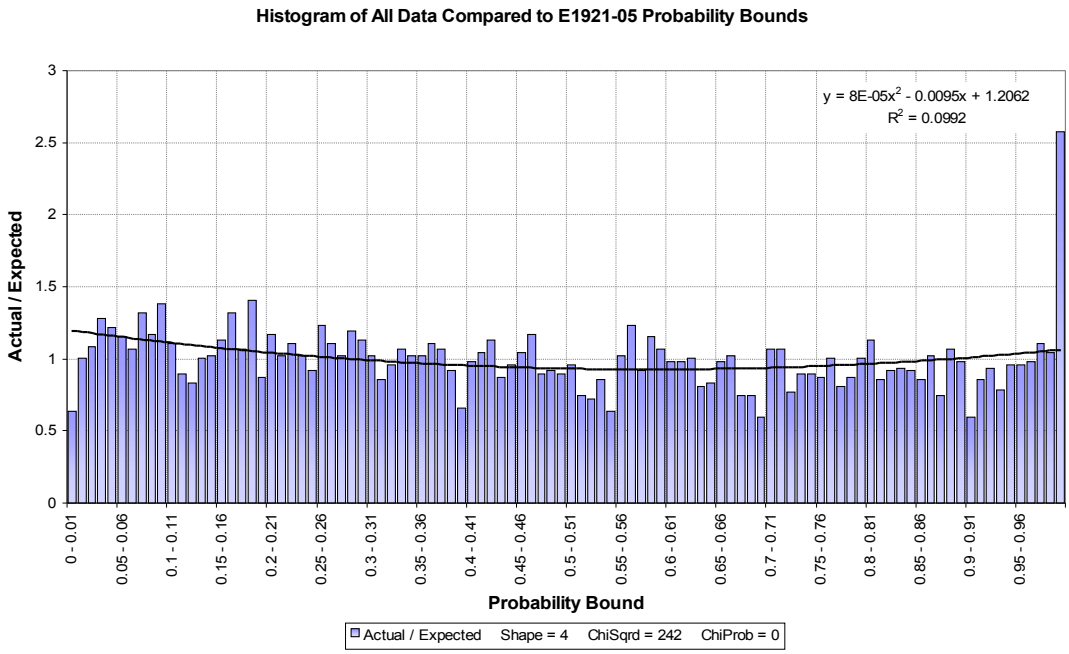

Figure C-8 - Histogram of Actual to Expected Data for All ASTM E1921-05 Data

Normalised by Reference Temperature, T_0

Weibull Shape Low Compared to Data

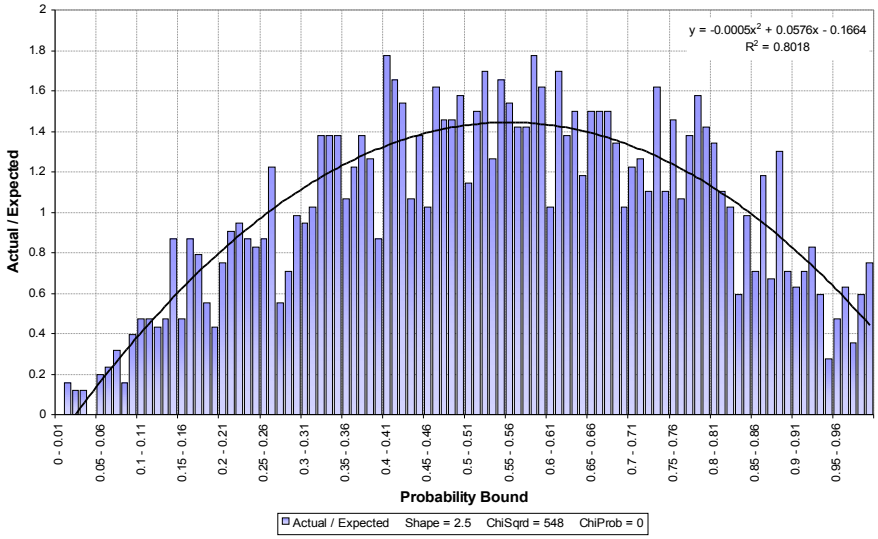

More data lie in the central region than predicted by the model giving a characteristic convex shape.

Weibull Shape High Compared to Data

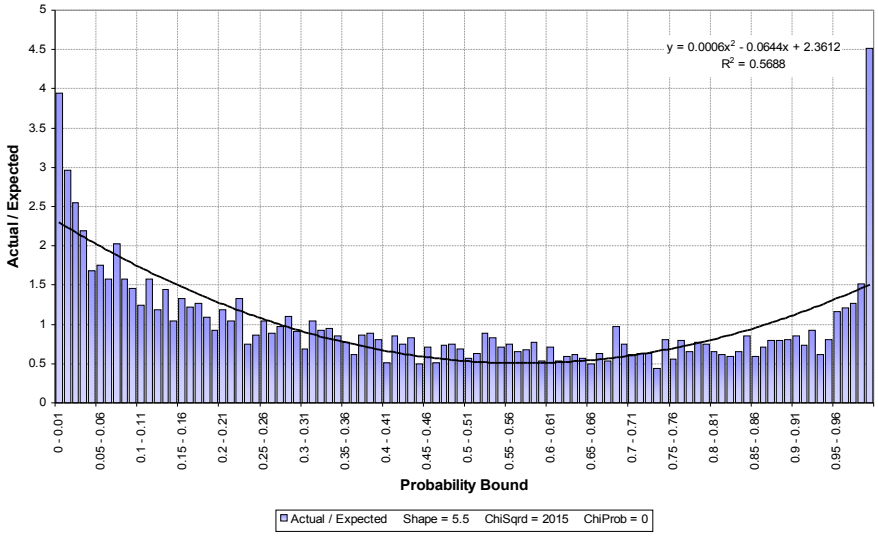

More data fall than predicted by the model in tails of the distribution giving a characteristic concave shape.

Figure C-9 - Effect of Weibull Shape on the Appearance of the All ASTM E1921-05 Data Histogram

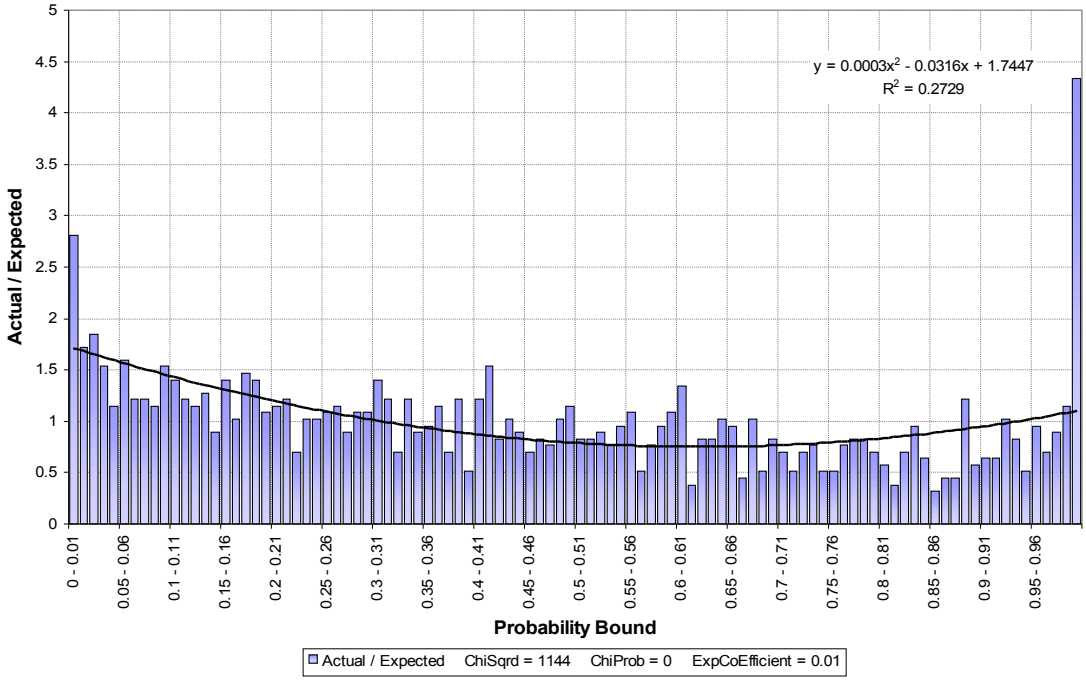

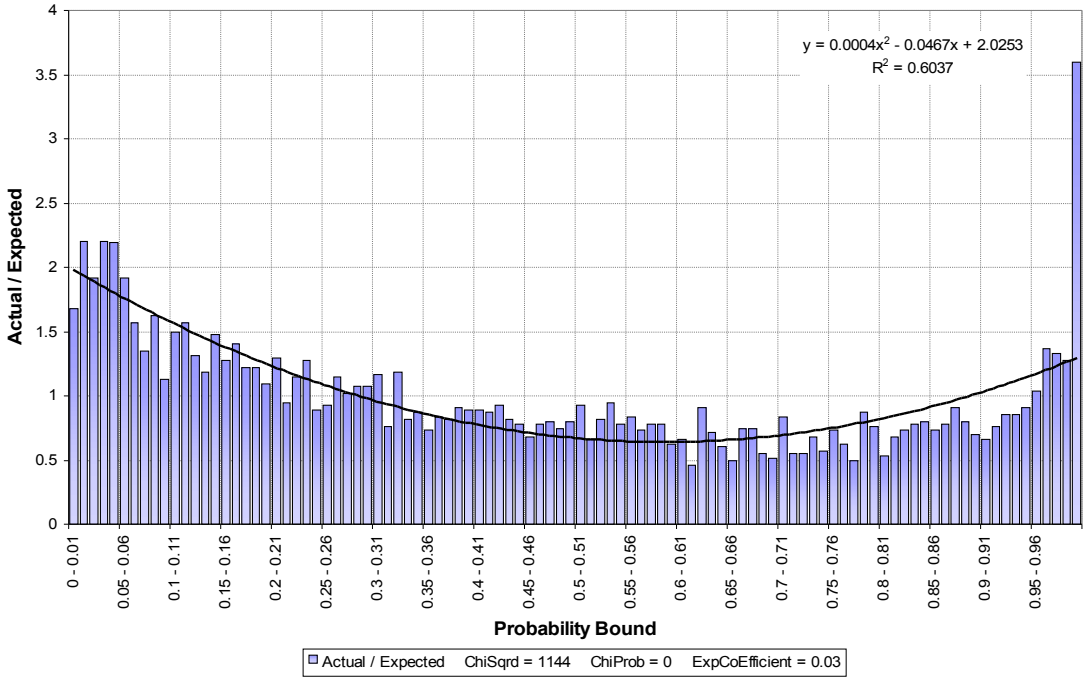

Figure C-10 - Effect of Scale Temperature Dependence on the Appearance of the All ASTM E1921-05 Data Histogram

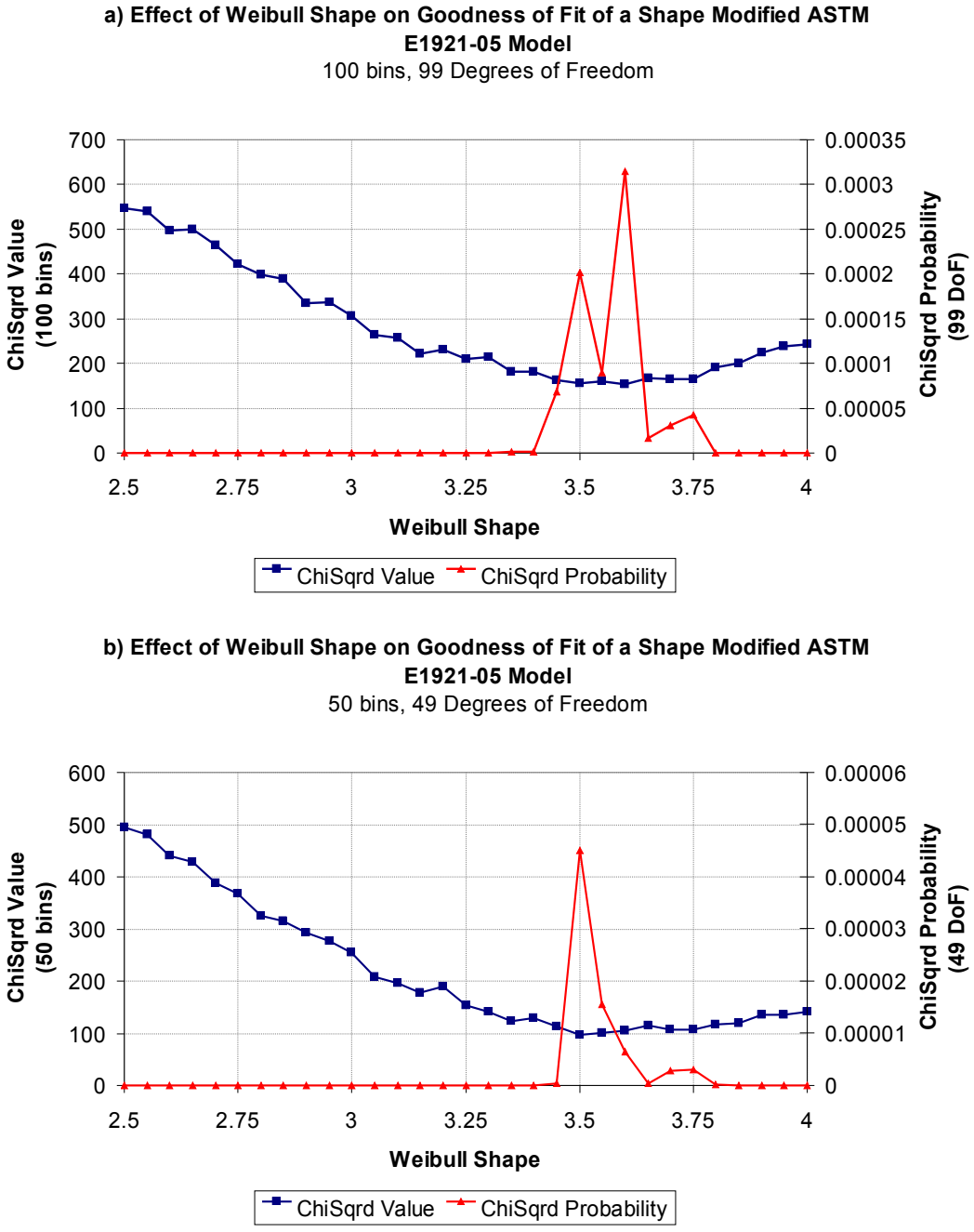

Figure C-11 - Effect of Weibull Shape on the Goodness of Fit Parameter, χ^2, for a Weibull shape modified ASTM E1921-05 model for a) 100 bins, and b) 50 bins

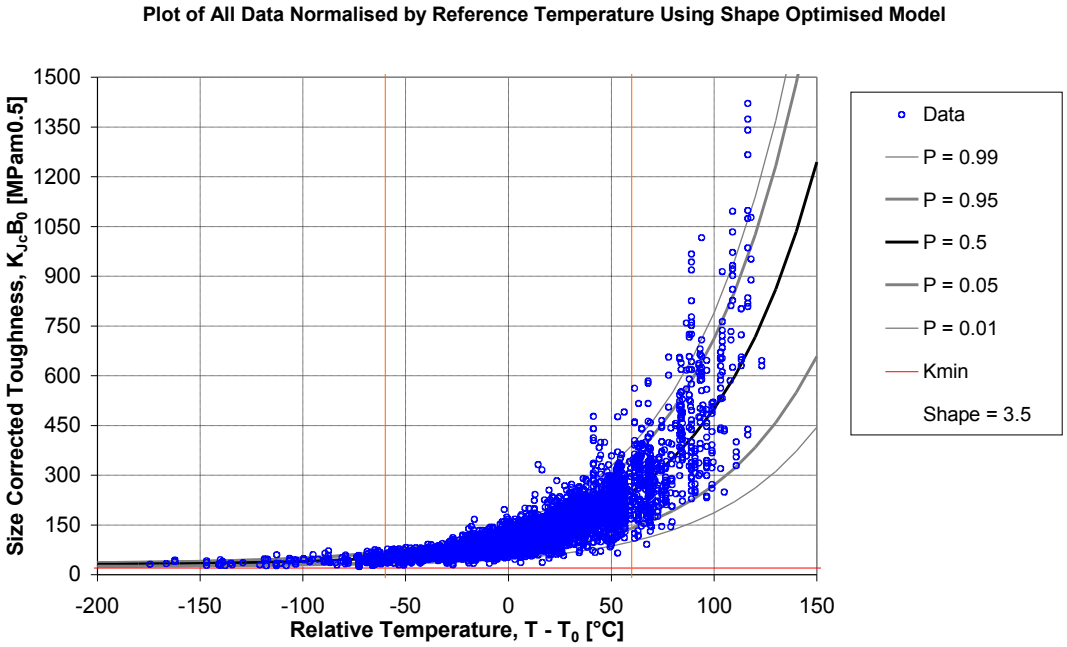

Figure C-12 - Shape Optimised Model for All Data Normalised by Reference Temperature, T_0

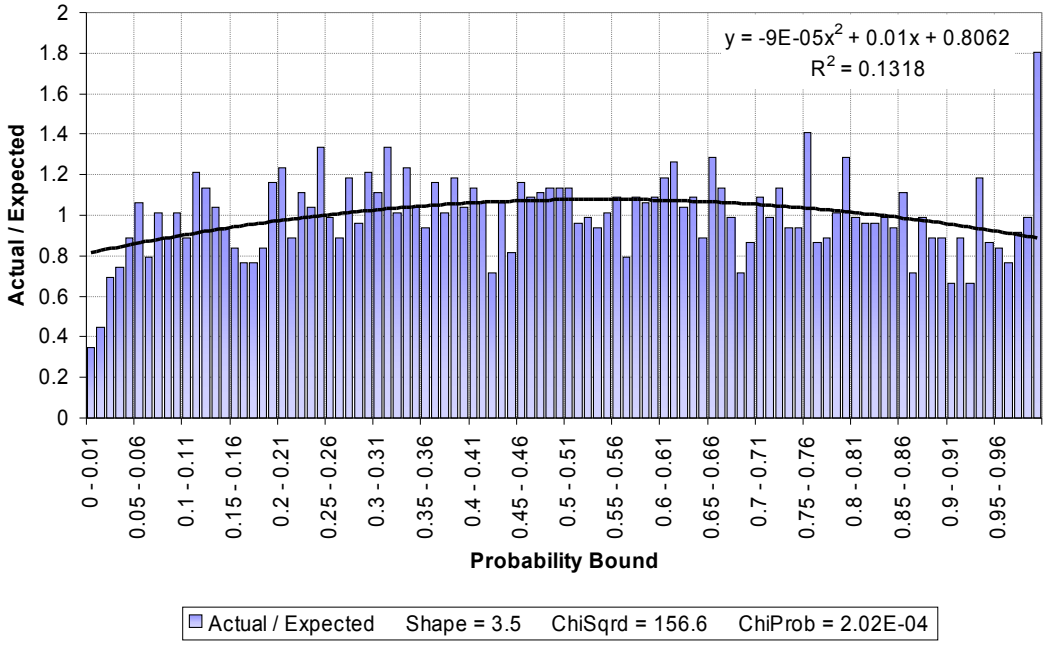

Figure C-13 - Histogram of Actual to Expected Data for Shape Optimised Model

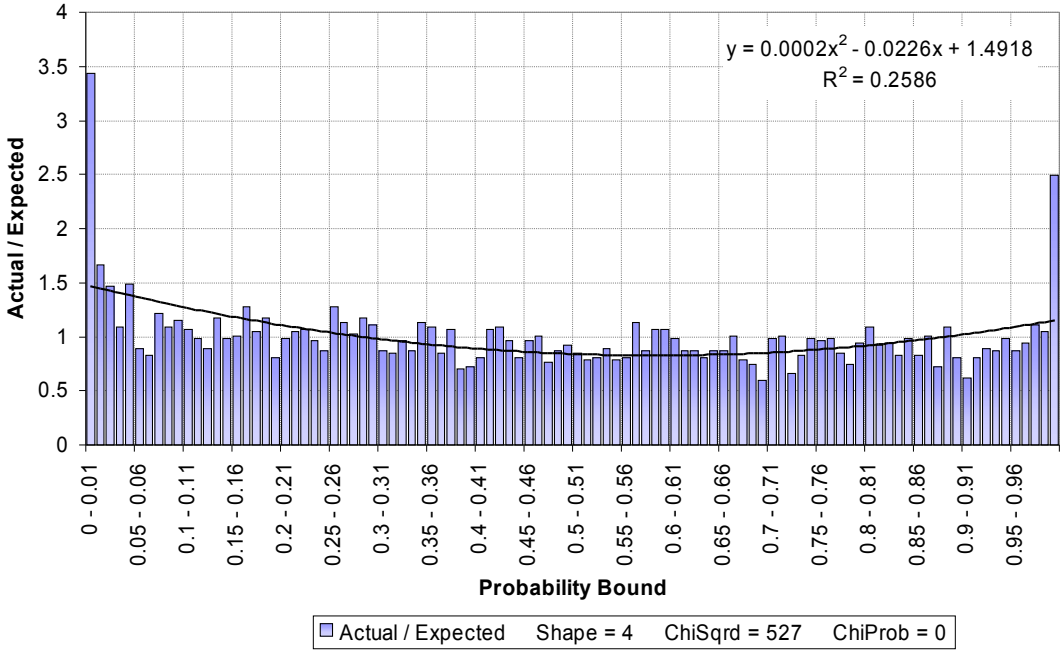

Figure C-14 - Effect of Applying Micro Arrest Concept to ASTM E1921-05 Model

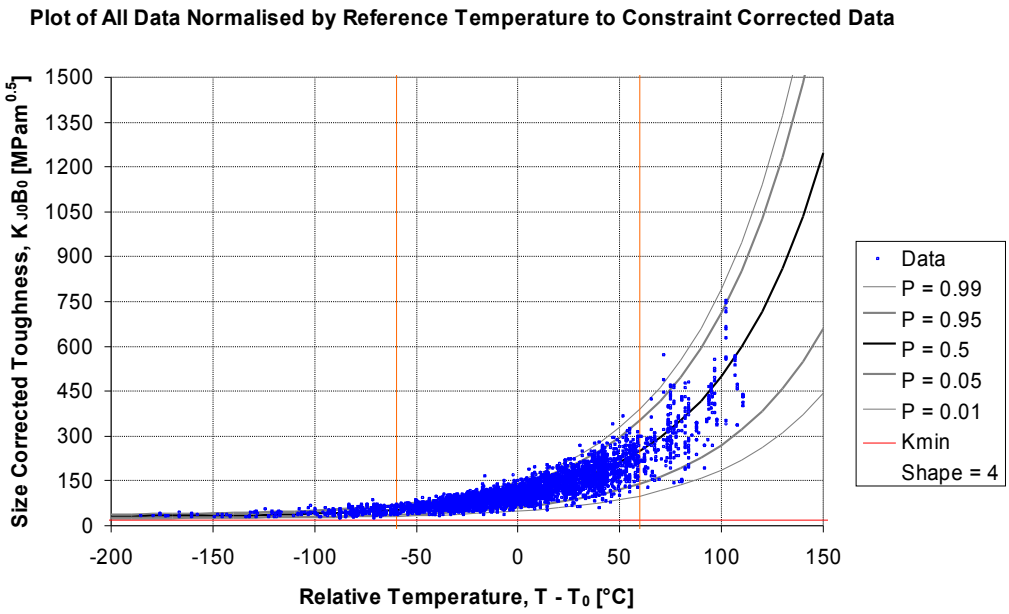

Figure C-15 - Constraint Corrected Model for All Data Normalised by Reference Temperature, T_0

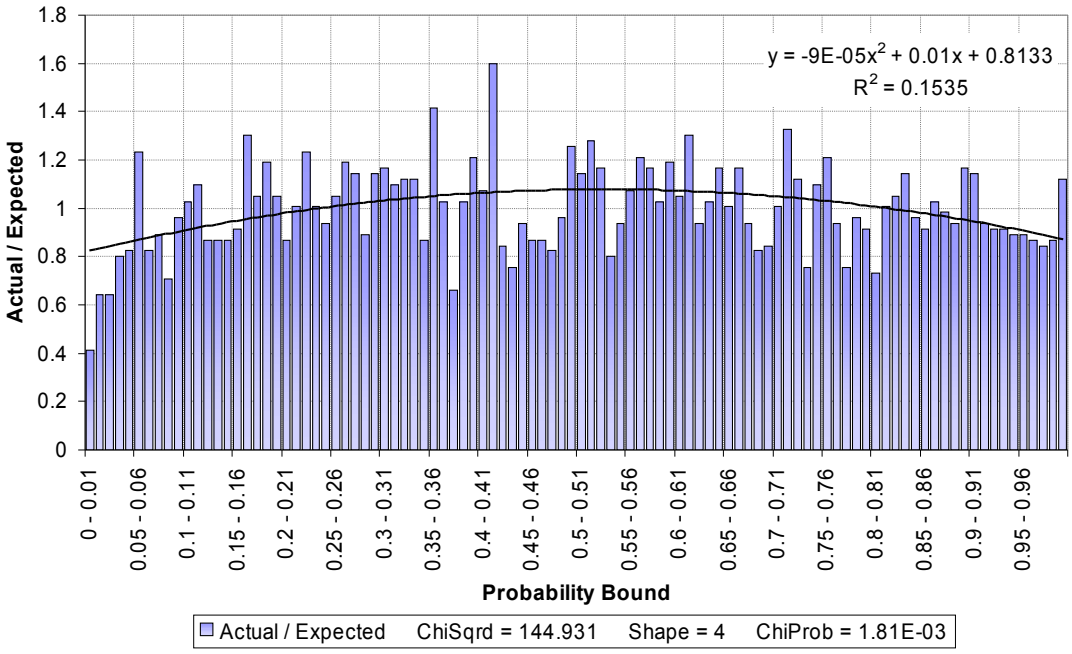

Figure C-16 - Histogram of Actual to Expected Data for Constraint Corrected Model

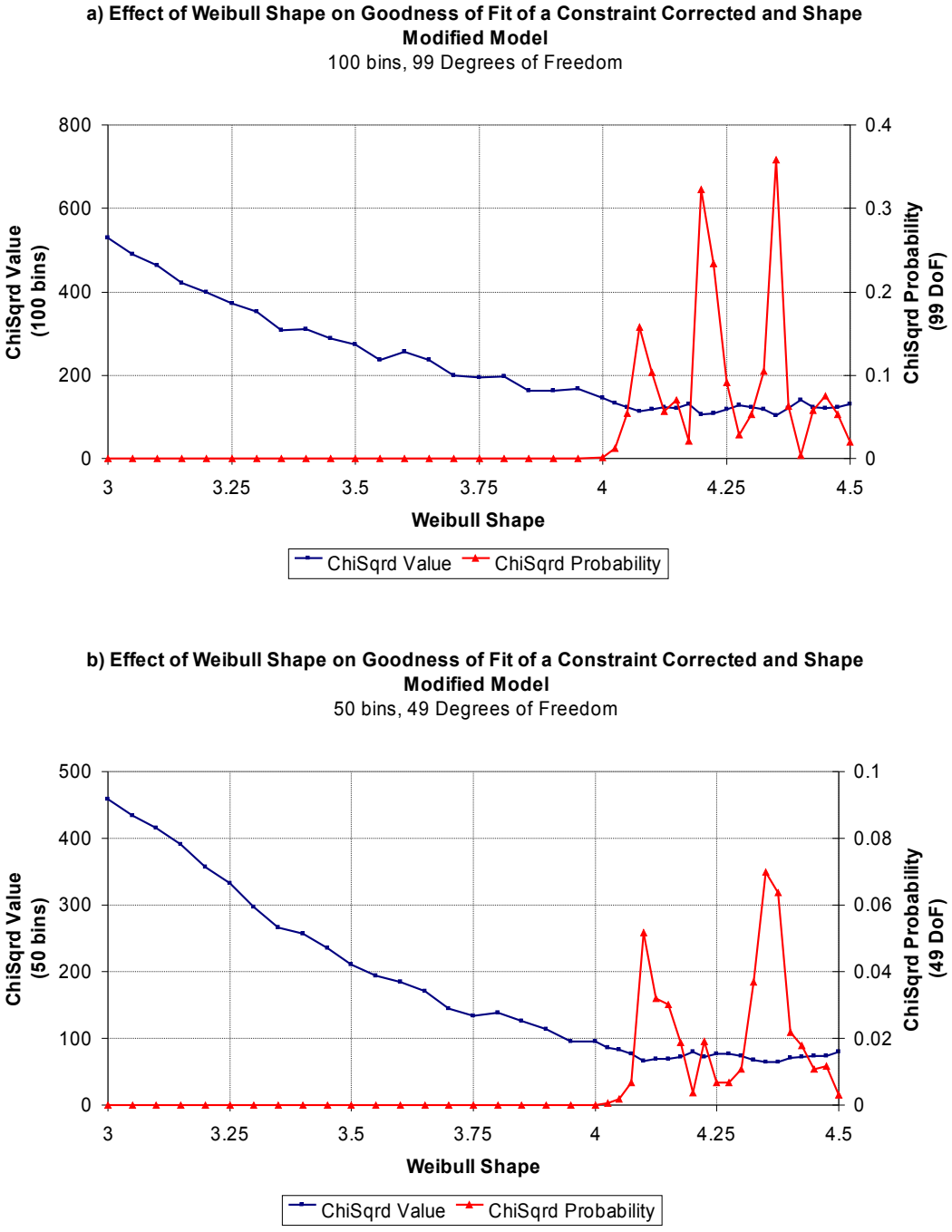

Figure C-17 - Effect of Weibull Shape on the Goodness of Fit Parameter, χ^2, for a Weibull shape modified Constraint Corrected model for a) 100 bins, and b) 50 bins

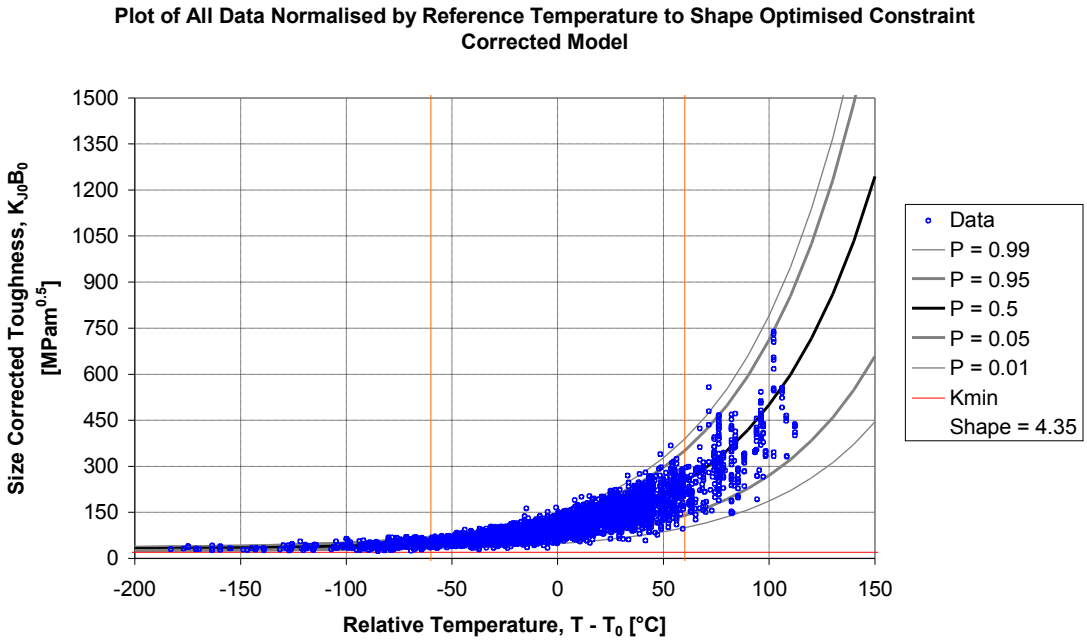

Figure C-18 - Shape Optimised Constraint Corrected Model for All Data Normalised by Reference Temperature, T_0

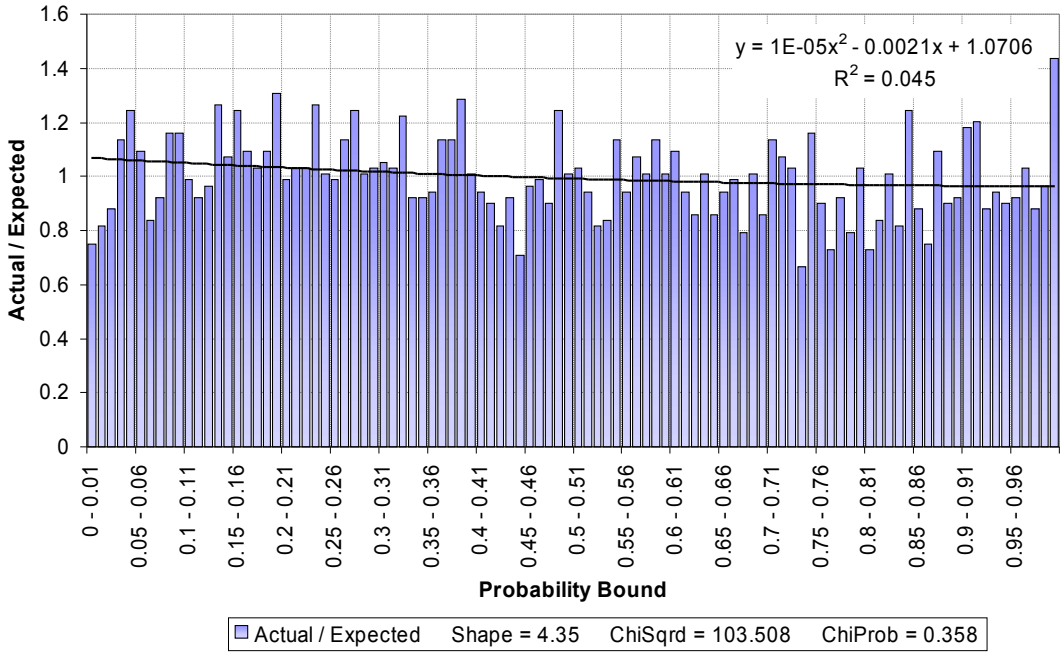

Figure C-19 - Histogram of Actual to Expected Data for Shape Optimised Constraint Corrected Model

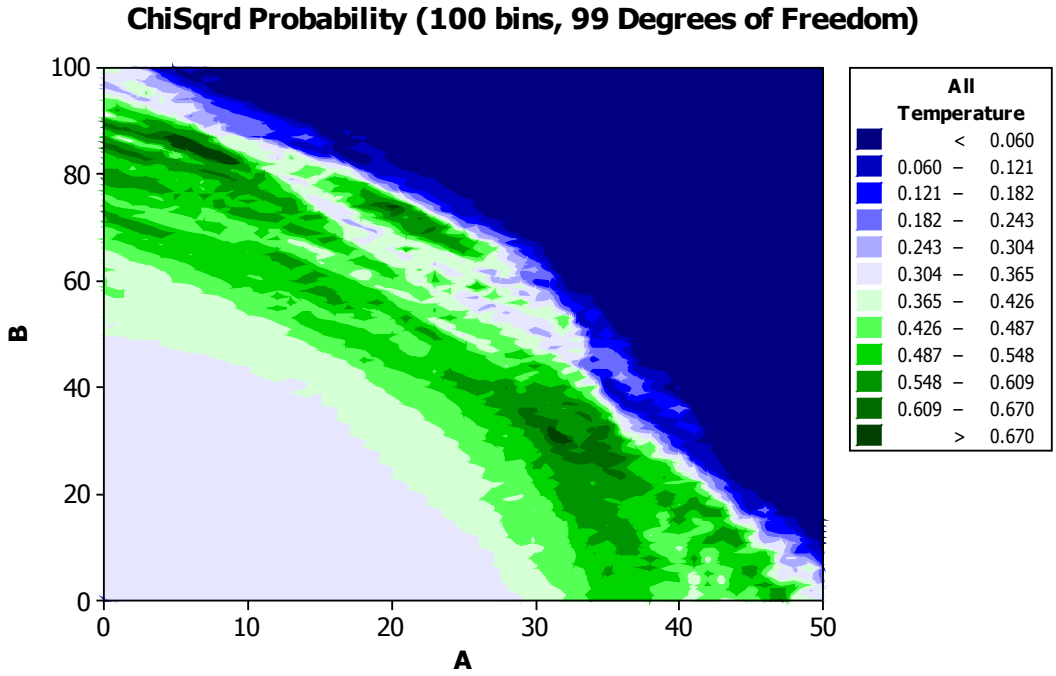

Figure C-20 - Effect of Varying Arrest Model Parameters on the Goodness of Fit (χ^2 Probability) for the Shape Optimised Constraint Corrected Model

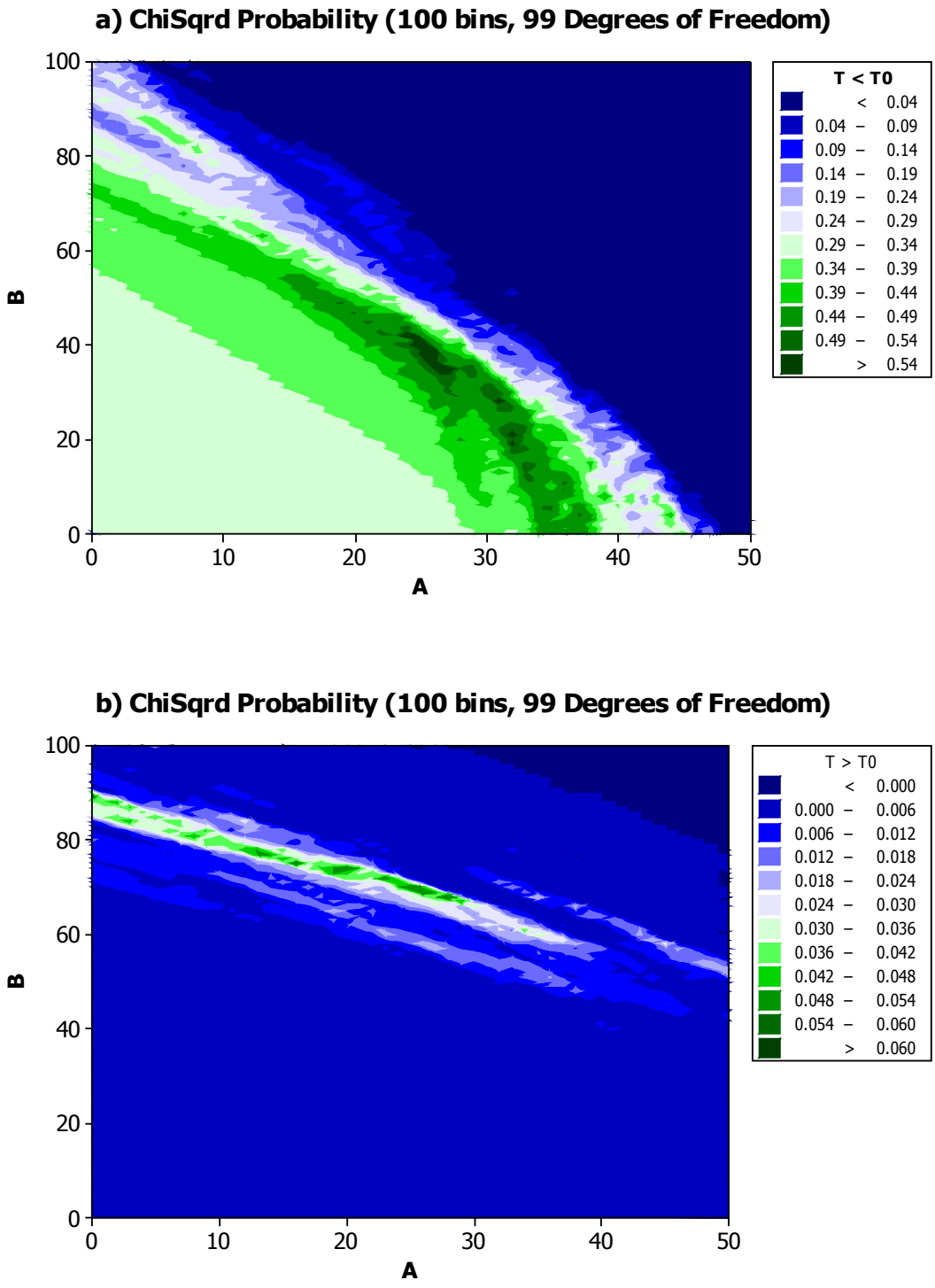

Figure C-21 - Effect of Varying Arrest Model Parameters on the Goodness of Fit (χ^2 Probability) for the Shape Optimised Constraint Corrected Model for a) below T_0, and b) above T_0

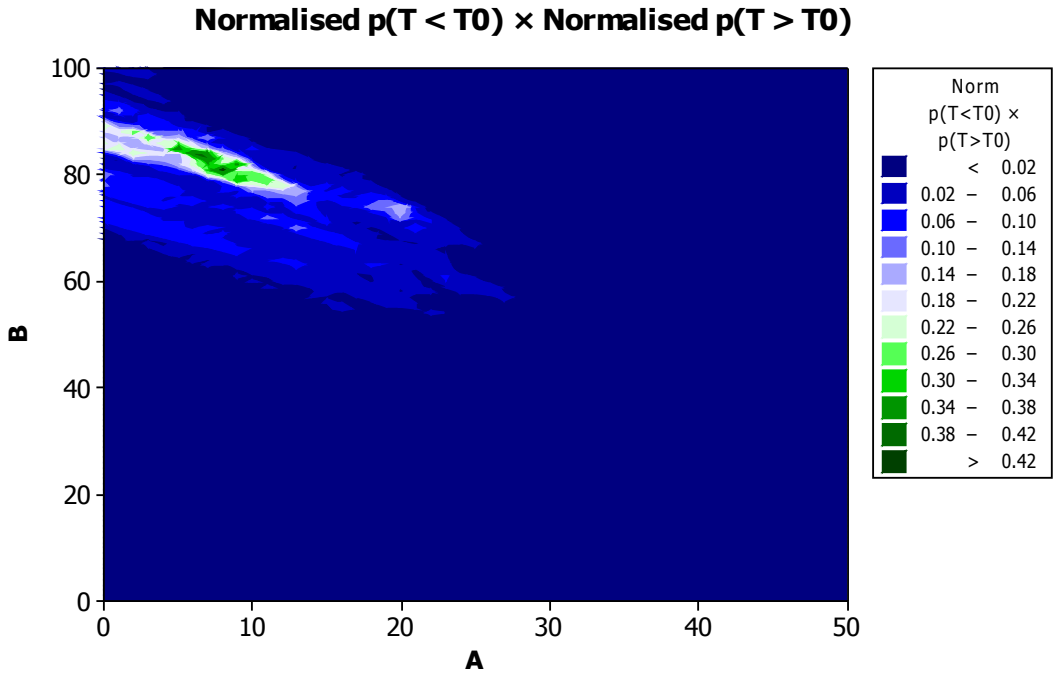

Figure C-22 - Comparison of Low and High Temperature Ranges, $p(T < T_0) \times p(T > T_0)$

Each Normalised by Maximum Value

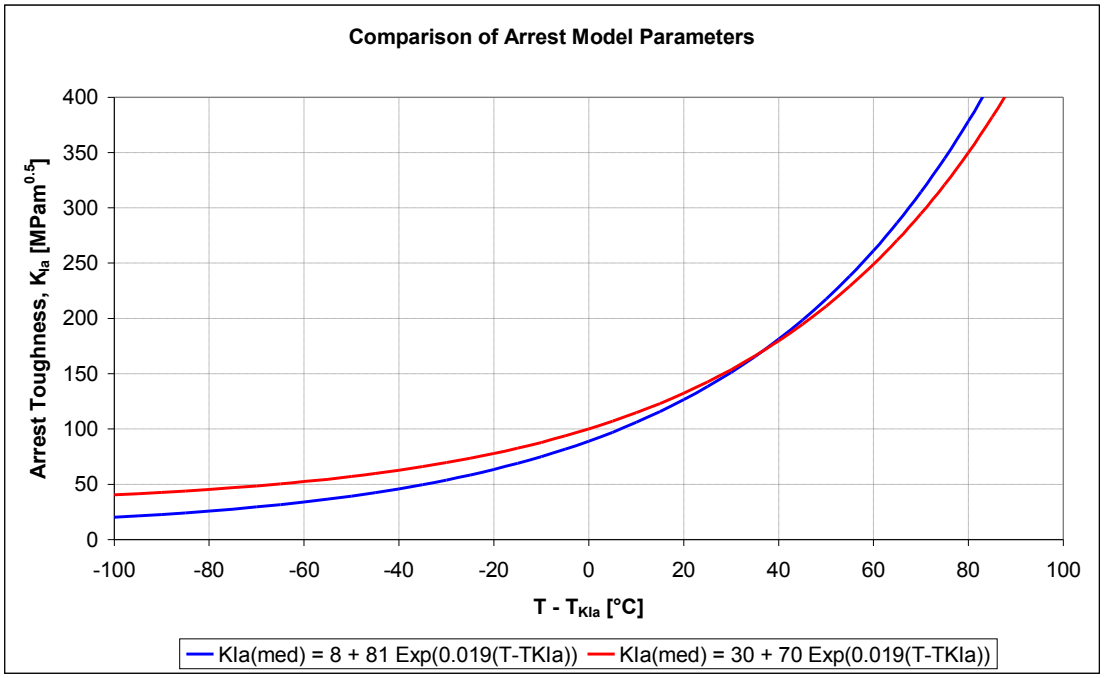

Figure C-23 - Comparison of Arrest Distribution Parameters

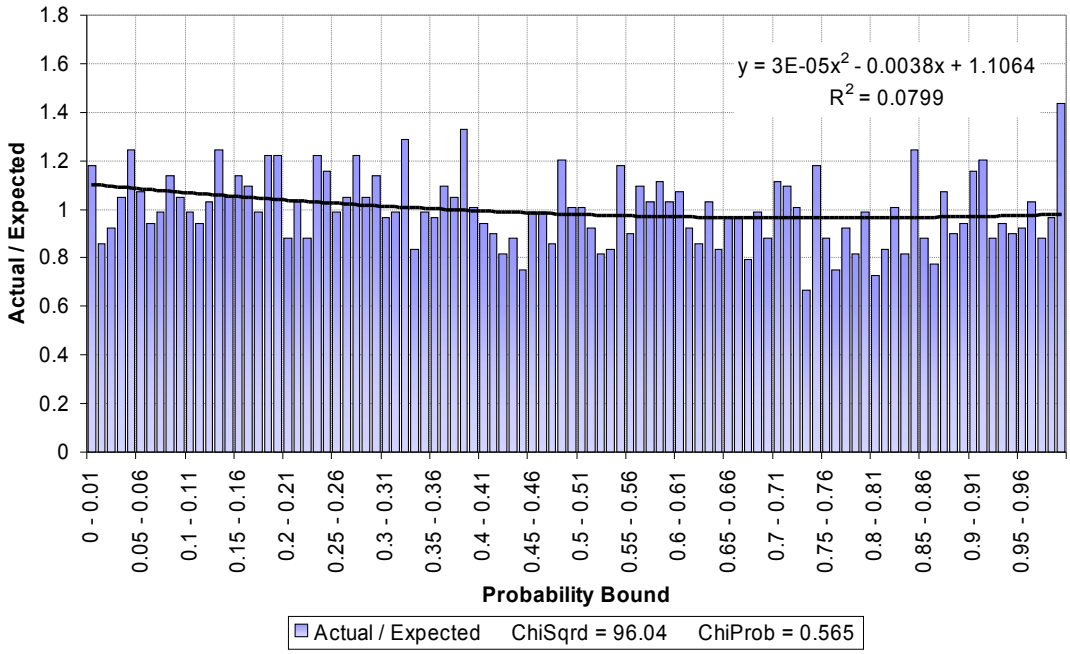

Figure C-24 - Histogram of Actual to Expected Data for Micro Arrest Modified Shape Optimised Constraint Corrected Model

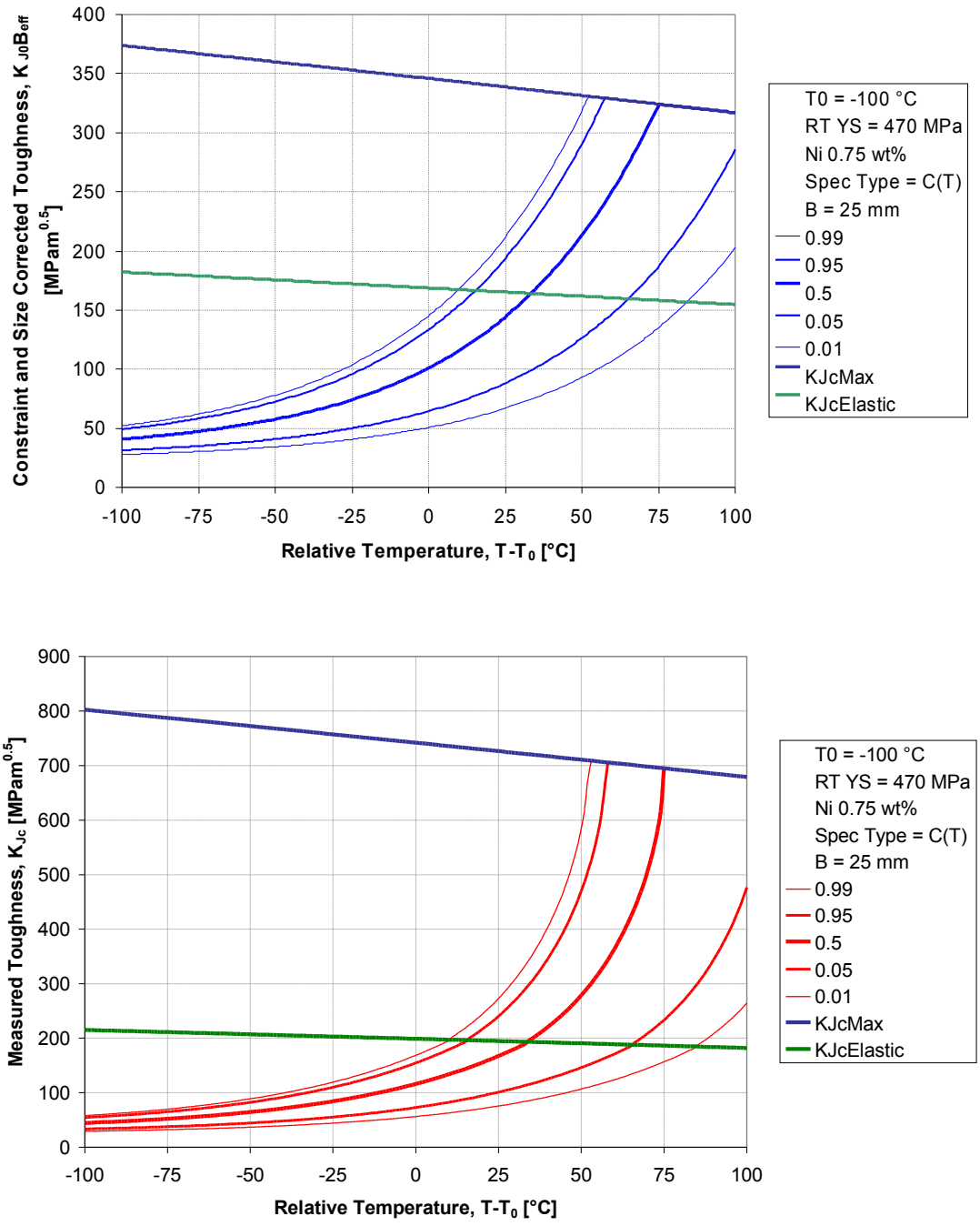

Figure C-25 - Failure Tolerance Bounds Predicted from the Micro Arrest Constraint Corrected Model for Typical A508-3 in the Start of Life Condition

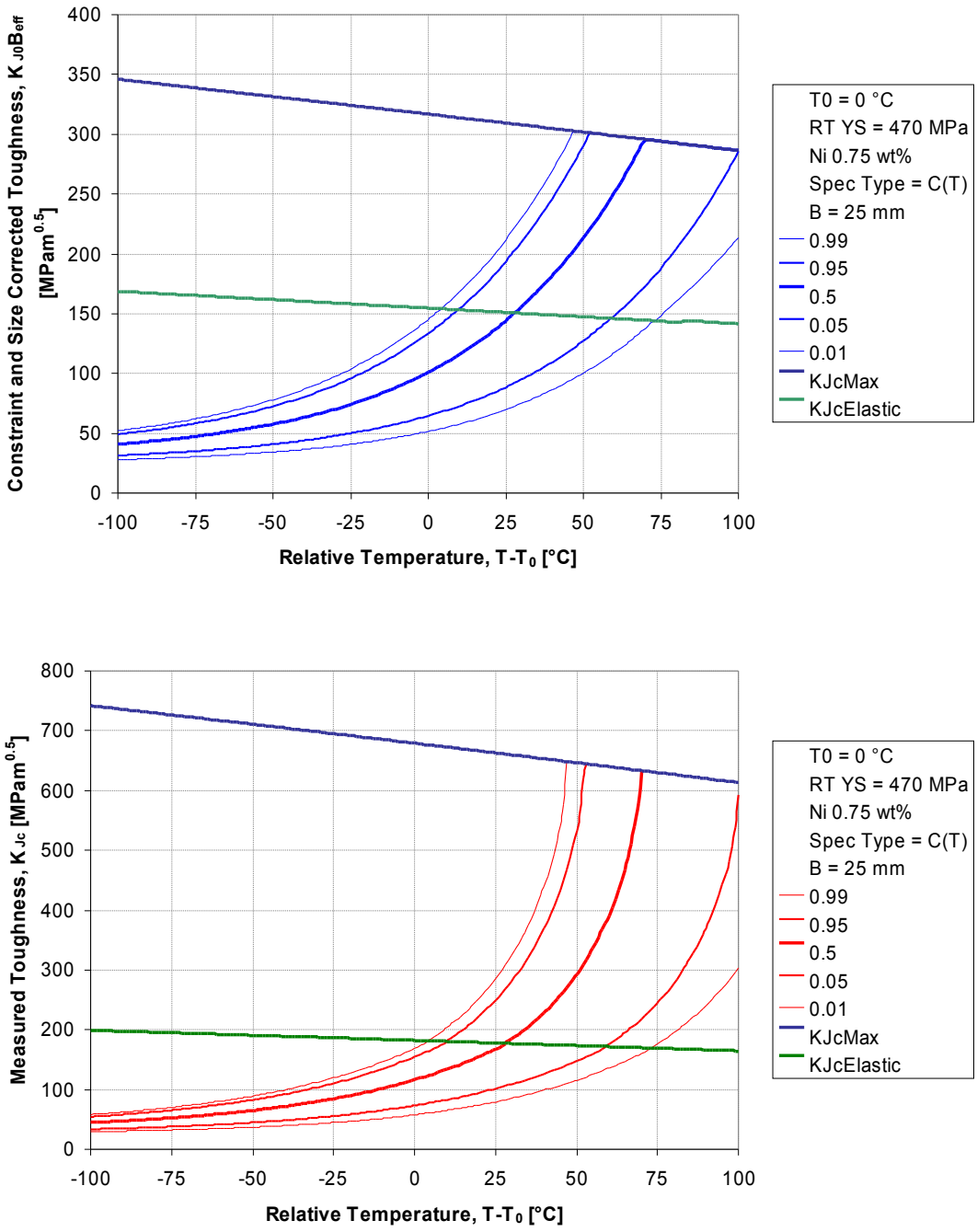

Figure C-26 - Failure Tolerance Bounds Predicted from the Micro Arrest Constraint Corrected Model for Typical A508-3 in the End of Life Condition

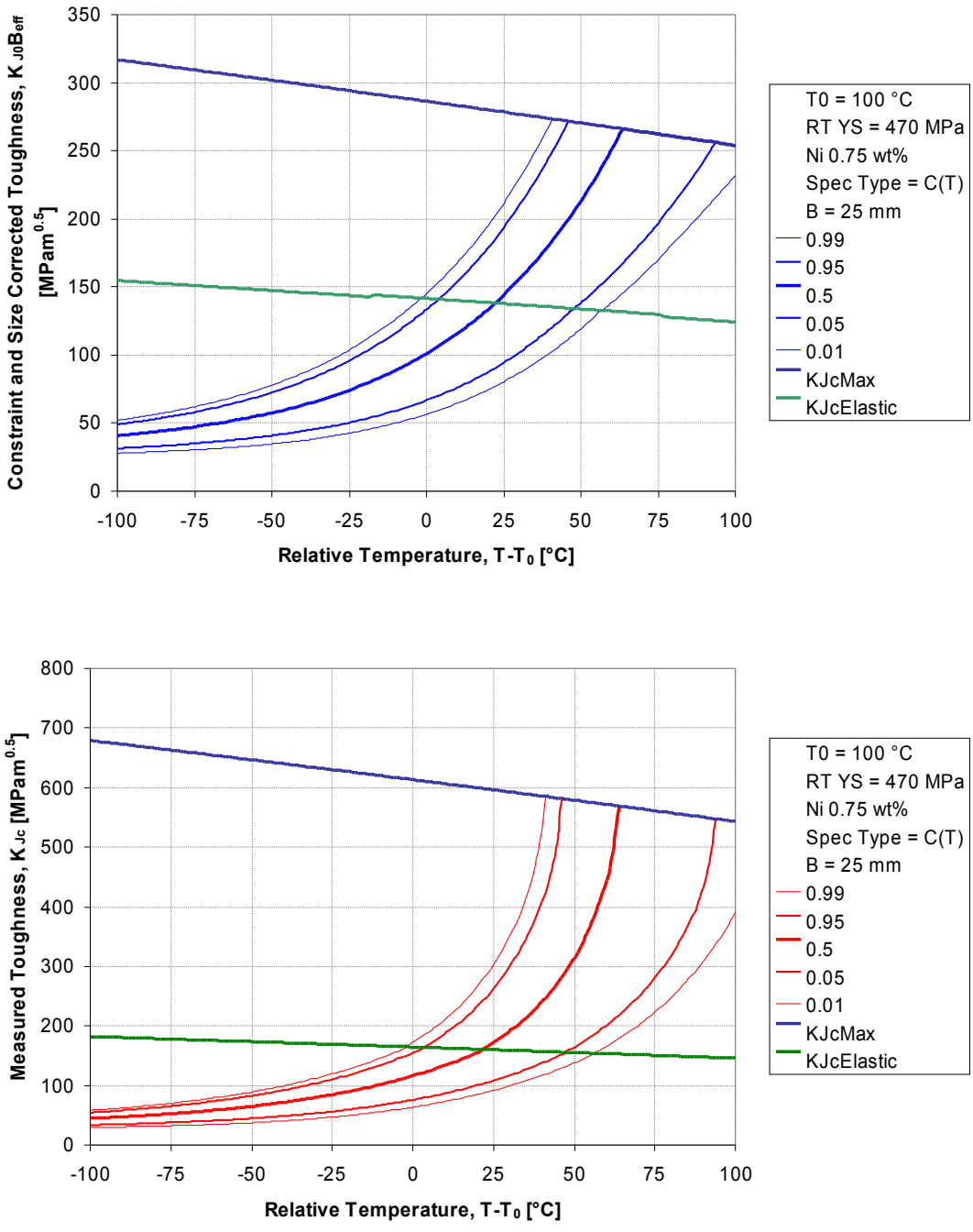

Figure C-27 - Failure Tolerance Bounds Predicted from the Micro Arrest Constraint Corrected Model for Typical A508-3 Following Extended Irradiation

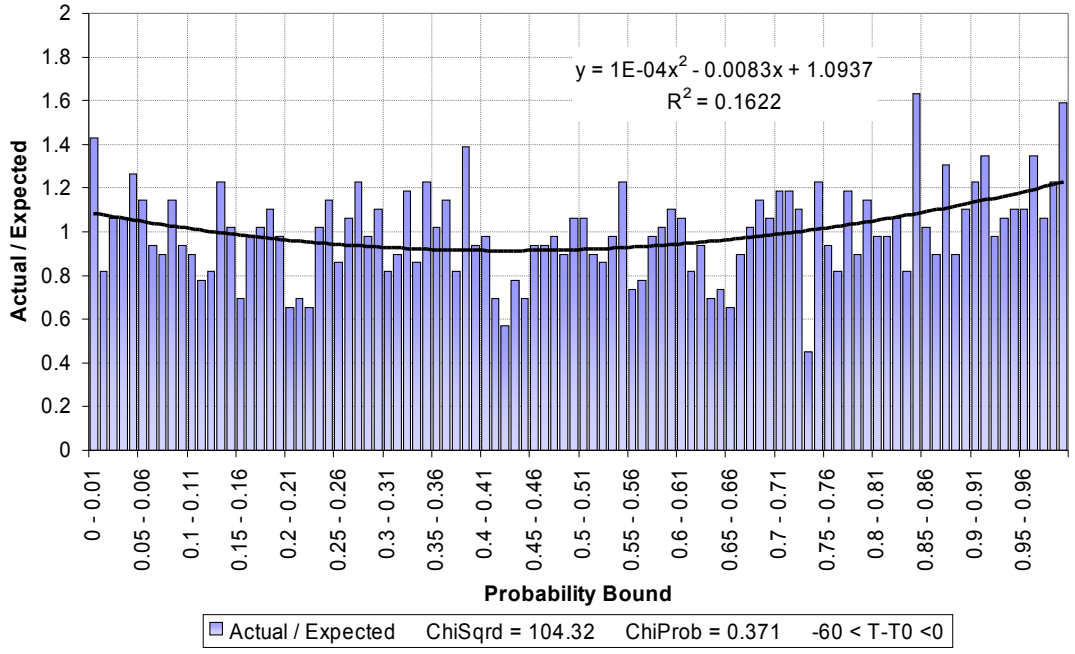

Figure C-28 - Histogram of All Below Reference Temperature Data Vs Expected for the Microarrest Constraint Corrected Model

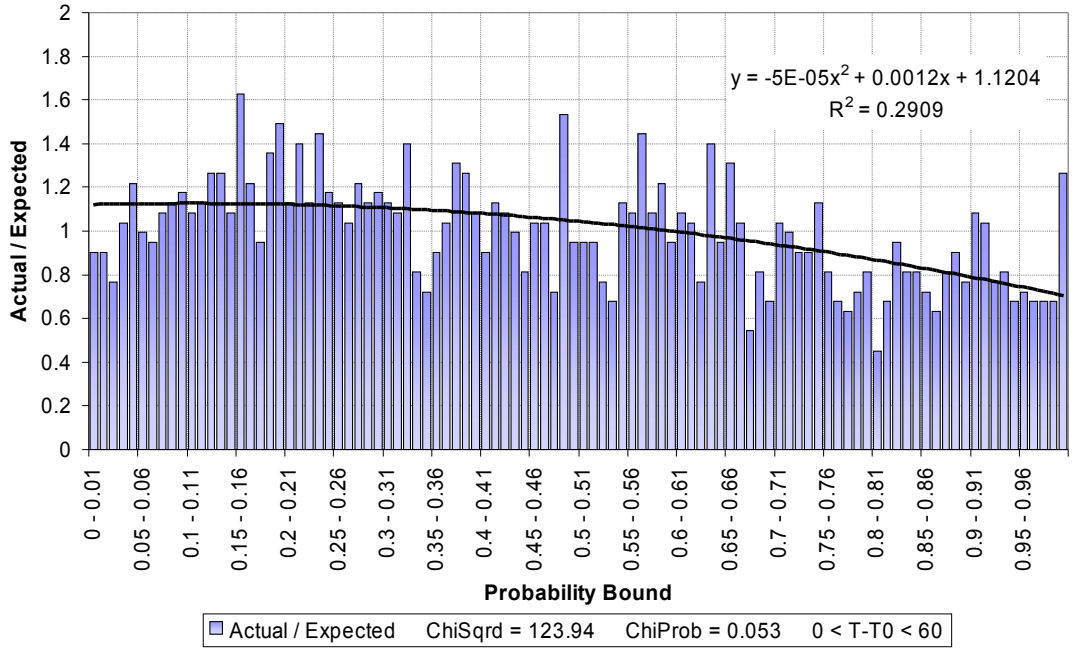

Figure C-29 - Histogram of All Above Reference Temperature Data Vs Expected for the Microarrest Constraint Corrected Model

C.11 References

1. Barlow, R.J., *Statistics: A guide to the use of statistical methods in the physical sciences*. 1989, Chichester: John Wiley & Sons.
2. Lawless, J.F., *Statistical Models and Methods for Lifetime Data*. 1982, New York: Wiley.
3. *ASTM E1921-05 Standard Test Method for Determination of Reference Temperature, T_0, for Ferritic Steels in the Transition Range*. 2005, West Conshohocken: ASTM International.
4. Sieurin, H. and R. Sandström, *Fracture toughness of a welded duplex stainless steel.* Engineering Fracture Mechanics, 2006. **73**(4): p. 377-390.
5. Pisarski, H.G. and K. Wallin, *The SINTAP fracture toughness estimation procedure.* Engineering Fracture Mechanics, 2000. **67**(6): p. 613-624.
6. Bannister, A.C., J. Ruiz Ocejo, and F. Gutierrez-Solana, *Implications of the yield stress/tensile stress ratio to the SINTAP failure assessment diagrams for homogeneous materials.* Engineering Fracture Mechanics, 2000. **67**(6): p. 547-562.
7. Ainsworth, R.A., A.C. Bannister, and U. Zerbst, *An overview of the European flaw assessment procedure SINTAP and its validation.* International Journal of Pressure Vessels and Piping, 2000. **77**(14-15): p. 869-876.
8. Weibull, W., *A statistical theory of the strength of materials.* Ingeniors Vetenskaps Akademien, 1939. **151**(3): p. 45-55.
9. Weibull, W., *A statistical distribution function of wide applicability.* J. Appl. Mech.-Trans., 1951. **18**(3): p. 293-297.
10. Guinea, G.V., F.J. Rojo, and M. Elices, *Brittle failure of dry spaghetti.* Engineering Failure Analysis, 2004. **11**(5): p. 705-714.
11. Nevalainen, M. and R.H. Dodds Jr, *Numerical investigation of 3-D constraint effects on brittle fracture in SE(B) and C(T) specimens.* International Journal of Fracture, 1995. **74**(2): p. 131-161.
12. Nevalainen, M. and R.H. Dodds Jr, *NUREG/CR-6317 Numerical Investigation of 3-D Constraint Effects on Brittle Fracture in SE(B) and C(T) Specimens*, O.o.N.R. Research, Editor. 1996, U.S. Nuclear Regulatory Commission.
13. Eno, D.R., *Single temperature error formulation*, D. Cogswell, Editor. 2008.
14. *Flaw evaluation procedures: ASME Section XI, EPRI SR-719*, T.U. Marston, Editor. 1978, Electric Power Research Institute.
15. Wallin, K., *Statistical re-evaluation of the ASME KIC and KIR fracture toughness reference curves.* Nuclear Engineering and Design, 1999. **193**(3): p. 317-326.
16. Williams, T.J., D.I. Swan, and G. Dixon, *Modification of the lower tail of the Master Curve distribution*, in *IAEA Specialist Meeting*. 2004: Moscow.
17. Dodds, R.H., *Personal communication*, D.J. Cogswell, Editor. 2008.
18. Dodds Jr, R.H., M. Tang, and T.L. Anderson, *Numerical procedures to model ductile crack extension.* Engineering Fracture Mechanics, 1993. **46**(2): p. 253-264.